IOWA STATE UNIVERSITY
Digital Repository

2013

Advancing the seismic design of reinforced concrete bridge columns

Aaron Trask Shelman
Iowa State University

Advancing the seismic design of reinforced concrete bridge columns

by

Aaron Trask Shelman

A dissertation submitted to the graduate faculty

in partial fulfillment of the requirements for the degree of

DOCTOR OF PHILOSOPHY

Major: Civil Engineering (Structural Engineering)

Program of Study Committee:
Sri Sritharan, Major Professor
Jeramy Ashlock
Igor Beresnev
Jon M. Rouse
Kejin Wang

Iowa State University
Ames, Iowa
2013

TABLE OF CONTENTS

LIST OF FIGURES

LIST OF FIGURES FOR APPENDIX A

LIST OF TABLES

ACKNOWLEDGEMENTS

ABSTRACT

Recent earthquakes near highly populated cities have reminded the world and engineers about the destructive capabilities of an earthquake event. This is especially true in the design of reinforced concrete bridge columns that need to survive an event to maintain life safety and provide operational capacity along major lifelines to provide immediate assistance to the regions affected. The research presented within this document examines the current state of practice and looks for ways to improve the design methodologies prior to an event that highlights unforeseen consequences. This is accomplished through a series of analytical and experimental studies that include: (1) the development of a new simplified method for the lateral load response of columns continuously supported on drilled shafts; (2) the behavior of concrete and soil when subjected to frozen conditions; and (3) the impacts of current methodologies for the establishment of transverse confinement reinforcement on the seismic response of reinforced concrete bridge columns.

A new approach is discussed within that defines an equivalent cantilever supported by a flexible base using a set of three springs for the establishing the lateral load response of columns continuously supported on drilled shafts in non-cohesive soils. This is an extension of the work presented in Appendix A in order to provide a consistent approach for both cohesive and non-cohesive soils that may be encountered near a bridge site. The effective height of the system was defined as the distance from column tip to the point of maximum moment to identify a critical design location for the establishment of transverse confinement reinforcement. The new method was found to adequately capture the response when

compared with the experimental work of Chai and Hutchinson (2002) and analytical models produced in LPILE.

Controlled material tests were performed on concrete and soil to examine the effects of seasonal freezing on their respective behaviors. Testing was conducted in controlled environments to maintain the temperature throughout the entire loading protocols. In each set of tests, it was concluded that significant changes would occur to the engineering properties when subjected to subzero conditions.

- Materials testing on confined and unconfined concrete provided evidence that both the confined and unconfined compressive strength would increase as temperature decreased. The strain at the peak compressive strengths increased for the confined concrete and decreased for the unconfined concrete. Furthermore, the modulus of elasticity increased in both instances. These changes are important in ensuring an accurate moment-curvature response of the reinforced concrete sections used in a seismic design.

- Soil testing found that an increase in strength by a factor of 10 and 100 would occur at temperatures of -1 °C (30.2 °F) and -20 °C (-40 °F) when compared with the warm weather testing at 20 °C (68 °F). This is of importance as the upper levels of soil cause changes that result in the shifting of the maximum moment location and increasing of the foundation shaft and column lateral shear demands.

The final portion of these studies was an investigation into the required amounts of transverse confinement reinforcement. The study indicated that the variation in requirements

xvii

could be as high as a factor of two to three depending on the approaches compared within the study. Furthermore, the information was extended to the impacts of the approaches on the curvature and displacement ductility capacity and demand. This study found that current equations may result in demand exceeding capacity and a new equation should be developed that takes into account the expected demand, axial load ratio, amount of longitudinal reinforcement, material properties and the ratio of the gross area to core area of the concrete cross-section.

CHAPTER 1: INTRODUCTION

1.1 Recent History

In recent years, numerous major to great earthquakes have taken place across the world in places like Chile ($M_w = 8.8$ in 2010), New Zealand ($M_w = 6.2$ in 2011) and Japan ($M_w = 9.0$ in 2011) that continue to remind the world and engineers about the destructive capabilities of a seismic event, and Figure 1-1 provides a few pictures of damage in these regions. The main reason these specific seismic events brought awareness to the forefront, even though these events regularly take place, was that they occurred in areas with large populations and significant infrastructure, and resulted in unexpected amounts of damage.

(a) (b) (c)
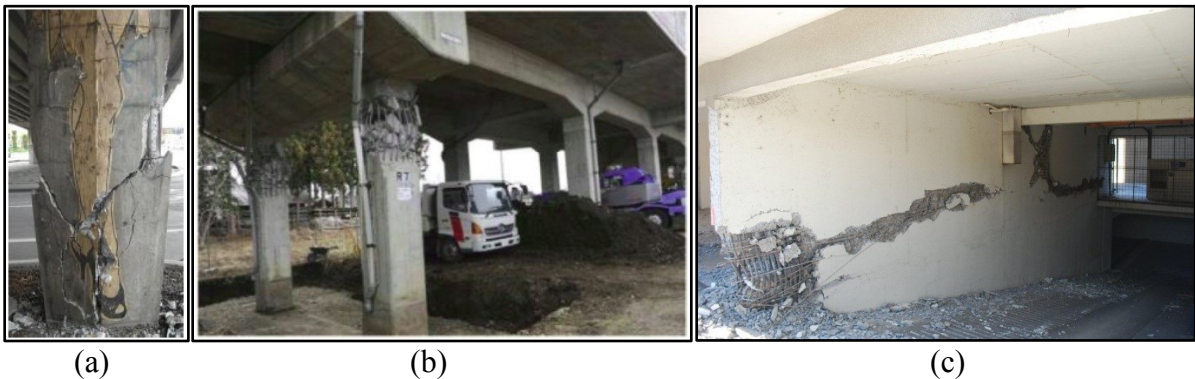
Figure 1-1: Damage of structures due to recent earthquakes: (a) bridge column from Christchurch Earthquake (Palermo et al. 2011); (b) bridge column from Tohoku Earthquake (Kawashima et al. 2011); (c) wall from Chile Earthquake (EERI 2012)

The New Zealand earthquake, commonly referred to as the 2011 Christchurch Earthquake, happened near the city of Christchurch, which is one of the most populous cities in the island nation. The 2011 earthquake caused large amounts of damage to the buildings within the city of Christchurch. Most buildings in the city of Christchurch were built with

masonry and concrete, and the damage occurred to older and most importantly modern buildings. The amount of demolition required within the city of Christchurch following the earthquake was approximately 78% of the buildings examined (~826 buildings) on the demolitions list provided by the Canterbury Earthquake Recovery Authority (CERA) (2012) with an additional 16% scheduled for partial demolition (~170 buildings). The list provided by CERA has three main categories of demolish, partial demolish and make safe with a total of 1058 buildings examined which does not encompass every building in the city. The partial demolish heading requires part of the building to be taken down immediately because of safety concerns and can include walls, facades and part of the overall structure. On this list are buildings with significance to the city that must be demolished including: (1) the tallest structure in the city known as the Grand Chancellor hotel that was leaning heavily, and; (2) the Crowne Plaza Hotel appeared to be in good condition on the outside but was still scheduled for demolition because of soil liquefaction in the surrounding area.

| (a) Grand Chancellor Building | (b) Crowne Plaza Hotel |

Figure 1-2: Images of buildings after the 2011 Christchurch Earthquake in New

Zealand

Bridge and road damage was also noted in the area such that 52% of the urban sealed roads needed rebuilding due to the earthquake (SCIRT 2012). Many of the bridges in the central business district survived the earthquake such that the vertical load carrying capacity was maintained, but the extent of the damage typically occurred near the abutments of the bridges since the liquefaction caused the bridges to act as a single strut between the two river banks (Palermo et al. 2011). The Earthquake Engineering Research Institute (EERI) and Pacific Earthquake Engineering Research (PEER) Center investigative team furthered this notion by stating that many of the bridges exhibited flexural cracking of the piles due to liquefaction and lateral spreading (2012). However, the density of bridges within the city area itself where significant building damage was widespread is very small. Other bridges throughout the world in regions with significant damage and ground motion may not perform in a similar manner as the surrounding soil may not liquefy and the structures themselves could unseat or experience other damage associated with earthquake ground motions. Further damage was noted, in the EERI Special Report, about the utilities that the bridges carried such that sewer and water lines broke spilling into the surrounding rivers and/or washing out embankments.

In the Tohoku Earthquake of 2011 (Japan), the large magnitude earthquake was also combined with a tsunami that caused massive flooding and damage. A key component gathered from this earthquake was that it had a rather long duration (3 minutes) and affected the infrastructure prior to the flooding of the tsunami waves. The bridges in the area tended to survive against the earthquake ground motion, but not necessarily the tsunami, if they were new or retrofitted to current standards in the Japanese design requirements (EERI 2012). The

older buildings, both residential and commercial, tended to show the most damage from the shaking, but the modern structures had less damage than expected (PEER et al. 2012). The lack of expected damage to structures due to the large magnitude shaking warrants further investigation by researchers.

The Chilean Earthquake of 2010 allowed for a great comparison between the U.S. codes in high seismic regions as they currently use a very similar practice and tend to use a number of reinforced concrete components. The damage resulting from this earthquake found that the base isolated structures tended to not be as damaged as the remaining structures, but those that were damaged had soft stories. Furthermore, the building damage was found to take place in locations where structural shear walls were placed such that they would not adequately take the seismically induced lateral loads. A number of walls in the reinforced concrete buildings had a lack of reinforcement steel in the edge regions (i.e., the boundary areas) of walls which lead to the crushing of concrete in these areas as seen in Figure 1-1(c). These three events and the unexpected amounts of damage emphasize the need for continual improvements in our understanding of earthquakes and how to design structures to withstand these events.

1.2 Design Approaches

In regions that have recently experienced major seismic events, many changes to the design approach used for reinforced concrete structures have occurred. However, two main approaches to the lateral design of a structure subjected to a design level or greater earthquake are in existence. These approaches consist of defining objectives based on forces or lateral displacements. The trend in the U.S. design approaches has begun to recognize the

importance of the direct displacement-based approach instead of the traditional force-based approach. A third method to design lateral force resisting members has arisen in current practice based on the desired performance of a structure or system with multiple objectives. This method in particular can be done using either a force-based or displacement-based approach.

1.2.1 Force-Based Design (FBD)

Force-based design has been around for nearly a century as Hardy Cross determined moment-distribution in the early 1920s (Leet et al. 2011). This method of analysis and other approaches (e.g., the flexibility and stiffness methods) developed later on allowed for relatively simple means of computing forces applied to a structural member. Members are then designed such that they will not fail under the applied load. In seismic situations, an equivalent static method is commonly used to determine the lateral forces and associated member forces that a design level earthquake would apply to a given structure. These forces, however, may not always control the sizing of a member because effects from dead load, live load, wind load, serviceability conditions and other design criteria influence the overall size of members. Furthermore, the lateral forces computed in this method are generally based on the natural period of the structure in the first mode only, which must be determined using known geometry from other loading cases or an approximation based on height of the structure. This process, however, does not typically take into account many factors including the fact that strength and stiffness are dependent on one another. Displacement has been generally only checked within the recent past decades using a pushover analysis, ignoring inertial effects, to ensure that any displacement requirements were satisfied once a design

was finalized. Should additional displacement be needed the design would be redone and most likely result in the use of additional confinement reinforcement. The volumetric ratio of transverse reinforcement, ρ_s, would then be increased implicitly for improvement as this would improve the ductility.

Following the 1971 San Fernando Earthquake and the extensive damage caused to structures designed using the force-based procedures, a shift in design philosophy began to take place, albeit at a slow pace. The damage throughout many structures indicated that the fundamental concepts of structures being designed to remain elastic under loading must be modified to ensure an adequate behavior. To attain the desired response, researchers began to focus on ways to increase the ductility of a system to prevent collapse. Out of this came the capacity design philosophy which focused on carefully selecting plastic hinge regions while ensuring no collapse under design-level and greater earthquakes (Priestley et al. 1996 and Priestley et al. 2007). Insufficient ductility and/or drift in a design was handled by implicitly increasing the transverse confinement reinforcement until a satisfactory result was attained.

1.2.2   Direct Displacement-Based Design (DDBD)

FBD demonstrated further weaknesses in the damage noted during the 1989 Loma Prieta and 1995 Kobe earthquakes because of the lack of adequately defining the seismic forces applied to a system and the handling of stiffness for any given structure. Instead of focusing purely on the improvement of force predictions, research began to focus on the idea of reaching a target displacement without failure. This led to the development of the direct displacement-based design (DDBD) methodology, where researchers began to target drifts

and/or displacements that a given structure should reach for a specific target hazard. The determination of an appropriate level of damping and ductility can then be used to determine an effective period for the structural member. This effective period can then be used to compute the effective stiffness of a member, which can then be related to a base shear force and distributed throughout to complete the design process. This method takes into account the fact that strength and stiffness are related to better improve the design process to prevent collapse under a design level or greater earthquake. In this approach, the amount of confinement reinforcement could be established based on the strain capacity of the confined concrete region. However, equations between the ultimate strain and desired curvature capacity seldom exist; thus, an iterative procedure is needed to define the confinement reinforcement needed for a system. For this purpose, an equation such as that recommended by Priestley et al. (1996), reproduced in Eq. (1-1), is used to link the amount of horizontal reinforcement to the targeted curvature capacity of the bridge cross-section based on the work of Mander et al. (1988). Sritharan et al. (1997) found that this recommendation suggested for design resulted in a reserve capacity of the confined concrete section by as much as 50%.

$$\varepsilon_{cu} = 0.004 + \frac{1.4\rho_s f_{yh}\varepsilon_{su}}{f'_{cc}} \qquad \text{Eq. (1-1)}$$

where: ε_{cu} = ultimate concrete strain;

ρ_s = volumetric spiral reinforcement;

f_{yh} = yield strength of hoop steel;

ε_{su} = ultimate strain of steel reinforcement; and

$$f_{cc}' \quad = \text{confined concrete compressive strength.}$$

1.2.3 *Performance-Based Design*

Performance-based design, although stated to have been around for quite a while by many sources, has emerged in the past couple of decades as the ideal design methodology for seismic situations. This method came to the forefront with the ATC-33 Project that attempted to create a standardized method for performance-based design and resulted in the publication of the *FEMA-273* (1997) and *FEMA-274* (1997) reports. In general, the performance-based methods for the seismic design of structures use multiple objectives with different criteria for each to define the desired response of a structure and can be completed using FBD or DDBD. The main sections suggested for performance-based design for seismic regions include (1) fully operational; (2) operational; (3) life safe, and; (4) near collapse (Priestley 2000). These sections of the design approach rely on the designer having to meet requirements such as the structure withstanding a certain magnitude earthquake, attaining a certain displacement ductility or drift, and/or meeting a specific level of damage. In the American Association of State Highway and Transportation Officials (AASHTO) *Guide Specification for LRFD Seismic Bridge Design* (2010), it is stated that the bridge must meet the life safety objective for an event with a seven percent probability of exceedance in 75 years (~1000 year return period). Furthermore, individual ductility demands must be less than a certain value based on the type of column bent (i.e., single vs. multiple) and the orientation of pier walls. The California Department of Transportation (Caltrans) extends this approach in the *Seismic Design Criteria (SDC)* by stating that the displacement ductility

capacity of a single member shall be greater than 3 while the demand should be established such that the displacement ductility demand shall be less than 4 (Caltrans 2010).

1.3 Limitations within practice

The aforementioned design approaches are highly prevalent in everyday practice throughout the United States and are constantly evolving, but each approach has it benefits and various methods are used to complete a design. The completion of any adequate design and analysis begins with a thorough understanding of the structural system and its components. This process requires accurate modeling and assumptions to be made about boundary conditions, material constitutive laws, ground motion and many other influences such as temperature. Numerous design models exist in practice to predict these effects and behaviors that are based off of theoretical and experimental simulations. Over the years, this has led to a more complicated design methodology, but changes in the overall process have typically only come about after significant events cause unforeseen damage. Counteracting this technique requires a proactive examination of the current design methodologies and models used in practice. With this in mind, it was found that the models used to produce adequate results tend to have some limitations. These limitations arise in the way in which materials are expected to behave, how the complexity of systems are handled and what components/quantity are important to a specific design. This ranges from the amount of confinement reinforcement needed in a critical region to the temperature at which a system should be designed. Each component involved in the modeling must be adequately accounted for as the overall response will be impacted and incorrect assumptions in some

parts may lead to catastrophic failure while other invalid assumptions may not lead to a failure in the system but a weaker understanding of the behavior.

1.3.1   Confinement Reinforcement

One area of improvement in our current design process is in the definition of confinement reinforcement that is typically used within critical regions of reinforced concrete columns and beams. This horizontal reinforcement ensures a ductile response of the system and component when subjected to a design level or greater earthquake. Confinement reinforcement in the form of closed loop ties or spirals resists the dilation of the concrete by providing lateral resistance when a load is applied to a system, thus increasing the overall capacity and ductility of the concrete section, Figure 1-3. Different guidelines and specifications suggest different methods of computing the appropriate amount of transverse reinforcement for confinement purposes [AASHTO (2012), Caltrans (2010), Priestley (1996), Standards New Zealand (2008), ATC (1996)] and each one uses some common and uncommon parameters about the concrete, steel reinforcement and cross-section details, as will be discussed further in Chapter 2.

(a) Spiral Reinforcement   (b) Tie/Hoop Reinforcement
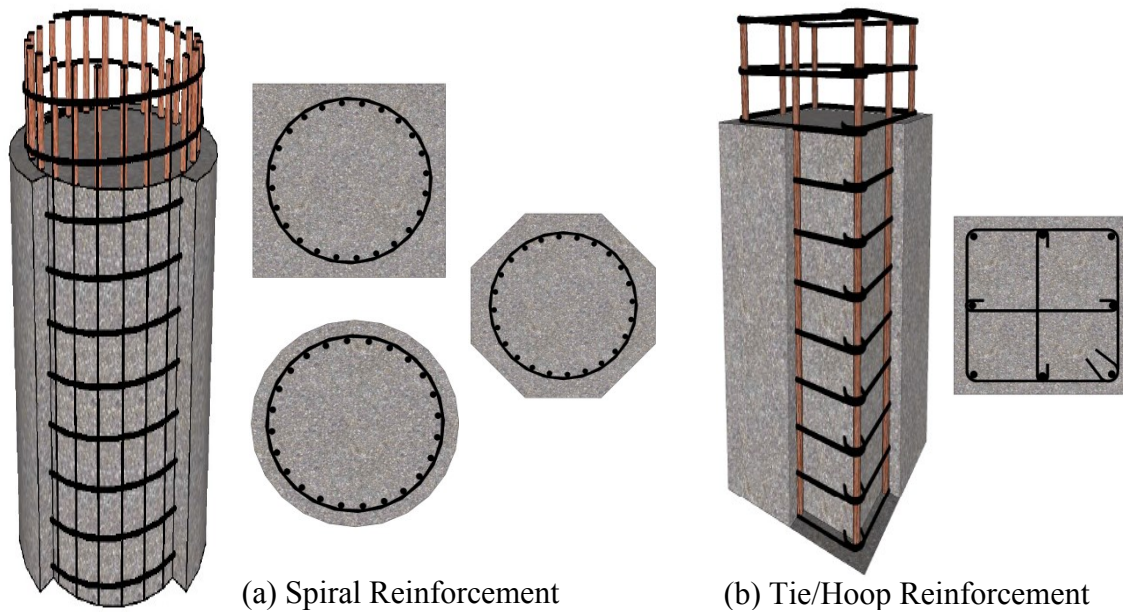
Figure 1-3: Examples of confinement in high seismic regions

Recent history and great earthquakes such as the Chilean earthquake of 2010 (Mw = 8.8) and the Tohoku Japan Earthquake of 2011 (Mw = 9.0) has shown that our current understanding of the transverse confinement reinforcement within a cross-section is still a work in progress, Figure 1-4. Examination of current guidelines, as part of a project for the California Department of Transportation (Caltrans), [Shelman and Sritharan 2013] has indicated that the different approaches for establishing adequate transverse reinforcement according to guidelines vary by as much as two to three times the smaller value with no consensus on the best available method. A sample of this variation is shown in Figure 1-5 through a comparison of methods by increasing only concrete compressive strength, f_c', and leaving the column diameter at 4 ft, the axial load ratio at 5%, longitudinal reinforcement ratio at 2% and a 3 in. cover with #5 bar horizontally.

Upper Left: Hanshin Expressway during the 1995 Kobe Earthquake

Lower Left: Nakasone Viaduct during the 2011 Great East Japan Eartquake (Kawashima et. al 2011)

Right: 1994 Northridge Earthquake (NOAA/NGDC 2013)
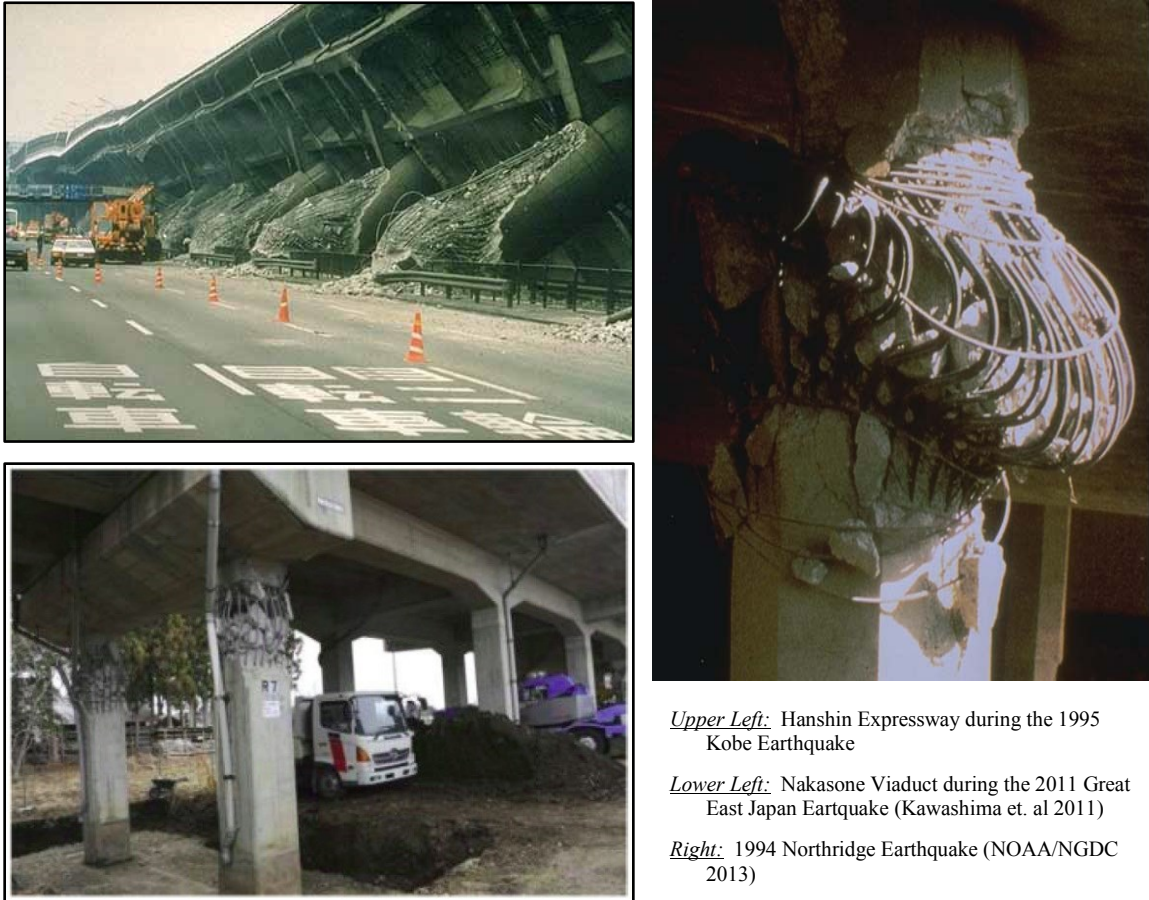
Figure 1-4: Confinement damage to reinforced concrete columns

Variation in the amount of transverse confinement reinforcement required for a design is also a function of the amount of longitudinal reinforcement, the applied axial load ratio, the ratio of the gross concrete area to the core concrete area, the expected demand and the material properties used in the cross-section. The material properties, however, are based on current understanding of the stress-strain behavior of confined and unconfined concrete (e.g., Mander et al. 1988 and Priestley et al. 1996). These approaches rely on the establishment of the ultimate concrete strain to determine the final capacity and ductility of the section. The definition of the strain is complicated by the fact that it must take into account additional

variables including: (1) amount of cross-section under compression; (2) the dual role of longitudinal reinforcement in the axial and transverse directions; (3) conservatism of an equation such as Eq. (1-1), and; (4) the size of the column tested for establishment.
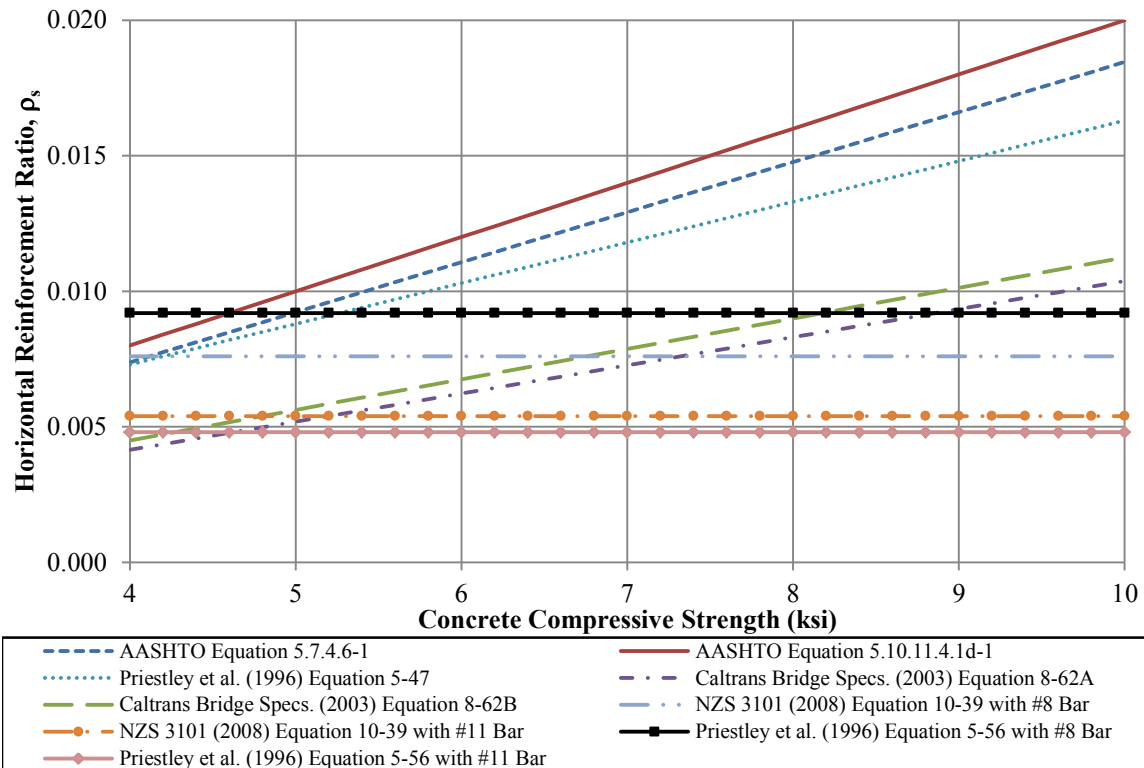
Figure 1-5: Impact of concrete compressive strength on horizontal reinforcement ratio

1.3.2 *Soil-Foundation-Structure-Interaction*

During the design process of integrated column-foundation systems, the effects of soil-foundation-structure-interaction (SFSI) complicate the lateral loading analysis and thus the design methodology. SFSI complicates the process for multiple reasons, but all hinges on one issue—how to correctly model the effects of the soil so that they can be accurately accounted for in structural design. Many researchers have examined ways of accounting for SFSI [e.g., Reese et al. (1975), Priestley et al. (1996), Budek et al. (2000), Chai (2002) and

Priestley et al. (2007)], but each method, whether complex or simple, has limitations. Some of the simplified methods, constructed to reduce computational time, assume that the system will behave in an elastic perfectly plastic manner while others remove soil altogether and treat the system as a fixed based cantilever. Although these methods provide results, the following concerns about their use were noted: (1) they were not necessarily calibrated to adequate experimental tests; (2) they tend to under predict the analytical plastic hinge length; (3) critical regions may not be identified accurately, and; (4) other limitations exist that are model dependent and not discussed herein.

A satisfactory approach throughout the years to capture these effects has been through the use of numerical analysis methods that model the soils using nonlinear springs, known as the Winkler foundation model (1867). These springs are assumed to support a beam and can thus be used to determine the force-displacement response of piles subjected to lateral loading in soil as well as the overall structural response. Other methods including full two-dimensional and three-dimensional finite element analyses have been shown to adequately capture the lateral loading response. In these complex and very detailed approaches, significant amounts of input information are generally required along with large amounts of computational time to complete the analyses.

Examples of some of these problems are found when using the model proposed by Chai (2002) in a cohesive soil medium although recommended by AASHTO (2010) to determine the lateral load behavior. The simplified model in this case assumes a uniform layer of soil and that the overall response of the system behaves in an elastic-perfectly plastic manner. In Shelman et al. (2010), comparisons were made between full-scale experimental testing, a

Winkler foundation model method and many simplified models used to account for SFSI in the design and analysis process of bridge columns. The results of one such analysis for Chai's simplified model (2002) is provided graphically in Figure 1-6, and the following limitations were found:

- The perfectly plastic response ignores the combined nonlinear behavior of reinforcing steel, concrete and soil between the yield and ultimate conditions.

- The maximum moment location was under predicted by 29.3%, thus altering the overall displacement of the system.

- The model established an analytical plastic hinge length using experimental testing in a cohesionless soil, but still recommended its use for cohesive soils. This resulted in an under prediction of the plastic rotation and plastic displacement by about 30% when compared with the Winkler Foundation model that adequately captures the lateral load response.
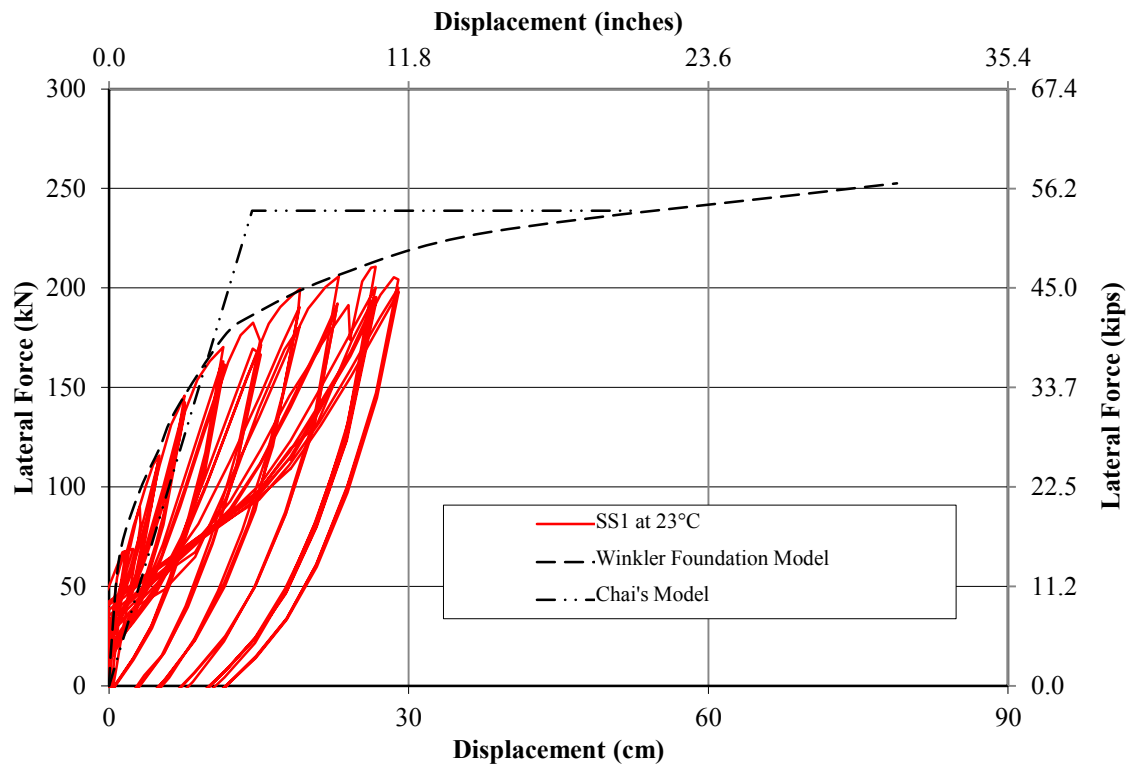
Figure 1-6: Comparison of experimental field data with analytical models used in design

In addition to the need for an appropriate simplified model for design purposes, the understanding of soil properties involved in SFSI, especially those near the ground surface, must be adequately addressed. Soil located near the ground surface typically has the greatest influence on the response of the system, as this is where the soil generally provides the largest amount of resistance to lateral movement but has the largest amount of variability because of weathering properties. Furthermore, soil stiffness along the foundation depth dictates the global and local displacements of the system, the local curvature demand and much more. Thus, all possible conditions and the resulting soil properties must be defined to ensure the best possible design to prevent failure.

1.3.3   *Temperature*

The effects of soil-foundation-structure-interaction are commonly taken into account during seasons of warm weather conditions. This is the case as the soil typically behaves in a more ductile manner which allows more displacement to occur in the overall structural system. Although the larger displacement must be accounted for so the appropriate seating length, column ductility and other seismic factors are accounted for, the effects of seasonal freezing must also be handled. This is currently a major deficiency in the field of earthquake engineering, as some of the largest earthquakes (e.g., 1811-1812 New Madrid Series and the 1964 Great Alaska earthquake) actually occurred in regions of the United States during winter months where ground freezing may take place. An exploratory research program by Sritharan et al. (2007) found that brittle failure of bridge columns may take place unless the effects of seasonal freezing are accounted for in seismic design. The effects of cold temperature are further exacerbated by the unknown effects caused to the moment-curvature response of a critical member section. The significance of these two issues are made more critical as they are in direct violation of the capacity design principles where a   designer should allow flexural yielding while preventing an undesirable failure mode. In the exploratory research that examined the performance of continuous columns supported on drilled shaft foundations, Suleiman et al. (2006) drew the following conclusions regarding the lateral load response of a full-scale test in wintry conditions with respect to the response of an identical system in warm conditions:

- effective elastic stiffness increased by 170%,

- lateral load resistance increased by 44%,

- maximum moment location shifted upwards by 0.84 m (33 in.),

- plastic region length reduced by 64% in the foundation shaft, and

- gap opening at the base of the column reduced by 60%.

Results for the cyclic responses of the two column-shaft systems are presented in Figure 1-7. These results demonstrate the drastic difference between seasonal wintry conditions and summer conditions where one can see a significant difference in the lateral force at a comparable displacement between the two experiments. Due to the large variation in the lateral response of the system, any new development in the seismic design process of an integrated column-foundation shaft should give consideration to this issue.

(a) SS1 at 23 °C   (b) SS2 at -10 °C
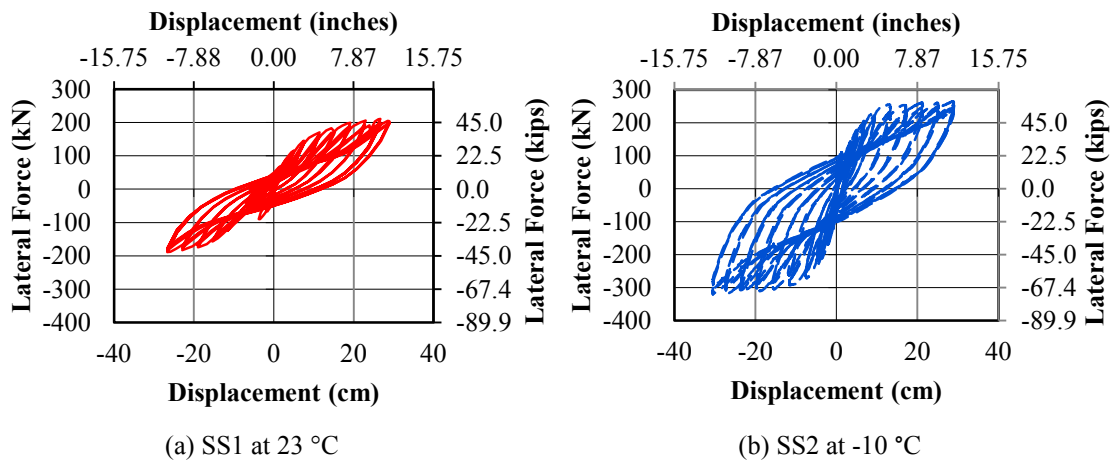
Figure 1-7: Cyclic load testing results (Suleiman et al., 2006)

Further analytical studies by Wotherspoon et al. (2010a & b) validated the studies performed by Sritharan et al. (2007) by reconstructing the model in a separate computer program, Figure 1-8. Besides comparison with the test models at Iowa State University, the authors examined seismic ground motions with periods between 25-years and 2500-years.

During this investigation it was found that: (a) the peak shear demand for the 2500-year return period was 56% of the section capacity in summer and 76% of the capacity in the winter; (b) 29% of the displacement capacity was reached in the summer compared to 62% of the displacement capacity in the wintry conditions for the 500-year return period; and (c) more cycles of high strain deformation occur in wintry times possibly resulting in low-cycle fatigue.

The broad impact of seasonal freezing and seismic conditions on bridge structures throughout the United States and Japan was investigated by Sritharan and Shelman (2008). This study showed that seismic response of approximately 50% of the 66,000 bridges in active seismic regions would be affected by seasonal freezing. Furthermore, when applying a minimum frost depth condition of 10 cm (4 in.), over 400,000 bridges or two-thirds of all bridges in the U.S. were found to be affected by seasonally frozen conditions, yet this issue is seldom addressed in routine design methods. The study was extended to the nation of Japan where the authors concluded that the northern part of Honshu Island and Hokkaido Island could experience similar conditions based on available historical earthquake and meteorological data.
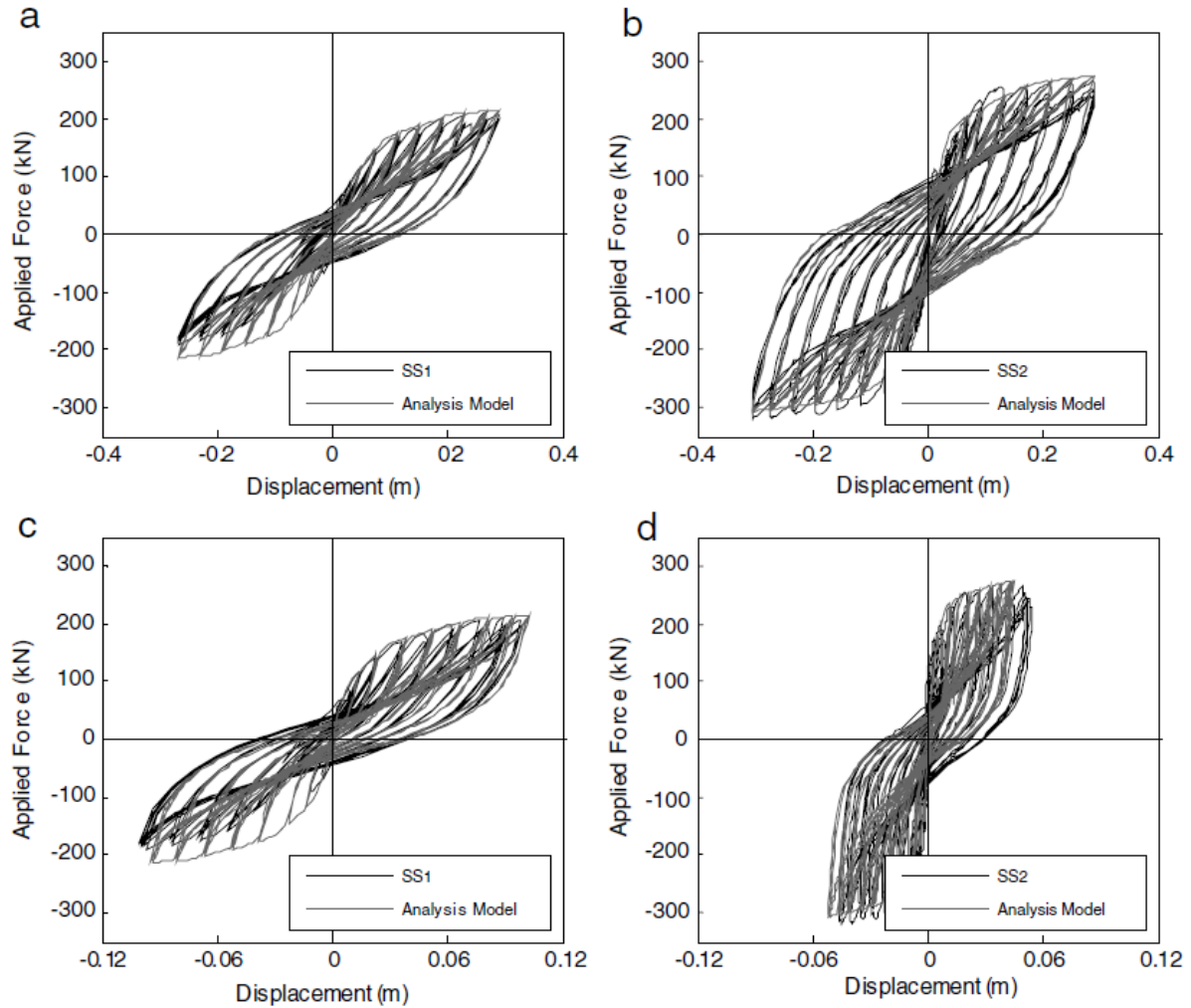
Figure 1-8: Cyclic force-displacement responses for (a) SS1 column top; (b) SS2 column top; (c) SS1 column base; (d) SS2 column base.

1.4 Research Objectives

Based on the limitations associated with the current design approaches and models used in practice, the research presented within this document looks to advance the current state of practice for the seismic design of reinforced concrete bridge columns. This will be accomplished through a proactive approach using both experimental and analytical means to further identify limitations and make recommendations for the improvement as it relates to the seismic design of reinforced concrete columns. The tasks completed within these studies

will validate and improve current models for both SFSI and confinement reinforcement while accounting for the influence of seasonal freezing.

1.4.1 Experimental Investigation

To better understand the behavior of materials and their impact on the seismic design of reinforced concrete bridge columns, a series of controlled material tests were performed at warm temperatures and cold temperatures expected to occur in regions of seasonal freezing throughout the United States and the world. This temperature range was between 20°C (68°F) and -30°C (-22°F) as this is common in high seismic regions including but not limited to Alaska, the central United States, northern California, China, and Japan. This is an important aspect to understand as approximately 50% of the bridges in high seismic regions can be affected by freezing temperatures (Sritharan and Shelman 2008). The main materials examined experimentally in this study are unconfined concrete, confined concrete and soil. Reinforcing steel was not examined in this document as it was investigated in a concurrent study at Iowa State University by Levings and Sritharan (2012).

Concrete, both confined and unconfined, must be examined at different temperatures to determine whether or not the current model commonly used in practice (i.e., Mander et al. 1988a & b) is still valid for the establishment of an adequate stress-strain curve for modeling purposes, Figure 1-9. Confined concrete testing at seasonally frozen temperatures was especially important as little to no information exists on the behavior of confined concrete at freezing temperatures although these temperatures can be seen in high seismic regions such as Alaska, California and the northern part of Japan. The concrete material testing was an exploratory study to examine the effects of temperature while considering multiple horizontal

reinforcement ratios, concrete compressive strengths and any possible effects of sample size that might arise. These tests will allow the establishment of the compressive behavior, ultimate strength, elastic modulus and critical points for strain on the stress-strain curve.

Soil testing at seasonally frozen temperatures is another important aspect in the behavior of reinforced concrete bridge columns as every system is supported on some sort of foundation that will be influenced by the response of the soil. Furthermore, bridge columns that extend into the ground as drilled-shaft foundations, which are fully surrounded by soil, are becoming more common due to the simplicity of construction, lack of a column-foundation connection and reduced construction costs. Therefore, this research examines the impact of seasonal freezing on the behavior of soil that is common near bridge structures. The study was an exploratory investigation into multiple soil types to examine the variation in soil stress-strain curves by identifying changes in critical parameters (e.g., unconfined compressive strength and modulus of elasticity) and the impact on the lateral loading of columns supported by a cast-in-drilled-hole (CIDH) shaft. The study investigated the influence of moisture content and unit weight at frozen temperatures to determine how they compare to the current understanding of warm weather behavior. The emphasis of the testing program was towards a cohesive soil as there is a significant amount of research on permafrost, sands and silts. The sandy and silty material was included in the study as most of the research has focused on the long term creep behavior of soils at frozen temperatures which is not ideal for a rapid loading situation commonly experienced in a seismic event.

Terminology:

f_c' = peak unconfined compressive stress;

E_c = concrete modulus of elasticity;

ε_{co} = strain at peak unconfined concrete stress;

ε_{co} = peak unconfined compressive strain;

f' = peak confined compressive stress;
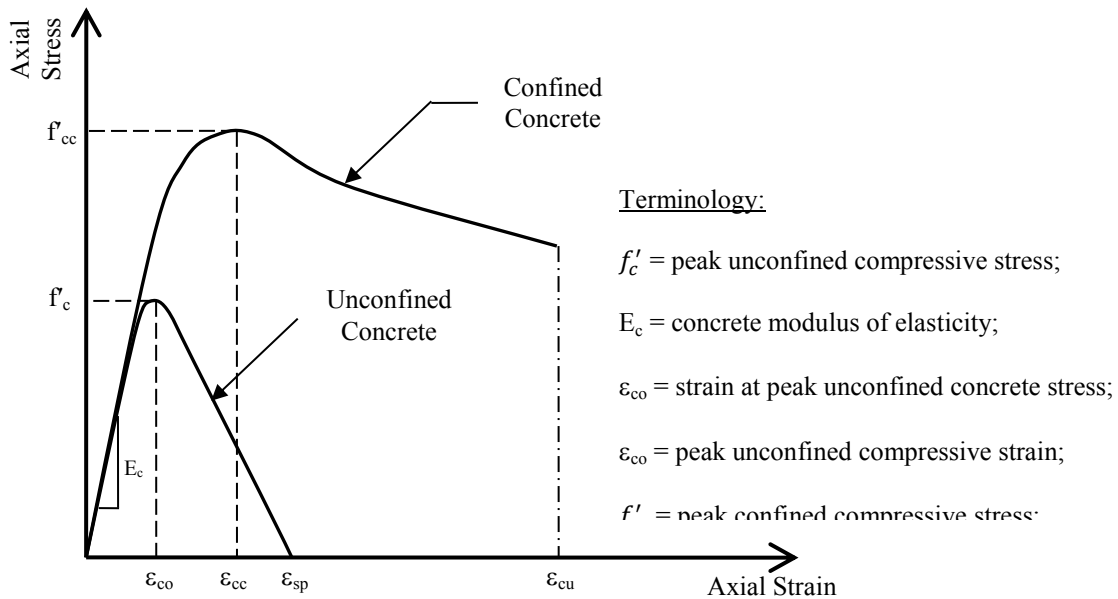
Figure 1-9: Idealized stress-strain behavior of confined and unconfined concrete subjected to an axial loading

1.4.2 *Analytical Investigation*

The analytical portion of the research presented within this document will take an in-depth look at the current models used in practice today to account for SFSI and the behavior of current confinement equations in reinforced concrete bridge columns. This will be completed through extensive literature reviews and computer modeling using open source software and packages used in industry. Each study provides recommendations as to the advancement of the seismic design of reinforced concrete bridge columns whether supported on CIDH shafts or another type of foundation system.

The first major topic investigated in this document shall be the influence of SFSI on bridge columns supported on CIDH shafts. Due to the systems being used on a more regular basis in practice, it is important to understand the behavior of both the column and foundation shaft when subjected to lateral loads under all conditions. To better understand

the behavior, a series of detailed computer based pushover analysis were performed and the results analyzed to compare with current simplified approaches for cohesionless soils. In addition, a new simplified approach was constructed to consist of a cantilever column supported by a flexible foundation. The flexible foundation method allows the system to be modeled in a computer based analysis program without having to include a significant amount of additional elements to handle the flexibility and resistance of the soil. This is a companion model to a similar approach developed for cohesive soils in Shelman (2009).

The remainder of the analytical work consists of a detailed investigation into the improvement of the confinement equations used for horizontal reinforcement in critical regions of reinforced concrete bridge columns. This includes a series of finite element analyses to establish moment-curvature, pushover and dynamic responses of multiple column heights and diameters with differing reinforcement ratios both horizontally and longitudinally. The dynamic responses examine the impact of real demands from significant earthquakes within the field of seismic engineering and how the current models for confinement perform under these loads. Using the results gained from these analyses a new confinement equation will be developed that takes into account the demands expected to be seen under real earthquake loads. The new approach will then be analyzed in a similar manner and shown to be a better option for the establishment of horizontal reinforcement in a reinforced concrete bridge column.

1.5 Chapter Layout

The information presented within this document will be provided in the form of articles written for submission to peer reviewed journals or conferences in the field of structural,

geotechnical and materials engineering. Following the introductory chapter, Chapter 2 presents the current state of the art in the field of seismic design for reinforced concrete bridge columns and the impacts of soil-foundation-structure-interaction. Chapter 3, a companion paper to one provided in the appendix, examines the effects of soil-foundation-structure-interaction and provides a new simplified model with the inclusion of seasonal freezing concerns for a cohesionless soil. Chapter 4 provides a paper that characterizes the behavior of seasonally frozen soils for the seismic design of foundations. Chapter 5 examines the impact of freezing temperatures on the material behavior of confined and unconfined concrete. Chapter 6 provides a conference style paper that presents research as to the impact on the seismic design of bridge columns using current equations in the appropriate guidelines for the establishment of adequate transverse confinement. The final chapter of this document will provide a summary of all the research presented throughout and any final recommendations.

1.6 References

American Association of State and Highway Transportation Officials (AASHTO) (2010). *Guide Specifications for LRFD Seismic Bridge Design 1st Edition with 2010 Interim Revisions.* Washington, D.C.: AASHTO.

AASHTO. (2012). LRFD *Bridge Design Specifications, customary U.S. units 6th Edition.* Washington, D.C.: AASHTO.

Applied Technology Council (ATC). (1996). *Improved Seismic Design Criteria for California Bridges: Provisional Recommendations.* Redwood City, CA: Applied Technology Council.

Budek, A. M., Priestley, M. J. N. and Benzoni, G. (2000). "Inelastic seismic response of bridge drilled-shaft rc pile/columns." *Journal of structural engineering* 126(4): 510-517.

Caltrans. (2010). Seismic *Design Criteria Version 1.6.* Sacramento, CA: Caltrans.

Canterbury Earthquake Recovery Authority (CERA). (2012). Demolition Lists. Retrieved on 28th August 2012. Available from: www.cera.govt.nz/demolitions/list

Chai, Y. H. (2002). "Flexural strength and ductility of extended pile-shafts I: Analytical model." *Journal of structural engineering* 128(5): 586-594.

Chai, Y. H. and Hutchinson, T. C. (2002). "Flexural strength and ductility of extended pile-shafts II: Experimental study." *Journal of structural engineering* 128(5): 595-602.

Earthquake Engineering Research Institute (EERI). (Accessed Online: August 2012). "Observations on building damage from Francisco Medina." *Chile earthquake clearinghouse.* Accessed at: http://www.eqclearinghouse.org/20100227-chile/

Earthquake Engineering Research Institute (EERI). (Accessed Online: September 2012). "Learning from Japan's ordeal." *Tohoku earthquake and tsunami clearinghouse.* Accessed at: http://www.eqclearinghouse.org/2011-03-11-sendai/

EERI and Pacific Earthquake Engineering Research (PEER) Center investigative team. (Accessed Online: September 2012). "Learning from Earthquakes, The M 6.3 Christchurch, New Zealand, Earthquake of February 22, 2011." *EERI Special Earthquake Report – May 2011.* Accessed Online at: https://www.eeri.org/products-publications/eeri-newsletter/

FEMA-273. (1997). *National* Earthquakes *Hazard Reduction Program (NEHRP) Guidelines for the Seismic Rehabilitation of Buildings (ATC-33 project).* Washington, D.C.: FEMA.

FEMA-274. (1997). *NEHRP* Commentary *on the Guidelines for the Seismic Rehabilitation of Buildings (ATC-33 project).* Washington, D.C.: FEMA.

Kawashima, K., Kosa, K., Takahashi, Y., Akiyama, M., Nishioka, T., Watanabe, G. Koga, H. and Matsuzaki, H. (2011). "Damage of Bridges during 2011 Great East Japan Earthquake." *Proceeding of 43rd Joint Meeting, US-Japan Panel on Wind and Seismic Effects*. Tsukuba, Japan: UJNR.

Leet, K. M., Uang, C. and Gilbert, A. M. (2011). *Fundamentals of Structural Analysis 4th Edition.* New York, NY: McGraw-Hill Companies, Inc.

Levings, J. and Sritharan, S. (2012). "Effects of cold temperature and strain rate on the stress-strain behavior of ASTM A706/A706M mild steel reinforcement." *Journal of materials in civil engineering (In publication)*

Mander, J. B., Priestley, M. J. N. and Park, R. (1988a). "Theoretical stress-strain model for confined concrete." *Journal of structural engineering* 114(8): 1804-1826.

Mander, J. B., Priestley, M. J. N. and Park, R. (1988b). "Observed stress-strain behavior of confined concrete." *Journal of structural engineering* 114(8): 1827-1849.

National Oceanic and Atmospheric Administration (NOAA) / National Geophysical Data Center (NGDC). (Accessed Online: May 2013). "Failed Bridge Support Picture by M. Celebi, U.S. Geological Survey." Accessed as part of the image database at: http://ngdc.noaa.gov/hazardimages/picture/show/459

Palermo, Alessandro; Wotherspoon, Liam; Wood, John; Chapman, Howard; Scott, Allan; Hogan, Lucas; Kivell, Anton; Camnasio, Elena; Yashinsky, Mark; Bruneau, Michel and Chouw, Nawawi. (2011). "Lessons learnt from 2011 Christchurch Earthquakes: analysis and assessment of bridges." *Bulletin of the New Zealand Society for earthquake engineering* 44(4): 319-333

PEER/EERI/GEER/Tsunami Field Investigation Team. (Accessed Online: September 2012). "Quick observations from the PEER/EERI/GEER/Tsunami Field Investigation Team." *Pacific Earthquake Engineering Website (News)*. Accessed at: http://peer.berkeley.edu/news/wp-content/uploads/2011/04/Tohoku-short-interim-report.pdf

Priestley, M. J. N., Seible, F. and Calvi, G. M. (1996). *Seismic Design and Retrofit of Bridges*. New York: John Wiley & Sons, Inc.

Priestley, M. J. N. (2000). "Performance-Based Seismic Design". *Proceedings of the 12th World Conference on Earthquake Engineering*. Auckland, New Zealand.

Priestley, M. J. N., Calvi, G. M. and Kowalsky, M. J. (2007). *Displacement-Based Seismic Design of Structures*. Pavia, Italy: IUSS Press.

Reese, L. C. and Welch, R. C. (1975). "Lateral loading of deep foundations in stiff clay." *Journal of geotechnical engineering division* 101(GT7): 633-649.

Shelman, A. (2009). *Seismic Design of Drilled Shafts in Clay.* Master's Thesis. Iowa State University.

Shelman, A., Levings, J. and Sritharan, S. (2010). *Seismic Design of Deep Bridge Pier Foundations in Seasonally Frozen Ground.* Final Report Prepared for the Alaska University Transportation Center and Alaska Department of Transportation and Public Facilities.

Shelman, A. and Sritharan, S. (2013: Under Review). *A Critical Review of Column Confinement Reinforcement used in Current Seismic Bridge Design Practice.* Final Report Prepared for the California Department of Transportation.

Sritharan, S., Priestley, M. J. N. and Seible, F. (1997). *Seismic Design and Performance of Concrete Multi-Column Bents for Bridges.* Report #SSRP-97/03. University of California San Diego, CA: Department of Structural Engineering.

Sritharan, S., Suleiman, M. T. and White, D. J. (2007). "Effects of seasonal freezing on bridge column-foundation-soil interaction and their implications." *Earthquake spectra* 23(1): 199-222.

Sritharan, S. and Shelman, A. (2008). "An assessment of broad impact of seasonally frozen soil on seismic response of bridges in the U.S. and Japan." *Proceedings of the 24th US-Japan bridge engineering workshop, Minneapolis.* FHWA: 429-440.

Standards New Zealand. (2008). *Concrete Structures Standard: Part 1 – The Design of Concrete Structures (NZS 3101: 2008).* Wellington, New Zealand: Standards New Zealand.

Stronger Christchurch Infrastructure Rebuild Team (SCIRT). (Accessed Online: August 2012). "Extent of road network damage" Accessed at: http://strongerchristchurch.govt.nz/work/roads/extent

Suleiman, M. T., Sritharan, S. and White, D. J. (2006). "Cyclic lateral load response of bridge column-foundation-soil systems in freezing conditions." *Journal of structural engineering* 132(11): 1745-1754.

Winkler, E. (1867). *Die Lehre von der Elastizitat und Festigkeit.* Prague, Czechoslovakia: Verlag H. Dominikus.

Wotherspoon, L. M., Sritharan, S. and Pender, M. J. (2010a). "Modeling the response of cyclically loaded bridge columns embedded in warm and seasonally frozen soils." *Engineering structures journal* 32:933-943.

Wotherspoon, L. M., Sritharan, S., Pender, M. J. and Carr, A. J. (2010b). "Investigation on the impact of seasonally frozen soil on the seismic response of bridge columns." *Journal of bridge engineering* 15(5):473-481.

CHAPTER 2: EXAMINATION OF THE CURRENT STATE OF THE ART

An adequate ductile design of bridge columns in high seismic regions requires a thorough understanding of the components involved within the entire structural system. For a reinforced concrete bridge column this starts with the definition of material properties within the cross-section of the bridge column. This includes the stress-strain behavior of the concrete within the cross-section, which includes both unconfined and confined concrete. This process relies on the use of theoretical models such as Mander et al. (1988) that were developed specifically for this purpose. The definition of the confined concrete properties, however, is further complicated as it relies on the amount of transverse confinement reinforcement surrounding the core region of the cross-section, which is essential for ensuring a ductile bridge response. Specifically, by providing spiral or hoop reinforcement, the concrete used in bridge columns is made possible to respond plastically, which allows the sudden and violent ground movement to be handled by limiting the seismic force imparted to the structure, enabling the structure to deform without significant degradation or collapse. Various design authorities specify how much of this transverse reinforcement is needed based on the size of the column by either a ratio of the volume of horizontal steel to volume of concrete, ρ_s, or by requiring the closed loop hoop steel to have a certain area (A_{sh}) and spacing, s, within a given length along the concrete member.

In addition to the concrete material properties, the materials surrounding the foundation must be adequately addressed. This is the case as the seismic ground motions enter the

structural system through this media. Furthermore, the soil surrounding the foundation introduces additional flexibility and resistance to the overall system. This additional flexibility and resistance influence the overall lateral response. In columns continuously supported on drilled shaft foundations, the soil surrounding the foundation shaft significantly alters the lateral load response of the system as the resistance to movement is dictated by the stiffness of the surrounding soil. The effects of seasonal freezing only further complicate the overall process as material properties are altered with the change in temperature.

The material property definition within the design allows for the local response of the system to be attained. This information can then be used to extrapolate the global lateral force-displacement response of the structural system to ensure the desired performance. Extrapolation out to the global response can be performed using methodologies from a very detailed and complex finite element analysis to simple methodologies that use a minimal number of inputs. This chapter investigates the available literature on the requirements for the definition of transverse confinement reinforcement, the definition of material properties with the inclusion of freezing temperatures and the design of columns continuously supported on drilled shaft foundations with the inclusion of soil-foundation-structure-interaction (SFSI).

2.1 Transverse Volumetric Ratio for Circular Columns

The wide discrepancy between the design and performance of reinforced concrete bridge columns in high seismic regions can be noted through the examination of design standards and guidelines published by the different authorities in the United States and world. Thus, a comparison was made between various state departments of transportation, national and

worldwide standards, research outcomes and guidelines for the design of concrete

confinement reinforcement. The list below defines the resources used for establishing the

comparison information for the seismic design in plastic hinge regions for transverse

reinforcement. The Alaska, Missouri and North Carolina Department of Transportations

were listed on the list first as these locations have seismic requirements within their design

guidelines in addition to federal requirements set forth by the Federal Highway

Administration (FHWA), but the standards do not necessarily fit into a specific chronological

order similar to the rest of the list. The guidelines list was extended to include the American

Concrete Institute's – *Building Code Requirements for Structural Concrete (ACI 318-08) and*

Commentary (ACI 318R-08) and the Standards New Zealand – *Design of Concrete Structures*

(NZS 3101) as these two references adopt a similar philosophy to seismic design as those of

the bridge design guidelines. Furthermore, the New Zealand Transport Agency (formerly

Transit New Zealand) states that the reinforced concrete design of bridges shall be performed

in accordance with NZS 3101 (Transit New Zealand 2005).

- Alaska Department of Transportation and Public Facilities (Alaska DOT&PF),
  Missouri Department of Transportation (MODOT) and North Carolina Department of
  Transportation (NCDOT);

- Watson, S.; Zahn, F. A.; and Park, R., (1994);

- Standards New Zealand – *Design of Concrete Structures (NZS 3101: 1995);*

- Applied Technology Council (ATC) – *Improved Seismic Design Criteria for*
  California Bridges: Provisional Recommendations (ATC-32) (1996);

- Caltrans - Bridge *Design Specifications Manual* (2003);

- South Carolina Department of Transportation - *Seismic Design Specifications for Highway Bridges Version 2.0* (2008);

- American Concrete Institute (ACI) – *Building Code Requirements for Structural Concrete (ACI 318-08) and Commentary (ACI 318R-08);*

- Standards New Zealand – *Design of Concrete Structures (NZS 3101: 2008);*

- AASHTO - Guide *Specifications for LRFD Seismic Bridge Design 1st Edition with 2010 interim revisions* (2010);

- Caltrans - Seismic Design *Criteria Version 1.6* (2010); and

- AASHTO – *LRFD* Bridge *Design Specifications* (2012).

2.1.1   Bridge Manual of Transit New Zealand

In the 1994 issue of the *Bridge Manual* of *Transit New Zealand* a set of equations were provided to quantify the appropriate amount of transverse reinforcement for concrete confinement. The equation provided in the 1994 edition of the standards is provided herein as Eq. (2-1) and is based on the required curvature ductility, axial load ratio, strength reduction factor and ratio of gross concrete area to core concrete area. Terms such as the curvature ductility and strength reduction factor are taking into account the local section design and resistance factors common in load and resistance factored design (LRFD). The presence of the curvature ductility requirement highlights the importance of considering demand within the establishment of the horizontal confinement reinforcement. The requirements specified for the design in this particular methodology is based on a displacement ductility of six at the ultimate limit state which results in the curvature ductility design being a value of 10 for potential plastic hinge regions above the bottom story. For the

bottom story, a curvature ductility of 20 is required. It is important to note that the

information input into this equation should be in megapascals and millimeters during

computations.

$$\rho_s = \frac{\left(\frac{\phi_u}{\phi_y} - 33 p_t m + 22\right)}{79} \frac{A_g}{A_c} \frac{f_c'}{f_{yt}} \frac{N^*}{\varphi f_c' A_g} - 0.0084 \qquad \text{Eq. (2-1)}$$

where: s = center to center spacing of transverse reinforcement;

   h″ = dimension of core of column at right angles to direction of transverse

     bars under consideration;

   A_g = gross area of column;

   A_c = core area of column;

   $\frac{\phi_u}{\phi_y}$ = curvature ductility factor required;

   ϕ_u = ultimate curvature;

   ϕ_y = curvature at first yield;

   p_t = A_{st}/A_g;

   A_{st} = total area of longitudinal column reinforcement;

   m = $f_y/(0.85 f_c')$;

   f_y = lower characteristic yield strength of longitudinal steel;

   f_{yt} = lower characteristic yield strength of transverse steel;

   N^* = axial compressive load on column; and

   φ = strength reduction factor = 0.85 for columns not protected by capacity

     design.

2.1.2 *Watson et al. (1994)*

These three researchers published a slightly different equation than the New Zealand equation in Section 2.1.1. The two equations differ by the value stated for use as the constant. In Watson et al. (1994) a value of 0.008 is published for use compared to the stated value of 0.0084 in the *Bridge Manual of Transit New Zealand* (1994). Although a slight difference is noted, there was no justification provided as to why there was a difference. Additionally, for low axial load ratios (ALR), $N/(f_c'A_g)$, in compression, the equation typically results in a negative number for the amount of confinement reinforcement within a cross-section. The same problem would occur for ALR that are in tension. Although this was the case, the researchers indicated that the current code provided a minimum amount of reinforcement that was deemed adequate at small ALR ratios. When positive volumetric ratios are obtained, the values are essentially identical to those specified in the Eq. (2-1) and thus the equation was not reproduced here. The researchers further indicated that when a more detailed ductility calculation is not needed a curvature ductility of 20 was sufficient for a ductile design, and a curvature ductility of 10 was sufficient for a limited ductile design.

2.1.3 *ATC-32 (1996)*

The Applied Technology Council (ATC) did a study to improve the seismic behavior of California bridges. In their final recommendations, they provided an equation, Eq. (2-2), to find the horizontal volumetric reinforcement ratio for spirally reinforced columns inside and outside the plastic hinge region.

$$\rho_s = 0.16 \frac{f_{ce}'}{f_{ye}} \left[0.5 + \frac{1.25P}{f_{ce}'A_g} \right] + 0.13[\rho_l - 0.01] \qquad \text{Eq. (2-2)}$$

where: f'_{ce} = expected concrete strength;

f_{ye} = expected yield strength of the reinforcement;

P = column axial load;

A_g = gross column area; and

ρ_l = longitudinal reinforcement ratio.

This equation utilizes the geometric properties and material properties, but was expanded to take into account the effects of the column axial load and the longitudinal reinforcement ratio. The inclusion of these additional parameters, make this approach the most detailed recommendation proposed in the United States. Although the detailed approach is defined by ATC, an additional requirement within the plastic end regions of ductile columns is specified. This requirement states that the volumetric ratio shall not be less than the value obtained from the previous equation, nor less than, Eq. (2-3), which is an anti-buckling requirement for the longitudinal bars and is not specifically for confinement alone.

$$\rho_s = 0.0002 n_b \qquad \text{Eq. (2-3)}$$

where: n_b = the number of longitudinal bars contained by the spiral or circular hoop

A second equation that accounts for the issue of anti-buckling within this text relates to the spacing needed between the spiral loops. This particular equation, Eq. (2-4), accounts for steel reinforcement that has an ultimate strength to yield strength ratio of less than 50%.

$$s \le \left[3 + 6\left(\frac{f_u}{f_y} - 1\right)\right] d_{bl} \qquad \text{Eq. (2-4)}$$

where: f_u = ultimate strength of the reinforcement;

f_y = yield strength of the reinforcement; and

d_{bl} = diameter of longitudinal reinforcement.

2.1.4   Alaska DOT&PF, MODOT and NCDOT

In the states of Alaska, Missouri and North Carolina, regions of high seismicity are present based on the past history of earthquakes and proximity to nearby known faults (USGS 2012). Although these sections of the United States are at risk for high ground motions, they do not maintain a specific set of standards or guidelines for use in the seismic design of bridges and structures (MODOT 2012, NCDOT 2012). Instead, they generally refer to the overall governing standards for the United States, typically considered to be the *AASHTO LRFD Bridge Design Specifications* (2012) and *AASHTO Guide Specifications for LRFD Seismic Bridge Design* (2010). For these specific states, it is important to note that this means the information presented in Sections 2.1.9 and 2.1.11 are the values for which confinement reinforcement must be met.

2.1.5   Caltrans Bridge Design Specifications Manual (2003)

Prior to the Seismic Design Criteria (SDC) used in practice today, Caltrans had a bridge design manual that provided specific requirements about the design of columns for all conditions. This set of specifications state that ties are permitted only where it is not practical to use spiral or circular hoop reinforcement. Additionally, the 2003 manual by Caltrans provided three equations to specify a volumetric ratio for the transverse reinforcement. The first and second equations, Eq. (2-5) and Eq. (2-6), are very similar to ACI and AASHTO approaches, but take into consideration the impact of the column axial

load as was the case in the ATC-32 specifications. Eq. (2-5) applies only when the column diameter is less than 3 ft (900 mm) in the plastic hinge region. Eq. (2-6) applies when the column diameter is greater than the limits applied to Eq. (2-5).

$$\rho_s = 0.45 \left(\frac{A_g}{A_c} - 1 \right) \frac{f_c'}{f_{yh}} \left(0.5 + 1.25 \frac{P_e}{f_c' A_g} \right)$$
<div align="right">Eq. (2-5)</div>

where: f_c' = specified compressive strength of concrete;

f_{yh} = specified yield strength of transverse reinforcement not to exceed 100,000 psi;

A_g = gross area of a concrete section;

A_c = cross-sectional area of a structural member measured to the outside edges of transverse reinforcement; and

P_e = column axial load.

$$\rho_s = 0.12 \frac{f_c'}{f_{yh}} \left(0.5 + 1.25 \frac{P_e}{f_c' A_g} \right)$$
<div align="right">Eq. (2-6)</div>

where: f_c' = specified compressive strength of concrete;

f_{yh} = specified yield strength of transverse reinforcement not to exceed 100,000 psi;

A_g = gross area of a concrete section; and

P_e = column axial load.

The third equation presented within this document, Eq. (2-7), appears throughout many of the references from the United States. This particular equation was recommended by many organizations as the intention is to ensure that the core of the column can sustain the

axial load after the exterior cover concrete has spalled off of the section (ACI 2008). The

third equation was also intended to be a minimum amount of steel required within the plastic

zone as this was the amount of steel needed to be provided outside the ductile region.

$$\rho_s = 0.45 \left(\frac{A_g}{A_{ch}} - 1 \right) \frac{f_c^{'}}{f_{yt}}$$
Eq. (2-7)

where: $f_c^{'}$ = specified compressive strength of concrete;

f_{yt} = specified yield strength of transverse reinforcement not to exceed

100,000 psi;

A_g = gross area of a concrete section; and

A_{ch} = cross-sectional area of a structural member measured to the outside

edges of transverse reinforcement.

2.1.6 *South Carolina DOT Seismic Design Specifications (2008)*

The South Carolina Department of Transportation (SCDOT) provides a set of design

specifications that must be followed for highway bridge design when subjected to seismic

conditions (SCDOT 2008). The specifications state that spiral reinforcement is not allowed

in a ductile design within the plastic hinge region of cast-in-place concrete, but rather the use

of butt-welded hoops is required. Additionally, the design specifications state that the

transverse reinforcement shall be sufficient to ensure adequate shear capacity and

confinement with the inclusion that the quantity of reinforcement meets the requirements of

Eq. (2-8). This equation, however, commonly appears as horizontal reinforcement

requirements within joint regions between columns and beams (AASHTO 2010). Due to this

being used as a joint requirement, the suggested equation was not included within later comparisons.

$$\rho_s \geq \frac{0.4A_{st}}{l_{ac}^2}$$
<div align="right">Eq. (2-8)</div>

where: ρ_s = volumetric ratio of transverse reinforcement;

      A_{st} = total area of longitudinal reinforcement in the column/shaft; and

      l_{ac} = anchorage length for longitudinal column reinforcement.

Besides the plastic hinge region, the SCDOT (2008) states that the transverse reinforcement outside of the plastic hinge region shall not be placed more than twice the spacing of the reinforcement in the plastic hinge region. Other information about the maximum spacing of transverse reinforcement meets the same requirements typically provided in AASHTO (2012) with those being the minimum of the following:

- Six inches inside the plastic hinge region;

- One-fifth the least dimension of the cross-section in columns or one-half the least cross-sectional dimension of piers;

- Six times the nominal diameter of the longitudinal reinforcement; and

- 12 inches outside the plastic hinge region.

2.1.7 *ACI 318-08*

The American Concrete Institute (ACI) *Building Code Requirements for Structural Concrete and Commentary* (ACI 2008) typically governs the concrete design of buildings and other structures. Although this is important to note, it is an appropriate source to

examine for the requirements of transverse reinforcement as it still deals with the design of columns subjected to lateral loading. In this set of requirements, two equations are provided to meet for the design of transverse reinforcement. The first one, Eq. (2-9), comes from Chapter 21 of *ACI 318-08* and states that the volumetric ratio of spiral or circular hoop reinforcement, ρ_s, shall not be less than this value. The commentary of this guideline states that the value was specified to ensure adequate flexural curvature capacity in yielding regions (ACI 2008).

$$\rho_s = 0.12 \frac{f_c'}{f_{yt}} \qquad \text{Eq. (2-9)}$$

where: f_c' = specified compressive strength of concrete; and

f_{yt} = specified yield strength of transverse reinforcement not to exceed 100,000 psi.

The second equation, Eq. (2-10), previously stated in Section 2.1.5 of this report comes from Chapter 10 of *ACI 318-08* and specifies that the volumetric ratio shall not be less than this value, which ensures sufficient capacity after spalling of the cover concrete.

$$\rho_s = 0.45 \left(\frac{A_g}{A_{ch}} - 1 \right) \frac{f_c'}{f_{yt}} \qquad \text{Eq. (2-10)}$$

where: f_c' = specified compressive strength of concrete;

f_{yt} = specified yield strength of transverse reinforcement not to exceed 100,000 psi;

A_g = gross area of a concrete section; and

A_{ch} = cross-sectional area of a structural member measured to the outside

edges of transverse reinforcement.

Although these equations are used to specify the amount of reinforcement needed for buildings and other structures, both equations are identical to the equations presented in AASHTO (2012). This is because both organizations want the desired behavior of concrete to be similar and the values produced by these equation came from numerous axially load tests on concrete columns.

2.1.8   Bridge Manual of Transit New Zealand (2005) and NZS 3101 (2008)

Since 1994, the *Bridge Manual of Transit New Zealand* has undergone revisions with one of the latest being from 2005. In this set of guidelines, the design process for concrete columns is now referred to the *Design of Concrete Structures Standard* produced by the Standards New Zealand Council (2008). In this standard, the amount of transverse reinforcement is required to meet different levels depending on whether or not it falls within a potential ductile plastic hinge region. In either approach, the updated standard provides a new equation, Eq. (2-11) or Eq. (2-12), that has been simplified from the 1994 version. Eq. (2-11) is the requirement to be met for confinement in general while Eq. (2-12) applies in the ductile plastic hinge region. This is a similar approach to that of Caltrans (2003) in which equations were given for the ductile and non-ductile zones. As in the other New Zealand equation, the units to be used are megapascals and millimeters.

$$\rho_s = \frac{(1\text{-}p_t m)}{2.4} \frac{A_g}{A_c} \frac{f_c^{'}}{f_{yt}} \frac{N^*}{\varphi f_c^{'} A_g} \text{-}0.0084 \qquad\qquad \text{Eq. (2-11)}$$

where: A_g = gross area of column;

A_c = core area of column measured to the centerline of the confinement

reinforcement;

p_t $= A_{st}/A_g$;

A_{st} = total area of longitudinal column reinforcement;

m $= f_y/(0.85f_c')$;

f_y = lower characteristic yield strength of longitudinal steel;

f_{yt} = lower characteristic yield strength of transverse steel;

N^* = axial compressive load on column; and

φ = strength reduction factor = 0.85 for columns not protected by capacity

design.

$$\rho_s = \frac{(1.3 - p_t m)}{2.4} \frac{A_g}{A_c} \frac{f_c'}{f_{yt}} \frac{N^*}{\varphi f_c' A_g} - 0.0084 \qquad \text{Eq. (2-12)}$$

where: A_g = gross area of column;

A_c = core area of column;

p_t $= A_{st}/A_g$;

A_{st} = total area of longitudinal column reinforcement;

m $= f_y/(0.85f_c')$;

f_y = lower characteristic yield strength of longitudinal steel;

f_{yt} = lower characteristic yield strength of transverse steel;

N^* = axial compressive load on column; and

φ = strength reduction factor = 0.85 for columns not protected by capacity

design.

The main difference between Eq. (2-1) and Eqs. (2-11) and (2-12) is that the curvature ductility term and a number of other constants were removed, thus simplifying the amount of input information required. Additionally, limits were placed on values within the equations. These limits include the following:

- A_g/A_c shall not be greater than 1.5 unless it can be shown that the design strength of the column core can resist the design actions;

- p_t*m shall not be greater than 0.4; and

- f_{yt} shall not exceed 800 MPa.

Besides the requirements specified above, *NZS 3101* states that the columns must be designed with an adequate amount of transverse reinforcement such that premature buckling does not occur. Again, the buckling equation is dependent on whether or not the design is taking place within a potential ductile plastic hinge region. Thus, Eq. (2-13) presented herein applies outside the ductile hinge region while Eq. (2-14) applies within the ductile hinge region.

$$\rho_s = \frac{A_{st}}{155d''} \frac{f_y}{f_{yt}} \frac{1}{d_b} \qquad \text{Eq. (2-13)}$$

where: A_{st} = total area of longitudinal column reinforcement;

$\quad\quad f_y$ = lower characteristic yield strength of longitudinal steel;

$\quad\quad f_{yt}$ = lower characteristic yield strength of transverse steel;

$\quad\quad d''$ = depth of concrete core of column measured from center to center of peripheral rectangular hoop, circular hoop or spiral; and

$\quad\quad d_b$ = diameter of reinforcing bar.

$$\rho_s = \frac{A_{st}}{110d''}\frac{f_y}{f_{yt}}\frac{1}{d_b}$$

Eq. (2-14)

where: A_{st} = total area of longitudinal column reinforcement;

f_y = lower characteristic yield strength of longitudinal steel;

f_{yt} = lower characteristic yield strength of transverse steel;

d'' = depth of concrete core of column measured from center to center of peripheral rectangular hoop, circular hoop or spiral; and

d_b = diameter of reinforcing bar.

2.1.9 AASHTO Guide Specifications for LRFD Seismic Bridge Design (2010)

The LRFD Bridge Design Specifications by AASHTO (2012) have been modified by a second set of guide specifications. This specification specifically addresses the seismic design of bridges (AASHTO 2010). In this set of guidelines, additional requirements on the amount of transverse reinforcement have been provided. These requirements for the volumetric ratio of transverse reinforcement in the core of the column do not take into account the column size or strength. The specifications, however, are based on the seismic design category for which they are designed. These values are provided in Eq. (2-15) and Eq. (2-16) and are minimum values for the design levels.

- For Seismic Design Category B:

$$\rho_s \geq 0.003$$

Eq. (2-15)

- For Seismic Design Categories C and D:

$$\rho_s \geq 0.005$$

Eq. (2-16)

The spacing requirements suggested in the AASHTO Seismic Bridge Design Specifications (2010) are the same as those provided in Section 2.1.2 for the SCDOT. For this reason they are not reproduced in this section.

2.1.10 Caltrans Seismic Design Criteria (2010)

Similar to the SCDOT, Caltrans has a specific set of seismic design criteria (SDC) (2010) that a design engineer must meet. The main idea presented in the design criteria is that enough confinement reinforcement must be provided such that the performance requirements as set by the Department of Transportation are adequately met in addition to the federal requirements of the FHWA. The performance requirements in the document are based on laboratory testing with fixed base cantilever columns. Additionally, the cantilever column and fixed-fixed column use the same detailing for geometry as well as horizontal and transverse reinforcement. This assumption and the laboratory testing resulted in the specifications such thata single member must have a minimum displacement ductility capacity of three. In addition to the capacity requirements, the sections must be designed such that the global demand displacement ductility meets the following criteria:

- Single Column Bents supported on fixed foundation $\mu_D \leq 4$;

- Multi-Column Bents supported on fixed or pinned footings $\mu_D \leq 5$;

- Pier Walls (weak direction) supported on fixed or pinned footings $\mu_D \leq 5$; and

- Pier Walls (strong direction) supported on fixed or pinned footings $\mu_D \leq 1$.

The intention of the displacement ductility values prescribed within the SDC is that the designer shall perform an inelastic pushover analysis to ensure the prescribed global displacement ductility is met. In this process the designer is also expected to ensure that the minimum displacement ductility of three is met for each member of the system. From this analysis, the amount of confinement reinforcement is determined such that the displacement ductility performance requirements are met. Furthermore, to prevent reinforcement congestion and higher ductility demand for an earthquake, the general practice is to keep an aspect ratio of the column to four or above. Once the ductile region design has been completed, SDC (2010) specifies that the transverse reinforcement outside the ductile region need not be less than half the amount of confinement reinforcement within the plastic hinge region.

2.1.11 AASHTO LRFD Bridge Design Specifications (2012)

The LRFD bridge design specifications published by AASHTO (2012) have numerous requirements on the amount of transverse reinforcement needed in a circular column, but are the exact same as those provided by ACI in Section 2.1.7 of this report. The equations for the volumetric ratio within the plastic hinge region that must be satisfied are reproduced again as Eq. (2-17) and Eq. (2-18).

$$\rho_s \geq 0.12 \frac{f_c'}{f_y} \qquad\qquad \text{Eq. (2-17)}$$

where: ρ_s = volumetric ratio of transverse reinforcement;

f_c' = specified compressive strength of concrete at 28 days, unless another

age is specified; and

f_y = yield strength of reinforcing bars.

$$\rho_s \geq 0.45 \left(\frac{A_g}{A_c} - 1\right) \frac{f_c'}{f_{yh}}$$
Eq. (2-18)

where: ρ_s = volumetric ratio of transverse reinforcement;

A_g = gross area of concrete section;

A_c = area of core measured to the outside diameter of the spiral;

f_c' = specified compressive strength of concrete at 28 days, unless another age is specified; and

f_{yh} = specified yield strength of spiral reinforcement.

The amount of reinforcement required must also meet some additional spacing requirements similar to those specified by the *SCDOT* (2008) and *ACI 318-08* (2008). These details are listed below:

- Clear spacing of the bars not less than 1 in. or 1.33 times the maximum aggregate size;

- The center to center spacing not greater than six times the diameter of the longitudinal bars;

- Spacing less than 4.0 in. in the confined region and 6.0 in. in non-confined regions; and

- Spacing less than one-quarter the minimum member dimension in the confined regions.

In addition to the spacing requirements and values of volumetric ratio of transverse reinforcement, a minimum amount of transverse reinforcement is required for shear both inside and outside the plastic hinge region.

2.2 Transverse Reinforcement Area Based Equations

Even though many guidelines provide information in regards to the volumetric ratio of horizontal reinforcement, ρ_s, some specifications provide transverse reinforcement details in the form of a specified area. This approach accounts for systems in which it may be beneficial to know the amount of area required for reinforcement instead of a volumetric ratio. For example, the area of transverse reinforcement may be more beneficial when there are two directions of concern with a column or beam having dimensions of cross-sections that vary in the principal direction of applied loading. To better understand all the possible equations that may come into confinement reinforcement, the area specifications and guidelines were also examined to demonstrate the differences that arise. Once the area of steel reinforcement is known for a given design, a volumetric ratio can be calculated to compare with other approaches if assumptions are made about the geometric dimensions of the column. In this section, it was assumed when appropriate that there was a column with equal dimensions in the primary directions was used along with a consistent area and number of reinforcement legs in either direction if a volumetric ratio is provided.

By assuming a column of this type with equal amounts of transverse reinforcement in either direction, the volumetric ratio of column can be computed using Eq. (2-19) and substituting the appropriate area equation in for A_{st}. The substituted area equation, however, must be divided by a factor of 2 as the reinforcement area computed will be used in a

minimum of two legs within the column cross-section. It is noted that Eq. (2-19) is a

summation of the total volumetric ratio within the cross-section (i.e., $\rho_s = \rho_{sx} + \rho_{sy}$).

$$\rho_s = \frac{4A_{st}}{D's} \qquad\qquad\text{Eq. (2-19)}$$

where: A_{st} = area of transverse reinforcement;

D' = dimension of core measured from center to center of transverse

reinforcement;

s = center to center spacing of transverse reinforcement; and

ρ_s = total volumetric ratio of transverse reinforcement.

The list below defines the resources used for establishing the comparison information

provided in the rest of Section 2.2 of this report based on the chronological history of the

equations used in the seismic design of bridge columns. The resources were selected to

match the documents chosen within Section 2.1 of this report where select references not

related to bridge column design were included based on design philosophy. The list was

extended to include the *Code for Design of Concrete Structures for Buildings* published by

the Canadian Standards Association (1994) and the *Standard Specification for Concrete

Structures 2007 "Design"* published by the Japan Society of Civil Engineers (2010). These

particular resources were selected for inclusion to expand the number of resources from high

seismic regions of the world that conduct additional research into confinement of reinforced

concrete columns. Furthermore, they were included within this section as they did not

directly provide equations for the volumetric ratio of transverse reinforcement.

- Canadian Standards Association - *Code for Design of Concrete Structures for Buildings (CAN3-A23.3-M94)* (1994);
- Watson, S.; Zahn, F. A.; and Park, R., (1994);
- Priestley, M. J.; Seible, F.; and Calvi, G. M. – *Seismic Design and Retrofit of Bridges* (1996);
- Applied Technology Council (ATC) – *Improved Seismic Design Criteria for California Bridges: Provisional Recommendations (ATC-32)* (1996);
- Caltrans - *Bridge Design Specifications Manual* (2003);
- American Concrete Institute (ACI) – *Building Code Requirements for Structural Concrete (ACI 318-08) and Commentary (ACI 318R-08);*
- Standards New Zealand – *Design of Concrete Structures (NZS 3101: 2008);*
- AASHTO - *Guide Specifications for LRFD Seismic Bridge Design 1st Edition with 2010 interim revisions* (2010) ;
- Japan Society of Civil Engineers – *Standard Specification for Concrete Structures 2007 "Design" (2010);*
- Caltrans – *Seismic Design Criteria Version 1.6* (2010); and
- AASHTO – *LRFD Bridge Design Specifications* (2012).

2.2.1   *Watson et al. (1994)*

The research provided in this reference is similar to the *NZS 3101* (2008) equations with some of the noted differences being that extra parameters are included and the anti-buckling requirements are not directly discussed with these volumetric equations. When the equation is converted from the area approach to volumetric ratio based on the column with equal reinforcement all around, Eq. (2-20) is attained. When extrapolating this equation out to the effective lateral confining stress assuming a curvature ductility of 20, a longitudinal steel ratio of two percent, a ratio of gross to core area of concrete of 1.22, material property ratio of 0.066 and an axial load ratio of 40% (to ensure positive numbers), the coefficient of effectiveness would end up being a value of 0.67 to match the effective lateral confining stress associated with the spiral reinforcement equation assuming a 0.95 coefficient of effectiveness. Priestley et al. (1996) suggests a coefficient of effectiveness of 0.95 for

circular sections, 0.75 for rectangular and 0.6 for rectangular walls. Thus, the effectiveness

of 0.67 seems to fall within a reasonable range.

$$\rho_s = 2 * \left(\frac{\frac{\varphi_u}{\varphi_y} - 33 p_t m + 22}{111} \frac{A_g}{A_c} \frac{f_c'}{f_{yh}} \frac{P}{\phi f_c' A_g} - 0.006 \right) \qquad \text{Eq. (2-20)}$$

where: s   = center to center spacing of transverse reinforcement;

       h″   = dimension of core of column at right angles to direction of transverse

            bars under consideration;

       A_g = gross area of column;

       A_c = core area of column;

       $\frac{\varphi_u}{\varphi_y}$ = curvature ductility factor required;

       φ_u = ultimate curvature;

       φ_y = curvature at first yield;

       p_t = A_{st}/A_g;

       A_{st} = total area of longitudinal column reinforcement;

       m   = $f_y/(0.85 f_c')$;

       f_y = lower characteristic yield strength of longitudinal steel;

       f_{yt} = lower characteristic yield strength of transverse steel;

       N^* = axial compressive load on column; and

       ϕ = strength reduction factor = 0.85 for columns not protected by capacity

            design.

2.2.2   *Priestley et al. (1996)*

In the *Seismic Design and Retrofit of Bridges* book by Priestley (1996), an area equation

was provided. Instead of reproducing that equation here, the volumetric ratio form, once

rearranged using the aforementioned process, is provided in this document. The resulting

equation, Eq. (2-21) is very similar to the ATC-32 (1996) approach with the only difference

being the assumption that rectangular hoops are not as efficient as circular hoops. Thus, the

multipliers in Eq. (2-21) are 50% and 100% higher than the spiral equation. When this

approach is extrapolated out to the effective lateral confining stress using a five percent ALR,

a two percent longitudinal reinforcement ratio and a ratio of material properties of 0.066, a

coefficient of 0.6 would be needed to match the spiral equation with a coefficient of

effectiveness of 0.95.

$$\rho_s = 0.24 \frac{f'_{ce}}{f_{ye}} \left[0.5 + \frac{1.25P}{f'_{ce}A_g} \right] + 0.26(\rho_l - 0.01) \qquad\qquad \text{Eq. (2-21)}$$

where: f'_{ce} = expected concrete strength;

f_{ye} = expected yield strength of the reinforcement;

P   = column axial load;

A_g = gross column area; and

ρ_l = longitudinal reinforcement ratio.

Anti-buckling requirements are specified by Priestley et al. (1996) in which a certain

amount of horizontal reinforcement must be provided to ensure that the longitudinal bar does

not buckle prematurely. The two equations are the same as those presented within Section

2.1.3 of this report. These equations are based on the number of longitudinal bars present in the cross-section and diameter of the longitudinal bar.

2.2.3 *ATC-32 (1996) and Caltrans (2003)*

In these two different approaches from the bridge manual published by Caltrans and the ATC-32 final recommendations, the resulting equations are the same as those published by Priestley et al. (1996). This means that they produce the same equation as provided in Eq. (2-21) for the design of columns with rectangular tie reinforcement. Thus, the equation is not reproduced herein.

2.2.4 *ACI 318-08*

Just like the spiral reinforcement equations, ACI provides two equations to give minimum area values for rectangular hoop reinforcement for rectangular columns. These equations are presented here as Eq. (2-22) and Eq. (2-23).

$$A_{sh} = 0.3 \frac{s b_c f_c'}{f_{yt}} \left[\left(\frac{A_g}{A_{ch}} \right) - 1 \right] \qquad \text{Eq. (2-22)}$$

where: A_{sh} = total area of hoop reinforcement;

f_c' = specified compressive strength of concrete;

f_{yt} = specified yield strength of transverse reinforcement not to exceed 100,000 psi;

A_g = gross area of a concrete section;

A_{ch} = cross-sectional area of a structural member measured to the outside edges of transverse reinforcement;

s = center to center spacing of transverse reinforcement; and

b_c = cross-sectional dimension of member core measured to the outside

edges of the transverse reinforcement composing area A_{sh}.

$$A_{sh}=0.09\frac{sb_c f_c'}{f_{yt}}$$ Eq. (2-23)

where: A_{sh} = total area of hoop reinforcement;

f_c' = specified compressive strength of concrete;

f_{yt} = specified yield strength of transverse reinforcement not to exceed

100,000 psi;

A_g = gross area of a concrete section;

A_{ch} = cross-sectional area of a structural member measured to the outside

edges of transverse reinforcement;

s = center to center spacing of transverse reinforcement; and

b_c = cross-sectional dimension of member core measured to the outside

edges of the transverse reinforcement composing area A_{sh}.

Rearranging the above equations and solving for the volumetric ratio Eqs. (2-24) and (2-25) are produced.

$$\rho_s=0.6\left(\frac{f_c'}{f_{yt}}\right)\left[\frac{A_g}{A_{ch}}-1\right]$$ Eq. (2-24)

where: f_c' = specified compressive strength of concrete;

f_{yt} = specified yield strength of transverse reinforcement not to exceed

100,000 psi;

A_g = gross area of a concrete section; and

A_{ch} = cross-sectional area of a structural member measured to the outside

edges of transverse reinforcement.

$$\rho_s = 0.18 \frac{f_c'}{f_{yt}}$$ Eq. (2-25)

where: f_c' = specified compressive strength of concrete; and

f_{yt} = specified yield strength of transverse reinforcement not to exceed

100,000 psi.

The above two equations, when compared back to Eqs. (2-9) and (2-10) are very similar in that the only difference is the multiplier at the beginning of the equations. Upon closer inspection, Eqs. (2-9) and (2-10) are obtained when Eq. (2-24) is multiplied by 75% and Eq. (2-25) by 66.5%. Thus, the specifications are assuming that additional steel is required when using rectangular hoops when compared to circular hoops and spirals for the confinement reinforcement. Similar to the prior sections, when the data is extrapolated out to the effective lateral confining stress, a coefficient of effectives for Eq. (2-23) and Eq. (2-24) would be 0.71 and 0.63, respectively. These assumptions are once again similar to the recommendations of Priestley et al. (1996) for the assumption on the effectiveness of the reinforcement.

2.2.5   NZS 3101 (2008)

The New Zealand concrete structure code states that the cross sectional area of rectangular hoop or tie reinforcement shall not be less than that given by the greater of four

different equations. Two of the equations are applicable to regions that are not expected to be ductile hinging regions and the other two are for regions with ductile hinging expected. In each set of equations the reinforcement must be greater than the two values produced. One of the equations is for anti-buckling and the other is just a set requirement that must be met. The equations for the ductile plastic hinge region are provided as Eq. (2-26) and Eq. (2-27) with the latter being for anti-buckling. These equations have the same form as the prior equations based on spiral reinforcement and must be in units of megapascals and millimeters.

$$A_{sh} = \frac{(1.3 - p_t m)s_h h''}{3.3} \frac{A_g}{A_c} \frac{f_c'}{f_{yt}} \frac{N^*}{\phi f_c' A_g} - 0.006 s_h h''$$ Eq. (2-26)

where: A_g = gross area of column;

A_c = core area of column;

p_t = A_{st}/A_g;

A_{st} = total area of longitudinal column reinforcement;

m = $f_y/(0.85 f_c')$;

f_y = lower characteristic yield strength of longitudinal steel;

f_{yt} = lower characteristic yield strength of transverse steel;

N^* = axial compressive load on column;

ϕ = strength reduction factor = 0.85 for columns not protected by

capacity design;

s_h = center to center spacing of hoop sets;

h'' = dimension of core of column at right angles to direction of

transverse bars under consideration; and

$$f_c' \quad = \text{specified compressive strength of concrete.}$$

$$A_{te} = \frac{\Sigma A_b f_y s}{96 f_{yt} d_b} \qquad\qquad\qquad \text{Eq. (2-27)}$$

where: ΣA_b = sum of the area of the longitudinal bars reliant on the tie;

$\qquad\quad f_y$ = lower characteristic yield strength of longitudinal steel;

$\qquad\quad f_{yt}$ = lower characteristic yield strength of transverse steel;

$\qquad\quad s$ = center to center spacing of stirrup-ties along member; and

$\qquad\quad d_b$ = diameter of reinforcing bar.

When converted to an equation for spiral volumetric ratio using the process provided in the prior sections, Eq. (2-28) and Eq. (2-29) are produced. When adjusted to examine the impacts on the effective lateral confining stress, the first equation results in an effectiveness coefficient of 0.64 when matching the value of confining stress using a 0.95 coefficient of effectiveness. It is assumed that the anti-buckling equation would result in a similar comparison.

$$\rho_s = \frac{2(1.3 - p_t m)}{3.3} \frac{A_g}{A_c} \frac{f_c'}{f_{yt}} \frac{N^*}{\phi f_c' A_g} - 0.012 \qquad\qquad \text{Eq. (2-28)}$$

where: A_g = gross area of column;

$\qquad\quad A_c$ = core area of column;

$\qquad\quad p_t$ = A_{st}/A_g;

$\qquad\quad A_{st}$ = total area of longitudinal column reinforcement;

$\qquad\quad m$ = $f_y/(0.85 f_c')$;

$\qquad\quad f_y$ = lower characteristic yield strength of longitudinal steel;

f_{yt} = lower characteristic yield strength of transverse steel;

N^* = axial compressive load on column;

ϕ = strength reduction factor = 0.85 for columns not protected by capacity design; and

f_c' = specified compressive strength of concrete.

$$\rho_s = \frac{2\Sigma A_b f_y}{96 f_{yt} d_b d''} \qquad \text{Eq. (2-29)}$$

where: ΣA_b = sum of the area of the longitudinal bars reliant on the tie;

f_y = lower characteristic yield strength of longitudinal steel;

f_{yt} = lower characteristic yield strength of transverse steel;

d_b = diameter of reinforcing bar; and

d'' = depth of concrete core of column measured from center to center of peripheral rectangular hoop, circular hoop or spiral.

Outside the ductile hinge regions, *NZS 3101* provides a series of equations that are about the same as Eqs. (2-11) and (2-13). The main difference once again was that the governing agency determined that ties were less efficient than spiral reinforcement. This is seen when comparing the effective lateral confining stress and the associated coefficient of effectiveness. In this instance the coefficient of effectiveness was found to be 0.58 when compared to the spiral effectiveness with a coefficient of 0.95. A similar trend is expected for the anti-buckling equations of *NZS 3101*. The resulting volumetric ratio equations are provided herein as Eq. (2-30) and Eq. (2-31) with the latter being the anti-buckling requirements.

$$\rho_s = \frac{2(1-p_t m)}{3.3} \frac{A_g}{A_c} \frac{f_c'}{f_{yt}} \frac{N^*}{\phi f_c' A_g} - 0.013 \qquad \text{Eq. (2-30)}$$

where: A_g = gross area of column;

A_c = core area of column;

p_t = A_{st}/A_g;

A_{st} = total area of longitudinal column reinforcement;

m = $f_y/(0.85 f_c')$;

f_y = lower characteristic yield strength of longitudinal steel;

f_{yt} = lower characteristic yield strength of transverse steel;

N^* = axial compressive load on column;

ϕ = strength reduction factor = 0.85 for columns not protected by capacity

design; and

f_c' = specified compressive strength of concrete.

$$\rho_s = \frac{2 \Sigma A_b f_y}{135 f_{yt} d_b d''} \qquad \text{Eq. (2-31)}$$

where: ΣA_b = sum of the area of the longitudinal bars reliant on the tie;

f_y = lower characteristic yield strength of longitudinal steel;

f_{yt} = lower characteristic yield strength of transverse steel;

d_b = diameter of reinforcing bar; and

d'' = depth of concrete core of column measured from center to center of

peripheral rectangular hoop, circular hoop or spiral.

2.2.6   *Japan Society of Civil Engineers (2010)*

Although an equation for the spiral volumetric ratio or area of hoop reinforcement

required for concrete columns was not provided, an area requirement was stated within the

concrete design specifications for seismic considerations. Specifically, Eq. (2-32) was

provided for columns that use spiral reinforcement and defines the converted cross-sectional

area of spirals, A_{spe}, which reduces the spiral area based on the spacing within the column.

This value must be less than 3% of the effective cross-section (i.e., the core section of the

column).

$$A_{spe} = \frac{\pi d_{sp} A_{sp}}{s} \leq 0.03 A_c \qquad \text{Eq. (2-32)}$$

where: d_{sp} = diameter of the effective cross section of spiral reinforced column;

A_{sp} = cross sectional area of spiral reinforcement;

A_c = effective cross-section of the column; and

s = spacing of spiral reinforcement.

When rearranged and solved for the volumetric ratio, the following expression, Eq. (2-

33), was found for the horizontal reinforcement needed when using spiral reinforcement in a

column design.

$$\rho_s = \frac{4 \pi A_{sp}}{s^2} \leq \frac{0.03 \pi d_{sp}}{s} \qquad \text{Eq. (2-33)}$$

where: d_{sp} = diameter of the effective cross section of spiral reinforced column;

A_{sp} = cross sectional area of spiral reinforcement; and

s = spacing of spiral reinforcement.

2.2.7 *AASHTO LRFD Bridge Design Specifications (2012)*

According to the bridge design specifications published by AASHTO (2012) the reinforcement in a rectangular column with rectangular hoop reinforcement, the total gross sectional area, A_{sh}, shall satisfy either Eq. (2-34) or Eq. (2-35).

$$A_{sh} \geq 0.30 \, sh_c \, \frac{f_c'}{f_y} \left[\frac{A_g}{A_c} - 1 \right] \qquad \text{Eq. (2-34)}$$

where: A_{sh} = total cross-sectional area of tie reinforcement, including supplementary cross-ties having a spacing of s and crossing a section having a core dimension h_c;

h_c = core dimension of tied column in the direction under consideration;

s = vertical center to center spacing of hoops, not exceeding 4.0 in.;

A_c = area of column core;

A_g = gross area of column;

f_c' = specified compressive strength of concrete; and

f_y = yield strength of tie or spiral reinforcement.

$$A_{sh} \geq 0.12 \, sh_c \frac{f_c'}{f_y} \qquad \text{Eq. (2-35)}$$

where: A_{sh} = total cross-sectional area of tie reinforcement, including supplementary cross-ties having a spacing of s and crossing a section having a core dimension h_c;

h_c = core dimension of tied column in the direction under consideration;

s = vertical center to center spacing of hoops, not exceeding 4.0 in.;

f_c' = specified compressive strength of concrete; and

f_y = yield strength of tie or spiral reinforcement.

Similar to ACI's requirements, AASHTO provided two equations based on different variables for the required area of transverse reinforcement. Note that the first equation provided by *ACI 318-08* (2008) as stated in Eq. (2-22) is identical to Eq. (2-34), and the second equation of *ACI 318-08* (2008), Eq. (2-23), differs from AASHTO within the coefficient by AASHTO's coefficient being 33% higher. Using the same process as in the ACI area computations, Eq. (2-35) was rearranged and solved for the volumetric ratio. The result was Eq. (2-36) where the ratio between the ACI and AASHTO approaches is still a 33% increase. Additionally, Eq. (2-36) results in a coefficient of effectiveness of 0.5 to match the effective lateral confining stress of a spiral section with a coefficient of effectiveness of 0.95 and a material ratio of 0.066.

$$\rho_s = 0.24 \frac{f_c'}{f_{yt}}$$ Eq. (2-36)

where: f_c' = specified compressive strength of concrete; and

f_{yt} = specified yield strength of transverse reinforcement not to exceed 100,000 psi.

As a side note, Eq. (2-36) is identical to that of the 1994 Canadian Code (*CAN3-A23.3-M94*) for the design of concrete structures (Bayrak and Sheikh 2004).

2.3 Comparison of Available Confinement Equations

Across the world, there are many different approaches for determining the amount of confinement as well as which parameters are important in the lateral design process. Some of the older approaches (e.g., New Zealand 1994) included the local design parameters based on the curvature limit states of the column cross-section while others in practice today do not account for such a demand parameter. The large variation in design parameters for determining the adequate amount of horizontal reinforcement are summarized in Tables 2-1 through Table 2-3.

Upon examination of the tables, it can be noted that there is a significant difference in complexity of equation and amount of parameters used in each approach. Although this was the case, there was no general consensus as to what is the best approach to determining an adequate amount of horizontal reinforcement when dealing with lateral loading.

Table 2-1: Summary of variables used for determining spiral transverse confinement reinforcement

Source	Eqn.	f'_c	f_{yt}	f'_{ce}	D'	A_g	A_{core}	ALR	ρ_l	f_{yl}	ϕ_u/ϕ_y	l_{ac}	LRFD Resistance Factor (ϕ)	Constant
AKDOT, MODOT, NCDOT		See AASHTO Requirements												
SC DOT	(2-8)								X			X		
AASHTO Bridge ('12)-1	(2-17)	X	X											
AASHTO Bridge ('12)-2	(2-18)	X	X			X	X							
AASHTO Seismic	(2-15) (2-16)													X
ACI 318-08 – 1	(2-9)	X	X											
ACI 318-08 – 2	(2-10)	X	X			X	X							
ATC-32	(2-2)		X	X				X	X					
Caltrans 2003 (Dia. 3 ft. or less)	(2-5)	X	X			X	X	X						
Caltrans 2003 (Dia. > 3 ft.)	(2-6)	X	X					X						
New Zealand (1994)	(2-1)	X	X			X	X	X	X	X	X		X	X
Watson et al. (1994)	(2-1)	X	X			X	X	X	X	X	X		X	X
NZS 3101 (2008) - 1	(2-11)	X	X			X	X	X	X	X			X	X
NZS 3101 (2008) - 2	(2-12)	X	X			X	X	X	X	X			X	X

Note: X – indicates the use of term in specified equation

Table 2-2: Summary of variables used for volumetric equations based on specification of required area

Source	Eqn.	f'_c	f_{yt}	f'_{ce}	D'	A_g	A_{core}	ALR	ρ_l	f_{yl}	ϕ_u/ϕ_y	s	LRFD Resistance Factor (ϕ)	Constant
ACI 318-08 – 1	(2-24)	X	X			X	X							
ACI 318-08 – 2	(2-25)	X	X											
AASHTO Bridge ('12)-1	(2-36)	X	X											
AASHTO Bridge ('12)-2	(2-24)	X	X			X	X							
AASHTO Seismic	(2-15) (2-16)													X
Priestley (1996)	(2-21)		X	X				X	X					
ATC-32 (1996) & Caltrans (2003)		See Priestley (1996)												
NZS 3101 (2008) - 1	(2-28)	X	X			X	X	X	X	X			X	X
NZS 3101 (2008) - 2	(2-30)	X	X			X	X	X	X	X			X	X
Watson et al. (1994)	(2-20)	X	X			X	X	X	X	X	X		X	X
JSCE (JGC No. 15)	(2-33)				X							X		

Note: X – indicates the use of term in specified equation

Table 2-3: Summary of variables used in anti-buckling equations for determining ρ_s

Source	Eqn.	f_u	f_{yt}	ρ_l	A_{st}	f_y	d_b	d''
NZS 3101 (2008)–1	(2-13)		X		X	X	X	X
NZS 3101 (2008)–2	(2-14)		X		X	X	X	X
Priestley et al. (1996) and ATC-32 (1996)	(2-3)			X				
Priestley et al. (1996) and ATC-32 (1996)	(2-4)	X				X	X	

Note: X – indicates the use of term in specified equation

The prior sections, as summarized in Table 2-1 through Table 2-3, indicate that the numerous methodologies specifying the required amount of transverse confinement reinforcement many different variables. To better understand the differences in the equations, a direct look at the impact of the unconfined concrete compressive strength, column diameter, axial load ratio and longitudinal reinforcement ratio on the requirements was undertaken. The comparisons were made using spiral or butt welded hoops for the transverse reinforcement in a circular column as the previous sections indicated that rectangular ties and hoops were about 70% as effective as the circular confinement.

2.3.1 *Concrete Compressive Strength*

The first set of analyses examined the impact of the unconfined concrete compressive strength on the requirement for horizontal confinement reinforcement ratio. This was done by examining the equations summarized in Table 2-1 and Table 2-3 with duplicates removed. Upon closer inspection of the *NZS 3101* (2008) equation, the data set was not included in this process as it was found to result in a negative value until the axial load ratio exceeded approximately 15% - 20%. Axial load ratios higher than 15% were not examined within this portion as exterior bridge columns of multi-column bents are assumed to not exceed a 15% axial load ratio. Furthermore, Park (1996) stated that this requirement shall not control over the anti-buckling requirements until about a 30% axial load ratio was attained. Thus, the *NZS 3101* (2008) equation for anti-buckling within the ductile plastic hinge region was included in the comparison as this would produce the most confinement reinforcement from the New Zealand Standard. The SCDOT value was not provided in the comparison as this

was typical joint reinforcement requirements (Sritharan 2005), but was stated as a

requirement to meet for the design of column confinement.

For comparison purposes, a 4 ft diameter column with a longitudinal reinforcement ratio

of 2% and an axial load ratio of 5% was selected based on expected usage within high

seismic regions. Additionally, it was assumed that both horizontal and longitudinal steel

reinforcement would have a yield strength of 60 ksi. The cover to the main longitudinal bar

was selected to be 3 in. as this would be a conservative approach based on the *AASHTO*

(2012) requirements for a bridge in a coastal region and would produce a higher ratio of

gross concrete area to core concrete area. The transverse confinement bar would be a #5 bar

(d_{bh} = 0.625 in., where d_{bh} is the diameter of the horizontal reinforcement) when needed in a

given confinement equation. In the buckling equations specified by *ATC-32* (1996) and *NZS*

3101 (2008), the number and size of the longitudinal bars within the column cross-section

was needed to compute the horizontal volumetric ratio. In these equations, the bar size was

specified as #8 bar (d_{bl} = 1.0 in., where d_{bl} = diameter of longitudinal bar), #11 bar (d_{bl} = 1.41

in., where d_{bl} = diameter of longitudinal bar) or #14 bar (d_{bl} = 2.25 in., where d_{bl} = diameter

of longitudinal bar) to capture a range of values that may be experienced with a 2%

longitudinal reinforcement ratio within a 4 ft diameter bridge column. Concrete compressive

strength was varied in these equations from 4 ksi to 8 ksi as this range was typical when

using normal strength concrete in a bridge column design.

The results of the comparison are provided in Figure 2-1. This figure demonstrates that

when it comes to concrete compressive strength, a number of equations were not affected

while others were highly influenced to the point where buckling equations might control the

design of the transverse reinforcement as was the case between 4 and 4.5 ksi depending on the size of the longitudinal bar. The equations that remained constant throughout the variation in the concrete compressive strength were related to the prevention of buckling in the longitudinal bar. These equations are independent of concrete compressive strength as they are based on the strength and quantity of longitudinal steel in the bridge column cross-section. Furthermore, the equations using #8 bar in the details required a higher level of confinement as the number of bars increased compared to the #11 bar and #14 bar detailing in order to maintain the 2% longitudinal reinforcement ratio. The remaining equations within the comparison have a linear increasing trend from 4 ksi to 8 ksi as all the equations include a term for the ratio between the unconfined concrete compressive strength and the steel yield strength. This ratio constantly increases as the steel yield strength remains constant throughout the comparisons.
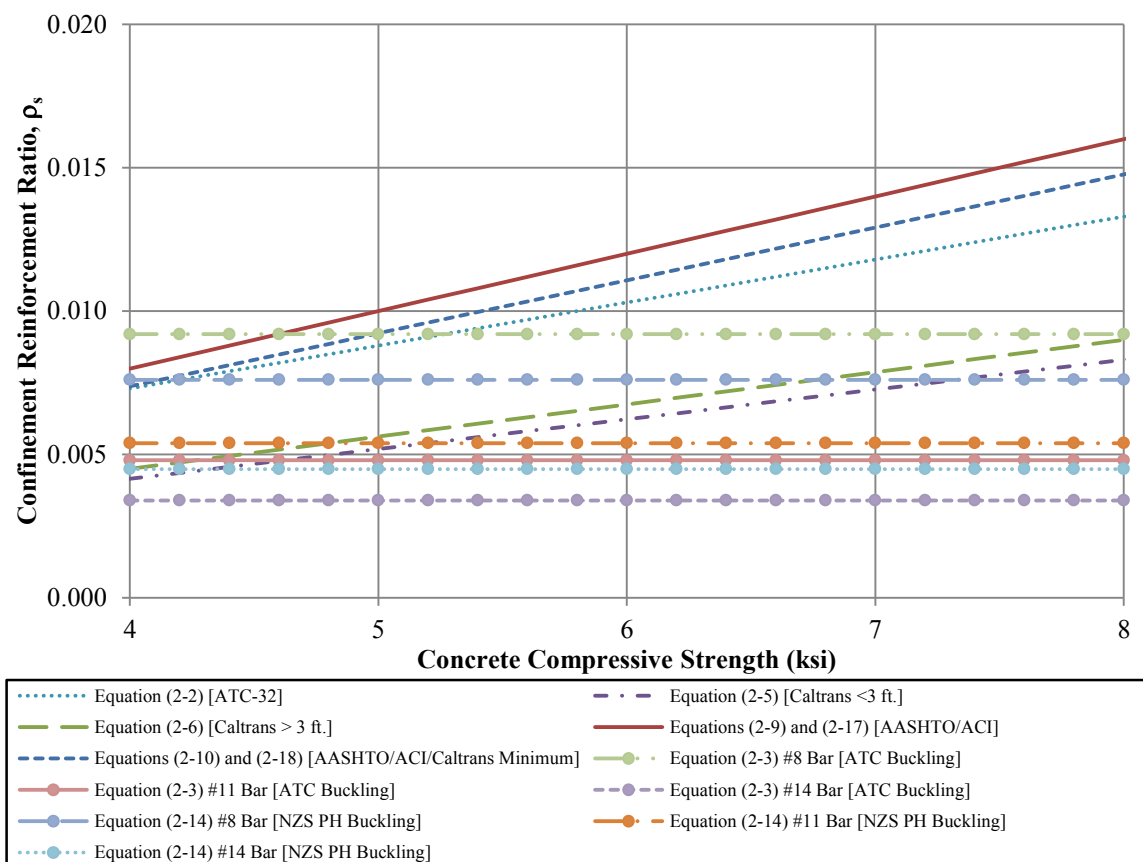
Figure 2-1: Impact of unconfined concrete compressive strength on horizontal confinement reinforcement ratio [Note: PH = within the plastic hinge region]

Examination of the transverse confinement equations presented in Figure 2-1 indicate that the highest level of reinforcement requirements as a function of concrete compressive strength were specified within *AASHTO* (2012), *ACI* (2008), *Caltrans* (2003) and *ATC-32* (1996) when ignoring the impacts associated with premature buckling of the longitudinal reinforcement. With this assumption in mind, the highest value of the required volumetric horizontal ratio comes from Eq. (2-9) and Eq. (2-17) in which the requirements were

specified to ensure an adequate flexural curvature capacity. This particular equation is purely a function of the concrete and steel reinforcing material properties within the system but resulted in a reinforcement ratio between 0.8% and 1.6%. The second highest term, ranging between 0.75% and 1.45%, was based on the minimum requirements specified within the *Caltrans* (2003), *AASHTO* (2012) and *ACI* (2008) documents that ensured the axial capacity of the core of the bridge column section without the cover concrete was the same as the gross concrete section. The recommended equation provided by *ATC-32*, Eq. (2-2), produced the next highest amount of reinforcement as the concrete compressive strength increased from 4 ksi to 8 ksi. The resulting amount of confinement reinforcement varied from 0.75% to 1.33%. This methodology was within 20% of the two aforementioned equations and took into account the highest number of variables during definition of the required transverse reinforcement; thus, the additional variables within this equation were investigated to determine the associated impact on the amount of required confinement reinforcement. The modified equations of *Caltrans* (2003) that take into account the importance of axial load ratio, Eq. (2-5) and Eq. (2-6), were approximately half the value of Eq. (2-9) and Eq. (2-10) which would have controlled the design of the cross-section.

Although ignored originally, the anti-buckling equations would have controlled the amount of transverse confinement steel at low concrete compressive strengths for the column and reinforcement setup used for the comparison, see Figure 2-1, if a #8 bar was used for the longitudinal reinforcement. However, if a #11 bar was used in the cross-section, the value could be exceeded by Eq. (2-9) by up to three times at a concrete compressive strength of 8

ksi. Furthermore, once the concrete compressive strength exceeded 4.6 ksi, Eq. (2-9) and Eq. (2-17) would control the amount of confinement steel in the system.

2.3.2   *Axial Load Ratio*

The next parameter investigated within the transverse confinement reinforcement equations was the axial load ratio. This parameter was selected for investigation as axial load influences the moment-curvature response of the section behavior; thus, the curvature ductility and associated displacement ductility would be similarly affected, which is a main component in the seismic design of reinforced concrete bridge columns. Similar to the concrete compressive strength a comparison was made with a 4 ft diameter column with a 2% longitudinal reinforcement ratio. The cover, horizontal bar and steel properties were maintained the same as the previous comparison. The main difference was that the design concrete strength would be 4 ksi as this is commonly specified in bridge design throughout the United States. The results of the comparison are provided in Figure 2-2.
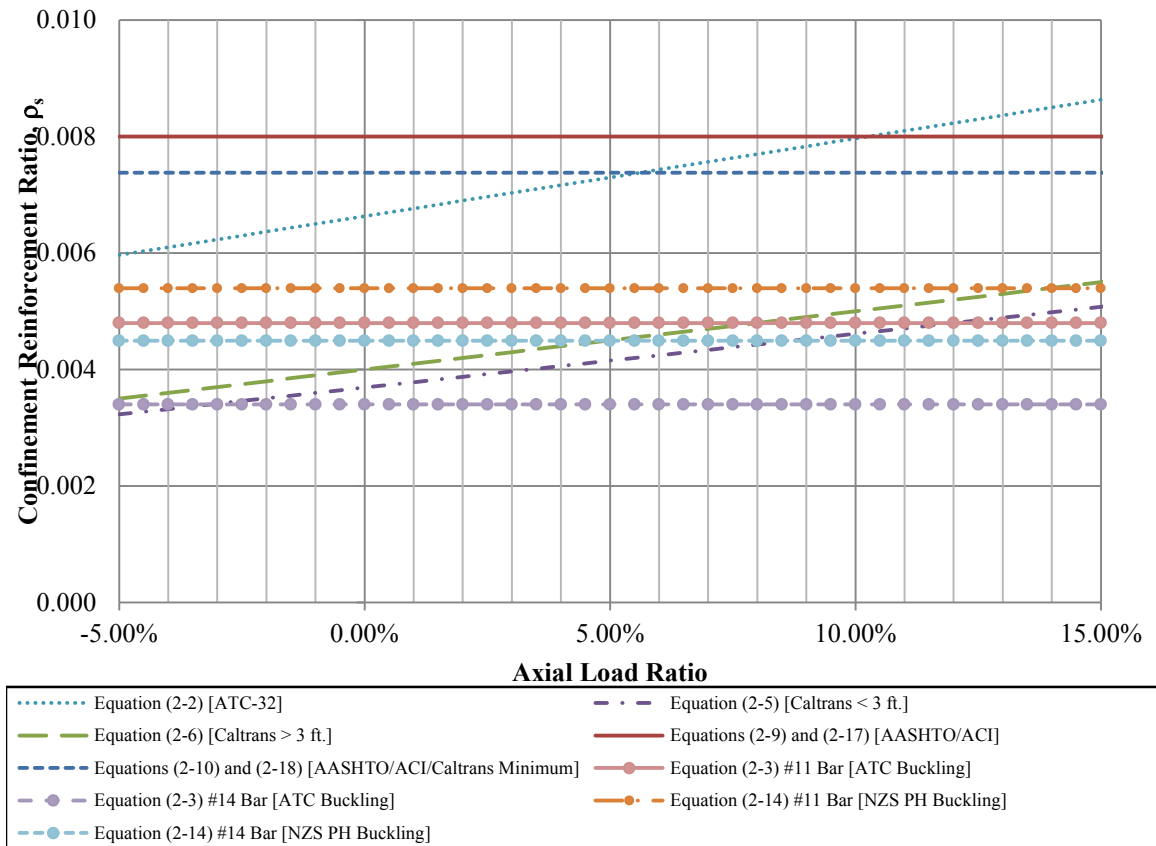
Figure 2-2: Impact of axial load ratio on horizontal confinement reinforcement ratio

[Note: PH = within the plastic hinge region]

Figure 2-2 provides a series of curves in which linearly increasing and constant trends were present within the requirements for horizontal confinement reinforcement. The #8 bar buckling equations were investigated and resulted in higher requirements for the horizontal confinement reinforcement than any other equations; however, this diameter bar would result in the use of 36 bars for a 4 ft diameter cross-section and would not be practical in most designs. The constant trends within the data set were from both the buckling equations and the requirements of *AASHTO* (2012) and *ACI* (2008). The use of a larger diameter longitudinal reinforcing bar resulted in the buckling equations not controlling the design of

the concrete bridge column based on the applied axial load ratio. The elimination of the

buckling equations resulted in Eq. (2-9) and Eq. (2-10) requiring the most amount of

transverse confinement reinforcement within the cross-section examined up to an axial load

ratio between 5% and 10%. Eq. (2-9), specified to ensure an adequate flexural curvature

capacity in the cross-section, was consistently higher than Eq. (2-10) for the system

examined as a function of axial load ratio. The approach suggested by *ATC-32* (1996)

exceeded this value at an axial load ratio of 10%. However, the equation designed to

maintain axial load capacity, Eq. (2-10) was exceeded at an axial load ratio of 5%. Since

axial load ratios in excess of 10% are common in exterior columns of multi-column bents,

the results of the analytical comparison demonstrate that the axial load ratio should be

included into any future volumetric ratio equation.

To account for the impact of axial load ratio, modifications to Eq. (2-9) and Eq. (2-10)

were specified in *Caltrans* (2003) that include axial load ratio as a variable, Eq. (2-5) and Eq.

(2-6). Figure 3-2 indicates that these equations experienced a linearly increasing trend from -

5% to 15%. However, the data resulting from these equations was generally one and a half

to two times lower than the minimum requirements specified in *AASHTO* (2012) and *ACI*

(2008) over the entire range examined. Furthermore, these equations were lower than the

buckling equations specified by *ATC-32* (1996) and *NZS 3101* (2008) up to approximately a

5% ALR. The *NZS 3101* (2008) buckling equation utilizing a #11 bar longitudinally was

higher than both of the *Caltrans* (2003) equations over the range examined within Figure 2-2.

This reinforces the need to include multiple variables within any future proposed design

equation for transverse confinement reinforcement.

2.3.3 Column Diameter and Ratio of Core to Gross Concrete Area

The column diameter, and thus the ratio of the gross to core cross-sectional area, of the section was investigated next as this term defines a key geometric property in any design. The diameters chosen for investigation ranged from 12 in. to 96 in., which are common throughout bridge designs. The concrete compressive strength was taken as 4 ksi, the steel yield strength was 60 ksi, a 5% axial load ratio was maintained and a longitudinal reinforcement ratio of 2% was selected as the average values for a concrete bridge column design. The cover for the main steel was not changed and #11 and #14 bars were used in the buckling equations. It was concluded that the #8 bar should no longer be provided in the comparison based on the probability of use in a 4 ft. diameter bridge column with a 2% longitudinal reinforcement ratio.

Comparisons of results are provided in Figure 2-3, which shows evidence that the column diameter highly influences the amount of horizontal confinement reinforcement needed in a bridge column. This was noted based on the opposite trends within the results that indicate a polynomial decrease in the *Caltrans* (2003) minimum equation, Eq. (2-10), and a polynomial increase provided by the equations for anti-buckling, Eq. (2-3) and Eq. (2-14). The decreasing polynomial trend in the *Caltrans* (2003) minimum equation, Eq. (2-10), would control the design up to a column diameter of approximately 44 in. based on the need to ensure axial capacity without the presence of the cover concrete. At this point, a constant trend in the results based on the specification of transverse confinement such that an adequate flexural curvature capacity is attained, Eq. (2-9), controls until a 62 in. to 72 in. diameter column is reached. At this point, the anti-buckling equations, Eq. (2-3) and Eq. (2-14),

control for the remainder of the diameters examined within this comparison. The exact

controlling equation, however, depended on the diameter of the longitudinal bar being

examined as it may not be practical to use #11 bars in a 96 in. diameter cross-section. The

opposite trends in the results were somewhat expected as the decreasing polynomial trend

contains a term based on the ratio between the gross-area of concrete and the core area of

concrete in the bridge column. The increasing polynomial trend occurred as the anti-

buckling equations rely on the number of bars present within the cross-section of a bridge

column and must increase with column diameter to maintain the specified 2% longitudinal

reinforcement ratio for the comparison.

Differences in requirements between a 24 in. diameter column and 72 in. diameter

column were approximately a factor of 2 with the *Caltrans* (2003) minimum equation, Eq.

(2-10), for the transverse confinement controlling the design at column diameters less than 48

in. This particular equation was expected to control the design within this range as many

resources including *Caltrans* (2003) and *Priestley et al.* (1996) stated that this equation was

for a bridge column with a diameter of less than 3 ft. The buckling equations used in Figure

2-3 may not always control the design for bridge columns in excess of 60 in. as an increased

longitudinal bar diameter would result in a lower amount of required horizontal confinement

reinforcement. Additionally, the equations presented in *Caltrans* (2003) that accounted for

the influence of axial load ratio were once again two times lower than the controlling

equations. The controlling equation in Figure 2-3 indicates that the ratio of the gross section

area to the core section area is important in the overall design as noted by the polynomial

behavior. Since the area of the core and overall section take into account the column

diameter, this means that a future developed design equation should take into account the
column diameter or the ratio of the gross section to the core section.
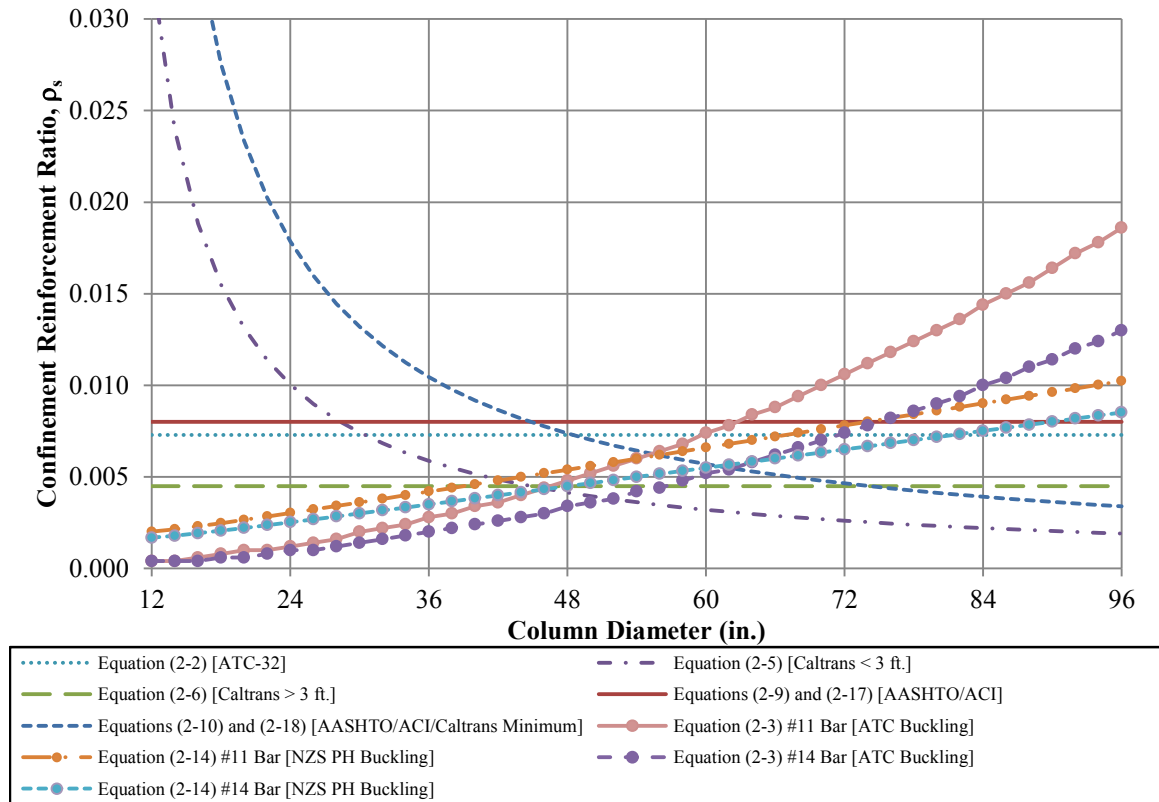
Figure 2-3: Impact of column diameter on the horizontal confinement reinforcement ratio [Note: PH = within the plastic hinge region]

2.3.4 Longitudinal Reinforcement

The final comparison made to examine the impact of variables on the design of horizontal
confinement reinforcement was for the amount of longitudinal reinforcement in the bridge
column. To make this comparison, a number of assumptions were made about the average
concrete column design throughout California and the United States. This meant that a 4 ft.
diameter column with a concrete compressive strength of 4 ksi and axial load ratio of 5% was

again selected. Additionally, the steel had a yield strength of 60 ksi and the reinforcing bar was a #11 or #14 bar when the bar diameter was used as a variable in quantifying the transverse reinforcement. To make the comparison, the longitudinal reinforcement ratio was varied between 1% and 4% as these are typically the upper and lower limits that are used in a bridge column design.

The results of the comparison are shown in Figure 2-4, which contains both linear and constant trends as the longitudinal reinforcement ratio increases from 1% to 4%. The increasing trends in Figure 2-4 were from the anti-buckling and *ATC-32* (1996) equations as these equations included terms that account for the amount of steel within the bridge column cross-section. The constant trends within the comparison were based on the minimum equations presented in *AASHTO* (2012) and *ACI* (2008), which do not contain a term related to the amount of longitudinal reinforcement. These particular equations are a function of material and geometric properties of the bridge column design.

The *ATC-32* (1996) equation for confinement exceeded the requirements of *AASHTO* (2012) between a longitudinal reinforcement ratio of 2% and 2.5%. The minimum requirement specified by *AASHTO* (2012) and *Caltrans* (2003) was exceeded at approximately a 2% reinforcement ratio while the additional equation based on flexural curvature was exceeded at a 2.5% longitudinal reinforcement ratio. Once again, the equations presented in *Caltrans* (2003) based on the adjustment for axial load ratios were exceeded by a factor of two at a minimum. Furthermore, the buckling equations exceeded the requirements of *AASHTO* (2012) and *ACI* (2008) at the high end of the longitudinal reinforcement comparison when using a #11 bar within the bridge column. Additionally, the

NZS 3101 (2008) buckling equation exceeded the required amount of confinement

reinforcement using a #14 bar longitudinally. The *ATC-32* (1996) equation was exceeded at

approximately a 3.4% longitudinal reinforcement ratio by the *NZS 3101* (2008) buckling

equation using a #11 bar in the cross-section. However, it should be noted that a 3.4%

longitudinal reinforcement ratio would contain 40 bars within a 4 ft. diameter cross-section

and would not be realistic for a design.
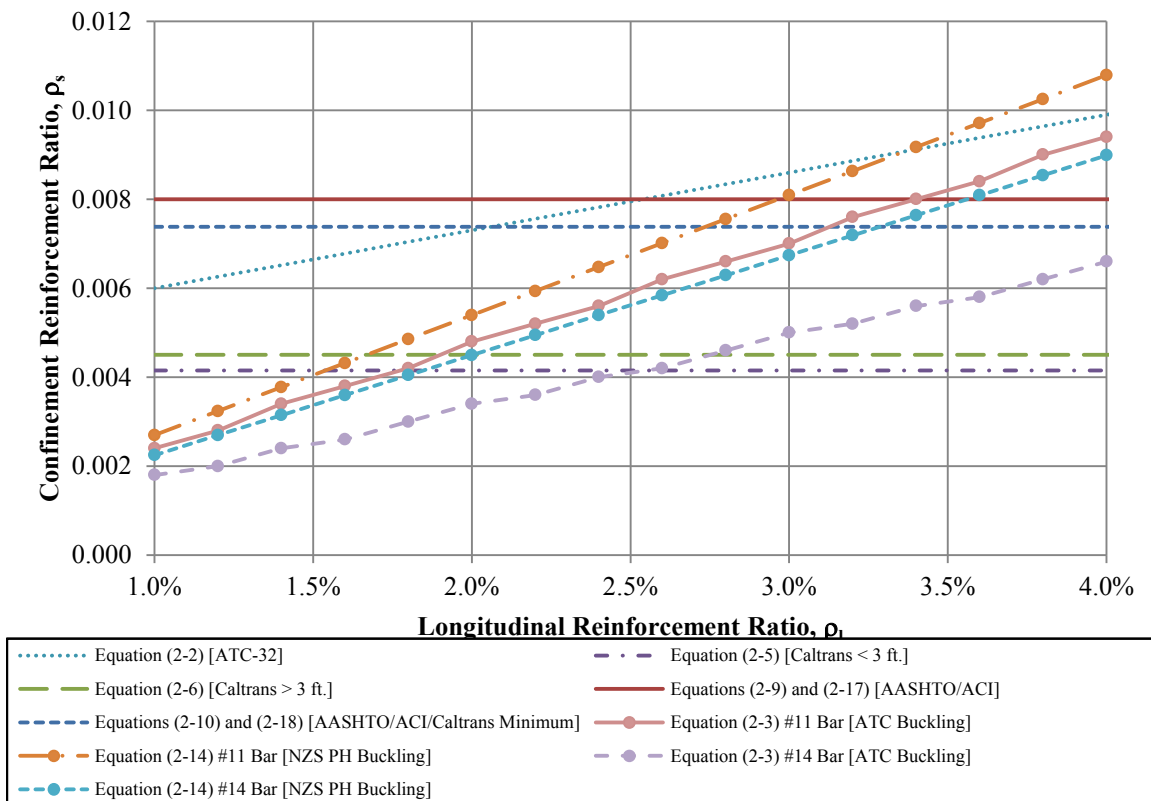
Figure 2-4: Impact of the amount of longitudinal reinforcement on the horizontal

   confinement reinforcement ratio [Note: PH = within the plastic hinge

   region]

2.4 Soil – Foundation – Structure – Interaction (SFSI)

The complexity of designing reinforced concrete bridges in seismic situations is furthered based on the presence of the foundation supporting the entire superstructure. This is the case as any additional flexibility must be sufficiently accounted for in the design to make sure demand does not exceed capacity (AASHTO 2010). Flexibility in the foundation region can come from the detailing of the connection to the response of the soil surrounding the overall foundation. In high seismic regions, columns continuously supported on drilled shaft foundations are commonly employed due to reduced construction costs, simplicity of construction and elimination of column-foundation connection. This type of system, however, is highly influenced by the interaction between the soil and foundation shaft and must be accounted for to ensure sufficient capacity.

Over the years, researchers have been constantly improving the methods of accounting for soil-foundation-structure-interaction (SFSI) through experimental and analytical studies,

Table 2-4. The goal of each study normally falls within two categories—improvement or simplification of the soil spring concept (Hetenyi 1946) used in practice, depicted graphically in Figure 2-5. This methodology relies on ensuring equilibrium between the foundation shaft and soil including the full nonlinearity of the material properties, the applied boundary conditions and the desired loading, Figure 2-6 and Eq. (2-37).

Table 2-4: Studies on lateral loading of drilled shafts

Researcher	Year	Type of Study	Study Overview
Reese and Welch	1975	Experimental	Development of soil subgrade reaction-displacement curves (p-y curves) in clay soils for use in the Winkler soil spring concept
Crowther	1990	Experimental	Modification of curves by Reese and Welch for use in frozen clay soils
Priestley et al.	1996	Analytical	Determination of inelastic rotation and ductility of a column/foundation shaft in cohesionless soils
Budek et al.	2000	Analytical	Parametric study on the inelastic seismic response of reinforced concrete bridge column/pile shafts in non-cohesive soils to simplify Winkler model. Verified against experimental and in-situ testing.
Chai	2002	Analytical	Analytical model for the flexural strength and ductility of drilled shafts subjected to lateral loads in cohesive and non-cohesive soils
Chai and Hutchinson	2002	Experimental	Experimental testing on full scale drilled shafts in cohesionless soils. Used to verify the analytical model proposed by Chai (2002)
Suleiman et al.	2006	Experimental	Experimental testing on full scale integrated column/foundation systems in cohesive soil to examine the effects of seasonal freezing on the lateral response.
Suarez and Kowalsky	2007	Analytical	Parametric study on cohesive and non-cohesive soils for the displacement-based seismic design of drilled shafts. Verified against experimentation by Chai and Hutchinson (2002)
Sritharan et al.	2007	Analytical	Parametric study to examine the effects of seasonal freezing in clay soils.
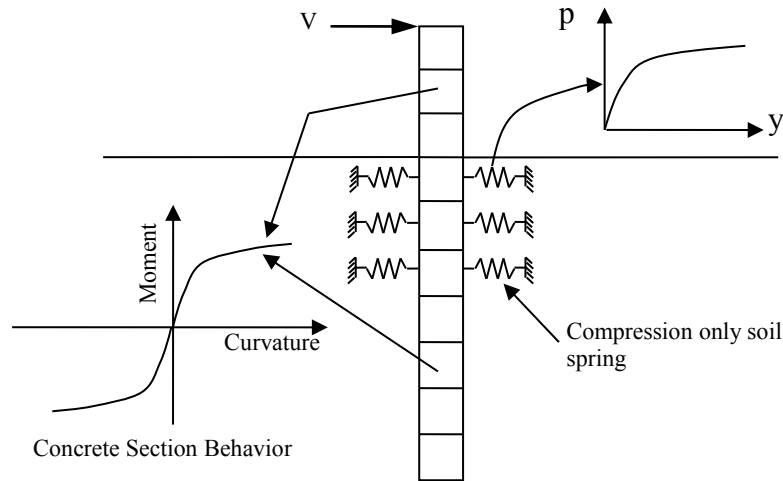
Figure 2-5: Winkler foundation model

Note:
$dV_v/dx = p$
$d^2M/dx^2 = EI(d^4y/dx^4)$
$p = -E_sy$
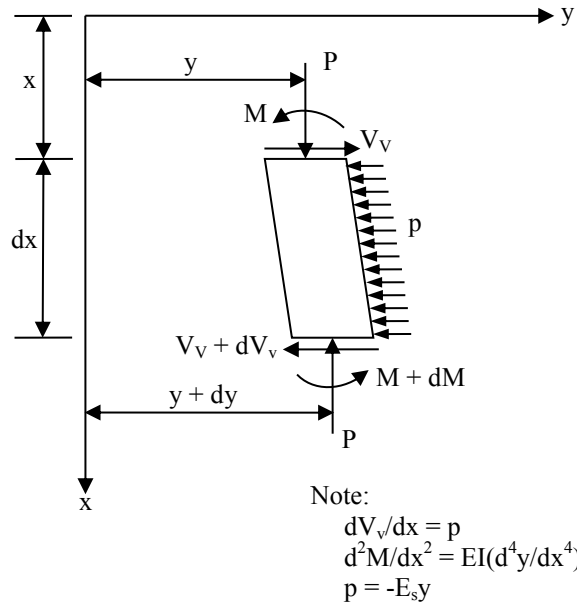
Figure 2-6: Beam-column element used in differential equation derivation

$$EI\frac{d^4y}{dx^4} + P\frac{d^2y}{dx^2} - p = 0; \quad p = -E_sy \qquad \text{Eq. (2-37)}$$

where, EI = flexural stiffness of foundation;
      y = lateral deflection of beam-column element and soil;
      x = length along foundation;
      P = axial load on column/foundation shaft
      E_s = soil modulus; and
      p = soil subgrade reaction.

A recent study performed by the research team at Iowa State University (Shelman et al. 2010) concluded that although a number of models were currently in existence for the simplification of accounting for SFSI a number of shortcomings still existed in the design of columns continuously supported on drilled shaft foundations in cohesive soils. These shortcomings consisted of:

- plastic action within the inelastic range of the system was generally underestimated as the analytical plastic hinge length in some models was based on experimentation in cohesionless soils;

- although recommended for use in cohesive soils, most of the current models were only verified against experimental testing performed in cohesionless soils as the engineering properties are easier to control;

- none of the current models considered the effects of seasonal temperature variation on material properties during their development;

- the maximum moment location was generally found to not coincide with that of a detailed analysis in cohesive soils; and

- localized effects (e.g., curvature and translation) at the point of the maximum moment were not accurately captured in most of the models although this is where the most damage will occur in an integrated column/foundation system subjected to design level or greater seismic events.

Identification of these shortcomings led to the development of a new equation based simplified model as presented in Appendix A. This model was developed as a cantilever supported on a flexible base at the point of maximum moment, Figure 2-7. The overall

height of the system was dictated at the maximum moment location as this would be a critical

location in seismic design to ensure that enough transverse confinement reinforcement would

be provided to attain the desired performance location. The flexible base consists of two

springs, one rotational and one translational, to capture the movement of the shaft occurring

below this point. The third spring in the model was included half-way between the ground

surface and maximum moment location to account for the resistance of the soil within this

region. The use of springs in this manner improved the versatility of the approach with

computer simulations.
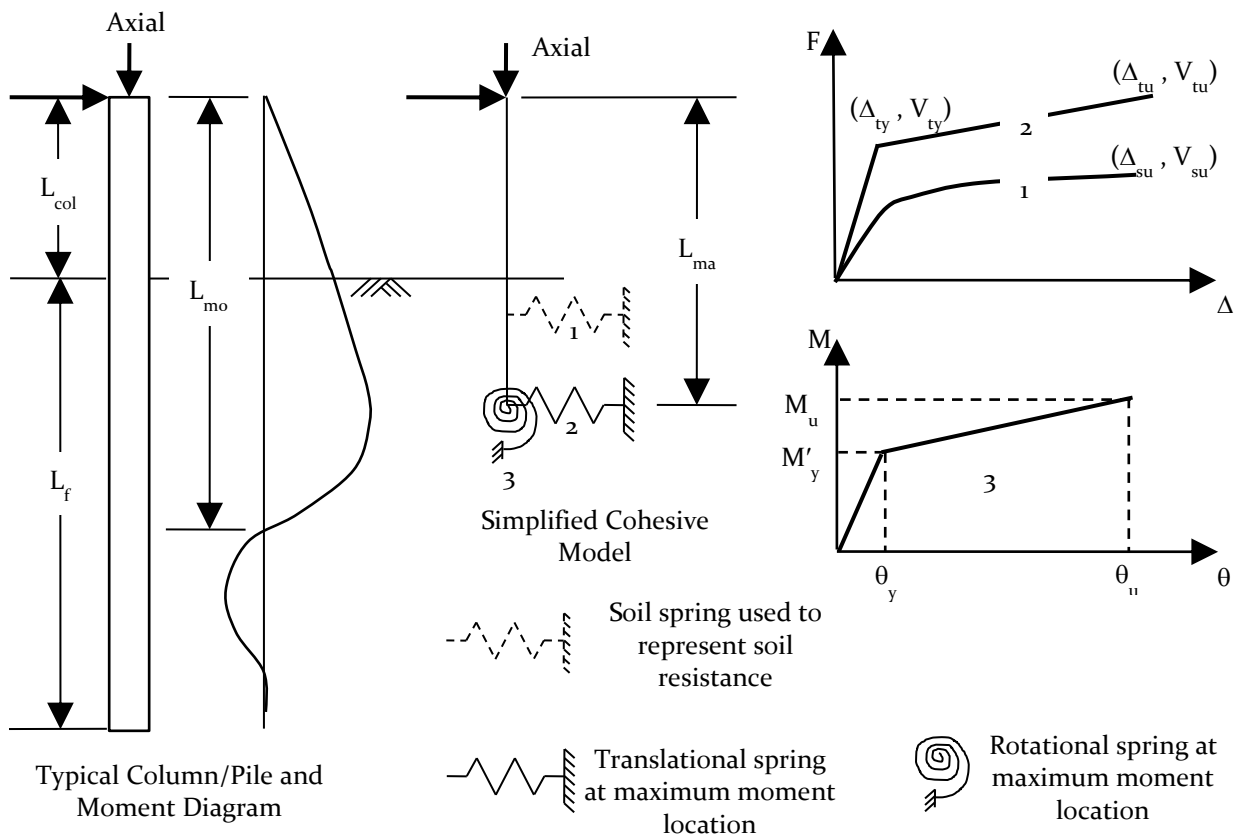
Figure 2-7: Proposed simplified model for SFSI in cohesive soils (reproduced from

Shelman and Sritharan 2013)

As with any proposed model, verification needed to be performed to ensure adequacy within the local and global response of the system. These verifications were performed against computer simulations as well as experimental testing of Suleiman et al. (2006) and Stewart et al. (2007). In all instances, the model was found to sufficiently capture the lateral load response of the system. A sample of the global verification to the experimental testing of Suleiman et al. (2006) is provided in Figure 2-8. This verification was provided herein to demonstrate the ability of the model to account for seasonal temperature variation and the large range of undrained shear strength that can be used with the model. The figure provides additional evidence as to the need for accounting for the fluctuations in temperature as noted by the change in lateral force and displacement at the first yielding and ultimate limit states used by the proposed method.
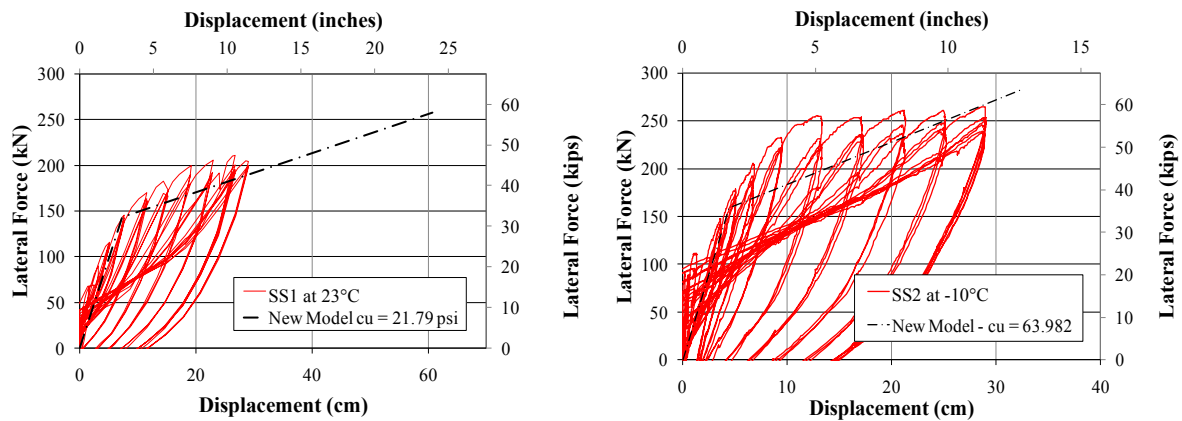
Figure 2-8: Graphical comparison of proposed simplified model with experimental testing of Suleiman et al. (2006)

2.5 Impact of Seasonal Freezing

Some of the largest earthquakes recorded in the history of the United States and the world have taken place during times of seasonal freezing. Examples include the New Madrid earthquake sequence of 1811-1812, the Great Alaska earthquake of 1964 ($M_L = 9.2$), the Nisqually earthquake of 2001 ($M_L = 6.9$) in Washington, and several large magnitude Hokkaido earthquakes in Japan. Although the occurrence of major future earthquakes cannot be predicted, seasonal temperature variations across the United States are well known. In areas expected to seasonally freeze, the following temperature variations are expected:

- Alaska: from -40 °C to 20 °C (variation of 110 °F),

- Midwest: from -20 °C to 20 °C (variation of ~75 °F),

- Eastern seismic region: from -20 °C to 20 °C (variation of ~75 °F), and

- Western seismic region: from -20 °C to 15 °C (variation of ~60 °F).

Despite these drastic temperature changes, they are not accounted for in routine design although SFSI and to a certain extent structural behavior will be greatly influenced. Understanding the influences of cold temperatures on the response of SFSI systems are critical within the field of seismic engineering to prevent undesirable failure modes in accordance with the capacity design philosophy.

2.5.1 *Effects of Seasonal Freezing*

In order to understand the effects of seasonal freezing on deep bridge pier foundations, Sritharan et al. (2007) undertook an exploratory research program into the lateral response of integrated bridge column/foundation systems with a CIDH shaft subjected to seasonal

freezing. The exploratory research program consisted of analytical and experimental

components. Following completion of the experimental investigation (Suleiman et al.,

2006), analytical studies were performed by Sritharan et al. (2007) and Wotherspoon et al.

(2010 a&b)

Based on the experimental data, a number of conclusions were drawn on the effects of

seasonal freezing to the lateral loading of integrated column/foundation systems. The

following conclusions were reported in Suleiman et al. (2006):

1. As expected, the continuous shaft increased the flexibility of the system due to the

    maximum moment forming below the ground surface.

2. With respect to the warm weather conditions, the cold weather system experienced

    the following changes in the lateral load response:

    - increased effective elastic stiffness by 170%,

    - increased lateral load resistance by 44%,

    - upward shift of the maximum moment location by 0.84 m (~33 in.),

    - reduced plastic region length by 64% in the foundation shaft, and

    - reduced the gap opening at the base of the column by 60%.

3. Seasonal wintry conditions must be accounted for in the seismic design of continuous

    column to drilled shaft foundations because of the drastic changes seen in the lateral

    response of these systems.

The analytical investigation undertaken by Sritharan et al. (2007) examined the

generalized effects of freezing temperatures and associated design implications on integrated

column/foundation systems. LPILE (2004), which uses the finite difference method and the Winkler soil spring concept, was used to complete the analytical portion. The soil spring properties were constructed based on the work of Reese and Welch (1975) with modifications based on the work of Crowther (1990). In regions not defined using "user-specified" curves, the soil springs were constructed by specifying the undrained shear strength, strain at fifty percent soil-strength, unit weight and a soil subgrade modulus for the predefined models available in LPILE (2004). The concrete properties were adjusted based on the work of Lee et al. (1988); while, the steel properties were adjusted based on the work of Filiatrault and Holleran (2001).

Using the above modifications, the analyses were run and compared to the experimental results as appropriate. These comparisons concluded that the modeling would accurately capture the effects of seasonally frozen conditions, allowing the remaining analyses at different temperatures to be legitimized. A number of conclusions were drawn from this study, which are as follows:

1. A 2-D model that uses beam-column elements to represent the column and foundation shafts and compression only springs satisfactorily captured the measured response of the column/foundation system in warm and freezing conditions. This correlates well with the design recommendations presented in AASHTO (2010 and 20012) in which a method involving soil springs is the primary recommendation.

2. With respect to warm weather conditions, the response of a column to drilled shaft system at -1 °C (30.2 °F) to -20 °C (-4 °F) will change the lateral response as follows:

   • increase the effective lateral stiffness by 40% - 188%,

- reduce the lateral displacement capacity by 17% - 63%,

- increase the lateral load resistance and shear demand in the column by 25% - 30%,

- increase the shear demand in the foundation shaft by 25% - 80%,

- shift the maximum moment location upwards by 0.54 m - 0.82 m, and

- reduce the length of plastic action in the foundation shaft by 19% - 68%.

3. The change in soil stiffness plays a more significant role in dictating the lateral response of column/foundations systems than the change in concrete and steel properties.

4. The depth of frozen soil and axial load do not greatly alter the response of the system in the frozen state (see Figure 2-9).
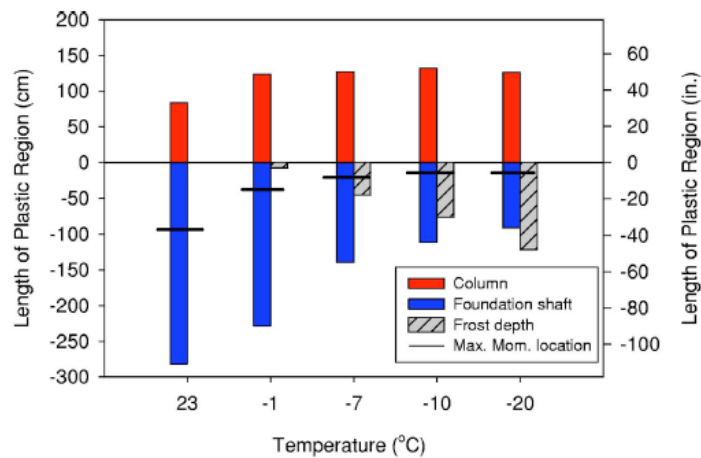
Figure 2-9: Frost depth, maximum moment location and plastic hinge length at ultimate condition for column-foundation shafts (Sritharan et al., 2007)

5. Seasonal freezing will significantly alter the seismic response of integrated bridge column-foundations systems. Therefore, unless these effects are accounted for in

design, they will have serious implications in areas where seasonal freezing occurs

around the world (see Figure 2-10).
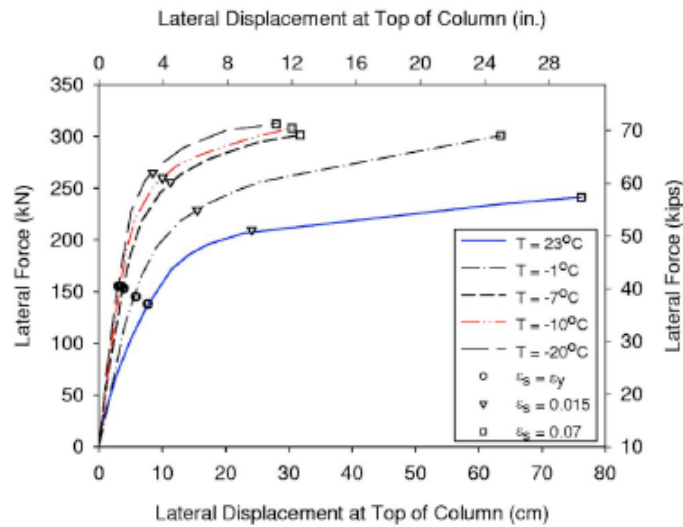
Figure 2-10: Global force-displacement response as temperatures decrease for a

column-foundation shaft system (Sritharan et al., 2007)

In addition to the monotonic analytical modeling performed by Sritharan et al. (2007),

analytical investigations were conducted by Wotherspoon et al. (2010 a&b) to construct a full

cyclic model of the lateral force-displacement response of the two systems examined by

Suleiman et al. (2006). The research was conducted using Ruaumoko (Carr 2005) and the

Winkler soil spring concept including the presence of gap opening and reattchment. The

structural behavior of the reinforced concrete column and foundation shafts were modeled

using experimental material properties through the use of moment-curvature responses

constructed using a fiber based approach available in OpenSees. Cyclic loading was applied

to the top of the column based on the experimental testing by applying increasing target

displacements with no less than three cycles at each target displacement.

Wotherspoon et al. (2010a) concluded that through the use of elements available in Ruaumoko, the full-scale cyclic response of a column/foundation shaft could successfully capture both summer and winter conditions for local and global behavior. This was accomplished by modeling structural nonlinearity, gap development and soil nonlinearity in compression. Global force-displacement comparisons used in the model validation are provided herein as Figure 2-11 and Figure 2-12. The modeling in Ruaumoko further validated the findings of Sritharan et al. (2007) in which the range of temperatures experienced by the system must be included in the design process to ensure adequate response during a seismic event.
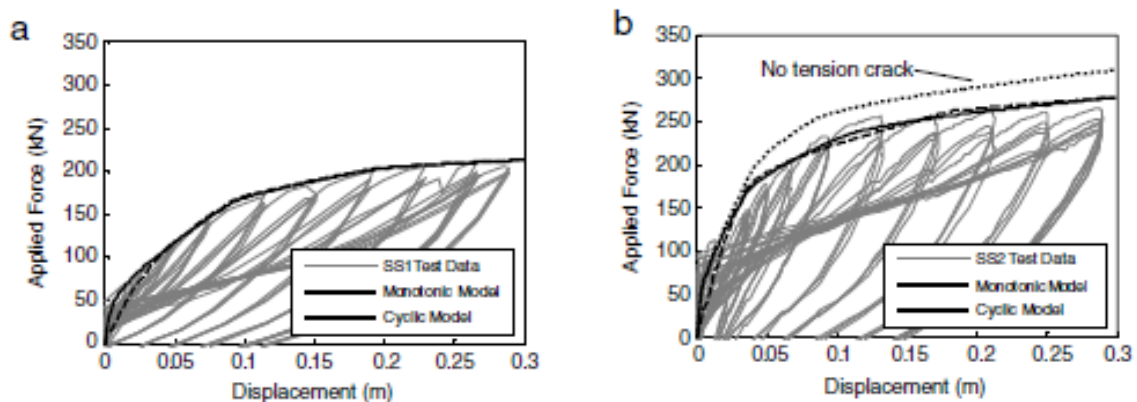
Figure 2-11: Comparison of the force-displacement characteristics at the column top for the monotonic and cyclic Ruaumoko models (a) warm testing; (b) cold testing
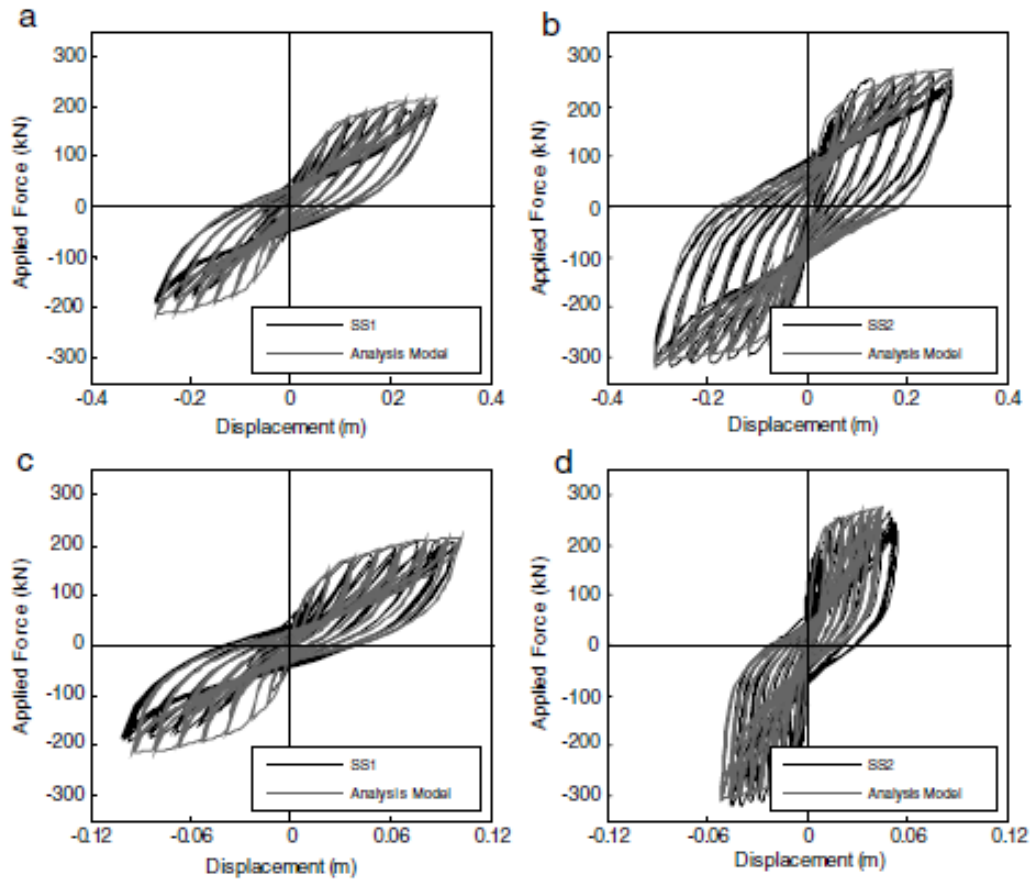
Figure 2-12: Cyclic force-displacement responses for (a) SS1 column top; (b) SS2 column top; (c) warm testing column base; (d) cold testing column base.

2.6 Broad Impacts

To better understand the broad impacts of seasonal freezing, an investigation was undertaken to examine the potential of seismic events and seasonal freezing to occur simultaneously within the United States and Japan (Sritharan and Shelman, 2008). In the United States, one commonly assumes that a significant freezing condition would only occur within the Central and Eastern United States and Alaska, but this is not an accurate assumption. In fact, a depth as small as 10 cm (4 in.) can alter the lateral loading response of

integrated bridge column/foundation systems according to Sritharan et al. (2007).

DeGaetano and Wilks (2001) suggested a depth of this nature can be expected in the seismic

region of the western United States including the northeastern part of California (see Figure

2-13). In Japan, the northern portion of Honshu Island and the Island of Hokkaido should

experience seasonal freezing and high seismic activity as well (see Figure 2-14).
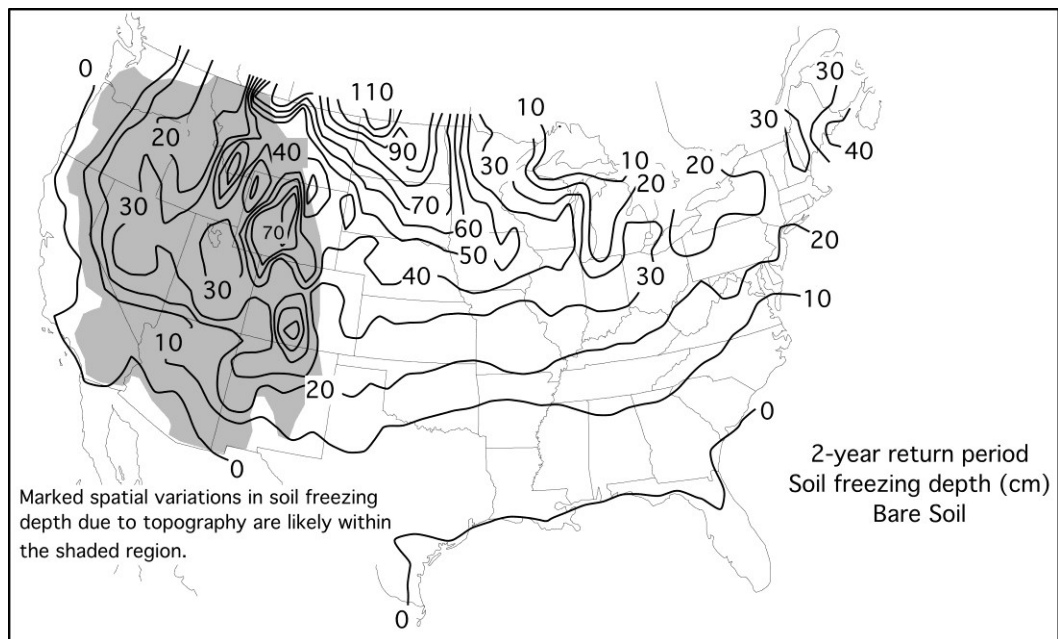
Figure 2-13: Frozen soil depth contours produced for a two-year return period by

DeGaetano and Wilks (2001)
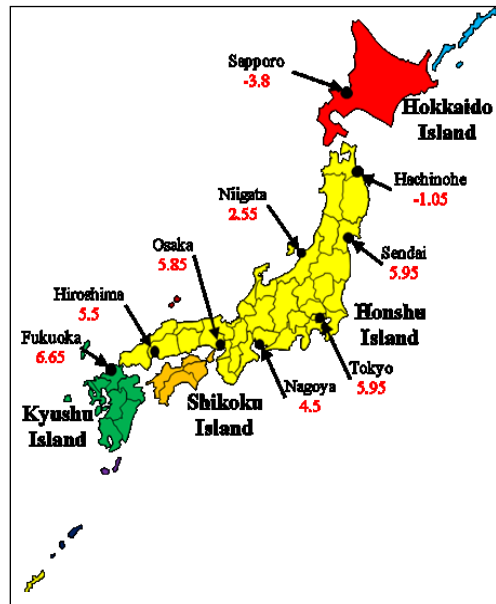
Figure 2-14: Average winter temperatures for Japan's larger cities (Japanese

   Meteorological Agency, 2009)

To better understand the significance of soil freezing and the seismic response of bridges,

an impact study was performed for the United States and Japan. For the United States, the

number of bridges within each state was determined and then compared to the frost depth

contour map in Figure 2-13 and a seismic hazard map. Due to a lack of information, it was

assumed that the number of bridges in a state were uniformly distributed, Figure 2-15. The

chosen seismic map for this study was the 0.2-second spectral acceleration map with a 10%

probability of exceedance in 50 years as published by the United States Geological Survey

(2002). With a limiting criterion that the bridges should experience at least 0.2g spectral

acceleration at a period of 0.2-second, 66,000 bridges were estimated to be in seismic

regions. Overlaying frost contours with the seismic hazard map, as shown in Figure 2-16,

found that the number of bridges that may experience both a minimum of 10 cm (~ 4 in.) of

frost depth and 0.2g spectral acceleration was approximately 50% of those in seismic regions. When only the minimum frost depth condition was used (i.e., the bridge site should experience a frost depth greater than or equal to10 cm [~ 4 in.]), over 400,000 bridges or two-thirds of all bridges in the U.S. were found to be affected by seasonally frozen conditions, yet this issue is seldom addressed in routine design methods.
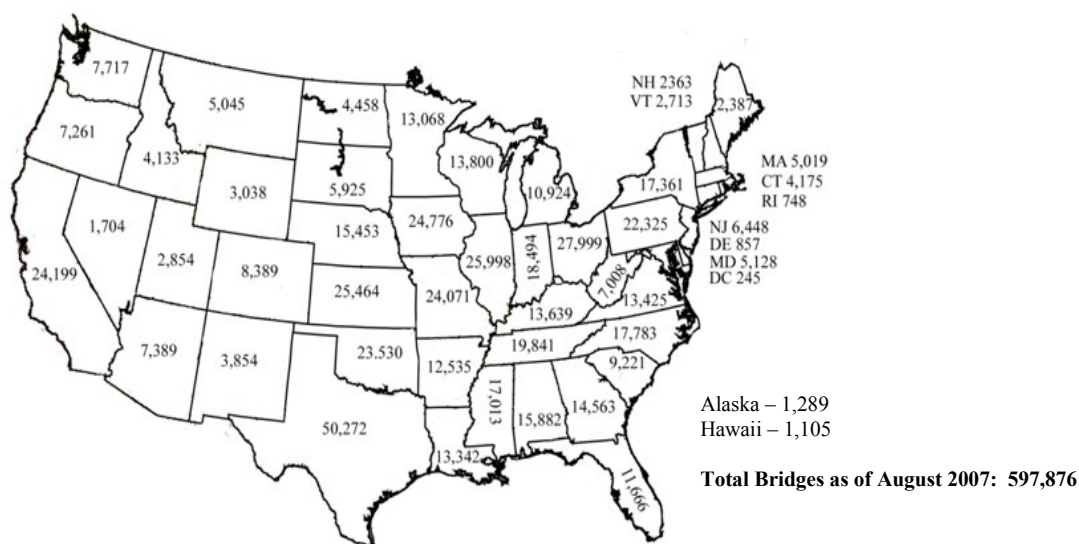
Figure 2-15: Statewide distribution of bridges in the United States (Bureau of Transportation Statistics, 2007)

Notes:
1. Hawaii omitted because of no frost concerns.
2. Entire State of Alaska would experience greater than 10cm frost depth
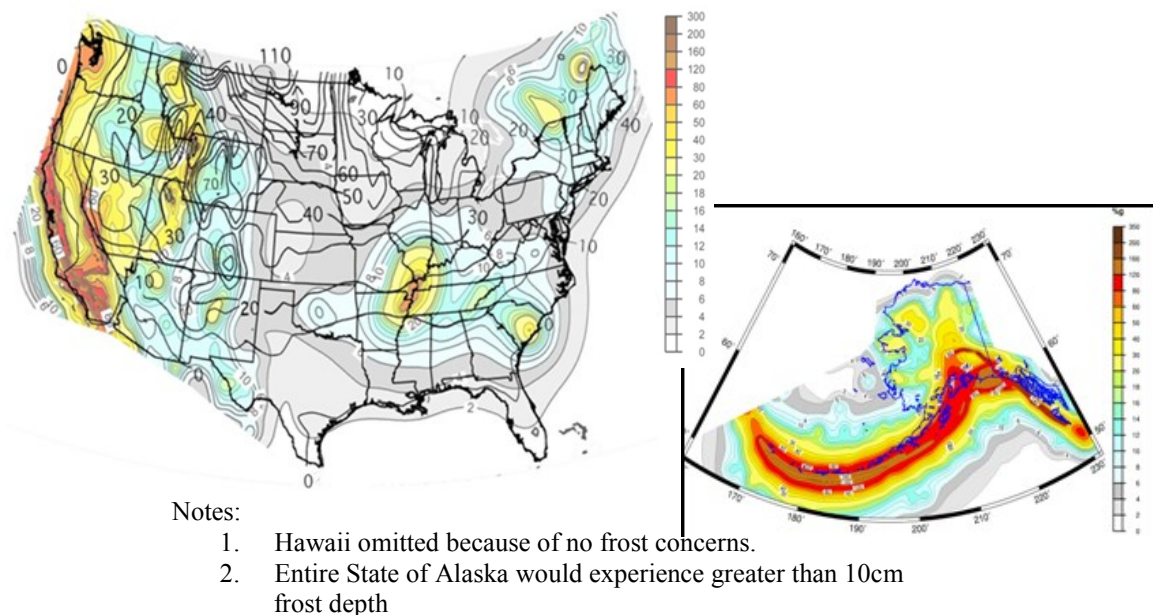
Figure 2-16: USGS seismic hazard map (2002) overlaid with frost depth contours shown in Figure 2-13

The broad impact study of Japan consisted of examining the average winter temperatures and comparing the locations of possible frozen soils to seismic hazards and population distribution. Figure 2-14 demonstrated the locations for possible frozen soils were Hokkaido Island and the northern part of Honshu Island. Within this region, seismic hazards were found, using the National Earthquake Information Center's historical and present data, and compared with the frozen soils area. With this information, the population distribution was examined to provide a qualitative risk estimate, as bridge locations were unavailable. It was noted that some major cities were located within this region, such as Sapporo. A final map correlating with Figure 2-14 was produced that shows the population distribution and seismic events in the area in Figure 2-17. It appears that bridges in four major cities and the south-eastern part of the island may be affected by both earthquakes and seasonally frozen

conditions. This area was verified as a high seismic region in the recent 2011 Tohoku

earthquake as this event corresponded well to this predicted region.
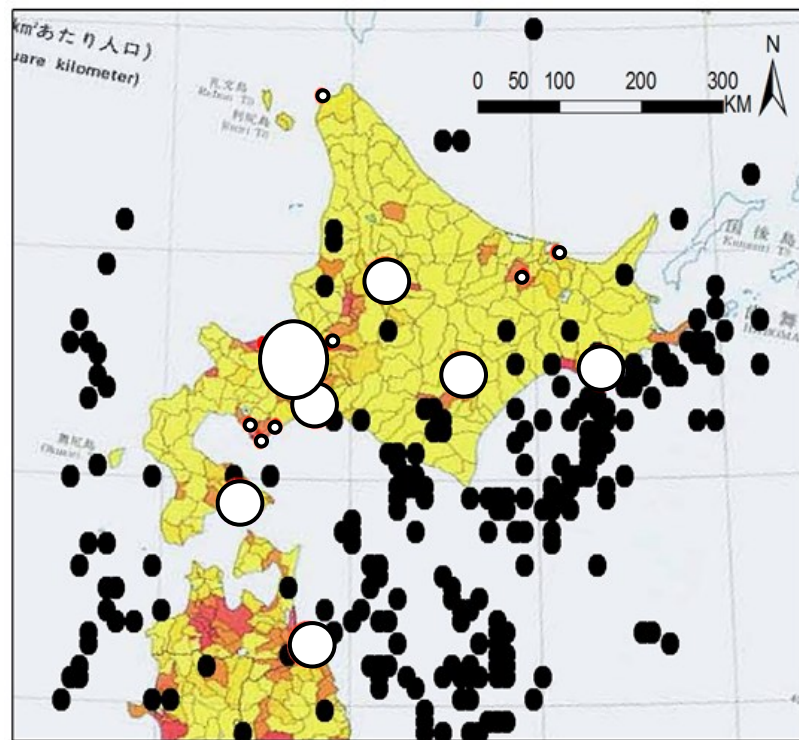
Key:
1. Small black circles are magnitude 5.5 or greater earthquakes
2. Open circles are population centers of 35,000 to 1.8 million persons

Figure 2-17: Seismic activity of Japan near Hokkaido Island circa year 2000

2.7 Material Behavior

When examining the lateral response of columns supported on CIDH shafts, the material

behavior must be defined for concrete, soil and steel. These definitions are even more

critical during times of seasonal freezing in which material properties are markedly different

from warm weather conditions. The section below provides information on the studies

performed in freezing conditions for soil and concrete. These studies are critical to

understand the local response of a confined concrete member so the moment-curvature response is correctly captured. Steel will not be presented in this work as a recent study at Iowa State University by Levings and Sritharan (2012) conducted similar work and will not be discussed further within this dissertation.

2.7.1 *Concrete*

Sritharan et al. (2007) demonstrated in an exploratory research program that concrete material properties will change as temperature decreases. Although they state that these changes in the material properties do not cause as significant an impact as the change in soil properties, they must be accounted for to correctly handle the effects of seasonal freezing in design. Currently, a limited amount of research is present to show the influence of cold temperatures, as warm weather conditions are generally used for the design process. The following section will discuss prior research that has been completed on the effects of cold temperatures to concrete material properties.

Sehnal et al. (1983)

Prior research in material testing of concrete has shown that as temperature decreases the compressive strength, elastic modulus and bond strength of concrete increases. Sehnal et al. (1983) demonstrated that as temperature decreased, concrete compressive strength increased according to a polynomial curve in normal strength concrete. The curve produced by this study, reproduced in Figure 2-18, showed that between 20 °C (68 °F) and -25 °C (-13 °F) an increase of 25% in compressive strength could be expected. Although experimentation was performed on 41.4 MPa (6 ksi) concrete, it was assumed that this was applicable over varying strengths as the testing was performed on plain Type II Portland cement concrete for

a w/c ratio of 0.6 which is high for typical bridge designs throughout Alaska and the United States. They also provided evidence, based on statistical modeling, that the rate at which concrete test specimens were cooled to testing temperature was independent of the compressive strength (1983).
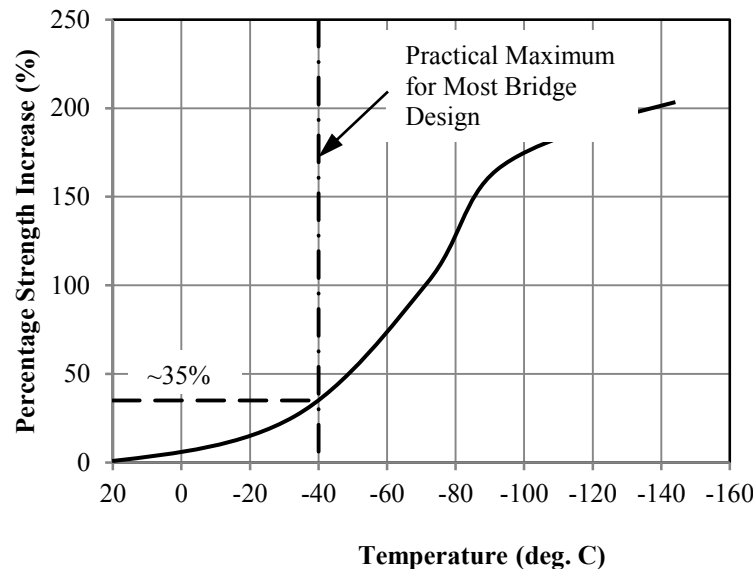
Figure 2-18: Percentage increase of concrete strength with reduction in temperature

(after Sehnal et al., 1983)

Lee et al. (1988)

The information provided by Sehnal et al. (1983) was furthered in 1988 by Lee et al. (1988a). This research demonstrated the compressive strength increased in a polynomial manner as suggested by Sehnal et al. (1983). Lee et al. (1988a) further concluded the modulus of elasticity and bond strength would increase at lower temperatures. These researchers noted that the increase in modulus of elasticity occurred at a slower rate than the rate of increase of concrete compressive strength (e.g., at -70 °C [-94 °F] the compressive

strength increased by 151.3% compared with the elastic modulus increase of 114.7%). This rate of decrease is as expected, as most codes suggest E_c is a function of the square root of the unconfined compressive strength. The bond strength in confined concrete was also noted to increase with lower temperatures, since bond strength is correlated with the unconfined compressive strength of concrete. In the study it was found that at -70 °C [-94 °F] the bond strength would increase by 145.1% compared with the 128.6% increase of the concrete compressive strength. The data also demonstrate a non-uniform increase of bond strength was experienced as temperature decreased from ambient room temperature.

In a follow-up paper published by Lee et al. (1988b), the effects of high strength concrete at low temperatures provided conclusions in terms of compressive strength, modulus of elasticity and bond strength. The main conclusions drawn were that the respective properties increased at a similar rate to that of normal strength concrete; however, the percent of increase tended to be lower than those of normal strength concrete at similar temperatures. This difference may be due to the variation in water to cement ratio between the normal strength, w/c = 0.48, and high strength, w/c = 0.35, tests; however, the authors do not provide any reasons for the differences experienced between the two types of concrete.

In the two papers published by Lee et al. in 1988 (a & b), the researchers expanded the information available on Poisson's ratio. They reported that the past studies conclude Poisson's ratio should be taken to be approximately 0.20 regardless of compressive strength and that Poisson's ratio will decrease as the compressive strength of the concrete increases. This suggests that no matter the temperature of concrete a constant value of 0.20 should be used for Poisson's ratio in concrete. However, Lee et al. (1988a, 1988b) has shown in both

normal strength concrete and high strength concrete that as temperature decreases and unconfined compressive strength increases, the Poisson's ratio will increase. The researchers provide data that suggest that at a temperature as low as -70 °C [-94 °F], Poisson's ratio will increase by approximately 50% in normal strength concrete and 25% in high strength concrete with interpolation required to attain increases at other subzero temperatures.

2.7.2 *Soil*

Frozen soil can be both an advantage and disadvantage when designing or constructing a structure in civil engineering projects. This is the case, as the inherent impervious nature of ice within the frozen soil construct allows for weak and soft soils to be bridged temporarily for stabilizing slips, underpinning structures, sampling weak or non-cohesive soils, temporary roads, protecting sensitive equipment and many other advantages (Harris 1995). All of these benefits rely on the stiffening of soil which is a concern for the seismic design of columns supported on drilled shafts as previously shown. Thus, the mechanical properties of the soil must be adequately established.

To define engineering properties correctly, the effects of moisture content and ice on the unconfined compressive strength of concrete must be understood. According to Tsytovich (1975), the range in which water experiences a significant phase transformation, the factors determining the strength of frozen soils, both seasonally and permanently, are the overall amounts of ice and unfrozen water and how they vary with temperature. The range discussed in Tystovich (1975) was suggested as 0 °C to -0.5 °C (32 °F to 31.1 °F) for sandy soils and 0 °C to -5 °C (32 °F to 23 °F) for clayey soils. The variation of unfrozen water content with temperature for different soils was examined during a project undertaken by Williams

(1988). The data attained during this investigation, Figure 2-19, demonstrate that between 0 °C to -5 °C (32 °F to 23 °F) the amount of unfrozen water in a soil specimen will change rapidly as the water undergoes a phase change from a liquid to a solid. In addition, the information provided suggests the rate of change in the unfrozen water content is a function of the soil type which is most likely due to the variation in the molecular structures.

After understanding the formation of ice in soil, the next step is to examine how the overall freezing of the soil affects engineering properties (e.g., compressive strength and modulus of elasticity). In 1978, Andersland and Anderson provided a summary of the work conducted by Sayles (1966 and 1968) on the effects of temperature on the unconfined compressive strength of soils. This summary was provided graphically and is provided here as Figure 2-20. Figure 2-20 shows that as temperature decreases from 0 °C (32 °F) to approximately -150 °C (-238 °F) an overall increase in the unconfined compressive strength of the soil occurs. In addition to the soil curves, three curves representing the increase in compressive strength of ice were provided to demonstrate the hardening that takes place with temperature. The combination of soil and ice curves demonstrates the influence of ice forming within the pores of the soil contributes to the overall unconfined compressive strength gain. However, the figure also provides evidence suggesting that as temperatures decreases, the influence of ice reduces and the contact between the microscopic particles has a direct impact on the unconfined compressive strength of soil.
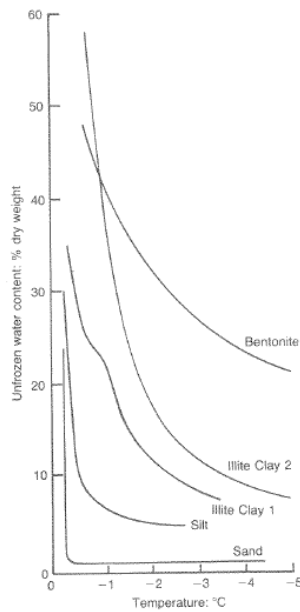
Figure 2-19: Typical curves of unfrozen water content against temperature (after

Williams, 1988) [Harris, 1995]
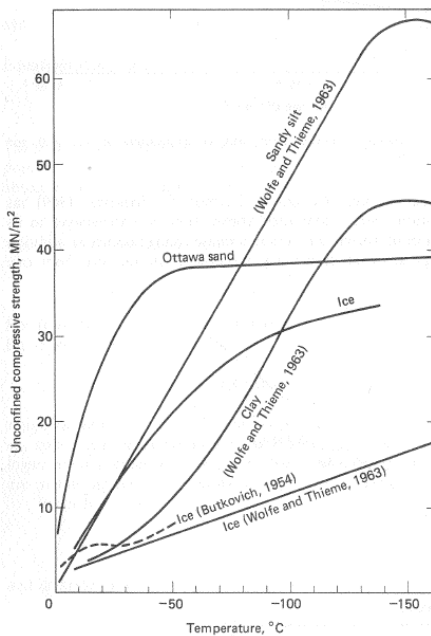
Figure 2-20: Temperature dependence of unconfined compressive strength for several

frozen soils and ice (after Sayles, 1966) [Andersland and Anderson, 1978]

Besides the work performed by Sayles (1966), Tsytovich (1975) provided a table, Table

2-5, on past investigations that noted the increase in ultimate compression strength of soil

when subjected to freezing temperatures. Additional information was provided by Tsytovich

(1975) on the temperature effects on the strength of permafrost, but the data sets have not

been included due to the focus of the report being on seasonally frozen ground.

Table 2-5: Ultimate strength of frozen soils in uniaxial compression (after Tsytovich, 1975)

Designation of Soil	Total Moisture W_d, %	Temperature °C (°F)	Strength σ_{ul}, MPa (tsf)	Investigator
Quartz sand (100% content of 1 – 0.05 mm fraction)	14.7	-1.8 (28.8)	6.08 (63.5)	N. A. Tystovich (1930)
	14.3	-3.0 (26.6)	7.65 (79.9)	
	14.0	-6.0 (21.2)	9.71 (101.4)	
	14.1	-9.0 (15.8)	11.57 (120.8)	
	14.9	-12.0 (10.4)	13.14 (137.2)	
	14.3	-20.0 (-4)	14.91(155.7)	
Silty sandy loam (61.2% of 0.05 – 0.005 mm fraction; 3.2% < 0.005 mm)	21.6	-0.5 (31.1)	0.88 (9.2)	N. A. Tystovich (1940)
	23.1	-1.8 (28.8)	3.53 (36.9)	
	22.1	-5.1 (22.8)	7.65 (79.9)	
	21.3	-10.3 (13.5)	12.55 (131.1)	
Clay (50% content of < 0.005 mm fraction)	34.6	-0.5 (31.1)	0.88 (9.2)	N.A. Tystovich (1940)
	36.3	-1.6 (29.1)	1.27 (13.3)	
	35.0	-3.4 (25.9)	2.26 (23.6)	
	35.3	-8.2 (17.2)	4.41 (46.1)	
Quartz sand (100% content of 1 – 0.05 mm fraction	16.7	-20.0 (-4)	14.71 (153.6)	N. K. Pekarskaya (1966)
Cover Clay (44.3 content of < 0.005 mm fraction)	32.0	-20.0 (-4)	8.92 (93.2)	N. K. Pekarskaya (1966)

Tsytovich (1975) furthered the information on frozen soils through an examination of the

tensile strength of soil, both instantaneously and long term. This data set, Table 2-6, suggests

that as temperature decreases the tensile strengths of soil will increase. Therefore, when a

system is subjected to a lateral load during a time of seasonal freezing, larger tensile cracks

will form, decreasing the soil confinement on the foundation shaft.

Table 2-6: Instantaneous and ultimate long-term tensile strengths of frozen soils (after Tsytovich, 1975)

Designation of Soil	Total Moisture W_d, %	Temperature °C (°F)	Strength, σ_{inst} MPa (tsf)	Strength, σ_{lt} MPa (tsf)	Investigator
Clay (45% content of fraction < 0.005 mm)	19.4	-1.2 (29.8)	0.96 (10.0)	--	N. A. Tsytovich (1952)
	19.4	-2.5 (27.5)	1.65 (17.2)	--	
	19.4	-4.0 (24.8)	2.12 (22.1)	--	
Cover Clay	32.0	-2.0 (28.4)	1.13 (11.8)	--	N. K. Pekarskaya (1966)
	32.0	-5.0 (23.0)	1.35 (14.1)	--	
	32.0	-10.0 (14.0)	2.60 (27.1)	--	
Heavy loam (22.5% content of fraction < 0.005 mm)	31.8	-3.0 (26.6)	1.18 (12.3)	0.25 (2.7)	S.E. Grechishchlev (1963)
Heavy sandy loam	34.0	-4.0 (24.8)	1.67 (17.4)	0.20 (2.0)	N. A. Tsytovich (1952)
Quartz Sand	17.0	-2.2 (28.0)	0.62 (6.5)	--	N. K. Pekarskaya (1966)
	17.0	-5.0 (23.0)	0.77 (8.1)	--	
	17.0	-10.0 (14.0)	1.57 (16.4)	--	

In addition to the temperature being a significant contributor to the ultimate compressive

strength of the soil, the total moisture content of the soil will influence the strength.

Tsytovich (1975) found that as the moisture content increases the ultimate compressive

strength of the soil will increase until just short of complete water saturation and decrease

thereafter, similar to unfrozen soil. Tsytovich's figure is provided within this report as

Figure 2-21.

Harris (1995) further expanded on the strength of frozen soil by providing information on

the work of Zhu and Carbee (1984) performed on frozen silt (Plasticity Index, $I_p = 4$). The

work concluded that as the strain rate applied to the specimens increased the strength of the soil increased, as shown in Figure 2-22. Additionally, Figure 2-22 shows the failure mode of the silt switched from a ductile failure at slower rates of loading to a more brittle failure at the higher rates of loading. A closer examination of the data provided evidence to suggest that the sharp bend in the stress-strain curves at less than 1% strain is most likely due to the cracking of the ice matrix.

The elastic modulus of soil is a major component when determining the deformation of the soil, as this property dictates the initial portion of a p-y curve. Tsytovich (1975) examined the effects of negative temperatures on the modulus of elasticity of soil. This investigation found that as temperature decreased the elastic modulus would increase as expected, since the soil modulus of elasticity is proportional to soil strength. Tsytovich found that the modulus could be predicted by a power series or a third order polynomial function, as depicted by the data shown in Figure 2-23. However, if the temperature of the specimen is not within the phase changing range of water a linear approximation can be used with coefficients determined using experimental means. It was also noted that the applied external pressure will influence the coefficients used to determine modulus of elasticity through the suggested relationships.
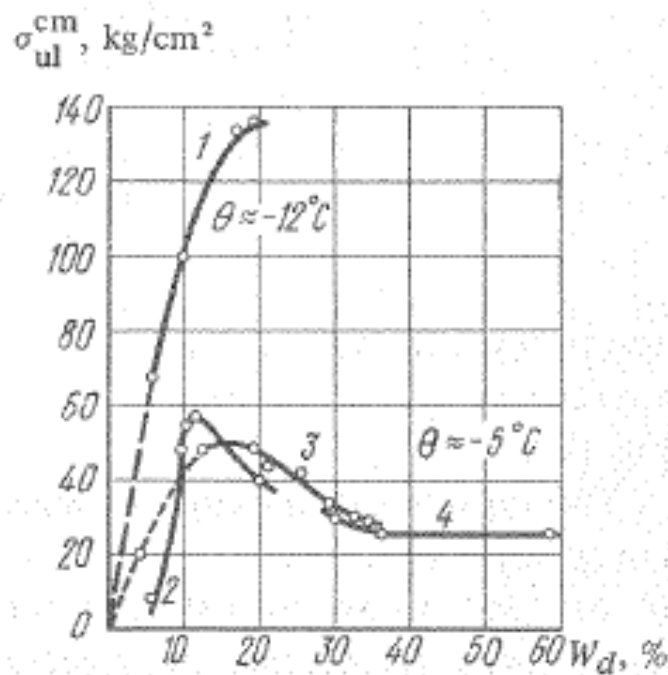
Figure 2-21: Ultimate compressive strength of frozen soils as a function of their total moisture content: (1) sand; (2) sandy loams; (3) clay (51% content of 0.005 mm fractions); (4) silty clay (63% content of fraction < 0.005 mm). [Tsytovich, 1975]

Another deformation component examined by Tsytovich (1975) was Poisson's coefficient to examine the effects of temperature on the lateral elastic deformation of soil. This examination was performed using direct measurements of experimental test specimens. Data retrieved from this testing, Table 2-7, show that as temperature decreases Poissson's ratio will substantially reduce. In addition, the data demonstrate that as the temperature approaches 0 °C (32 °F) the coefficient approached 0.5, similar to an ideal plastic body at lower temperatures.
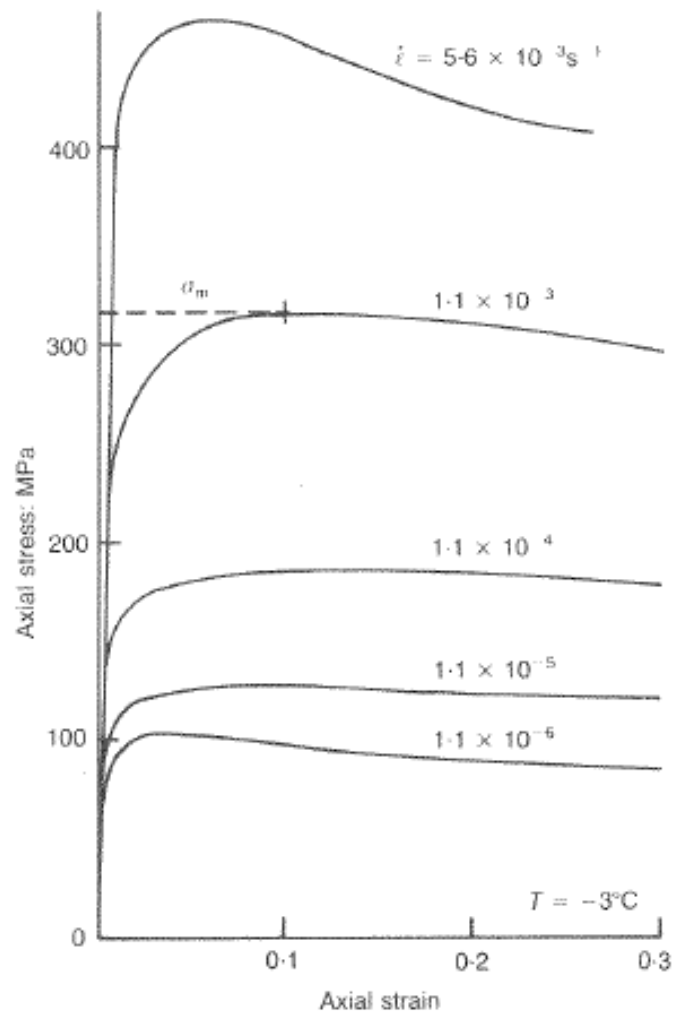
Figure 2-22: Stress-strain curves for uniaxial compression of a remoulded silt (after

Zhu and Carbee, 1984) [Harris, 1995]
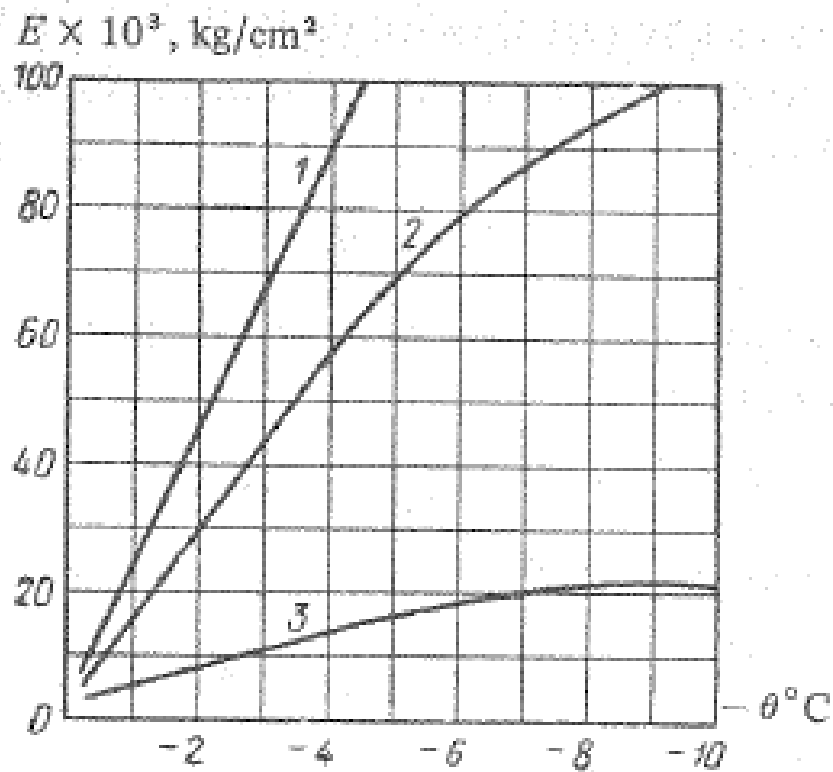
Figure 2-23: Modulus of normal elasticity E, kg/cm², of frozen ground at constant

pressure σ = 2 kg/cm². (1) Frozen sand; (2) frozen silty soil; (3) frozen clay.

(Tsytovich, 1975)

Table 2-7: Values of Poisson's coefficient for frozen soils (after Tsytovich, 1975)

Designation of Soil	Total Moisture W_d, %	Temperature °C (°F)	Axial Stress, σ_t MPa (tsf)	Poisson's Coefficient
Frozen Sand	19.0	-0.2 (31.6)	0.20 (2.0)	0.41
	19.0	-0.8 (30.6)	0.59 (6.1)	0.13
Frozen Silty Loam	28.0	-0.3 (31.5)	0.15 (1.5)	0.35
	28.0	-0.8 (30.6)	0.20 (2.0)	0.18
	25.3	-1.5 (29.3)	0.20 (2.0)	0.14
	28.7	-4.0 (24.8)	0.59 (6.1)	0.13
Frozen Clay	50.1	-0.5 (31.1)	0.20 (2.0)	0.45
	53.4	-1.7 (28.9)	0.39 (4.1)	0.35
	54.8	-5.0 (23.0)	1.18 (12.3)	0.26

2.8 References

American Association of State and Highway Transportation Officials (AASHTO). (2012). *LRFD Bridge Design Specifications, customary U.S. units 6th Edition.* Washington D.C.: AASHTO.

AASHTO (2010). *Guide Specifications for LRFD Seismic Bridge Design 1st Edition with 2010 Interim Revisions.* Washington D.C.: AASHTO.

American Concrete Institute (ACI). (2008). *Building Code Requirements for Structural Concrete (ACI 318-08) and Commentary (ACI 318R-08).* Farmington Hills, MI: ACI.

Andersland, O. B. and Anderson, D. M. (1978). *Geotechnical engineering for cold regions.* U.S.A.: McGraw-Hill Inc.

Applied Technology Council (ATC). (1996). *Improved Seismic Design Criteria for California Bridges: Provisional Recommendations.* Redwood City, CA: Applied Technology Council.

Bayrak, O. and Sheikh, S. (2004). "Seismic Performance of High Strength Concrete Columns Confined with High Strength Steel." *Proceedings of the 13th World Conference on Earthquake Engineering.* Vancouver, B.C., Canada: IAEE

Budek, A. M., Priestley, M. J. N. and Benzoni, G. (2000). "Inelastic seismic response of bridge drilled-shaft rc pile/columns." *Journal of structural engineering* 126(4): 510-517.

Bureau of Transportation Statistics. (Accessed Online: 2007). "Conditions of U.S. Highway Bridges By State." Washington D.C.: United States Department of Transportation. http://www.bts.gov/current_topics/2007_08_02_bridge_data/html/bridges_by_state.html

California Department of Transportation (Caltrans). (2003). *Bridge Design Specifications.* Sacramento, CA: Caltrans.

Caltrans. (2010). *Seismic Design Criteria Version 1.6.* Sacramento, CA: Caltrans.

Canadian Standards Association. (1994). *Code for Design of Concrete Structures for Buildings (CAN3-A23.3-M94).* Rexdale, Ontario, Canada: Canadian Standards Association.

Carr, A. J. (2005) *3D Ruaumoko: inelastic three-dimensional analysis program.* Christchurch, NZ: University of Canterbury – Department of Civil Engineering.

Chai, Y. H. (2002). "Flexural strength and ductility of extended pile-shafts I: Analytical model." *Journal of structural engineering* 128(5): 586-594.

Chai, Y. H. and Hutchinson, T. C. (2002). "Flexural strength and ductility of extended pile-shafts II: Experimental study." *Journal of structural engineering* 128(5): 595-602.

Crowther, G. S. (1990). "Analysis of laterally loaded piles embedded in layered frozen soil." *Journal of geotechnical engineering* 116(7): 1137-1152.

DeGaetano, A. T., and Wilks, D. S. (2001). "Development of Frost Depth Maps for the United States." *Research report.* Upper Marlboro, Maryland: National Association for Home Builders (NAHB) Research Center, Inc.

Filiatrault, A. and Holleran, M. (2001a). "Stress-strain behavior of reinforcing steel and concrete under seismic strain rates and low temperatures." *Materials and structures* 34: 235-239.

Filiatrault, A. and Holleran, M. (2001b). "Characteristics of reinforced concrete bridge components under seismic strain rates and low temperatures." *Proceedings of the 18th US-Japan bridge engineering workshop, St. Louis.* FHWA: 49-63.

Harris, J. S. (1995). *Ground freezing in practice.* London, England: Thomas Telford Services Ltd.

Hetenyi, M. (1946). *Beams on elastic foundation.* Ann Arbor, Michigan: University of Michigan Press.

Japanese Meteorological Agency. (Accessed Online: August 2008). Accessed at: http://www.jma.go.jp/jma/indexe.html

Japan Society of Civil Engineers. (2010). *Standard Specifications for Concrete Structures 2007 – "Design"* (JGC No. 15). Japan: Japan Society of Civil Engineers.

Lee, G. C., Shih, T. S. and Chang, K. C. (1988a). "Mechanical properties of concrete at low temperature." *Journal of cold regions engineering* 2(1): 13-24.

Lee, G. C., Shih, T. S. and Chang, K. C. (1988b). "Mechanical properties of high-strength concrete at low temperature." *Journal of cold regions engineering* 2(4): 169-178.

Levings, J. and Sritharan, S. (2012). "Effects of cold temperature and strain rate on the stress-strain behavior of ASTM A706/A706M mild steel reinforcement." *Journal of materials in civil engineering (In publication)*

Mander, J., Priestley, M. and Park, R. (1988). "Theoretical Stress-Strain Model for Confined Concrete". *Journal of Structural Engineering* 114(8): 1804-1826. USA: American Society of Civil Engineers.

Mander, J., Priestley, M. and Park, R. (1988). "Observed Stress-Strain Behavior of Confined Concrete". *Journal of Structural Engineering* 114(8): 1827-1849. USA: American Society of Civil Engineers.

Missouri Department of Transportation (MODOT). (Accessed Online: May 2012). *Engineering Policy Guide.* Missouri, USA: MODOT. Accessed at: epg.modot.org.

North Carolina Department of Transportation (NCDOT). (Accessed Online: May 2012). North Carolina, USA: NCDOT. Accessed at: www.ncdot.gov.

Park, R. (1996). "The Revised New Zealand Concrete Design Standard." *Proceedings of the Eleventh World Conference on Earthquake Engineering – Acapulco, Mexico*. Mexico: Elsevier Science Ltd.

Priestley, M. J. N., Seible, F. and Calvi, G. M. (1996). *Seismic Design and Retrofit of Bridges*. New York: John Wiley & Sons, Inc.

Reese, L. C. and Welch, R. C. (1975). "Lateral loading of deep foundations in stiff clay." *Journal of geotechnical engineering division* 101(GT7): 633-649.

Reese, L. C., Wang, S. T., Isenhower, W. M., Arrellaga, J. A. and Hendrix, J. (2004). *LPILE plus 5.0, user's manual.* Austin: Ensoft, Inc.

Reese, L. C., Wang, S. T.. Isenhower, W. M. and Arrellaga, J. A. (2004). LPILE plus 5.0, *technical manual.* Austin: Ensoft, Inc.

Sayles, F. H. (1966). "Low temperature soil mechanics." *Technical note.* Hanover, N.H.: Cold regions research and engineering laboratory.

Sayles, F. H. (1968). "Creep of frozen sands." *Technical Report 190.* Hanover, N.H.: Cold regions research and engineering laboratory.

Sehnal, Z. A., Kronen, H. and Marshall, A. L. (1983). "Factors influencing the low temperature strength of concrete." *Proceedings 2nd international conference on cryogenic concrete, Amsterdam.* London: Concrete Society of UK. pp. 1-11.

Shelman, Aaron, Levings, Jared and Sritharan, Sri. (2010). Seismic Design of Deep Bridge Pier Foundations in Seasonally Frozen Ground: *Final Report # UAF08-0033*. Fairbanks, Alaska: Alaska University Transportation Center.

South Carolina Department of Transportation (SCDOT). (2008). *Seismic Design Specifications for Highway Bridges Version 2.0*. Columbia, SC: SCDOT.

Sritharan, S. (2005). "Strut-and-tie analysis of bridge Tee joints subjected to seismic actions." *Journal of Structural Engineering* 131(9): 1321 - 1333

Sritharan, S., Suleiman, M. T. and White, D. J. (2007). "Effects of seasonal freezing on bridge column-foundation-soil interaction and their implications." *Earthquake spectra* 23(1): 199-222.

Sritharan, S. and Shelman, A. (2008). "An assessment of broad impact of seasonally frozen soil on seismic response of bridges in the U.S. and Japan." *Proceedings of the 24th US-Japan bridge engineering workshop, Minneapolis.* FHWA: 429-440.

Standards New Zealand. (1995). *The Design of Concrete Structures (NZS 3101:1995).* Wellington, New Zealand: Standards New Zealand.

Standards New Zealand. (2008). *Concrete Structures Standard: Part 1 – The Design of Concrete Structures (NZS 3101: 2008).* Wellington, New Zealand: Standards New Zealand.

Suarez, V. and Kowalsky, M. J. (2007). "Displacement-based seismic design of drilled shaft bents with soil-structure interaction." *Journal of earthquake engineering* 11: 1010-1030.

Suleiman, M. T., Sritharan, S. and White, D. J. (2006). "Cyclic lateral load response of bridge column-foundation-soil systems in freezing conditions." *Journal of structural engineering* 132(11): 1745-1754.

Tanabe, T. (1999). *Comparative Performances of Seismic Design Codes for Concrete Structures.* New York, USA: Elsevier.

Transit New Zealand. (2005). *Bridge Manual Second Edition with July 2005 Amendments.* Wellington, New Zealand: Transit New Zealand.

Tsytovich, N. A. (1975). *The mechanics of frozen ground.* U.S.A.: Scripta Book Company

United States Geological Service. (2002). (Accessed Online: August 2008). "0.2 second spectral acceleration with a 10 percent probability of exceedance in 50 years seismic hazard map." *USGS.* Accessed at: http://earthquake.usgs.gov/research/hazmaps/products_data/2002/maps/.

United States Geological Service (USGS). (Accessed Online: May 2012). Earthquake Hazards Program. Washington D.C., USA: USGS. Accessed at: earthquake.usgs.gov.

Watson, S., Zahn, F. A. and Park, R. (1994). "Confining Reinforcement for Concrete Columns". *Journal of Structural Engineering* 120(6): 1798-1824. USA: American Society of Civil Engineers.

Williams, P. J. (1988). "Thermodynamic and mechanical conditions within frozen soils and their effects." *Proceedings of the 5th International Conference on Permafrost, Trondheim.* International Permafrost Association: 493-498

Wotherspoon, L. M., Sritharan, S. and Pender, M. J. (2010a). "Modeling the response of cyclically loaded bridge columns embedded in warm and seasonally frozen soils." *Engineering structures journal* 32:933-943.

Wotherspoon, L. M., Sritharan, S., Pender, M. J. and Carr, A. J. (2010b). "Investigation on the impact of seasonally frozen soil on the seismic response of bridge columns." *Journal of bridge engineering* 15(5):473-481.

Zhu, Y. and Carbee, L. (1984). "Uniaxial compressive strength of frozen silt under constant deformation rates." *Cold regions science and technology*. 9:3-15

CHAPTER 3: RATIONAL MODEL FOR CHARACTERIZING THE MONOTONIC LATERAL RESPONSE OF DRILLED SHAFTS IN NON-COHESIVE SOILS

A modified version of a paper to be submitted to the American Society of Civil Engineers Journal of Stuctural Engineering or similar journal

Aaron Shelman [1] and Sri Sritharan [2]

3.1 Abstract

Lateral loading on superstructures and substructures comes in many different forms, but the design process of these elements is further complicated by the soil surrounding the foundation. This paper presents a new rational model for the computation of the monotonic lateral load response of columns supported continuously supported on drilled shaft foundations. The new rational model establishes critical design location and a bilinear lateral load response for the overall behavior of the system through the establishment of a cantilever supported on a flexible foundation at the maximum moment location using a series of simple equations. Additional features of the proposed model include: (1) the ability to estimate ultimate shear demand and its associated location, and; (2) the ability to account for the

[1] Research Assistant, Department of Civil, Construction and Environmental Engineering, Iowa State University, Ames, IA 50011

[2] Wilson Engineering Professor, Department of Civil, Construction and Environmental Engineering, Iowa State University, Ames, IA 50011

effects of seasonal temperature variations. Verification of the model is provided using both analytical and experimental means that represent a column supported on a drilled shaft in non-cohesive soils.

CE Database Keywords: Foundations; Seismic design; Soil-Structure Interaction; Models; Concrete; Cold Temperature; Cohesive Soil

3.2 Introduction

Deep foundation design for structures requires the investigation of overturning since lateral loads (e.g., wind and seismicity) may cause high lateral forces and displacements within the structural systems. For bridges in regions of high seismicity, it has become common to use columns continued directly into the ground as drilled shaft foundations to reduce the construction costs. These deep foundation systems are highly influenced by the effects of soil-foundation-structure-interaction (SFSI), thus increasing the difficulty of characterizing the monotonic lateral load response of drilled shafts. Besides maintaining equilibrium along the entire length of the shaft with the inclusion of nonlinear material behavior, the effects of temperature further complicate the process as critical locations and force demands vary significantly [Suleiman et al. 2006, Sritharan et al. 2007, Wotherspoon et al. 2009, and Wotherspoon et al. 2010]. This paper describes an improved rational model for reducing the computational time within detailed approaches while still characterizing the monotonic lateral response of drilled shafts in non-cohesive soils.

3.3 Background

Methodologies that aim at reducing the complexity of engineering calculations are constantly being investigated to improve the efficiency of the overall design process. The challenge associated with these models, however, is to maintain accuracy without losing the simplicity of the approach. When accounting for the impacts of SFSI on a drilled shaft foundation and its aboveground superstructure, pushover analyses are the common approach to construct an equivalent cantilever that matches the stiffness of the combined column and foundation shaft such that the displacement at the column tip matches.

AASHTO (2010) specifies a simple system that relates the ratio of the pile's flexural rigidity to the modulus of elasticity of the soil, but only applies when the system behaves in a linear elastic manner. In high seismic regions, however, structural systems commonly include nonlinearity from the combined behavior of the soil and reinforced concrete under lateral demands. Thus, AASHTO (2010) suggests approaches presented in work by Chai (2002) and Priestley et al. (2007).

Chai (2002) defines a simplified model that uses two points, the point of fixity and the maximum moment, to establish the flexural strength and ductility of the system when surrounded by soil to an equivalent elasto-plastic cantilever system. This methodology relates the strength and ductility by relating the pile flexural rigidity, rate of increase of the horizontal subgrade reaction and the Rankine passive earth pressure. The soil properties in these instances were established as a function of the relative density and friction angle of the cohesionless soil. The elasto-plastic response of the system results in a perfectly plastic

displacement response post yielding that ignores the nonlinearity associated with steel, concrete and soil.

Priestley et al. (2007) provides the work of Suarez and Kowalsky (2007) that establishes the design level displacement of the system using a series of nomographs or equations. This methodology presents information solely based on the friction angle of the cohesionless soil and the boundary condition at the top of the column shaft. Lateral shear demand is then found by approximating the viscous damping of the system due to elastic and hysteretic damping based on the design level spectral and displacement curves.

Similar methodologies were developed for use in cohesive soils, but a recent study (Shelman and Sritharan 2013) found that a number of challenges were associated with their usage. One noted challenge within this system was that the maximum moment location was commonly defined at the point of fixity within the system although inconsistent with the expected behavior of the overall structural system, Figure 3-1. Additional shortcomings included: (1) the adequate capturing of the nonlinearity from soil, steel and concrete; (2) the definition of the analytical plastic hinge length in cohesive soils; (3) the minimal applicable range of soil parameters; (4) defining multiple points for establishing strength and ductility, and; (5) the lack of inclusion of seasonal temperature fluctuations. To address these shortcomings, a rational method that captures both the force and displacement behavior was constructed as shown in Figure 3-2. The proposed methodology used a set of three springs that established an equivalent cantilever supported on a flexible foundation at the point of maximum moment. The flexible foundation effectively located the critical location for

damage and plastic deformation, while defining the rotation and translation that occurs from movement below this location. The third spring in the model accounted for the resistance of the soil between the maximum moment location and the ground surface which improved the ability to handle seasonal temperature fluctuations. Although a set of springs were used in the model to improve its versatility with structural analysis software, simple equations were provided based on structural equilibrium that define the global response at the first yield and ultimate limit states over the elastic and inelastic loading range.

3.4 Formulation of Model in Non-Cohesive Soils

Based on the development of a successful approach for accounting for SFSI in cohesive soils, equations were developed for a consistent approach in non-cohesive soils. Using accurate representation of material nonlinearity, analytical models were constructed in LPILE Plus v 5.0 (Reese et al. 2004) and trends identified within the resulting data sets. Soil p-y curves were established according to the American Petroleum Institute recommendations for sand above the water table (1987). Soil parameters were chosen for a uniform layer of sand to maintain compatibility between unit weight, relative density and effective friction angle, Table 3-1, using the correlations for strength characteristics for granular soils in the Soil Mechanics Design Manual 7.01 published by the Naval Facilities Engineering Command (1986).

3.4.1   *Maximum Moment Location*

The maximum moment location establishes the effective height of the cantilever model, the critical region for inelasticity, locates all plastic rotation and locates the overall flexible

base for the model. The results of the pushover analyses, Figure 3-3, indicated that the non-dimensional maximum moment location (L_{ma}/D) varied in a quadratic manner based on the normalized above ground column aspect ratio (L_{col}/D) in agreement with current literature. The data further indicates that the variation in the coefficients for the quadratic trends would be a function of the effective friction angle such that the smaller the friction angle the larger the friction angle the smaller the maximum moment location. The maximum moment location can be found using Eq. (3-1), where α_{ma}, β_{ma} and χ_{ma} are coefficients calculated based off of the soils effective friction angle with a comparison between the equation and analytical data set in Figure 3-3.

$$L_{ma} = D\left[\alpha_{ma}\left(\tfrac{L_{col}}{D}\right)^2 + \beta_{ma}\left(\tfrac{L_{col}}{D}\right) + \chi_{ma}\right]$$
<div align="right">Eq. (3-1)</div>

where: α_{ma} = 0.0013*[ϕ(deg.)] - 0.027

β_{ma} = -0.0056*[ϕ(deg.)]+0.75
χ_{ma} = -0.114*[ϕ(deg.)]+8.07

3.4.2 *Zero Moment Location*

The next point established in the model definition identifies the point on the moment profile of Figure 3-2 where zero moment first occurs after the maximum moment location and translation is negligible. This point is used to define the plastic rotation, translation and elastic rotation at the maximum moment location. The results of the pushover analyses, Figure 3-3, indicate that the non-dimensional location (L_{m0}/D) would vary according to a power series, similar to the cohesive approach, based on the effective friction angle of the non-cohesive soil. The magnitude and rate of decay of the power series was a function of the

aboveground column aspect ratio as indicated by the stacking in Figure 3-3. The zero

moment location is found using Eq. (3-2), where α_{m0} and β_{m0} are coefficients based on the

above ground height of the column with a comparison between the equation and analytical

data provided in Figure 3-3.

$$L_{m0}=D\alpha_{m0}[\phi(deg)]^{\beta_{m0}}$$ Eq. (3-2)

where: $\alpha_{m0}=19.076*e^\wedge(49.9584/[L_{col}/D+10.9317])$

$$\beta_{m0}=-0.0044\left(\tfrac{L_{col}}{D}\right)^2+0.124\left(\tfrac{L_{col}}{D}\right)-1.5$$

3.4.3   Translational Spring at Maximum Moment Location

The lateral displacement occurring at the maximum moment location is handled with the

translational spring as part of the flexible base. A linear relationship between the non-

dimensional translation (Δ_t/D) and the non-dimensional distance between the maximum

moment and zero moment location (L_{mb}/D) was found in the data; however, the slope and

intercept were a function of the relative density of the soil. This arose as the relative density

of the soil causes the coefficient for the soil modulus as a function of depth to increase by a

factor of 3.6 and 9 for medium and dense sands when compared to loose sands, Figure 3-4

(API 1987). Eq. (3-3) and Eq. (3-4) define the translation at the ultimate and first yield limit

states, respectively. Spring forces are computed using equilibrium of a free-body diagram

associated with the proposed cantilever system at the ultimate and first yield limit states.

$$\Delta_{tu}=D\left[a\left(\tfrac{L_{mb}}{D}\right)+b\right]$$ Eq. (3-3)

where: $a=\begin{cases} 0.0577 \text{ for loose sands} \\ 0.0465 \text{ for medium sands} \\ 0.0411 \text{ for dense sands} \end{cases}$ and

$$b = \begin{cases} -0.3216 \text{ for loose sands} \\ -0.1942 \text{ for medium sands} \\ -0.1434 \text{ for dense sands} \end{cases}$$

$$\Delta_{ty} = \Delta_{tu} / \begin{cases} 4.90 \text{ for loose sand} \\ 5.94 \text{ for medium sand} \\ 6.07 \text{ for dense sand} \end{cases} \qquad \text{Eq. (3-4)}$$

3.4.4 Rotational Spring at Maximum Moment Location

Elastic rotation within the system at the ultimate and first yield limit states was found to be correlated to the relative density of the non-cohesive soil and vary linearly with L_{mb}/D. To account for the plastic action within the system, an analytical plastic hinge length, L_p, relating the section curvature to the total plastic rotation, θ_p, was established as a function of L_{mb}/D. Eqs. (3-5) to (3-8) establish the rotational aspects of the bilinear spring at the ultimate limit state based on flexural failure of the cross-section. At the first yield limit state, the elastic rotation component is defined using Eq. (3-9). The moment value for each of the limit states is taken as the ultimate and first yield moments of the foundation shaft within the expected plastic region produced from a moment-curvature analysis that adequately addresses material behavior through all seasons (e.g., see Shelman et al. 2010 and Levings and Sritharan 2012).

$$\theta_{ebu} = 0.0045 \left(\frac{L_{mb}}{D} \right) - \begin{cases} 0.011 \text{ for loose sands} \\ 0.008 \text{ for medium sands} \\ 0.0066 \text{ for dense sands} \end{cases} \qquad \text{Eq. (3-5)}$$

$$L_p = 2(0.13 L_{mb}) \qquad \text{Eq. (3-6)}$$

$$\theta_p = \phi_p L_p = (\phi_u - \phi_e) L_p \qquad \text{Eq. (3-7)}$$

$$\theta_u = \theta_{ebu} + \theta_p \qquad \text{Eq. (3-8)}$$

$$\theta_y = \theta_{eby} = 0.0027 \left(\frac{L_{mb}}{D}\right) - \begin{cases} 0.0076 \text{ for loose sands} \\ 0.0055 \text{ for medium sands} \\ 0.0045 \text{ for dense sands} \end{cases} \qquad \text{Eq. (3-9)}$$

3.4.5   Translational Spring representing Soil

The spring or multiple springs improve the models ability to account for P-Δ effects

occurring in the large deformations at the ultimate flexural failure, and the ability to account

for seasonal freezing is further improved with this spring. The p-y curve for the soil spring is

established using the procedures of API-RP2A (1987) for a non-cohesive soil with

appropriate modifications made for the influence of temperature on the soil material

behavior.

When a hand calculation is desired for establishing the tip lateral load and displacement,

the ultimate soil pressure, p_u, is computed and then multiplied by the effective height of the

spring, h (h = L_{ma} - L_{col} for a single spring), to determine the resistance of the soil at the

ultimate limit state, V_{su}. A similar process is needed at the first yield limit state, but

calibration of the pushover data sets found that a coefficient η, Eq. (3-10), could adjust the

ultimate limit state to the first yield limit state through the use of a constant value. The

adjustment is performed by multiplying the soil resistance at the ultimate limit state by the

coefficient η.

$$\eta = 0.93 \qquad \text{Eq. (3-10)}$$

3.4.6   Force-Displacement Response at Tip

The global force-displacement bilinear response envelope can be found by summing the

following individual components: (1) the total elastic displacement of the sytem, Δ_e; the total

plastic displacement, Δ_p; and (3) the initial translation at the maximum moment location, Δ_t. The total elastic displacement accounts for the elastic rotation below the maximum moment location, Δ_{eb}, and the elastic displacement above the maximum moment location, Δ_{ea}, due to the cantilever action produced from loading applied at the column tip. The initial translation at the maximum moment location is found using Eq. (3-3) or (3-4) depending on the limit state that is being analyzed. The plastic displacement is due to the plastic rotation, θ_p, concentrated at the maximum moment location. The final equation, Eq. (3-11), requires iteration on the tip elastic displacement, Δ_{ea}, to account for the P-Δ effects present in the overall system. The force at the column top, V_{top}, is found at each limit state using a summation of moments about the flexible base accounting for the P-Δ effects.

$$\Delta_{final}=(\Delta_{eb}+\Delta_{et})+\Delta_p+\Delta_t \qquad\qquad \text{Eq. (3-11)}$$

$$\text{where, } \Delta_{eb}=\theta_{eb}L_{ma}$$
$$\Delta_{et}=\frac{V_{top}L_{ma}^3}{3EI_e}$$
$$\Delta_p=\theta_p L_{ma}$$
$$\Delta_t=\Delta_{tu} \text{ or } \Delta_{ty}$$

3.5 Maximum Shear Calculations

Although the maximum moment location and top lateral force has been effectively established, the maximum shear does not typically occur within this region but rather deeper into the soil. Two methods establish the point of maximum shear by relating the point of maximum shear to the point of maximum moment in Eq. (3-12) as long as the ratio between

clear height of the column and diameter is greater than 2. If it is less than a value of 2, the maximum shear typically occurs at the column tip.

$$L_{vu} = L_{ma}\left[-0.021\left(\frac{L_{col}}{D}\right) + 1.52\right]$$
<div align="right">Eq. (3-12)</div>

The first method computes the maximum shear based on the soil causing a distributed loading on the foundation shaft between the maximum moment and maximum shear locations as shown in Figure 3-5. The loading is approximately parabolic in shape with a zero slope occurring at approximately 0.14 to 0.35 the length between the maximum moment location and the maximum shear location depending on the column aspect ratio. In this method, the shear at the maximum moment location is taken to be a value of zero as expected from general beam theory and the maximum shear is then calculated as $\alpha(p_u @ L_{ma})(L_{vu}-L_{ma})$ where α is a coefficient that better defines the shape of the distributed load based on the aspect ratio of the above ground column, Eq. (3-13). The α value computed by Eq. (3-13) approximately varies between 0.66 and 2.4, corresponding to different degrees of increase and decrease within the parabolic shape. Alternatively, Eq. (3-14) may be used to conservatively compute the maximum shear associated with the distributed loading of soil along the foundation shaft.

$$\alpha = 0.66e^{0.13*L_{col}/D}$$
<div align="right">Eq. (3-13)</div>

$$V_u = V_{top}\left[0.93e^{0.27\left(\frac{L_{col}}{D}\right)}\right]$$
<div align="right">Eq. (3-14)</div>

3.6 Verification of Proposed Method

Model verification was performed using data from full-scale testing of CIDH shafts in non-cohesive soils [Chai (2002)] and multiple nonlinear analyses of column-foundation systems using LPILE Plus v 5.0 (Reese et al. 2004). These techniques allowed for the comparison of both local and global responses produced by the model. This included an examination of the global force-displacement response, the maximum moment location, the elastic and plastic rotations, the displacement at the maximum moment location, and the location of the zero moment.

3.6.1 Experimental Verification – Chai and Hutchinson (2002)

At the University of California – Davis (UCD) a series of full-scale field tests on two sets of identical continuous column/foundation systems using a quasi-static push pull sequence were constructed in medium dense and dense sand. Using the structural and geotechnical information provided by Chai (2002), the experimental tests and proposed new method were compared graphically for the column top force-displacement response in Figure 6 and found to adequately capture the overall behavior. A numerical comparison was conducted for the maximum moment location and found that the location was found within 9% - 35% accuracy. This difference may be related to the translation of the maximum moment location between the yield and ultimate limit states. The analytical models constructed using LPILE are also provided in Figure 3-6 where the difference in the ultimate limit states can be contributed to the conservatism within the model used for the determination of the plastic displacement of the overall system. The conservatism is indicated in Figure 3-7, which demonstrates the differences as a function of friction angle and column aspect ratio.

3.7 Conclusions

A rational method accounting for the effects of SFSI was presented within this paper that improves upon the traditional approaches used for simplifying detailed finite element approaches. The method was constructed to create a consistent approach with cohesive soils that was previously developed and produced a rational method that captures both the lateral force and displacement response of the column shaft. This was accomplished by constructing an equivalent cantilever supported by a flexible foundation at the critical design location for maximum moment using an equation based approach. Verification of the proposed rational method was performed against experimental test specimens in a wide range of soils and analytical models using varying soil and structural parameters. These verifications indicated that the model would perform adequately throughout the expected loading range with the assumption of a flexural failure at the point of maximum moment in the column or foundation shaft.

3.8 References

American Association of State Highway and Transportation Officials (AASHTO). (2009). *Guide Specifications for LRFD Seismic Bridge Design,* Washington D.C.

American Petroleum Institute (API). (1987). *Recommended Practice for Planning, Designing and Constructing Fixed Offshore Platforms, API Recommended Practice 2A (RP 2A), 17th Edition,* Washington D. C.

Chai, Y. H. (2002). "Flexural strength and ductility of extended pile-shafts. I: analytical model." *Journal of Structural Engineering* 128(5), 586-594.

Chai, Y. H. & Hutchinson, T. C. (2002). "Flexural strength and ductility of extended pile-shafts. II: experimental study." *Journal of Structural Engineering* 128(5), 595-602.

Levings, J. and Sritharan, S. (2012). "Effects of cold temperature and strain rate on the stress-strain behavior of ASTM A706 Grade 420 (60) steel reinforcement." *Journal of Materials in Civil Engineering* 24(12): 1441-1449.

Naval Facilities Engineering Command. (1986). *Soil Mechanics Design Manual 7.01,* U.S. Navy: Alexandria, Virginia.

Priestley, M. J. N., Seible, F. & Calvi, G. M. (1996). *Seismic Design and Retrofit of Bridges,* John Wiley & Sons, Inc.: New York.

Priestley, M. J. N., Calvi, G. M. & Kowalsky, M. J. (2007). *Displacement-Based Seismic Design of Structures*, IUSS Press: Pavia, Italy.

Reese, L. C., Wang, S. T., Isenhower, W. M., Arrellaga, J. A. and Hendrix, J. (2004). *LPILE plus 5.0, user's manual.* Ensoft, Inc.: Austin.

Reese, L. C., Wang, S. T.. Isenhower, W. M. and Arrellaga, J. A. (2004). *LPILE plus 5.0, technical manual.* Ensoft, Inc.: Austin .

Shelman, A. and Sritharan, S. (2013: In Progress). "A rational model for characterizing the monotonic lateral response of drilled shafts in cohesive soils." *Journal of structural engineering.*

Shelman, A., Levings, J. and Sritharan, S. (2010) "Seismic design of deep bridge pier foundations in seasonally frozen ground." *Final Report submitted to AUTC and ADOT&PF.*

Sritharan, S., Suleiman, M. T. and White, D. J. (2007). "Effects of seasonal freezing on bridge column-foundation-soil interaction and their implications." *Earthquake spectra* 23(1): 199-222.

Suarez, V. & Kowalsky, M. J. (2007). "Displacement-based seismic design of drilled shaft bents with soil-structure interaction." *Journal of Earthquake Engineering* 11, 1010-1030.

Suleiman, M. T., Sritharan, S. and White, D. J. (2006). "Cyclic lateral load response of bridge column-foundation-soil systems in freezing conditions." *Journal of structural engineering* 132(11): 1745-1754

Wotherspoon, L. M., Sritharan, S., Pender, M. J. (2009). "Modelling the response of cyclically loaded bridge columns embedded in warm and seasonally frozen soils." *Engineering structures* 32(2010): 933-943.

Wotherspoon, L. M., Sritharan, S., Pender, M. J. and Carr, A. J. (2010). "Investigation on the impact of seasonally frozen soil on seismic response of bridge columns." *Journal of bridge engineering* 15(5): 473-481.

Table 3-1: Correlations used in the establishment of the constitutive soil models

Relative Density	Coefficient for Modulus	Dry Unit Weight	Effective Friction Angle	Moisture Content
%	MPa/m (lb/in^3)	kN/m^3 (lb/ft^3)	deg	%
25	6.79 (25)	16.65 (106)	30.1	Assumed drained well enough such that $\gamma_d \sim \gamma_m$
		14.35 (91.33)	29.0	
		15.6 (99.22)	29.5	
50	24.43 (90)	17.55 (111.7)	33.6	
		15.08 (96.02)	31.8	
		16.34 (104.04)	32.7	
75	61 (225)	18.43 (117.3)	37.0	
		15.92 (101.33)	34.54	
		17.16 (109.23)	35.72	

Ground Surface

Maximum Moment
Location

Typical Fixity
Location for
Displacement
Equivalency

Equivalent System

Typical System   Expected Displacement   Expected Moment Profile
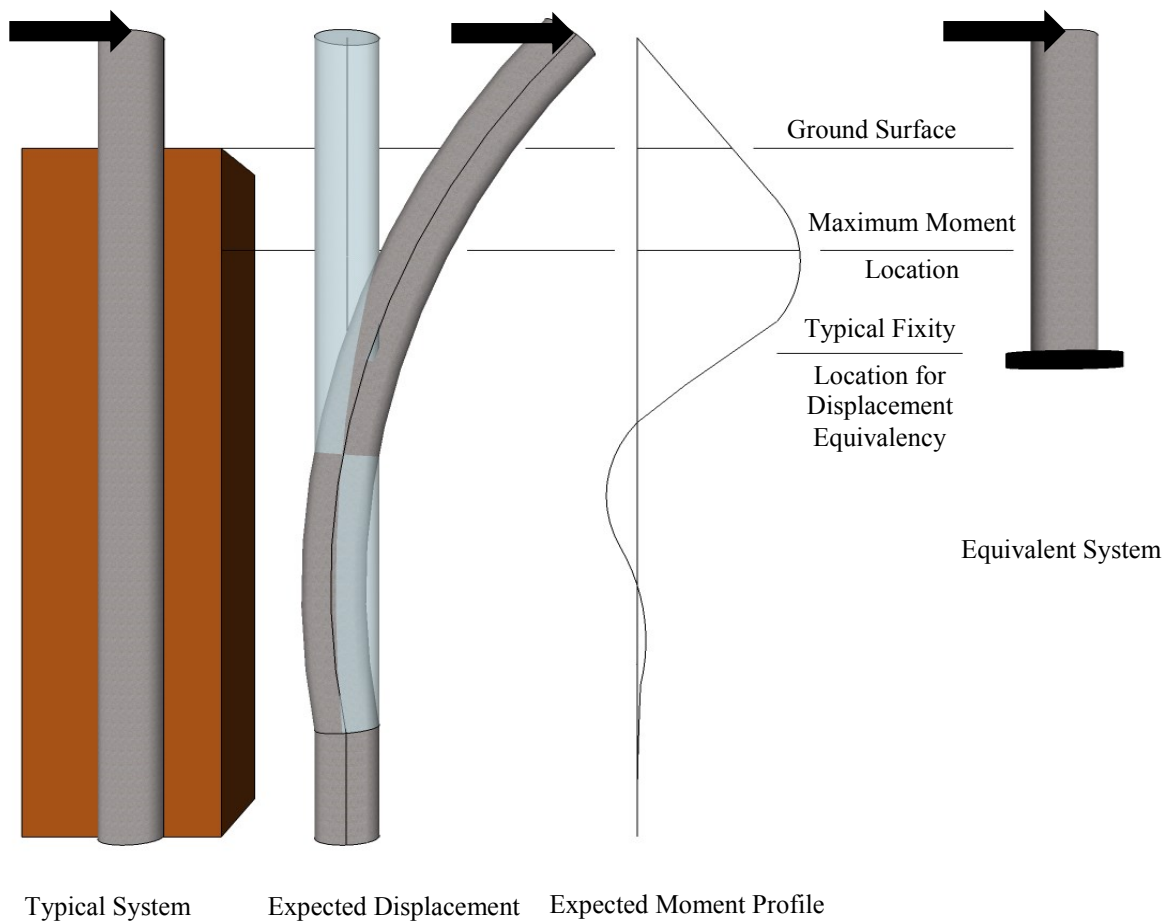
Figure 3-1: Typical response of a drilled shaft subjected to a lateral force [reproduced

from Shelman and Sritharan 2013]

Axial

L_{col}

L_{mo}

L_f

Typical Column/Pile and
Moment Diagram

Axial

L_{ma}

1

2

3

Simplified Cohesive
Model

Soil spring used to
represent soil
resistance

Translational spring
at maximum moment
location

Rotational spring at
maximum moment
location

F

(Δ_{ty}, V_{ty})

2

(Δ_{tu}, V_{tu})

1

(Δ_{su}, V_{su})

Δ

M

M_u

M'_y

3

θ_y

θ_u

θ
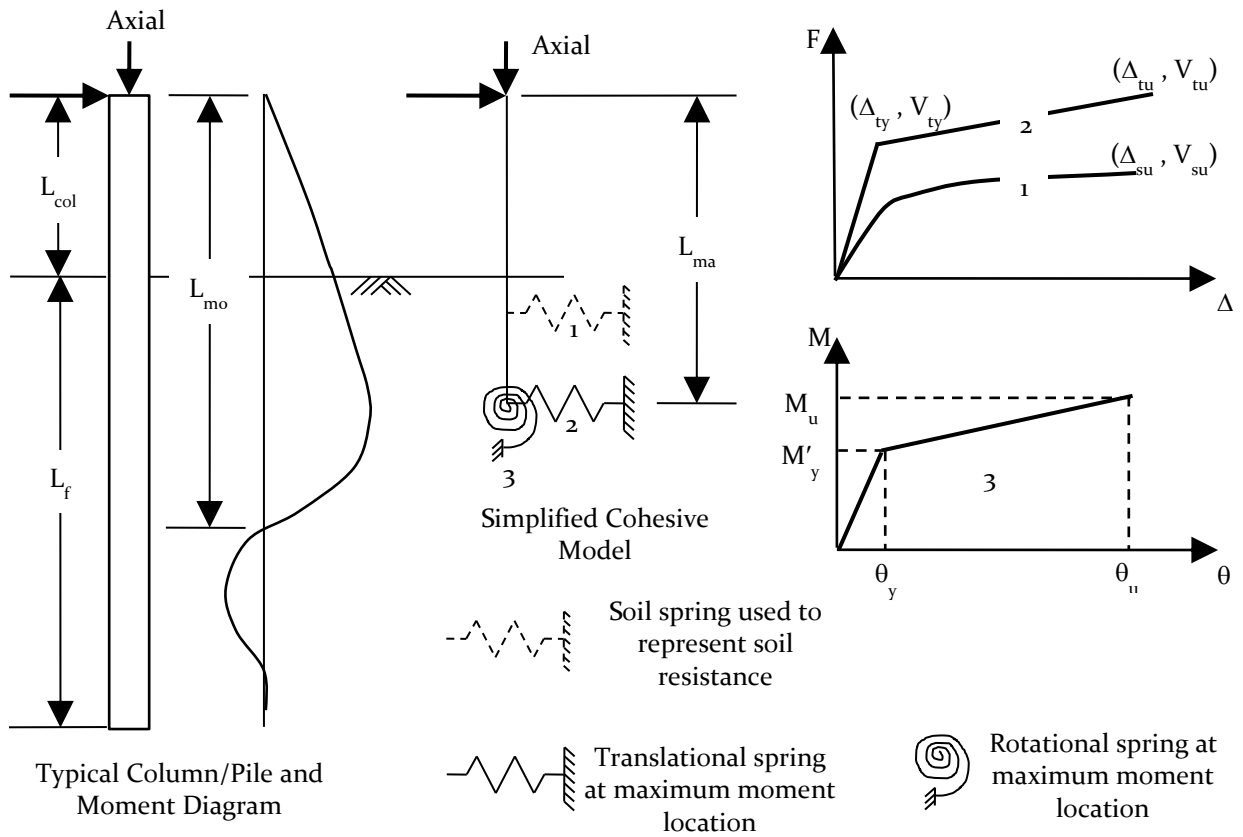
Figure 3-2: Proposed new method [Reproduced from Shelman and Sritharan 2013]
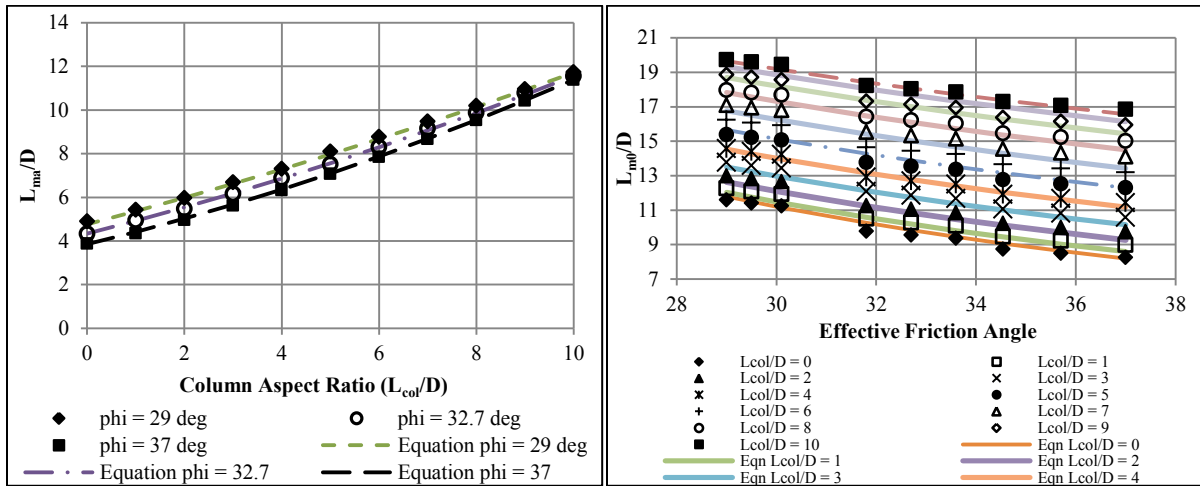
**Figure 3-3: Comparison of equation-based methods to analytical LPILE models (left)
maximum moment location; (right) zero moment location**
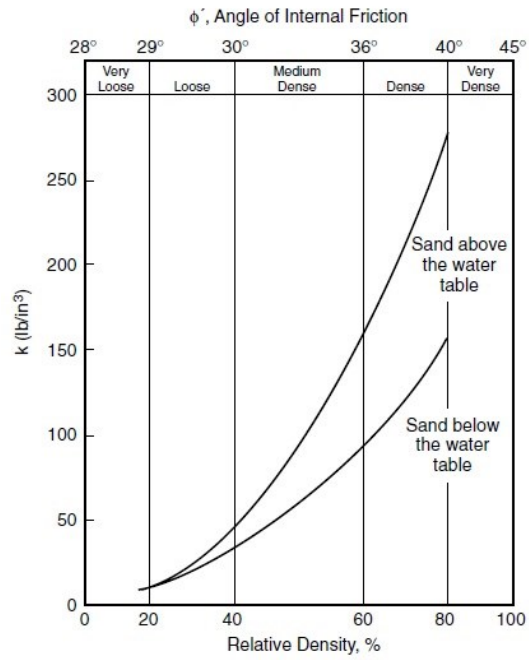
Figure 3-4: Variation in the coefficient for subgrade modulus with depth as a function of friction angle and relative density (after API 1987)
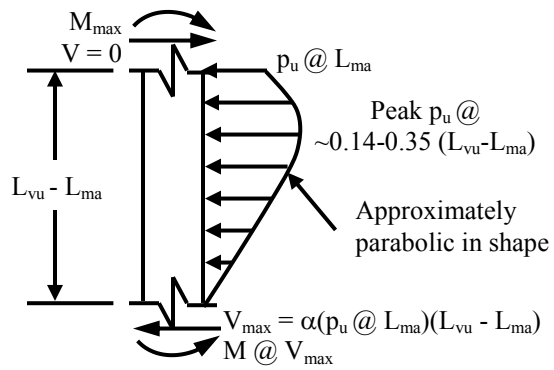
Figure 3-5: Free body diagram for determining the ultimate shear in the foundation shaft
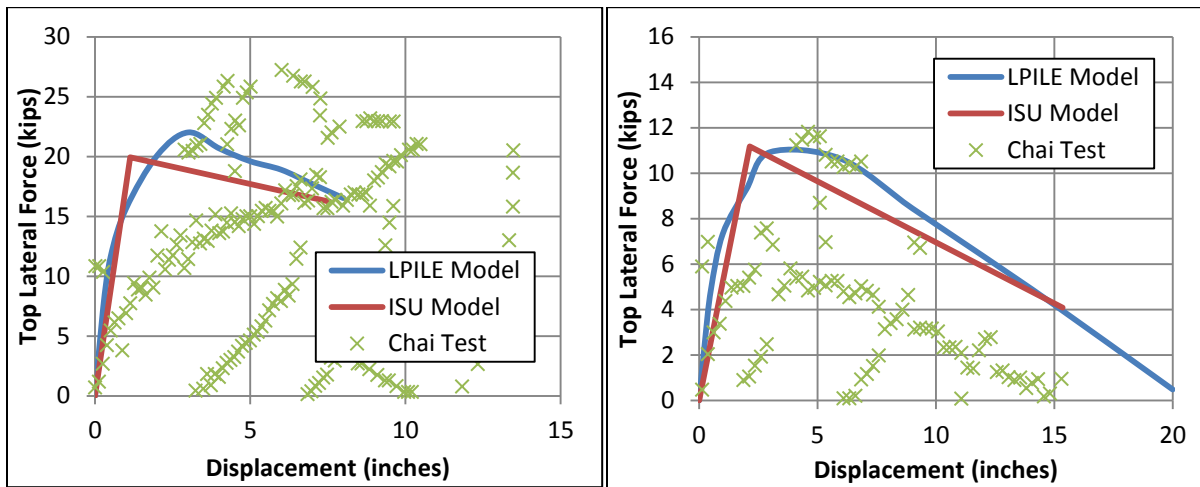
(a) Aspect Ratio 2 with Medium Sand   **(b) Aspect Ratio 6 with Dense Sand**

Figure 3-6: Verification of the proposed method with experimental work by Chai (2002) and analytical LPILE models
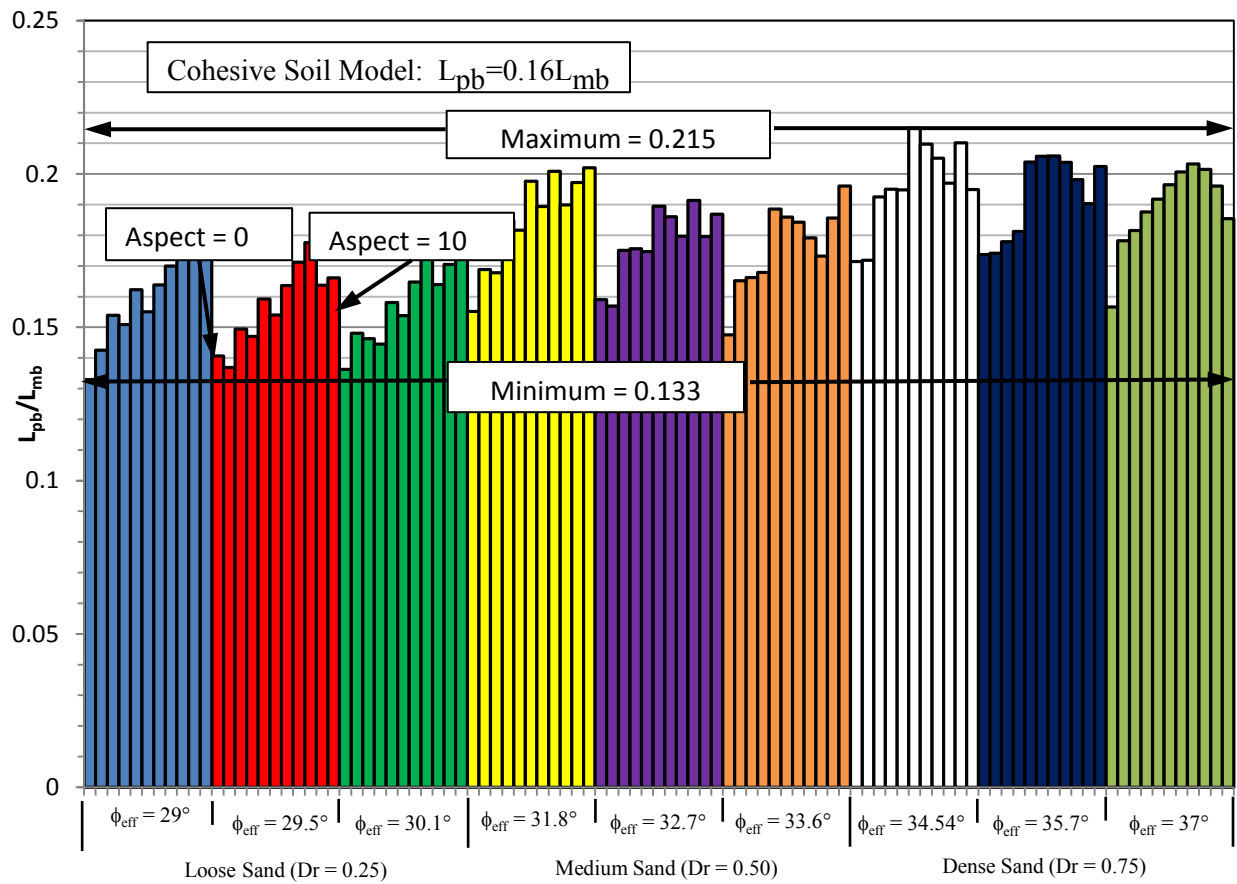
Figure 3-7: Analytical plastic hinge length as a ratio of the normalized distance between the zero and maximum moment locations

CHAPTER 4: CHARACTERIZATION OF SEASONALLY FROZEN SOILS FOR SEISMIC DESIGN OF FOUNDATIONS

A modified version of a paper submitted to the American Society of Civil Engineers (ASCE) Journal of Geotechnical and Geoenvironmental Engineering

Aaron Shelman[3], James Tantalla[4], Sri Sritharan, M. ASCE[5], Sissy Nikolaou, M. ASCE[6], Hugh Lacy, F. ASCE[7]

4.1 Abstract

An experimental investigation was performed on five widespread soil types common in the United States to characterize the effects of freezing temperatures on the unconfined compressive strength (q_u), the modulus of elasticity (E) and strain at the unconfined compressive strength (ε_{qu}). Soil specimens were subjected to monotonic and cyclic loading with varying strain rates at temperatures ranging from 20°C (68°F) to -23°C (-9.4°F). When

[3] Main Researcher, Primary Author and Graduate Student, Dept. of Civil, Construction and Environmental Engineering, Iowa State University, Ames, IA 50011

[4] Associate, Mueser Rutledge Consulting Engineers, New York, NY 10122

[5] Wilson Engineering Professor and Associate Chair, Dept. of Civil, Construction and Environmental Engineering, Iowa State University, Ames, IA 50011

[6] Senior Associate and Geoseismic Director, Mueser Rutledge Consulting Engineers, New York, NY 10122

[7] Consultant, Mueser Rutledge Consulting Engineers, New York, NY 10122

compared with test results at 20°C (68°F), testing at -20°C (-4°F) showed an increase in q_u by a factor of 100, an average increase in E by a factor of 300 and an average decrease in ε_{qu} by 5% strain. Increase in the soil compaction, moisture content and applied strain rate amplified the cold temperature effects on q_u. Additional testing at -20°C (-4°F) resulted in an increase in ε_{qu} with no change in E when the applied strain rate was increased. Cyclic experimentation produced data trends comparable to the monotonic experimentation for the mechanical properties, but allowed residual deformation as a function of cold temperature to be identified. To assist with current seismic design practice, experimental trends were incorporated into a p-y curve development and the impact of observed soil response as a function of temperature is demonstrated using a series of pushover analyses on a column continued into the subsurface as a drilled shaft foundation.

CE Database Keywords: Foundations, Seismic design, Soil properties, Soil-structure interaction, Cold temperature effects

4.2 Introduction

Despite the fact that past and present earthquakes have occurred across the world during times of seasonal freezing and that nearly 50% of bridges in seismic regions of the US can experience winter earthquakes (Sritharan and Shelman 2008), the influence of temperature on the effects of soil-foundation-structure-interaction (SFSI) under seismic conditions is not well understood. The effects of SFSI in wintry conditions were studied in an exploratory study performed at Iowa State University (Suleiman et al. 2006 and Sritharan et al. 2007). This study consisted of experimental and analytical programs to identify additional

considerations that may be required for the design of columns supported on cast-in-drilled-hole (CIDH) shafts. The study found that the effects of freezing on concrete, steel and soil would influence the lateral load behavior of the drilled shafts with the soil component having the largest impact. Although a stiffer soil causes less lateral deflection to the overall system, the column and CIDH shafts are adversely affected to the extent of brittle failure because the critical moment location [i.e., in-ground plastic hinge] shifts towards the ground surface, the shear and moment demands increase in both the column and foundation shafts, and the plastic hinge length decreases.

Further investigation (Wotherspoon et al. 2010) on the dynamic response of CIDH shafts subjected to seismic ground motions, with return periods between 25-years and 2500-years, concluded the following: (a) maximum bending moment and shear demands would be larger in winter conditions than in summer conditions; (b) the peak shear demand for the 2500-year return period in the summer was 56% of the section capacity compared to 76% in the winter; (c) for the 500-year return period, 29% of the displacement capacity of the column and foundation system was reached compared to 62% of the displacement capacity in times of seasonal freezing; and (d) more cycles of high strain deformation will occur in wintry times that may result in failure of the drilled shafts due to low-cycle fatigue.

To address the aforementioned challenges in routine seismic design practice involving pushover models, appropriate modifications need to be introduced. Given that the largest influence to lateral response in these models comes from the temperature effects on the properties of soil surrounding the foundation, the main focus of this paper was to characterize

the behavior of soil at different cold temperatures using monotonic loads so that suitable p-y curves can be appropriately developed. Specifically this paper examines the monotonic characteristics of five soil types that are widespread in seismic regions of the United States as a function of cold temperatures. Influence of variables such as unit weight, moisture content, strain rate and cyclic loading were also examined

4.3 Background

Frozen soil appears throughout the world due to fluctuations in seasonal temperature and permanent ground freezing in the form of permafrost. Engineering behavior of permafrost for the design of structures in artic regions has been studied by numerous researchers. Additionally, seasonal freezing of soil has been found to have many benefits during the construction process due to the stiffening of soil surrounding a given location therefore creating a safer working environment.

Mechanical properties of frozen soils have been studied in the past by researchers to improve the design of foundations under non-seismic conditions (Tsytovich 1975, Andersland and Anderson 1978, Andersland and Ladayani 1994 and Harris 1995). Typically, the main focus of these studies was on properties related to the long term creep behavior of permafrost through loading applied over long time periods and the heave associated with frozen soil. Although these are important topics for the design of structures in soil that experience permanent freezing, several outcomes of these studies are not directly applicable to seismic design that deals with loading over a short duration.

However, the general trends established for the frozen soils in these studies are valuable, and are thus summarized herein. The shear strength of soil increases with the decrease in temperature (Figure 4-1), increases with an increase in applied strain rate, decreases with duration of applied load, and increases as the amount of unfrozen water content decreases (Tsytovich 1975, Andersland and Ladayani 1994 and Harris 1995). Figure 4-1 provides information on the strength gain of ice, indicating the impact of ice as a function of cold temperature; however, variation exists as ice compression strength varies with crystal structure, rate of freezing, chemical composition, testing temperature and many other factors. Studies have reported that the shear strength of sands, clays and silts increase by a factor of two to four times when the temperature went from -1°C (30.2°F) to -10°C (14°F) and an eightfold increase as the temperature decreased from 20°C (68°F) to -2°C (28.4°F) (Tsytovich 1975, Andersland and Anderson 1978, Andersland and Ladayani 1994).

Deformability of soil reduced when subjected to freezing temperatures, established by examining either the initial secant modulus of elasticity or secant modulus of elasticity at 50% of the peak stress (Tsytovich 1975 and Andersland and Ladayani 1994). The modulus of elasticity in sands and silts increased when temperature decreased and resulted in a factor of four to one hundred increase between -1°C (30.2°F) and -10°C (14°F) (Tsytovich 1975 and Andersland and Ladayani 1994). Additionally, Poisson's ratio was found to decrease with a decrease in temperature (Tsytovich 1975 and Shibata et al. 1985) suggesting that the deformability decreases as lateral spread cannot occur as easily.

Limited studies confirm that applied strain rate affects the overall compressive strength and deformability characteristics (Zhu and Carbee 1984 and Andersland and Ladanyi 1994). Testing on frozen sands (Andersland and Ladanyi 1994) between 0.006% and 20% strain per minute provided data suggesting that as strain rate increased, the compressive strength increased by a factor of two to five while experiencing a shift in the failure mode from plastic to brittle. Frozen silt strength was found increase by a factor of 25 as strain rate was increased from 0.6% per minute to 30,000% per minute at -9.4°C (15°F). Cyclic testing on frozen sands at -4°C (24.8°F) with strain rates less than 0.05% strain per minute was found to result in lower peak stress than static testing performed at similar rates of loading.

Additional drawbacks of the previous research studies include: 1) testing completed and referenced back to a known temperature below 0°C (32°F); and 2) strain rate investigations were limited to sands and silts (Tsytovich 1975, Andersland and Anderson 1978, and Andersland and Ladanyi 1994). Using a known temperature allowed for easier relationships to be established for the design process, however, soil testing laboratories rarely have the capability for testing at frozen temperatures to establish a base value. A practical approach would be to establish seasonal temperature variations with respect to a common room temperature [e.g., 20°C (68°F)], enabling designers to more readily account for cold temperature effects in design and analysis.

4.4 Test Plan

In parallel with experimental investigations conducted on A706 steel reinforcing bar (Levings and Sritharan 2011) and concrete (Shelman et al. 2010), an experimental

investigation was undertaken to investigate the behavior of frozen soils. The main objectives of this study were 1) to identify trends for critical parameters (e.g., ultimate compressive strength, soil modulus of elasticity, etc.) of frozen soils with respect to a preselected temperature reference of 20°C (68°F); and 2) the establishment of modified stress-strain curves as a function of temperature to be used for defining p-y curves so that SFSI analyses can be performed with consideration to seasonal temperature effects. Although repeated loading and unloading of soils is common in high seismic regions, a monotonic approach is commonly employed to determine the lateral response of a structural system. Therefore the monotonic behavior of frozen soils was the main focus of the exploratory program with cyclic behavior being defined to examine potential degradation concerns.

In seismic regions of the United States, numerous soils are encountered during site investigations for foundation construction. The in-situ soils may range from alluvial to loess based on the depositional environment that each one may have experienced over time. The goal was to include multiple soils that could be found at bridge sites throughout the United States, while giving consideration to areas of high seismicity. A total of five soil types were chosen as shown in Table 1 based on geologic depositional nature, but for convenience, all soils were collected from the state of Alaska as a recent project was conducted with the Alaska Department of Transportation and Public Facilities (ADOT&PF) and the Alaska University Transportation Center (AUTC). The project area included soils with a depositional nature consisting of prior glacial expanses and nearby waters which led to the presence of glacial, alluvial and even lacustrine deposits. Moreover, the area undergoes

seismic events in freezing temperatures on a regular basis. The soil types were then classified as I through V based on the expected frequency of encounters at a bridge site with I being the most frequent type. The anticipated maximum cold temperature to be experienced by the soils was -30°C (-22°F).

4.5 Test Setup

In order to capture the changes in soil behavior and engineering properties at subzero temperatures, a specially designed triaxial chamber was used. The chamber allowed for a liquid (e.g., antifreeze or salt water) capable of maintaining frozen temperatures to be circulated around the soil specimen, thus creating a temperature-controlled environment. The testing apparatus that was designed and used at Mueser Rutledge Consulting Engineering (MRCE) firm in New York City is provided in Figure 4-2.

The chamber labeled 1 in Figure 4-2 consists of a top and bottom plate separated by a large diameter clear tube capable of sustaining a horizontal pressure. A rigid plate at the bottom of the tube created a surface for supporting the specimen as well as ports to put the desired liquid into the chamber. The top plate was modified to allow copper coils to be placed around the specimen that would constantly circulate the cold liquid with a pump in order to maintain the temperature and still allow a compressive axial load to be applied up to 44.5 kN (10 kip).

4.6 Specimen Preparation

Disturbed soil samples were obtained during drilling at various project sites and shipped to New York for testing. The samples were then separated into groupings proposed in Table

1 and kept in plastic containers until the time of sample preparation. At the time of

preparation, water was added to the soil to make the desired moisture content. Specimens

were then created by loosely placing soil into a mold supported on a hard surface while using

a consistent effort to compact the soil in three lifts. Depending on the desired moist unit

weight, the number of blows used in the compaction effort was either increased or decreased.

Upon completion, the specimens and molds were placed inside a freezer (2 in Figure 4-2) at -

25°C (-13°F) as needed and stored in the lab facilities until testing.

Prior to testing, frozen and unfrozen samples were extruded from the mold using standard

practices and trimmed to the correct two inch diameter with level ends for testing purposes.

Once all trimming was completed, the specimen was measured and placed between the upper

and lower loading plates and then covered with a neoprene membrane to protect the sample

from contamination inside the testing chamber.

4.7 Test Matrix

Using the information provided in Table 1, sixty soil samples were constructed from the

five soil types with three samples per soil type and testing temperature to allow for variation

in ice formation. As summarized in Table 2, the distribution of these samples covered the

influence of several variables including moist unit weight, moisture content, loading rate, and

the following final target temperatures: 20°C (68°F), -1°C (30.2°F), -10°C (14°F), and -20°C

(-4°F). 40% of the samples constructed were Type I soil and was expected to be the soil

most commonly encountered around a bridge site based on depositional environment and was

therefore a primary focus of the investigation (Shelman et al. 2010). The Type I alluvial soil

provided as part of this study was classified as a CH soil using the unified soil classification system (USCS) and would further improve the frozen soil information on a clay soil which was considered a main goal. The remaining four soil types were used for the establishment of general trends between the extreme testing temperatures. Moisture content and testing unit weight were specified based on average values expected to occur in the field (Shelman et al. 2010), but the actual testing values did not correspond with the specified values at all times. This was the case within the Type II and Type IV specimens where moisture content of 30% was specified and some of the Type IV specimens only reached 10% moisture content. In six of the Type I soil specimens, the moisture content was varied by ±15% to examine the impacts of additional water in the pore structure on the strength at -20°C (-4°F). Similarly, the moist unit weight was varied over a range of 3.6 kN/m^3 (22.7 pcf) to examine the variation in strength at -20°C (-4°F) without modifications to the moisture content. Furthermore, variable loading rates were used for identifying the differences in the modulus of elasticity and strength. In addition to the testing for material properties with variable temperature, additional testing was performed at -1°C (30.2°F) and -20°C (-4°F) under repeated loading and unloading with variable loading rates.

4.8 Loading Protocols

Monotonic testing in an unconsolidated, undrained state with minimal to no confining pressure was used for the majority of the testing since shallow soils have the greatest impact on the lateral response of the system [e.g., 10 cm (4 in.) can influence the response (Sritharan et al. 2007)]. This testing consisted of applying a compressive force to the soil specimens at

the desired loading rates of 0.1%, 1% and 10% strain per minute. The cyclic loading was performed on selected samples at two different loading rates, 1% and 10% strain per minute, with the overall pattern consisting of loading the samples to the set target strain, then fully unloading the specimen before proceeding to the next target strain. Once a strain of 1% was reached for the first time in the loading pattern, the effects of reloading to a certain strain level were examined by reloading to that strain point two additional times before proceeding to the next target strain. Each target strain in the pattern selected for the cyclic testing, 0.25% minimum and 15% maximum, was based on observations made of the stress-strain curves obtained from the monotonic triaxial testing on the alluvial soil (see Table 2). The goal of the three cycles at each level was to identify whether any loss in soil strength or change in the residual deformation would occur with the repeated nature of the loading.

4.9 Test Observations

Each specimen was allowed to stabilize at the desired temperature as measured by a steel probe thermocouple placed in the center of the triaxial chamber, taking between 3 and 24 hours. Upon stabilization, an external control loading system (3 in Figure 4-2) was activated to apply consistent loading at the desired strain rate. The applied force and vertical deformation to the sample were recorded in order to establish the stress-strain curves similar to that in Figure 4-3 as well as identify the following critical parameters: initial, secant and unload/reload moduli, shear strength, and strains. Unconfined compressive strength (q_u) of the soil was determined by the peak stress on the stress-strain curve and the associated strain was defined as ε_f. Undrained shear strength (c_u) was taken as one-half of the unconfined

compressive strength. Additionally, the modulus of elasticity (E) was approximated to a secant value between the origin and one-half the peak stress on the stress-strain curve, much like the approach in Reese and Welch (1975).

4.10 Results and Discussion

Between the testing temperatures of 20°C (68°F) and -22.8°C (-9°F), the mechanical properties of the five soil types experienced the following: (1) an increase in the elastic modulus; (2) an increase in the ultimate compressive strength; and (3) a decrease in the strain at peak stress. Figure 4-4 graphically describes this trend for a Type I soil in which the elastic modulus increased by a factor of 300, the ultimate compressive strength increased by a factor of 80, and the strain at peak stress decreased by 5% strain (i.e., $\Delta\varepsilon = 5\%$).

4.10.1 Unconfined Compressive Strength (UCS)

An analysis of the stress-strain curves for the five soil types was performed by constructing a chart of the UCS ratio (see Figure 4-5) for all soils and temperatures with respect to the measured warm weather unconfined compressive strengths at 20°C (68°F). The unconfined compressive strength of the Type IV soil was not provided at -1°C (30.2°F) as there was only a limited amount of material obtained for this soil type.

The data provided in Figure 4-5 suggests that the transition from pore water to pore ice significantly alters the ultimate compressive strength of the soil as the amount of partially frozen water decreases in the specimen as the temperature decreases. The relative increase in strength varies greatly between soil types at first examination, but a closer examination of the data reveals that the UCS of the soils has a consistent increase as a function of temperature.

This is depicted in Figure 4-5 where the relative increase is a factor of 10 at -1°C (30.2°F) and a factor of 100 at -20°C (-4°F), respectively.

4.10.2 Strain at UCS, ε_f

Each soil type tested resulted in a general decreasing trend in strain at UCS as the data set in Figure 4-6 demonstrates. Within Figure 4-6, a large scatter in the data exists as the strain at the peak stress will be dependent on soil type, internal structure, water content and other factors. Although the rate of decrease in individual soil types varied from 0.5% to 10% strain, a conservative estimate of the overall decrease in strain from 20°C (68°F) to -20°C (-4°F) at UCS would be 5% based on the trend for all the soil types.

4.10.3 Elastic Modulus

As expected, the strength gain and reduced ε_f with decreasing temperature resulted in the increase of the secant modulus of elasticity. The overall gain at -20°C (-4°F) varied between a factor of 200 and 400 with respect to the reference warm temperature, and followed a curvilinear trend as seen in Figure 4-7.

Type II Soil Effects

The Type II soil had noted differences from the other four soil types tested in this program. This was believed to be a result of the higher moisture contents throughout testing and the depositional environment of the ice contact deposits. The relative increase in the UCS was 140 at -1°C (30.2°F) and 740 at -20°C (-4°F). The strain at UCS experienced a decrease of 8% strain from 20°C (68°F) to -20°C (-4°F). The modulus of elasticity gain at -20°C (-4°F) was between a factor of 1000 and 1800.

__Additional Type I Soil Testing__

A number of additional tests were performed on the Type I soil to investigate the impact of moist unit weight, moisture content and strain rate at frozen temperatures.

4.10.4 Moist Unit Weight Effects

The Type I soil was tested to examine the effects of moist unit weight when tested at freezing temperatures. Classified as a CH soil, the moisture content was maintained at approximately 27% and moist unit wieght varied from 15.5 kN/m^3 (100 pcf) for the loose material to 19.0 kN/m^3 (120 pcf) for the dense material. At each level, three specimens were tested and results indicated a linear increase in strength as a function of moist unit weight, see Figure 4-8. This overall linear trend was expected based on the warm weather behavior where the friction increases in the internal matrix from additional compaction, assuming that the soil is not over the peak compaction and moisture content location.

4.10.5 Moisture Content Effects

The amount of moisture within the soil specimen directly impacts the undrained shear strength of the soil as it impacts the ice matrix and the peak point of the compaction versus moisture content curve. The results produced from varying the moisture content in the Type I soil are shown in Figure 4-9 with an additional point produced using data provided in Figure 4-8 (i.e., the square data point). This point corresponds to a moisture content of 28.1% at a moist unit weight of 17.0 kN/m^3 (108 pcf) with an undrained shear strength of approximately 3600 kPa (37.6 tsf). The data point adjusted the trend such that the effects of strength gain associated with reaching the optimum moisture content were not influencing

the overall trend. This point is plotted as the square in Figure 4-9, which concludes that as

moisture content increases at a consistent moist unit weight, the undrained shear strength

increases linearly as a function of moisture content.

4.10.6 Strain Rate

The strain rate was varied from 0.1% to 10% strain per minute for monotonic loading of

the Type I soil at -20°C (-4°F) and the results depicted an increase in the ultimate

compressive strength, strain at the ultimate compressive strength and the elastic modulus of

elasticity. Results for the strain and compressive strength are provided in Figure 4-10. The

modulus of elasticity increased by approximately 25% using the secant method, but a

relatively large scatter was present. A further examination of the stress-strain curves and

tangent modulus along the initial point of the stress-strain curves led to the conclusion that

the modulus did not change significantly over the tested strain rates.

4.10.7 Cyclic Loading

Cyclic testing was performed on the Type I soil at -1°C (30.2°F) and -20°C (-4°F) along

with variable loading rates of 1% and 10% strain per minute. The results for the cyclic

testing at 1% strain per minute are provided in Figure 4-11. The envelope of the data concurs

with the monotonic testing where an increase in the ultimate compressive strength and the

modulus of elasticity of the Type I soil were a function of temperature. Additionally, the

data sets indicate that the unloading and reloading moduli were approximately equal to the

initial soil modulus of elasticity found for the temperature at which the samples were tested.

A key result was that residual deformation occurred after each cycle and was a function of

temperature. At -1°C (30.2°F), the residual deformation was 93% of the peak strain while at -20°C (-4°F) the residual deformation was 80% of the peak strain. Furthermore, degradation occurred after the first loading level of a new cycle such that the peak stress in the second and third cycles was 80% of the peak stress in the first cycle. Further tests would be required to better define the amount of degradation associated with higher number of cycles similar to approaches in unfrozen soils. Additionally, increasing the strain rate from 1% to 10% caused a 30% increase in the UCS, while the secant modulus of elasticity to 50% of the peak stress, the unloading/reloading moduli and residual deformations were generally unaffected at -20°C (-4°F).

4.11 Integration into Seismic Design

In lateral loading of deep foundations subjected to a design level or greater seismic event, the presence of soil is typically accounted for using p-y curves, which can be constructed using laboratory stress-strain curves [e.g., Reese and Welch (1975)]. By representing the soil as a series of springs along the length of the foundation, the continuity between the soil and pile is adequately addressed. Sritharan et al. (2007) and Wotherspoon et al. (2009) demonstrated that this technique would work even at cold temperatures when using programs such as LPILE (Reese et al. 2004) and Ruamoko (Carr 2005).

The construction of p-y curves can be done by many methods, but a common approach suggested by Reese and Welch (1975) relates the shape of the stress-strain curve to the soil displacement using Eqns. (4-1) and (4-2) with the exponent $a = 0.25$ and $b = 0.5$ for warm weather conditions. Crowther (1990) suggested that $a = 0.43$ is a good estimate for frozen

soils and was shown to be successful in studies involving frozen soils (Sritharan et al. 2007 and Wotherspoon et al. 2009).

$$\left(\frac{y}{y_{50}}\right)^a = \left(\frac{\varepsilon}{\varepsilon_{50}}\right)^b \qquad\qquad\text{Eq. (4-1)}$$

where: y   = soil deflection

y_{50} = soil deflection at one-half the ultimate soil reaction

ε = strain in the soil

ε_{50} = strain at one-half maximum principal stress difference

$$\frac{p}{p_u} = 0.5\left(\frac{y}{y_{50}}\right)^a \qquad\qquad\text{Eq. (4-2)}$$

where: y   = soil deflection

y_{50} = soil deflection at one-half the ultimate soil reaction

p   = soil reaction

p_u = ultimate soil reaction

4.11.1 Example p-y curves

Starting with a typical stress-strain curve for the Type I soil subjected to monotonic loading at the warm weather, the cold temperature stress-strain curves up to the UCS can be approximated using the following relationships based on the experimental work presented herein: (a) UCS ratio of 10 at -1°C (30.2°F) and 100 at -20°C (-9°F) based on Figure 4-5, where $q_{u,warm}$ is at 20°C (68°F); (b) a decrease in strain, ε_f, of 1.25E-3 ε/°C (6.5E-4 ε/°F) as shown in Figure 4-6; (c) an increase in the stiffness ratio ($E_{frozen}/E_{roomtemp}$) equal to 36.86e⁻

$^{0.083[T(in\ Celsius)]}$-5.30 (see Figure 4-7); (d) E = $0.5q_u/\varepsilon_{50}$ and stress-strain curve is linear up to

the point of $(\varepsilon_{50}, 0.5q_u)$; and, (e) after reaching $0.5q_u$, the stress-strain curve follows a

logarithmic trend up to the adjusted UCS and ε_f location. As with current practice (e.g.,

Reese et al. 2004), after construction of the adjusted stress-strain curve, the degradation of

soil subjected to loading and unloading could be accounted for at this stage by multiplying

the resulting stresses in the curve by a factor of 0.8 based on the cyclic degradation observed

in this study for a CH soil or a value deemed appropriate for other soils based on engineering

judgment. The p-y curves are then constructed using Eqns. (4-1) and (4-2). This process

was performed for a 0.6 m (24 in.) diameter foundation shaft at a soil depth of 10 cm (4 in.)

surrounded by the Type I soil with a moist unit weight of 19.5 kN/m^3 (124.1 pcf). The

resulting stress-strain and p-y curves are provided in Figure 4-12, where the increase of 10

and 100 for the stress-strain curves relate to an increase of 10.9 and 109, respectively, in the

p-y curves.

4.11.2 Impact on Lateral Response

To understand the significance of the modified p-y curves, pushover analyses were

condicted using a full nonlinear analysis at three different temperatures [i.e., 20°C (68°F), -

1°C (30.2°F) and 2 at -20°C (-9°F)] in LPILE (Reese et al. 2004) similar to the approach

presented by Sritharan et al. (2007). A 0.61 m (24 in.) diameter (D) drilled shaft that

extended above the ground 4.42D and into the ground 17.1D was specified with a 2%

longitudinal reinforcement ratio, a 0.9% horizontal reinforcement ratio, and a 5% axial load

ratio to represent a typical seismic bridge column. Materials and the associated properties

were consistent with the following: (a) concrete compressive strength of 27.6 MPa (4000 psi); and (b) reinforcing steel of A706 Grade 60 steel. The nonlinear moment-curvature behavior for the column and foundation shaft was established through a section analysis program available at Iowa State University (Levings 2009). For the purposes of this study, the influence of temperature on concrete and steel were not included for the following reasons: 1) the impact of frozen soil alone was desired and 2) previous research has shown that these material properties have a minimal impact on the response (Sritharan et al. 2007). The soil surrounding the foundation shaft had properties as specified in the p-y curve example section and was considered to be uniform along the entire length in the unfrozen state and no water table was present. The frozen state at the two cold temperatures was handled by including a uniform frozen soil to a depth of 10 cm (~4 in.) from the ground surface based on the work of Sritharan et al. (2007), having unfrozen soil properties below that location. A further analysis was conducted at -20°C (-9°F) with the more realistic frozen depth of 1.2 m (47.25 in.), appropriate for this temperature (Sritharan et al. 2007).

The results of the pushover analyses summarized in Figure 4-13 and Figure 4-14 indicate that as the temperature decreased, the lateral displacement at the top of the column decreased as expected, but the shear demand increased significantly. With only a frozen soil depth of 10 cm (~4 in.), shear demand in the foundation shaft increased by up to 19% while the shear demand in the column increased by up to 61%. These changes in the structural demands of the system arise with the shifting of the maximum moment location towards the ground surface by 1.77 m (5.8 ft) and the length over which plastic action takes place (i.e., length for

which yield moment was exceeded) decreasing over the temperature range examined. These results indicate the potential for brittle failure and that the plastic hinge will not form in the desired location identified during the warm weather condition.

The results of the second pushover analysis at -20°C (-4°F) with a frozen soil depth of 1.2 m (47.25 in.) indicate a further increase in the shear demand while decreasing the displacement. Although the impact of the increase in frozen soil appears to be minimal in the force-displacement responses in Figure 4-13, the foundation shear demand in this case increased by 128%, while the column shear demand did not change significantly.

4.12 Conclusions

This paper presented an investigation into the characterization of frozen soils for use in the seismic design of foundations and incorporation into p-y curves in SFSI modeling. Suggestions for this characterization were based off the experimental testing of five soil types representing areas expected to experience seasonal freezing.

Testing was performed in a specially designed triaxial chamber under monotonic and cyclic loading with variable loading rates and temperatures. Temperatures of 20°C (68°F) and -23°C (-9.4°F) were used as the upper and lower limit testing temperatures as they corresponded to the temperature range expected throughout the United States where freezing occurs. The conclusions drawn from this study are as follows:

1. The unconfined compressive strength of soil significantly increases with colder temperatures. The multiple soil types tested (Type I through V, excluding II) typically had the strength ratio increase by a factor of 10 at -1°C (30.2°F) and 100 at -20°C (-4°F).

2. The strain at the unconfined compressive strength decreased by $0.05\,\varepsilon$ between the upper and lower limit testing temperatures for all soils. This corresponds to a drop in strain of 1.25E-3 $\varepsilon/°C$ (6.5E-4 $\varepsilon/°F$) as a function of temperature for all the soil types tested.

3. The stiffness ratio increased in an exponential manner to an average factor of 300 at -20°C (-4°F) for Type I through Type V soils, excluding Type II soils.

4. Increasing the moist unit weight of the soil specimens caused an increase in the unconfined compressive strength at -20°C (-4°F). Additionally, the increased moisture content caused a higher amount of ice in the void spaces, which led to an increased unconfined compressive strength at -20°C (-4°F).

5. The Type II soils tested in this program did not follow the same magnitudes of increase for the UCS and soil modulus of elasticity. In this instance, the UCS ratio increased by 140 and 740 at -1°C (30.2°F) and -20°C (-4°F), respectively. The stiffness ratio increased by a factor of 1000 to 1800 at -20°C (-4°F).

6. Additional testing of Type I soils was performed to examine the influence of moist unit weight, moisture content and strain rate. The increasing trends for the moist unit weight and moisture content tests were as expected based on the current understanding of warm weather behavior. Variation in the rate of monotonic loading of the Type I soils between 0.1% and 10% strain per minute resulted in an increase of the unconfined compressive strength and strain at the associated level. However, the modulus of elasticity was unaffected by strain rate over the testing range.

7. Cyclic loading of the warm and frozen soil specimens produced data trends similar to that of the monotonic testing for the strength ratio, stiffness ratio and strain at the unconfined compressive strength. The residual deformation of the soil type tested was 93% of the peak strain value at -1°C (30.2°F) and 80% of the peak strain at -20°C (-4°F). Additionally, strain rate effects were the same as the monotonic specimens at -20°C (-4°F).

8. The influence of frozen soil on the lateral load response of a column continuously supported on a CIDH was found to be significant. The column and foundation shear demands increased by 19% to 128%, depending on the depth of frozen soil and temperature being examined. Additionally, the critical design location shifted towards the ground surface by over a meter at the extreme testing temperature of -20°C (-4°F), emphasizing the importance of accounting for seasonal temperature variation.

4.13 Acknowledgements

4.14 References

Andersland, O. B. and Anderson, D. M. (1978). *Geotechnical engineering for cold regions,* McGraw-Hill Inc., USA

Andersland, O. B. and Ladayani, B. (1994). *An introduction to frozen ground engineering,* Chapman & Hall, USA.

Carr A. J. (2005). *3D Ruaumoko: Inelastic three-dimensional dynamic analysis program,* University of Canterbury, Christchurch, NZ.

Crowther, G. S. (1990). "Analysis of laterally loaded piles embedded in layered frozen soil." *Journal of Geotechnical Engineering* 116(7): 1137-1152.

Das, B. M. (2004). *Principles of Foundation Engineering*, 5th Edition, Thomson, Brooks/Cole, USA.

ENSR (2002). "Fort Wainwright Meteorological Station Data." University of Fairbanks. URL: http://ine.uaf.edu/werc/projects/ftww/metdata/metdata.html.

Harris, J. S. (1995). *Ground freezing in practice,* Thomas Telford Services Ltd., London, England.

Levings, J. (2009). "Development of a versatile section analysis tool for use in seismic design." *Master's Thesis*. Iowa State University, Ames, Iowa.

Levings, J. and Sritharan, S. (2012). "Effects of cold temperature and strain rate on the stress-strain behavior of ASTM A706/A706M mild steel reinforcement." *Journal of materials in civil engineering (In publication)*

Reese, L. C. and Welch, R. C. (1975). "Lateral loading of deep foundations in stiff clay." *Journal of geotechnical engineering division* 101(GT7): 633-649.

Reese, L. C., Wang, S. T., Isenhower, W. M., Arrellaga, J. A. and Hendrix, J. (2004). *LPILE plus 5.0, user's manual*, Ensoft, Inc., Austin, TX.

Sayles, F. H. (1966). "Low temperature soil mechanics." *Technical note.* Cold regions research and engineering laboratory, Hanover, NH.

Sayles, F. H. (1968). "Creep of frozen sands." *Technical Report 190.* Cold regions research and engineering laboratory. Hanover, NH.

Shelman, A., Levings, J. and Sritharan, S. (2011) "Seismic design of deep bridge pier foundations in seasonally frozen ground." *Final Report submitted to AUTC and ADOT&PF.* Access Online from: http://ine.uaf.edu/autc/final-reports/

Sritharan, S., Suleiman, M. T. and White, D. J. (2007). "Effects of seasonal freezing on bridge column-foundation-soil interaction and their implications." *Earthquake spectra* 23(1): 199-222.

Sritharan, S. and Shelman, A. (2008). "An assessment of broad impact of seasonally frozen soil on seismic response of bridges in the U.S. and Japan." *Proceedings of the 24th US-Japan bridge engineering workshop, Minneapolis,* FHWA: 429-440.

Suleiman, M. T., Sritharan, S. and White, D. J. (2006). "Cyclic lateral load response of bridge column-foundation-soil systems in freezing conditions." *Journal of structural engineering* 132(11): 1745-1754

Tsytovich, N. A. (1975). *The mechanics of frozen ground,* Scripta Book Company. USA

Williams, P. J. (1988). "Thermodynamic and mechanical conditions within frozen soils and their effects." *Proceedings of the 5th International Conference on Permafrost, Trondheim,* International Permafrost Association: 493-498

Wotherspoon, L. M., Sritharan, S., Pender, M. J. (2009). "Modelling the response of cyclically loaded bridge columns embedded in warm and seasonally frozen soils." *Engineering structures* 32(2010): 933-943.

Wotherspoon, L. M., Sritharan, S., Pender, M. J. and Carr, A. J. (2010). "Investigation on the impact of seasonally frozen soil on seismic response of bridge columns." *Journal of bridge engineering* 15(5): 473-481.

Zhu, Y. and Carbee, L. (1984). "Uniaxial compressive strength of frozen silt under constant deformation rates." *Cold regions science and technology* 9:3-15

Table 4-1: Description of Collected Soils / Types

ID	Specified Soil Type	USCS*	Expected Saturated Moisture Content	Expected Dry Unit Weight
I	Alluvial Deposits	CH	10% - 50%	$10 \text{ kN/m}^3 - 30 \text{ kN/m}^3$
II	Glacial Till/Ice Contact Deposits	SP-SM	10% - 50%	$10 \text{ kN/m}^3 - 30 \text{ kN/m}^3$
III	Estuarine/Lacustrine	SM	15% - 30% / 90% - 150% (Silty,Clayey/Organic)	$8 \text{ kN/m}^3 - 20 \text{ kN/m}^3$
IV	Glacial Outwash	SP-SM	10% - 50%	$10 \text{ kN/m}^3 - 30 \text{ kN/m}^3$
V	Loess	ML	15% - 30%	$10 \text{ kN/m}^3 - 17 \text{ kN/m}^3$

* USCS classification based on the disturbed soil samples provided by the ADOT&PF for the specified soil types

Table 4-2: Soil Testing Parameters

Soil Type	No. of Tests	Test Temperature	Test Moisture Content (%)	Test Moist Unit Weight (kN/m³)	Loading Rate (%/min)
I: Alluvial Deposits	3	-23°C	27.23	18.61	1
	3	-20°C	28.03	18.60	1
	3	-10°C	22.05	17.97	1
	3	-1°C	23.06	18.53	1
	3	20°C	25.33	19.51	1
	3	-20°C	28	15.44	1
	3	-20°C	24	19.02	1
	3	-20°C	17.93	17.42	1
	3	-20°C	41.2	16.79	1
	2	-1°C	23.75	18.96	0.1
	2	-20°C	30.13	17.87	0.1
	2	-20°C	29.95	18.04	10
II: Glacial Till/Ice Contact Deposits	3	-20°C	35.13	17.47	1
	3	-1°C	35.1	17.55	1
	3	20°C	39.4	19.07	1
III: Estuarine/Lacustrine	3	-20°C	29.37	18.49	1
	3	-1°C	32.13	18.89	1
	3	20°C	31.47	19.18	1
IV: Glacial Outwash	3	-20°C	26.33	17.97	1
	3**	-1°C	30**	20**	1
	3	20°C	10.77	22.90	1
V: Loess	3	-20°C	26.88	18.53	1
	3	-1°C	25.78	18.61	1
	3	20°C	29.97	18.68	1
Total Tests	66 Samples				
Additional Testing – Repeated Loading and Unloading under Variable Loading Rates					
I: Alluvial Deposits	2*	-1°C	30	20	1
	2*	-20°C	30	20	1
	2*	-20°C	30	20	10
Total Additional Tests	6				

*Indicates cyclic loading at stated strain rate
**Not tested due to lack of material
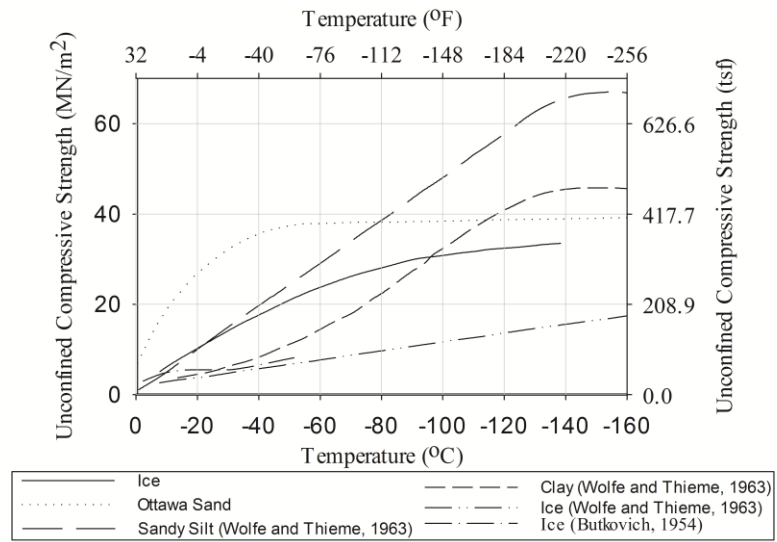
Figure 4-1: Temperature dependence of unconfined compressive strength for several frozen soils and ice [reproduced from Andersland and Anderson (1978)]
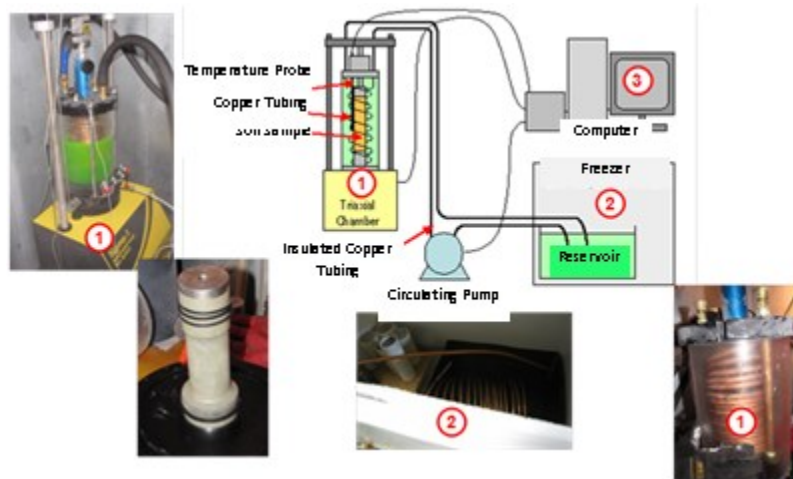
Figure 4-2: Schematic of test setup for frozen soils testing at MRCE
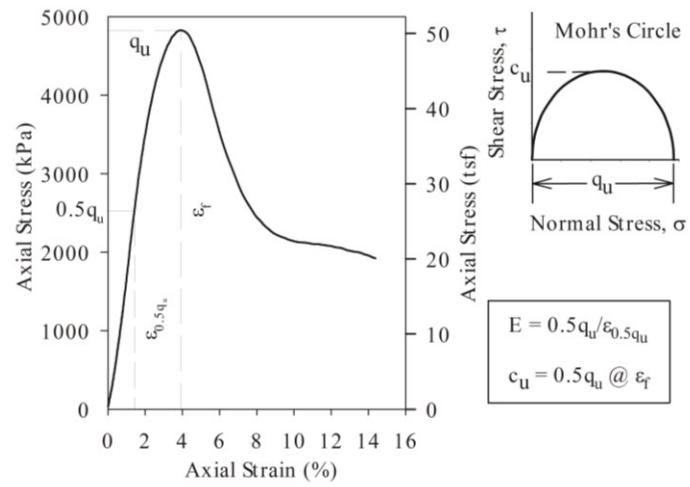
Figure 4-3: A measured stress-strain curve for a Type I soil sample at -20 °C (-4 °F)
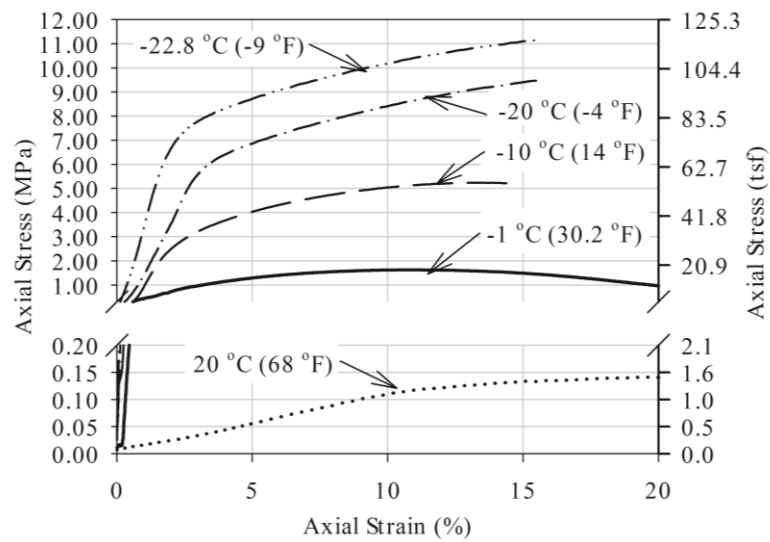
Figure 4-4: Stress-strain response of a Type I soil subjected to monotonic loading at different test temperatures
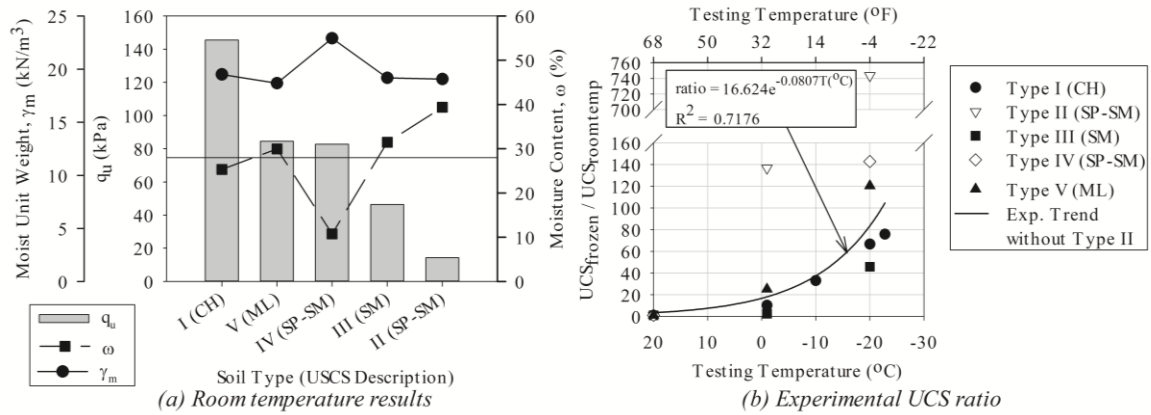
Figure 4-5: Strength comparison of soils tested at various temperatures (a) room temperature results; (b) unconfined compressive strength (UCS) ratio [Note: 1 kN/m3 = 6.3659 lb/ft3; 1 kPa = 0.01044 tsf]
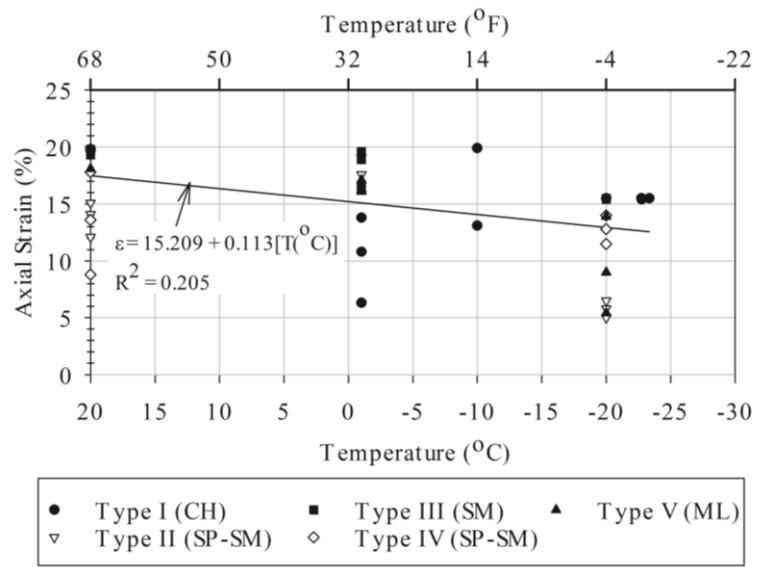
Figure 4-6: Variation of strain with temperature at q$_u$
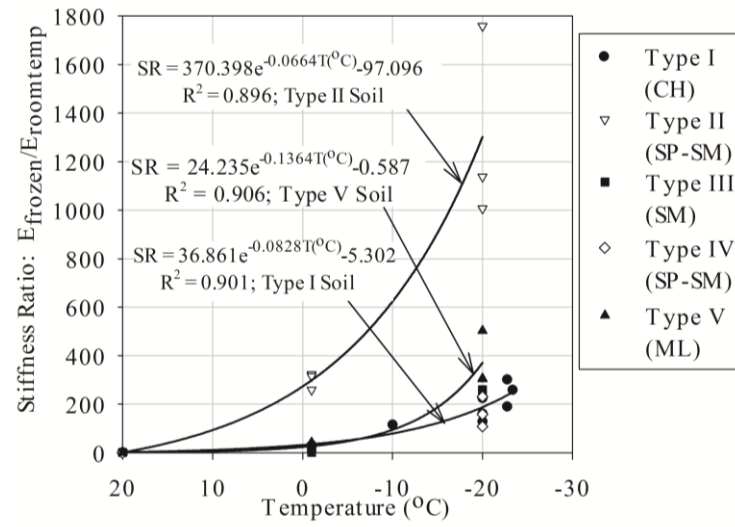
Figure 4-7: Effects of temperature on the stiffness ratio under monotonic loading
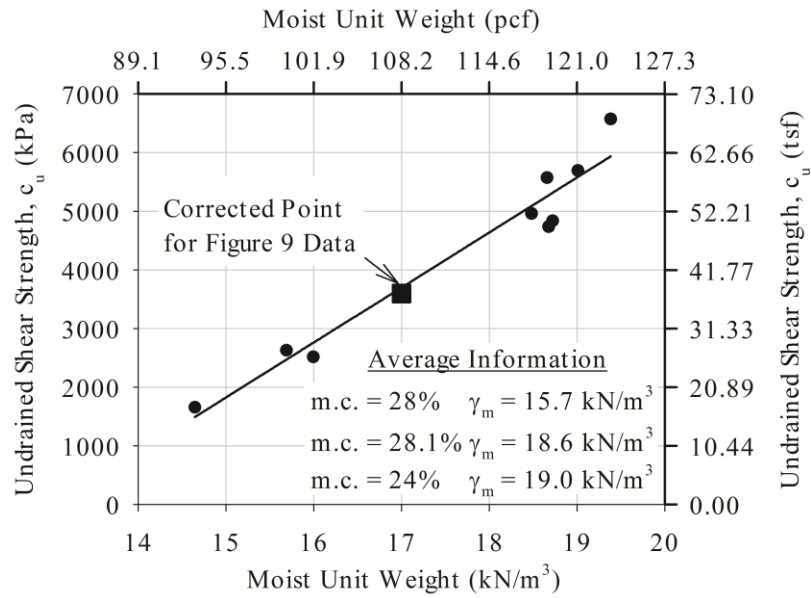
Figure 4-8: Effects of moist unit weight on the undrained shear strength of a CH soil at -20 °C (-4 °F)
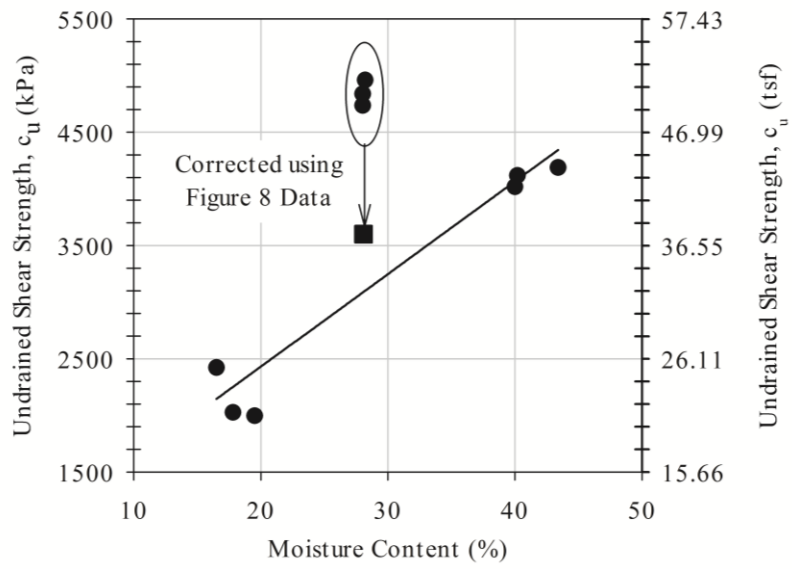
Figure 4-9: Effects of moisture content on the undrained shear strength of a CH soil at -20 °C (-4 °F)
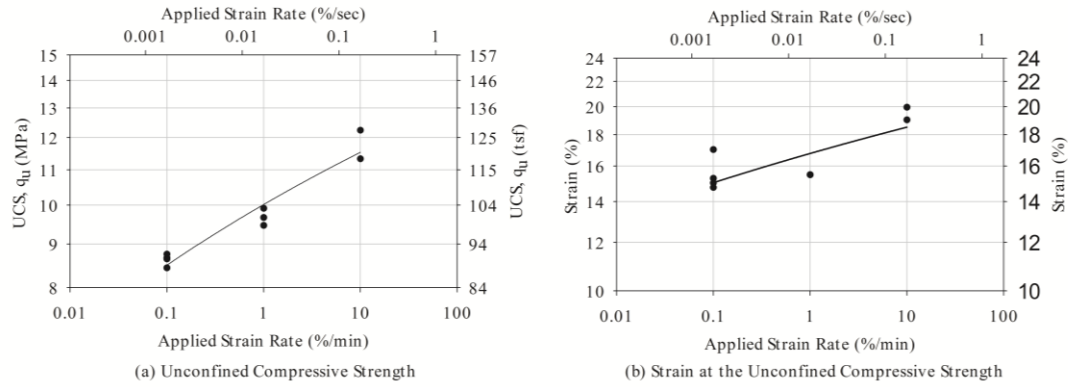
Figure 4-10: Effects of strain rate on a Type I soil at -20 °C (-4 °F)
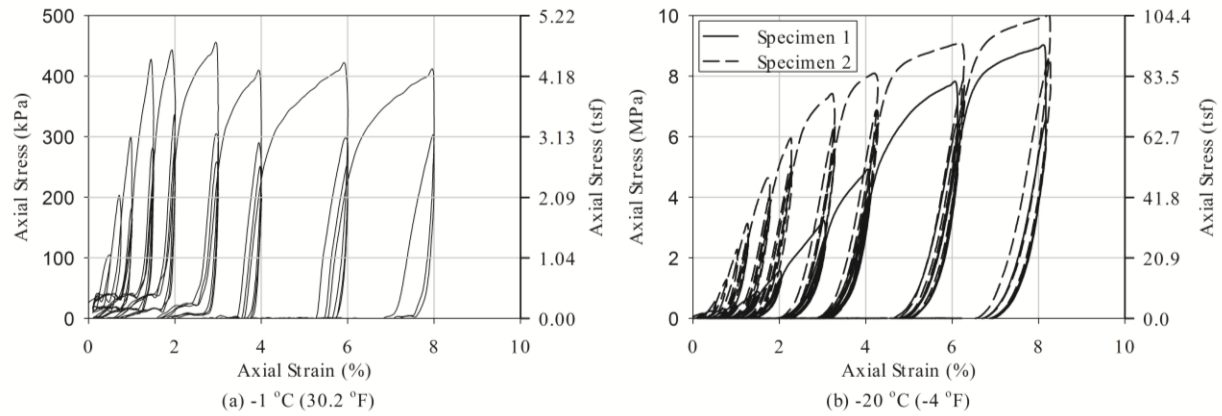
Figure 4-11: Experimental cyclic stress-strain results of a Type I soil subjected to subzero temperatures and a loading rate of 1% strain per minute
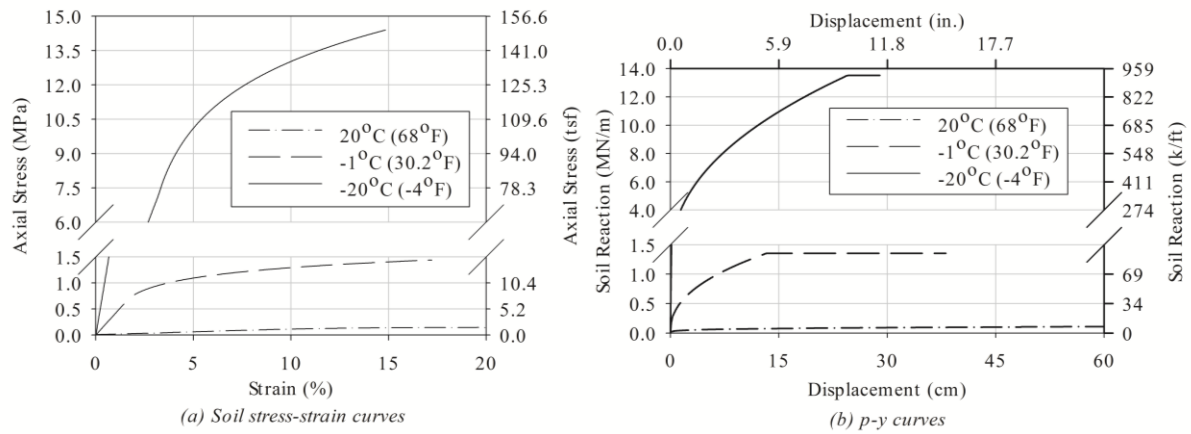
Figure 4-12: Stress-strain and p-y curves for a Type I soil using experimental recommendations
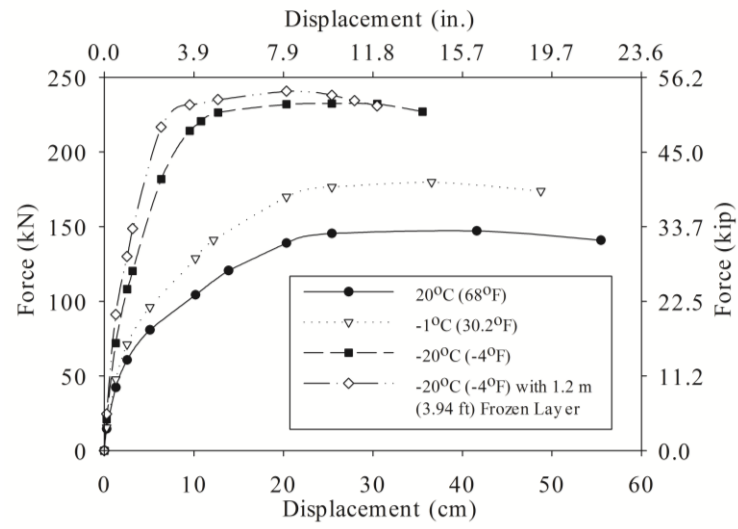
Figure 4-13: Monotonic force-displacement response of example column supported by a CIDH shaft
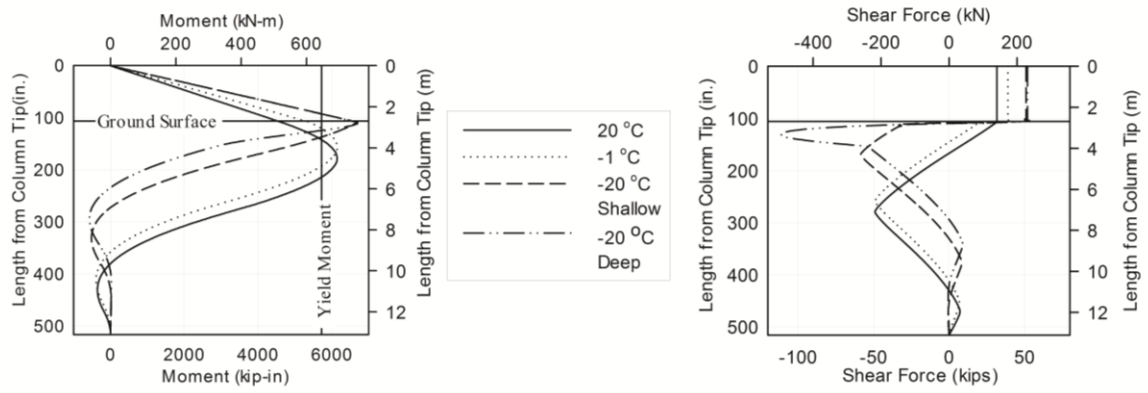
Figure 4-14: Shear and moment demand of example column supported by a CIDH shaft

CHAPTER 5: EFFECTS OF COLD TEMPERATURE ON THE BEHAVIOR OF CONFINED CONCRETE

A modified version of a paper to be submitted to the American Concrete Institute's (ACI) Materials Journal

Aaron T. Shelman[8] and Sri Sritharan

Biography: Aaron T. Shelman is a graduate research assistant at Iowa State University, Ames, Iowa. He received his BS in Civil Engineering from the University of Wisconsin at Platteville; MS and PhD in Civil Engineering (Structural Emphasis) from Iowa State University. His research interests include earthquake resistant design including soil-foundation-structure-interaction (SFSI) and cold temperatures.

Sri Sritharan is the Wilson Engineering Professor at Iowa State University, Ames, Iowa. He received his BS in Civil Engineering from the University of Peradeniya, Sri Lanka; MEng in Civil Engineering from the University of Auckland, New Zealand; PhD in Structural Engineering from the University of California. He is the chair of ACI Committee 341 and a member of ACI Committees 445, 447 and the faculty network. His research interests include earthquake resistant design, structural concrete and SFSI.

---

[8] Primary Author and Researcher

5.1 Abstract

This paper presents the results of an experimental investigation conducted on confined and unconfined normal strength concrete at varying temperatures to aid in seismic design of structures that experience seasonal freezing. Test data was collected by performing monotonic testing of concrete specimens with multiple levels of confinement at 20°C (68°F), -1°C (30.2°F), -20°C (-4°F), and -40°C (-40°F) within a controlled environment. Key parameters used in defining the stress-strain behavior of confined concrete were investigated in this study including: compressive strength, modulus of elasticity, strain at peak compressive strength, and ultimate concrete strain. Compressive strength and modulus of elasticity were found to increase while the strain at peak compressive strength decreased as temperature decreased. Ultimate concrete strain was found to be unaffected by temperature. The study further indicated that confined concrete behavior does not follow recommendations used in practice simply by adjusting the expected material properties when subjected to cold temperatures.

Keywords: Cold Weather; Stress-Strain Diagram; Confined Concrete; Material Behavior; Temperature

5.2 Introduction

In a study by Sritharan and Shelman (2008) it was found that approximately two-thirds of the bridges within the United States have the potential for being impacted by seasonal freezing with 33,000 of those being located in high seismic regions. This number of structures could easily be increased with the inclusion of buildings and the respective

foundations located within these regions. Researchers have performed studies to identify the change in key stress-strain parameters such as concrete compressive strength, Poisson's ratio and modulus of elasticity at cold temperatures. Studies by Sehnal et al. (1983) and Lee et al. (1988) found that the unconfined concrete compressive strength would increase by up to 35% at -40 °C (-40 °F). Lee et al (1983) found that Poisson's ratio would increase in unconfined concrete by as much as 50% at -70 °C (-94 °F) in normal strength concrete. These studies, however, have focused on the behavior of unconfined concrete for use in cryogenic applications or the bond behavior between reinforcing steel and unconfined concrete. Extension of such studies to the confined concrete region of a structure should be investigated to ensure the desired ductile behavior of the structural system especially in a seismic situation. Therefore, an experimental study was undertaken to identify the changes in the stress-strain behavior of confined concrete with varying levels of horizontal and longitudinal reinforcement between 20°C (68°F) and -40°C (-40°F) in a controlled temperature environment.

5.3 Research Significance

Recent research has found that the effects of cold temperature significantly alter the seismic performance of concrete bridge columns supported on drilled shaft foundations (Suleiman et al. 2006, Sritharan et al. 2007, Shelman et al. 2011, and Wotherspoon et al. 2009 & 2010). The performance of such systems starts at the section and material level where one must be able to define the moment-curvature response with due consideration to temperatyre effects. Current knowledge on unconfined concrete at cold temperatures needs

to be expanded to the confined concrete region as the next logical step. This paper presents an experimental investigation into the behavior of confined concrete at cold temperatures and comparisons to a commonly used constitutive model.

5.4 Experimental Investigation

As part of a larger study at Iowa State University (ISU) examining the impacts of cold temperatures on seismic behavior of deep foundations, the material behavior of A706 reinforcing steel (Levings and Sritharan 2012), soil (Shelman et al. 2011) and concrete were tested at cold temperatures for establishing a consistent data set. This paper discusses the experimental testing of confined concrete at cold temperatures using 101.6 mm (4 in.) and 76.2 mm (3 in.) diameter cylinders with horizontal volumetric reinforcement ratios ranging from unconfined to full encasement in a steel shell (~1.3% horizontal reinforcement ratio) for temperatures between 20°C (68°F) and -40°C (-40°F). This investigation was accomplished through the use of two different concrete mix designs with specified concrete strengths from 27.6 MPa (4 ksi) to 55.2 MPa (8 ksi) to represent the expected concrete strengths prevalent in structures. For each reinforcement ratio and desired testing temperature, three specimens were tested under monotonic loading as was consistent with literature on confined concrete testing used in seismic design [Mander et al. (1988)]. Loading rate was selected as 1 mm/min (0.05 in/min) which corresponds to the procedures of ASTM C 39/C 39M (2003) and was similar to the testing rate of Lee et al. (1988) at 1.8 mm/min (0.07 in/min). The remainder of this section describes the materials selection, testing matrix, specimen construction and testing setup used as part of the study.

5.4.1 Materials

The concrete selected for this study was specified to have unconfined compressive strengths of 27.6 MPa (4 ksi) and 55.2 MPa (8 ksi) to capture strengths expected in bridge structures. Batch properties of the final mix designs including strength, slump, air content and temperature at time of batching are provided in Table 5-1 based on the field testing procedures established by ACI for a Grade I Technician.

The small scale testing of confined cylinders required the use of 3.8 mm (0.15 in.) diameter smooth steel wire with a yield strength of 413.7 MPa (60 ksi) as transverse reinforcement. The difference in strength between Grade 60 reinforcing steel, yield strength of 413.7MPa (60 ksi), and the steel reinforcing in the experiment was accounted for by adjusting the spacing of the horizontal confinement reinforcing steel as discussed in the specimen construction portion of this paper. The steel shell reinforcement used for a number of samples was made of a 0.381 mm (0.015 in.) shim stock with a yield strength of 248.2 MPa (36 ksi).

5.4.2 Testing Matrix

Based on the desired testing temperatures and concrete mix designs, a testing plan was constructed to capture the cold temperature behavior of confined concrete as shown in Table 2. The experiment focused on cylinders with a concrete compressive strength of 27.6 MPa (4 ksi) as the reference since this compressive strength represents a common concrete strength specified in design throughout the United States. The remaining concrete mixes were used to verify whether or not similar trends existed for different concrete strengths.

The specified level of the horizontal volumetric reinforcement ratio was taken as 0, 0.006, 0.009, 0.012 and steel shell (with an equivalent ratio of 0.013) based on the expected level of reinforcement in high seismic regions throughout the United States. The unconfined concrete specimens were used to establish the baseline concrete compressive strength at each testing temperature for use in the analytical comparisons of the confined specimens.

5.4.3   Specimen Construction

Using the information in Table 5-2, the confined and unconfined concrete samples were constructed to create the desired testing specimen as provided in Figure 5-1. For the spirally reinforced and unreinforced concrete specimens, the forms were made of plastic cylinder molds of 101.6 mm by 203.2 mm (4 in. by 8 in.) for the 27.6 MPa (4 ksi) concrete mix. In addition, 76.2 mm by 152.4 mm (3 in. by 6 in.) cylinder molds were used for the 55.2 MPa (8 ksi) unconfined and spirally reinforced concrete samples based on the capacity of the testing apparatus. Each mold then had spiral reinforcement inserted with the spacing determined such that the amount of horizontal reinforcement ratio would be the equivalent of a concrete cylinder confined by Grade 60 deformed reinforcing bar. After placement of the spiral reinforcement, two horizontal bars placed in an ubonded state were placed through the mold so that gauges could be placed for measuring vertical strain over the middle third of the specimen to capture the stress-strain behavior. Additionally, a thermocouple was placed within the center of each specimen to ensure the entire sample was at the desired testing temperature.

In addition to the plastic molds, a number of steel shell cylinder molds were constructed for testing purposes. To ensure the shell would act as lateral confinement only, the shell height was intentionally cut 6.3 mm (0.25 in.) short overall to allow for compression of the concrete cylinder without applying direct load to the steel shell. The next step was to create the remainder of the mold by removing the top and bottom of a plastic cylinder and attaching them to the shell such that the appropriate height of concrete was obtained for testing. Furthermore, the horizontal rods and thermocouples needed for measurements during testing were inserted into the final concrete cylinder.

Concrete was placed at local concrete batch plants within the molds using three lifts per mold and consolidation through rodding and tapping procedures dictated in the appropriate field testing guidelines. The specimens were then covered and allowed to cure for one day prior to transporting the specimens back to the structures laboratory at ISU. Once at the lab, the specimens were field cured by leaving them in the molds for 28 days and covering them with a thin layer of water and plastic wrap to lock in the moisture at the top of the concrete specimens. After the full cure time of 28 days had elapsed, the specimens were removed from the molds, capped using high strength sulfur and stored in the lab until testing was possible.

5.4.4 Testing Procedures

After curing, capping and pre-freezing as needed to reduce testing time, specimens were taken to the testing apparatus at the time of testing. The loading frame consisted of an MTS uniaxial testing frame and an environmental chamber as depicted in Figure 5-2. The

environmental chamber uses pressurized liquid nitrogen to cool the interior of the chamber to the testing temperature and maintain the level for the specified cylinder. To test a specimen within this chamber, two extensions were designed and milled at ISU to extend from the wedge grips into the center of the chamber and safely obtain the maximum compressive capacity of the loading frame of 489.3 kN (110 kips). Compression platens were then attached to the end of the rods to apply the compressive force.

The remaining component needed for testing purposes was the instrumentation setup for each cylinder as shown in Figure 5-3. This consisted of a displacement gauge on either side of the cylinder, attached to the top bar of horizontal thread rods, to measure the change in length experienced in the center of the specimen due to compression loading, determining a vertical strain for the concrete specimen to go along with the frames load cell measuring the applied compressive force. A thermocouple was placed at the center of the specimen prior to placement of the concrete to provide confidence that the entire specimen had reached the desired testing temperature. The laterally confined specimens using spiral reinforcement or external steel shells had two strain gauges placed on opposite sides of the cylinder to measure the hoop strain developed from the steel resisting the dilation of the concrete. Two additional displacement gauges were placed along the plane perpendicular to that of the thread rods and measured the vertical strain over the entire height of the specimen. The multiple displacement gauges produced corresponding data until significant cracking caused the thread rod gauges to deviate and not adequately capture the softening of the concrete.

Loading Protocols

The loading of the multiple concrete specimens was performed using a monotonic procedure as initial testing at Iowa State University (Thiemann 2009) indicated that the peak behavior of a cyclic test could be sufficiently captured using monotonic means. Monotonic testing began by seating the specimen within the testing apparatus. After this stage, the machine automatically applied compressive force to the specimen using the specified loading rate until raching one of the following states: (1) the ultimate capacity of the testing apparatus [490 kN (110 kip)]; (2) complete failure of the unconfined specimen; (3) failure of the lateral reinforcement, or; (4) an additional head displacement of 12.7 mm (0.5 in.) was reached without failure. The last value was selected, as this would correspond to an approximate confined compressive strain of 0.06 which exceeds strains typically used in seismic design. In addition, the axial stress being maintained at this level is typically below 40% of the maximum stress experienced by the specimen at the peak load. At this point, the specimen was unloaded and removed from the environmental chamber so that another specimen could be instrumented and tested, Figure 5-4.

5.5 Analytical Investigation

In seismic design, the satisfactory behavior of the confined concrete is important to establish a satisfactory level of ductility in a structural system. The model suggested by Mander et al. (1988) and discussed in Priestley et al. (1996) is commonly used to establish the stress-strain response of confined concrete, Figure 5-5. This model establishes the behavior of the concrete using the unconfined concrete properties for strength along with the effectiveness of the confining reinforcement to define the behavior, Eq. (5-1) through Eq. (5-

4). For a logical comparison as part of the experimental study, it was important to determine whether or not the approach discussed in Priestley et al. (1996) would sufficiently capture the response indicated within the experimental investigation at cold temperatures.

$$f_c = f'_{cc} * x * r / (r - 1 + x^r) \qquad \text{Eq. (5-1)}$$

$$f'_{cc} = f'_c \left(2.254 \sqrt{1 + 7.94 f'_l / f'_c} - 2 f'_l / f'_c - 1.254 \right) \qquad \text{Eq. (5-2)}$$

$$\varepsilon_{cc} = \varepsilon_{co} \left[1 + 5 \left(f'_{cc} / f'_c - 1 \right) \right] \qquad \text{Eq. (5-3)}$$

$$r = E_c / \left(E_c - E_{sec} \right) \qquad \text{Eq. (5-4)}$$

5.6 Experimental Results and Discussion

5.6.1 Unconfined Concrete

The results of the unconfined concrete testing undertaken as part of the experimental investigation are presented first to help define the expected behavior of the confined concrete specimens. According to the information presented in Eqns. (5-1) through (5-4), the most important behavior to understand with decreasing temperature was (1) the unconfined concrete compressive strength, f'_c; (2) the strain at the unconfined compressive strength, ε_{co}, and; (3) the modulus of elasticity, E_c.

The first parameter investigated was the unconfined concrete compressive strength. Based on the work of previous researchers (Sehnal et al. 1983 and 1988), the concrete compressive strength was compared to the strength at a room temperature of 20°C (68°F).

This comparison was accomplished by analyzing the strength gain factor (SGF) which was defined as the strength at the specified testing temperature divided by the average strength of three cylinders tested at the reference temperature. Figure 5-6 provides a comparison of the strength gain factor for an individual mix design and specimens discussed in Table 5-2 along with previous research. Figure 5-7 compares the average of the multiple mix designs tested as part of the experimental investigation with the inclusion of previous research for normal strength concrete materials only. Figure 5-7 data indicates an increasing trend in concrete compressive strength as temperature decreases between the upper and lower temperature testing range. Using the Lee et al. (1988a) data set along with the experimental data because of the similar water to cement ratio, a linear trend was established for the SGF as a function of temperature that accounts for the change in unconfined compressive strength of concrete at cold temperatures, Eq. (5-5). Although the tested cylinders ranged from a 76.2 mm (3 in.) to 101.6 mm (4 in.) diameter, the relative increase between the cold temperature and the room temperature specimens was consistent and size effects were deemed insignificant when related to cold temperature impacts.

$$\text{SGF} = f_c^{'}/f_{c,20}^{'} = -0.0047[T(°C)] + 1.094 \qquad \text{Eq. (5-5a)}$$

$$\text{SGF} = f_c^{'}/f_{c,68}^{'} = -0.0026[T(°F)] + 1.177 \qquad \text{Eq. (5-5b)}$$

Similar to the unconfined compressive strength experimental results, the variation in strain at the unconfined compressive strength with decreasing temperature was compared.

As expected, the experimental data indicated a decreasing trend with the change in temperature for the multiple concrete mix designs investigated as part of this study.

$$\varepsilon_{co,20}=6.9E\text{-}06[T(°C)]+1.86E\text{-}03 \qquad\qquad \text{Eq. (5-6a)}$$

$$\varepsilon_{co,68} = 3.8E\text{-}06[T(°F)] + 1.74E\text{-}03 \qquad\qquad \text{Eq. (5-6b)}$$

The third component investigated for the unconfined concrete specimens was the modulus of elasticity as this is typically assumed to be constant between confined and unconfined concrete. Figure 5-8 provides a comparison of the cold temperature modulus of elasticity by comparing to the average modulus of elasticity in the unfrozen state with removal of data points that exceed the 20% threshold. The relationship indicates that the value is related to the square root of Eqns. (5-5a) and (5-5b) as stated in Eq. (5-7). This relationship is in line with the common definition of modulus being a function of the square root of the unconfined compressive strength of the concrete (ACI 2008). Additionally, the confined concrete modulus was found to equal the unconfined concrete modulus at each respective testing temperature which was consistent with the theory for warm weather conditions (Priestley et al. 1996)

$$RV_{Modulus}=\sqrt{SGF} \qquad\qquad \text{Eq. (5-7)}$$

5.6.2 Confined Concrete

Using the relationships established for the unconfined concrete strengths, the analytical investigation was now used to compare the experimental data with the expected behavior of

the confined concrete by modifying the appropriate material properties in Eqns. (5-1) to (5-4). Material properties were modified in the analytical equations by taking the unconfined compressive strength established from the experimental testing of unconfined concrete and maintaining the strain at the compressive strength of 0.002. The first term analyzed using this technique was the confined concrete compressive strength for different levels of reinforcement. The experimental and analytical data are compared graphically in Figure 5-9 where the experimental data demonstrated a consistently lower trend than the expected confined concrete strength based on changes in unconfined concrete material behavior. Additionally, the low confinement ratio of 0.61% studied as part of this investigation behaved similar to unconfined concrete and was most likely due to the large spacing used on a small cylinder sample. The fully encased steel shell specimens consistently reached the capacity of the testing apparatus; thus, the data will not be provided for the remaining data sets.

The decrease in confinement effects with cold temperature can be contributed to the increase in Poisson's ratio with decreasing temperature as found by Lee et al. (1988). The researchers found that Poisson's ratio would increase between 25% and 45% at a temperature of -60°C (-76°F) when compared with testing at 20°C (68°F). The increase in Poisson's ratio would cause the confined concrete specimens to dilate quicker, thus reducing the effectiveness of the confining steel reinforcement. This suggests that the amount of reinforcement in a confined concrete region must be increased at cold temperatures to ensure the desired performance of the structure.

A comparison of the cold and warm temperature confined concrete compressive strength found that the amount of horizontal confinement reinforcement was independent of the amount of increase as a function of temperature, Figure 5-10. Thus, the amount of strength gain associated with the confined concrete strength with decreasing temperature can be related according to Eq. (5-8).

$$RV_{confined} = f'_{cc} / f'_{cc,20} = -0.00166[T(°C)] + 1.0332 \qquad \text{Eq. (5-8a)}$$

$$RV_{confined} = f'_{cc} / f'_{cc,68} = -0.00092[T(°F)] + 1.0627 \qquad \text{Eq. (5-8b)}$$

The next point analyzed in the data set was the strain and the confined concrete compressive strength as this point typically defines the change from strengthening to softening within an analytically developed stress-strain curve. The data, Figure 5-11, indicated that the strain at the peak confined concrete strength would increase linearly between 0% to 40% over the temperature testing range for this study. This was contrary to the analytical model suggested by Mander et al. (1988), in which a decreasing trend would be expected based on simple modifications to unconfined concrete material properties. Capturing the change in strain at the peak confined concrete compressive strength is possible using Eq. (5-9) with the strain at the reference temperature of 20°C (68°F) computed according to Mander et al. (1988) or an appropriate confined concrete methodology.

$$RV_{\varepsilon cc} = \varepsilon_{cc}/\varepsilon_{cc,20} = -0.0034[T(°C)] + 1.068 \qquad \text{Eq. (5-9a)}$$

$$RV_{\varepsilon cc} = \varepsilon_{cc}/\varepsilon_{cc,68} = -0.0019[T(°F)] + 1.128 \qquad \text{Eq. (5-9b)}$$

The ultimate strain of the confined concrete section was investigated with temperature as this point establishes the one of the ultimate limit state curvatures that would define the plastic behavior in a system. For this experiment, the ultimate concrete strain was defined as the first occurrence of fracture within the horizontal spiral reinforcement. The data indicated that the ultimate concrete strain was unaffected by temperature, Figure 5-12. Figure 5-12c shows that a minimal increase may be present with temperature, but this could be due to test specimens that did not result in adequate data for the ultimate concrete strain. Thus, the warm weather ultimate strain specified by a designer can be applied to cold temperatures up to -40°C (-40°F).

5.7 Conclusions

This paper discussed an experimental investigation into the behavior of confined concrete at cold temperatures on small scale specimens. The testing program provided data necessary for modifying the stress-strain curves that establish the behavior of confined concrete for use in structural design based on the equations presented herein based on the assumption that the starting strength is based on the start of an individual freezing cycle. These modifications were specified based on the specific property being analyzed including the concrete compressive strength, strain at peak compressive strength, modulus of elasticity and ultimate

concrete strain. The following conclusions were drawn from this study based on the

experimental testing at cold temperatures:

- The unconfined concrete compressive strength of concrete increased an average of

  28% when temperature decreased from 20 °C (68 °F) to -40 °C (-40 °F).

- The concrete strain at the peak of the unconfined concrete curve (ε_{co}) was found to be

  approximately 0.002 at 20 °C (68 °F). This value will decrease in a linear manner by

  approximately 23% as the temperature decreases to -40 °C (-40 °F).

- The modulus of elasticity for unconfined concrete (E_c) was found to increase by 13%,

  based on a square root relationship to compressive strength, as temperature decreased

  to -40°C (-40°F) from 20°C (68°F). Furthermore, the confined concrete modulus of

  elasticity was the same as the unconfined concrete modulus of elasticity.

- Similar to the unconfined compressive stress, the confined concrete compressive

  stress (f'_{cc}) was found to increase as temperature decreased from 20°C (68°F) to -

  40°C (-40°F). Additionally, the rate of increase in f'_{cc} was determined to be affected

  by the increase in Poisson's ratio of the concrete specimen as temperature decreases.

  The changing Poisson's ratio decreased the effectiveness of the confinement thus

  reducing the overall strength gain possible. However, additional steel added to the

  specimen will increase the ductility of the confined region as it does during a warm

  weather condition.

- In contrast to the unconfined concrete, the strain at the peak confined compressive

  strength increased between 0% and 40%, depending on the amount of horizontal

reinforcement present in the specimen, as temperature went from 20°C (68°F) to -40°C (-40°F).

- The modification of material properties alone in Mander's model will not adequately capture the behavior of confined concrete subjected to seasonal freezing as shown in Figure 5-9. The confined concrete curve must therefore be established through modification of the key parameters using its own relationships.

- The ultimate confined compressive strain was found to not be affected by decreasing temperature and recommended that the cold temperature value be the same as the warm temperature value.

5.8 Acknowledgements

5.9 Notations

ACI   = American Concrete Institute

ADOT&PF   = Alaska Department of Transportation and Public Facilities

AUTC   = Alaska University Transportation Center

°C   = degrees Centigrade

°F　　　　　　　= degrees Fahrenheit

E_c　　　　　　　= concrete modulus of elasticity

E_{sec}　　　　　　= secant modulus of elasticity to the confined concrete compressive strength

$RV_{Modulus}$　　　= reference value for the modulus of elasticity ($E_{c,cold}$/Average $E_{c,unfrozen}$)

$RV_{\varepsilon cc}$　　　　　= reference value for the confined concrete strain (ε_{cc} /$\varepsilon_{cc,unfrozen}$)

$RV_{confined}$　　　= reference value for the confined concrete strength (f'_{cc}/ $f'_{cc,unfrozen}$)

SGF　　　　　　= strength gain factor for unconfined concrete compressive strength

　　　　　　　　　($f'_{c,cold}$/Average $f'_{c,unfrozen}$)

T　　　　　　　= temperature with the units specified in the parentheses

f_c　　　　　　　= concrete compressive stress at the specified concrete strain

f'_c　　　　　　　= unconfined concrete compressive strength

$f'_{c,20}$ ($f'_{c,68}$)　　= unconfined concrete compressive strength at the unfrozen state of 20°C

　　　　　　　　　(68°F)

f'_{cc}　　　　　　= confined concrete compressive strength

f'_l　　　　　　　= effective lateral confining stress based on the horizontal volumetric

　　　　　　　　　reinforcing steel ratio and yield strength of steel

x　　　　　　　= ratio of specified strain to strain at the confined concrete compressive

　　　　　　　　　strength

r　　　　　　　= coefficient to define the shape of the concrete stress-strain curve

ε_{cc}　　　　　　= strain at the confined concrete compressive strength

$\varepsilon_{cc,20}$ $(\varepsilon_{cc,68})$ = strain at the confined concrete compressive strength at the unfrozen state of

20°C (68°F)

ε_{co} = strain at the unconfined concrete compressive strength, typically taken as

0.002 according to Priestley et al. (1996)

$\varepsilon_{co,20}$ $(\varepsilon_{co,68})$ = strain at the unconfined concrete compressive strength at the unfrozen state

of 20°C (68°F)

ρ_s = horizontal volumetric reinforcing steel ratio

5.10 References

American Concrete Institute (ACI). (2008). *Building code requirements for structural concrete (ACI 318-08) and commentary (ACI 318R-08)*. Farmington Hills, MI: ACI.

ASTM Standard C39/C39M-03, 2003, "Standard test method for compressive strength of cylindrical concrete specimens," West Conshohocken, PA: ASTM International.

Lee, G. C., Shih, T. S. and Chang, K. C., 1988a, "Mechanical properties of concrete at low temperature," *Journal of cold regions engineering* 2(1): 13-24.

Lee, G. C., Shih, T. S. and Chang, K. C., 1988b, "Mechanical properties of high-strength concrete at low temperature," *Journal of cold regions engineering* 2(4): 169-178.

Levings, J. and Sritharan, S., 2012, "Effects of cold temperature and strain rate on the stress-strain behavior of ASTM A706/A706M mild steel reinforcement," *Journal of Materials in Civil Engineering* 24(12): 1441–1449.

Mander, J. B., Priestley, M. J. N. and Park, R. (1988a). "Theoretical stress-strain model for confined concrete." *Journal of structural engineering* 114(8): 1804-1826.

Mander, J. B., Priestley, M. J. N. and Park, R. (1988b). "Observed stress-strain behavior of confined concrete." *Journal of structural engineering* 114(8): 1827-1849.

Sehnal, Z. A., Kronen, H. and Marshall, A. L., 1983, "Factors influencing the low temperature strength of concrete," *Proceedings 2nd International Conference on Cryogenic Concrete, Amsterdam,* London: Concrete Society of UK. pp. 1-11.

Shelman, A., Levings, J. and Sritharan, S., 2011, "Seismic design of deep bridge pier foundations in seasonally frozen ground," *Final Report submitted to AUTC and ADOT&PF.* Access Online from: http://ine.uaf.edu/autc/final-reports/

Sritharan, S., Suleiman, M. T. and White, D. J., 2007, "Effects of seasonal freezing on bridge column-foundation-soil interaction and their implications," *Earthquake Spectra* 23(1): 199-222.

Sritharan, S. and Shelman, A., 2008, "An assessment of broad impact of seasonally frozen soil on seismic response of bridges in the U.S. and Japan," *Proceedings of the 24th US-Japan Bridge Engineering Workshop, Minneapolis,* FHWA: 429-440.

Suleiman, M. T., Sritharan, S. and White, D. J., 2006, "Cyclic lateral load response of bridge column-foundation-soil systems in freezing conditions," *Journal of Structural Engineering* 132(11): 1745-1754

Thiemann, Z. J., 2009, "Pretest three-dimensional finite element analysis of the girder-to-cap-beam connection of an inverted-tee cap beam designed for seismic loadings," *Master's Thesis*, Ames, Iowa: Iowa State University.

Wotherspoon, L. M., Sritharan, S., Pender, M. J., 2009, "Modelling the response of cyclically loaded bridge columns embedded in warm and seasonally frozen soils," *Engineering structures* 32(2010): 933-943.

Wotherspoon, L. M., Sritharan, S., Pender, M. J. and Carr, A. J., 2010, "Investigation on the impact of seasonally frozen soil on seismic response of bridge columns," *Journal of Bridge Engineering* 15(5): 473-481.

Table 5-1: Batch Properties of Concrete Mix Designs

Mix ID	Trial 1	Trial 2
Specified f'$_c$ [MPa] ([ksi])	27.6 (4)	55.2 (8)
Mix Temperature [°C] ([°F])	21.1 (69.9)	21.7 (71)
Slump [cm] ([in.])	3.8 (1.5)	20.3 (8)
Air Content	3.50%	4.40%
Measured f'$_c$ [MPa] ([ksi])	37.1 (5.38)	54.5 (7.91)
w/c ratio	0.26	0.31

Table 5-2: Original test matrix for the experimental investigation of concrete cylinders

Specified Mix Design	f'_c [MPa] ([ksi])	Grade 60 Horizontal Volumetric Ratio, ρ_s	No. of Samples	Temperature [°C] ([°F])
Trial 1	27.6 (4)	Unconfined	12	20 (68), -1 (30.2), -20 (-4), -40 (-40)
		0.006	12	
		0.009	12	
		0.012	12	
		Steel Shell	12	
Trial 2	55.2 (8)	Unconfined	6	-1 (30.2), -20 (-4)
		0.009	6	
		Steel Shell	6	
Total			**96**	

Debonded Threaded
Steel Rods to Attach
Displacement Gauges

Gauge Length

Confined /
Unconfined
Concrete
Specimen

Varies between
152.4 mm (6 in.) and
203.2 mm (8 in.)

Varies between
76.2 mm (3 in.) &
101.6 mm (4 in.)
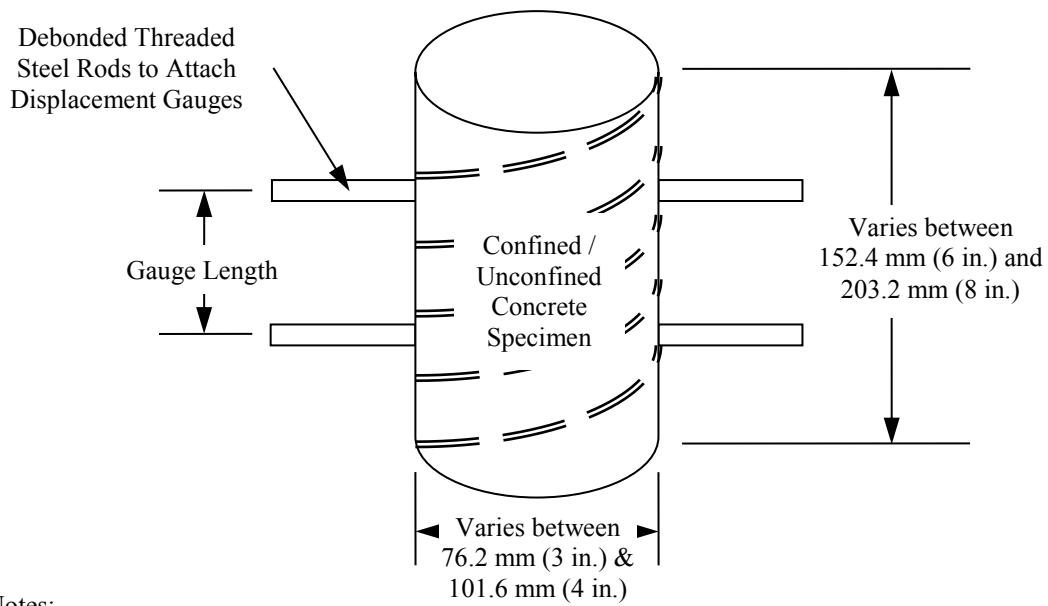
Notes:
- Spiral reinforcement shown as the dashed line was not present in all specimens.
- High strength sulfur caps used to ensure cylinder levelness on top and bottom.
- Instrumentation is not depicted.

Figure 5-1: Typical details of specimens used for testing of confined and unconfined concrete
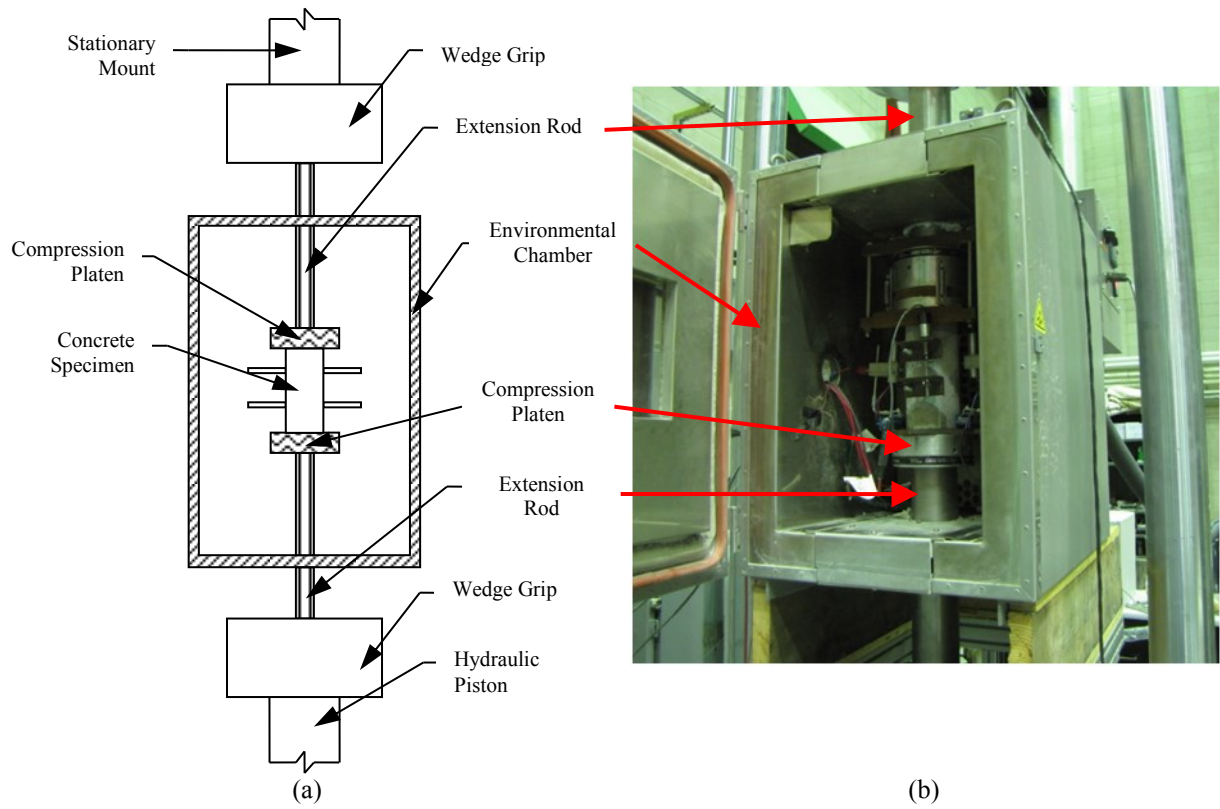
Figure 5-2: Loading frame setup for testing of cylindrical concrete specimens in an environmental chamber: (a) front schematic view; (b) actual view of testing apparatus

Pivoting Head Platen

Gauge Length 1

Gauge Length 2

Thermocouple

Strain Gauge

Fixed Head Platen

(a)

(b)
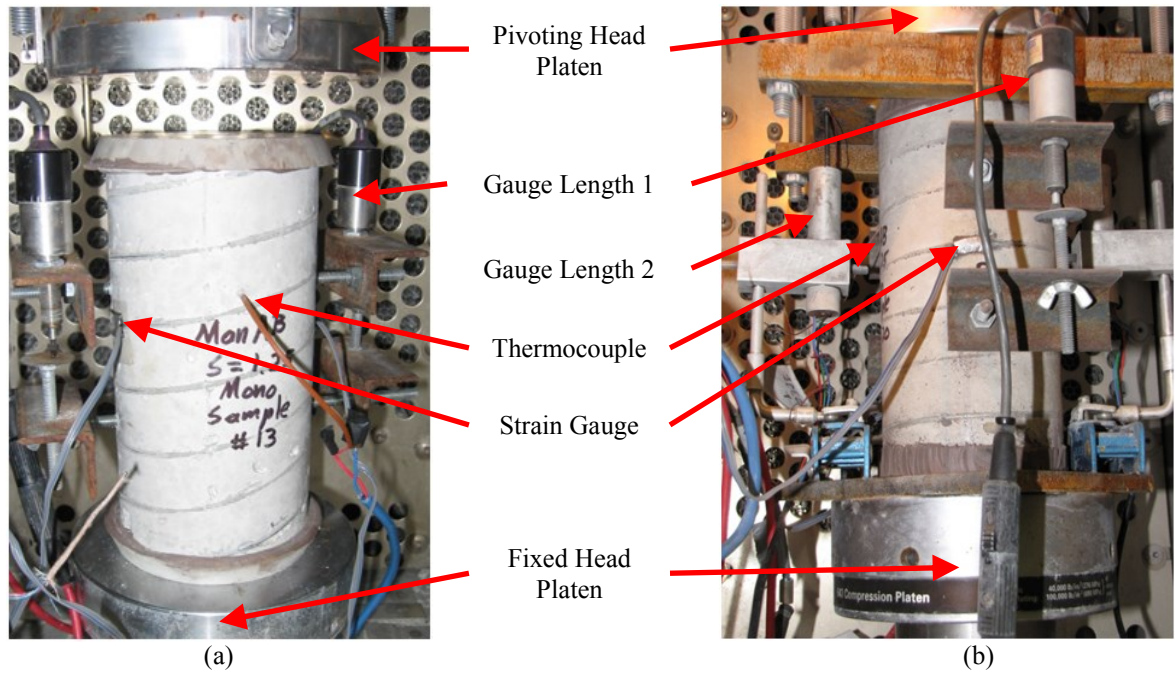
Figure 5-3: Concrete experimental instrumentation setup (a) original; (b) modified

Figure 5-4: A set of specimens after testing to ultimate limit state

Terminology:
f'_c = peak unconfined compressive stress;
E_c = concrete modulus of elasticity;
ε_{co} = strain at peak unconfined concrete stress;
ε_{sp} = unconfined compressive strain at crushing or spalling;
f'_{cc} = peak confined compressive stress;
ε_{cc} = strain at peak confined concrete stress;
ε_{cu} = ultimate confined compressive strain;
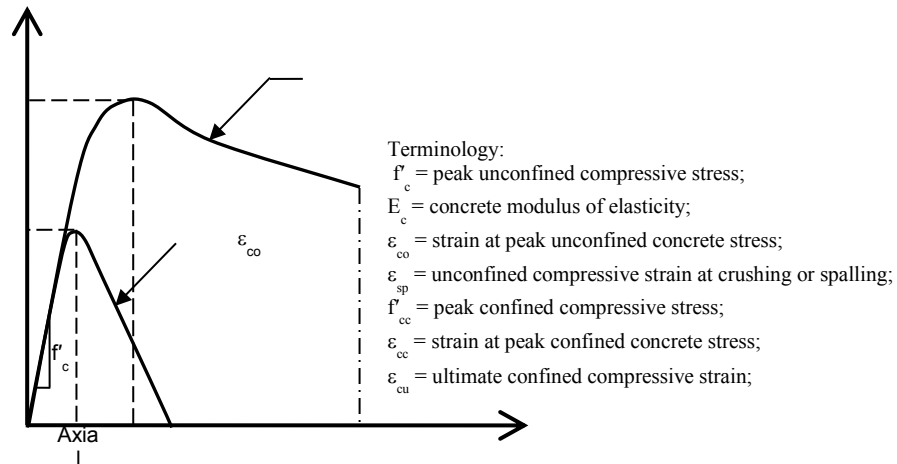
Figure 5-5: Terminology associated with stress-strain response of confined and unconfined concrete
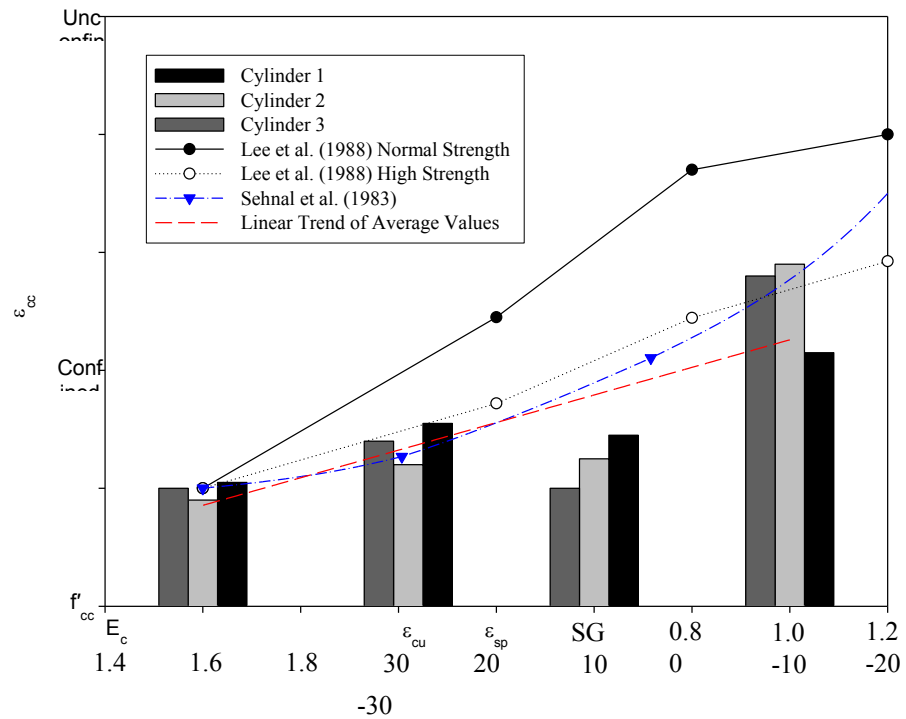
Figure 5-6: SGF for the Trial 1 (4 ksi) concrete mix as a function of cold temperature with comparison to previous research
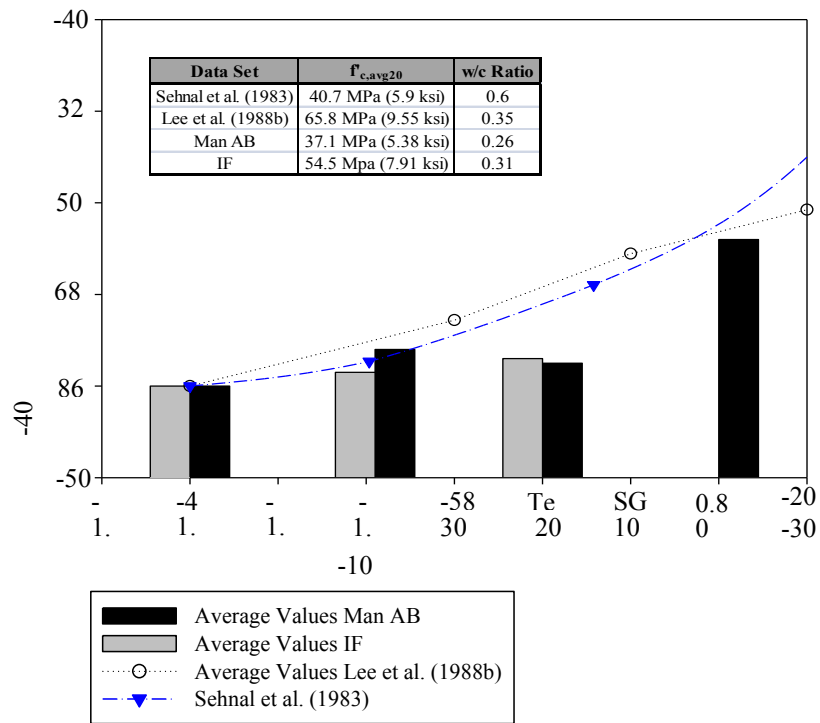
Figure 5-7: SGF of unconfined concrete at cold temperatures including multiple mix designs

205
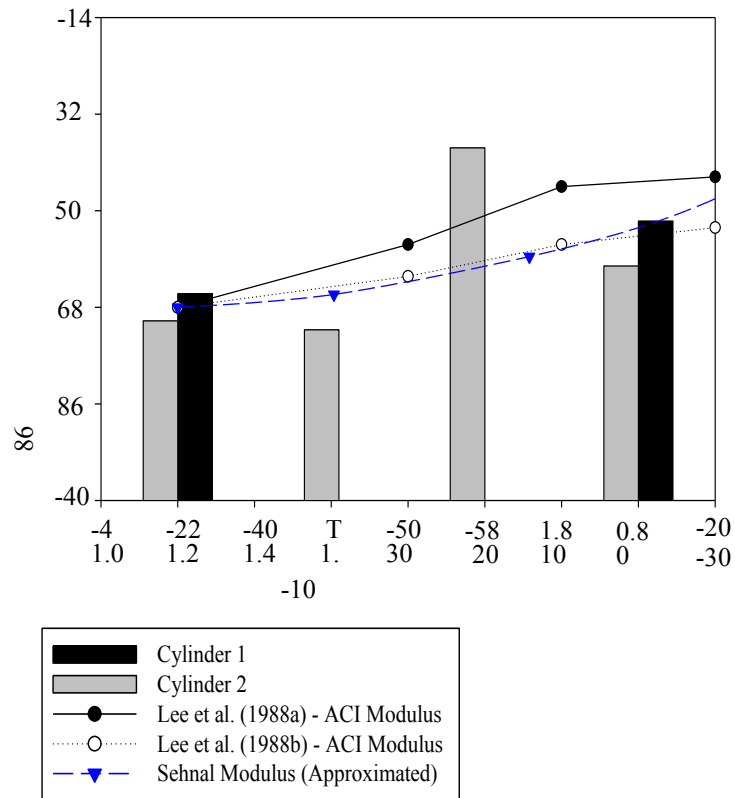
Figure 5-8: Influence of cold temperature on the unconfined modulus of elasticity
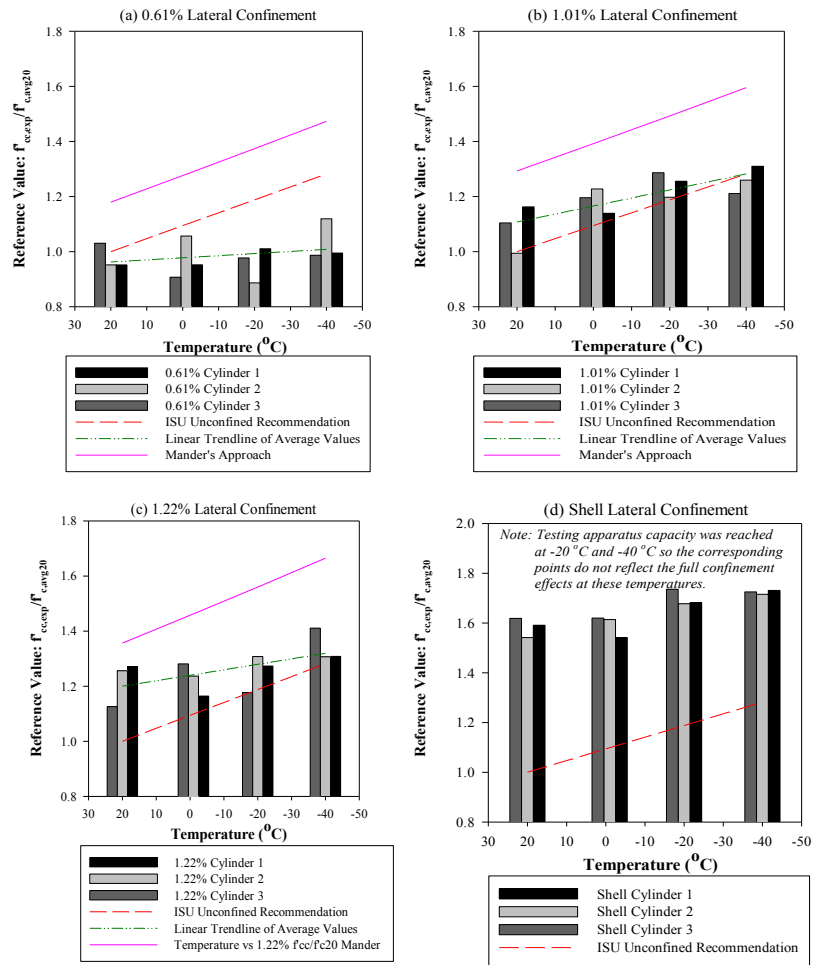
Figure 5-9: Change in confined concrete strength at cold temperatures compared to expected behavior and the behavior of unconfined concrete
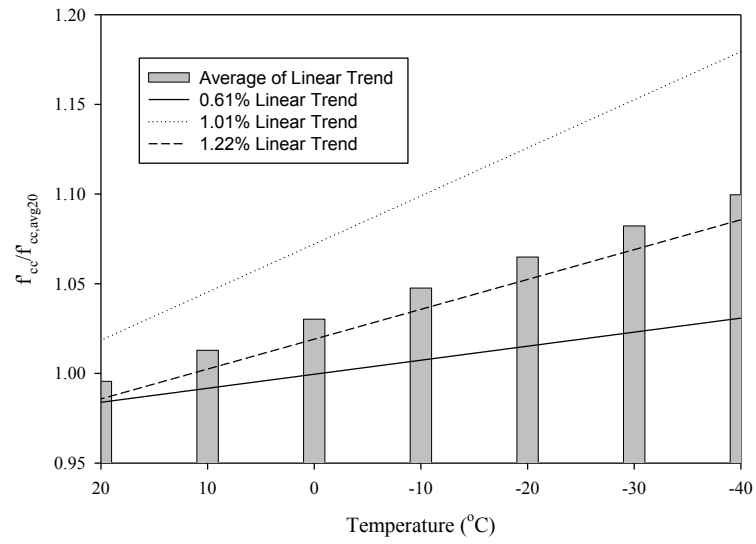
Figure 5-10: Confined concrete strength ratio deviation with temperature
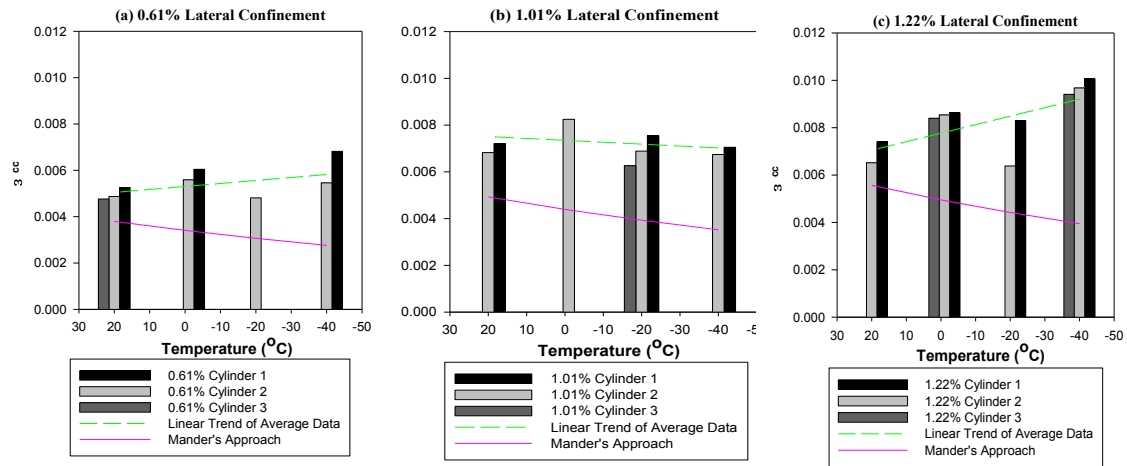
Figure 5-11: Comparison of strain at the confined concrete compressive strength
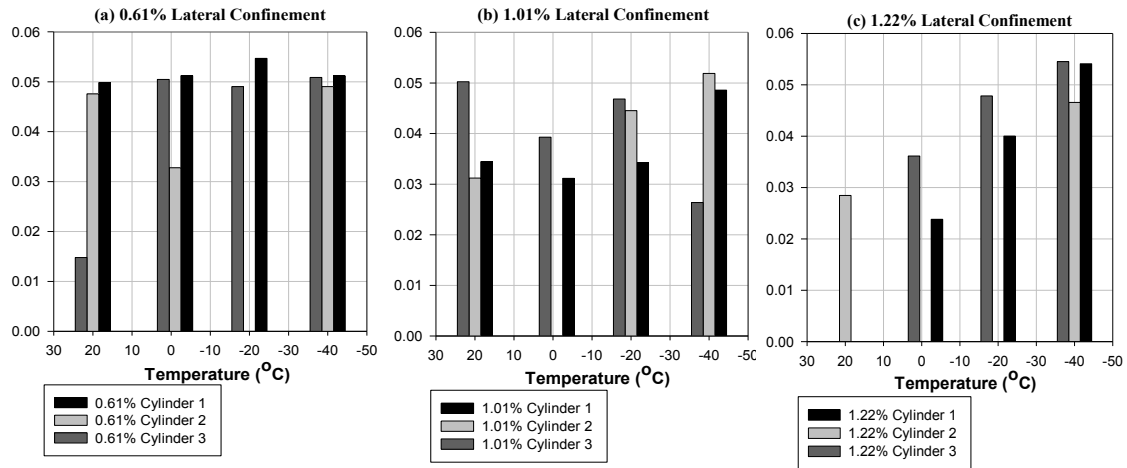
Figure 5-12: Ultimate concrete strain for the confined concrete specimens

CHAPTER 6: EXAMINATION OF METHODS USED FOR ESTABLISHING TRANSVERSE CONFINEMENT REINFORCEMENT FOR BRIDGE COLUMNS

A modified version of a paper to be submitted to a conference related to concrete or earthquake engineering

Aaron T. Shelman[9] and Sri Sritharan[10]

6.1 Abstract

Ductile behavior is an important aspect for the design of structures subjected to lateral loading from events such as earthquakes. Attaining ductile behavior relies on the establishment of adequate amounts of transverse confinement reinforcement in critical regions. Numerous design authorities have specified different approaches, but such approaches vary in the required amount by factors as high as two or three. A recent study at Iowa State University investigated these differences and their impacts on the seismic design of structures. After demonstrating the differences in a few of the different approaches, the impacts to the seismic design of bridge structures is presented based on computer simulations using a fiber-based analysis under static and dynamic loading with emphasis on curvature and displacement ductility demands.

---

[9] Primary Researcher and Author, Research Assistant at Iowa State University, Department of Civil, Construction and Environmental Engineering, Ames, Iowa 50011

[10] Wilson Engineering Professor at Iowa State University, Department of Civil, Construction and Environmental Engineering, Ames, Iowa 50011

6.2 Introduction

The design of structures in regions of high seismicity typically relies on meeting

performance-based design requirements such as (1) fully operational; (2) operational; (3) life

safety, and; (4) near collapse (Priestley 2000). These performance-based design requirements

and past history of earthquake damage has led to the design of structures that respond in a ductile

manner without collapse from undesirable failure modes. In the design of reinforced concrete

bridge columns, this process is normally achieved through the establishment of plastic hinge

regions that have sufficient transverse confinement reinforcement to achieve the desired level of

displacement ductility. Structural damage in recent earthquakes, such as shown in Figure 6-1,

however, has demonstrated that the current design methods employed to ensure an adequate

response still have room for improvement. This paper summarizes the results of a recent study at

Iowa State University that examined several current methods available to design engineers for

the establishment of transverse confinement reinforcement and how they impact the ductile

design of reinforced concrete bridge columns.

6.3 Currently Available Methods

Over the years various design authorities have specified the quantity of transverse

reinforcement needed in a design in the form of the volumetric ratio of transverse steel to

concrete area, which defines the required cross-sectional area within a given spacing and/or the

required level of displacement ductility. These recommendations range from constant values to

multi-variable equations that take into account some combination of terms related to section

geometry, material properties, applied loads, reinforcement detailing and section performance.

This section provides additional detail as to some of the current methods available for use by

design engineers without the inclusion of approaches suggested purely for design of shear reinforcement.

6.3.1 *American Association of State and Highway Transportation Officials (2012)*

Throughout the United States, the design of bridge structures is typically conducted according to the requirements of the LRFD Bridge Design Specifications (AASHTO 2012). According to these standards, the design of transverse reinforced concrete bridge columns must meet two different equations. The first of these equations, Eq. (6-1) was developed to ensure that the core of the cross-section maintains axial load capacity without the presence of the cover concrete associated with the gross area.

$$\rho_s = 0.45\left(A_g/A_{ch} - 1\right)f_c'/f_y \qquad \text{Eq. (6-1)}$$

where: A_g = gross area of concrete

A_{ch} = core area of concrete measured to outside edge of reinforcement

f_c' = unconfined compressive strength of concrete

f_y = yield strength of transverse confinement reinforcement

The second equation, Eq. (6-2), was specified such that an adequate flexural curvature capacity in yielding regions would be attained, thus establishing a sufficient curvature ductility.

$$\rho_s = 0.12f_c'/f_y \qquad \text{Eq. (6-2)}$$

where: f_c' = unconfined compressive strength of concrete

f_y = yield strength of transverse confinement reinforcement

6.3.2   Priestley et al. (1996)

In this approach, the design of the transverse confinement reinforcement was recommended to be designed in accordance with Eq. (6-3), which was based on the work of the ATC-32 project for the seismic design of bridges in the state of California. This particular equation takes into account the amount of longitudinal reinforcement in the section, the applied loads within the system and the material properties used in the design. The authors furthered this approach by stating that a certain amount of reinforcement should be provided to prevent buckling of the longitudinal bars. Additionally, this approach recommends applying Eq. (6-1) for columns less than three feet in diameter.

$$\rho_s = 0.16 f_c'/f_y \left[0.5 + 1.25 P/(f_c' A_g)\right] + 0.13\left[\rho_l - 0.01\right] \qquad \text{Eq. (6-3)}$$

where: A_g = gross area of concrete

P = axial load on the cross-section

f_c' = unconfined compressive strength of concrete

f_y = yield strength of transverse confinement reinforcement

ρ_l = volumetric ratio of longitudinal reinforcement

6.3.3   New Zealand Concrete Structures Design

Similar to the United States, New Zealand maintains its own specifications, NZS 3101 (2008), for the design of concrete structures. In ductile regions of the structure, the recommendations specify the use of Eq. (6-4) for the design of transverse confinement reinforcement. Eq. (6-4) is a modified form of an earlier equation published by the New Zealand group that took into account the curvature ductility of the system. The earlier equation stated

that for ductile regions at the bottom of a story a curvature ductility of 20 could be specified, while a curvature ductility of 10 could be used in limited ductile regions. Thus, Eq. (6-4) is believed to have indirectly included the desired curvature ductility of the system.

$$\rho_s = (1.3 - p_t m) A_g f_c' N^* / (2.4 A_c f_{yt} \varphi f_c' A_g) - 0.0084 \qquad \text{Eq. (6-4)}$$

where: A_g = gross area of column;

A_c = core area of column;

p_t = A_{st}/A_g;

A_{st} = total area of longitudinal column reinforcement;

m = $f_y/(0.85 f_c')$;

f_y = lower characteristic yield strength of longitudinal steel;

f_{yt} = lower characteristic yield strength of transverse steel;

N^* = axial compressive load on column; and

φ = strength reduction factor = 0.85 for columns not protected by

capacity design.

Overall, Eq. (6-4) takes into account numerous factors, but upon closer inspection the design will not be controlled by this equation until the axial load ratio exceeds thirty percent (Park 1996). Thus, requirements to ensure buckling of the longitudinal reinforcing bar does not take place were also included in this design guideline and typically control the overall design.

6.3.4 *Guide Specifications for LRFD Seismic Bridge Design (AASHTO 2010) and*

California Department of Transportation (Caltrans) Seismic Design Criteria (2010)

Although numerous guidelines provide specific equations that designers must meet for the design of transverse confinement reinforcement, the more recent shift towards a performance-based design has resulted in methodologies that provide requirements for the desired behavior of the system. AASHTO Seismic (2010) and the Seismic Design Criteria (SDC) published by Caltrans (2010) have adopted this approach by specifying that the amount of transverse confinement reinforcement should be provided such that a certain displacement ductility is attained. Within the SDC, the intent commonly associated with guidelines of this nature is such that a designer shall perform a pushover analysis on the global structural system and ensure that the prescribed displacement ductility level is satisfied (Shelman and Sritharan 2013). The specific level of displacement ductility depends on the type of bridge column being designed (e.g., a single column bent versus a multi-column bent); however, each individual component must satisfy a minimum displacement ductility level of three. Although not stated explicitly in the SDC, the conservatism built into the confinement equation is generally expected to provide a minimum displacement ductility level of four or greater for the local components of a structural system.

6.4 Impact of Available Equations

Understanding the differences in the above equations requires an examination of the data with respect to the section geometry, applied loads, concrete material properties and amount of longitudinal reinforcement. Comparison that have been conducted in this study related to these characteristics have indicated that the amount of transverse confinement reinforcement specified

for use within a bridge column could vary by a factor of two to three times depending on the equations examined. Furthermore, constant, linear and curvilinear trends were present within the data sets dependent on the approach and characteristic examined. As an example of a few of the results, Figure 6-2 provides the comparison for the influence of unconfined concrete compressive strength and the influence of the axial load ratio. These two comparisons indicate that Eq. (6-1) through Eq. (6-3) typically result in the highest amounts of transverse confinement reinforcement that would be needed for a given design. The exact methodology that would control the design, however, would vary depending on the characteristic variable being examined. The differences can be seen in the axial load ratio comparison (Figure 6-2b) where Eq. (6-3) exceeded the other two equations between a five and ten percent axial load ratio. It is important to note that axial load ratios between a tension value of five percent to a compression value of fifteen percent could be experienced in an exterior column of a multi-bent bridge design, thus suggesting the importance of the axial load ratio in the establishment of the transverse confinement reinforcement. Based on the high variability within the data sets and the fact that different approaches would control the design, the characteristics investigated within this study should be included in any future approach that defines the amount of transverse confinement reinforcement. This included the materials used in the cross-section, the applied axial loads, the amount of longitudinal reinforcement and the ratio of the gross concrete to the core concrete area of the cross-section.

6.4.1   Curvature Ductility

Although a comparison of the different equations and the amount of reinforcement that should be provided is critical, a better comparison for the seismic design of a reinforced concrete

bridge column is the study of the curvature ductility capacity. Such a study was completed, consisting of modeling a series of circular concrete bridge column sections in OpenSEES (2012) for a moment-curvature analysis using a fiber-based zero length element. The comparison consisted of columns with cross-section diameters ranging from 12 in. to 96 in., an axial load ratio of -5% to 15% and a longitudinal reinforcement ratio of 1% to 5%, using #11 bars or a size such that a minimum of 8 bars existed in the cross-section. The concrete material model, concrete07 (developed by the Iowa State Research Team for use in OpenSEES), was specified to have properties established using the recommendations of Priestley et al. (1996) for confined and unconfined concrete, with an unconfined concrete compressive strength of 4 ksi. The increase in the concrete compressive strength for the confined region was accounted for using the amount of transverse confinement according to Eq. (6-1), Eq. (6-2) or Eq. (6-3), since these provided the greatest amounts of transverse confinement reinforcement. The steel material model, steel02, was selected, utilizing a yield strength of 66 ksi longitudinally and a 2% secondary slope to capture strain hardening. Prior to completing the analysis, the OpenSEES model was verified using multiple commonly-used programs that perform a moment-curvature analysis (Shelman and Sritharan 2013).

The results of the analyses are provided in Figure 6-3 through Figure 6-5. Figure 6-3 provides the results of the analyses using Eq. (6-3). This figure indicates that the curvature ductility experiences a polynomial decrease and asymptotically approaches a singular value as the amount of longitudinal steel increased. Furthermore, the amount of decrease was a function of the axial load ratio and the diameter of the cross-section.

Similar trends were noted within Figure 6-4, which provides the impact of Eq. (6-2) on the curvature ductility capacity, established to ensure an adequate flexural curvature capacity. The results of the Eq. (6-2) comparison, however, resulted in a lower curvature ductility capacity than Eq. (6-3) as the amount of longitudinal reinforcement increased. Additionally, an examination of the data at a 2% longitudinal reinforcement ratio indicated that the curvature ductility ranges from 13 to 25 using Eq. (6-2) whereas Eq. (6-3) ranges from 14 to 21.

Figure 6-5 provides a comparison of the curvature ductility capacity using Eq. (6-1) to establish the amount of transverse confinement reinforcement. This particular equation results in a large variation in the overall capacity of the section in a seismic design process. This figure indicates the curvature ductility would vary from a value of 5 up to 25 based on the column diameter, where the cover concrete signifcantly alters the curvature ductility depending on column size, and the applied axial load within the system.

Regardless of the approach used, the amount of transverse confinement reinforcement typically resulted in a curvature ductility capacity less than 20. This specific value was suggested for use in ductile regions according to the design approach of New Zealand (1994). Furthermore, Eq. (6-3) typically resulted in the highest level of curvature ductility; thus, the data would provide the highest level of displacement ductility.

6.4.2 Displacement Ductility

The moment-curvature analyses using Eq. (6-3) were extended to a series of pushover and dynamic analyses. Eq. (6-3) was the approach investigated based on the fact that the highest level of curvature ductility capacity was typically attained with this approach. The pushover analyses were performed on a cantilever style column using values for the aspect ratio (ratio of

column length above the foundation to the column diameter) that varied from three to ten. The results of the static part of the analysis indicated that current equation-based approaches which account for strain penetration satisfactorily captured the global response (Shelman and Sritharan 2013). Furthermore, the data indicated that the selected equation resulted in a displacement ductility greater than 5.5 for all aspect ratios investigated, as shown in Figure 6-6. This level of displacement ductility was well suited to the requirements of the SDC (2010) and AASHTO (2010) guidelines, which have the intent of performing a pushover analysis to ideally ensure that the displacement ductility capacity exceeds a level of four to five.

Although the pushover analysis requirements of the guidelines were adequately met, a dynamic analysis was performed in OpenSEES (2012) to investigate the adequacy of the pushover analyses in determining the lateral behavior of the system. Three different unscaled earthquake records from the Imperial Valley (1940), Loma Prieta (1989) and Northridge (1994) events were applied in separate analyses for the dynamic portion of the investigation. These records were chosen to represent different magnitudes of ground acceleration as well as significant events in the design of bridge structures for seismic situations. Spectral acceleration charts of the 5% damped records are provided in Figure 6-7 along with two typical design spectrums provided by the SDC (Caltrans 2010) for a Type D soil. The bridge columns were specified to have a dynamic mass such that natural periods of 0.5 sec, 1.0 sec, 1.5 sec and 2.0 sec would exist prior to application of ground shaking. Viscous damping in the system was conservatively selected to be 3% of critical, based on information available in Chopra (2007), and applied to the tangent stiffness matrix per available literature [e.g., Priestley and Grant 2004].

The dynamic analyses resulted in both elastic and inelastic responses depending on the column aspect ratio, period of the structure and intensity of the applied ground motion. An example of one set of these analyses is provided in Figure 6-8 for the Northridge event, which has been identified as producing earthquake records with a velocity pulse. This particular event resulted in the capacity of the section being exceeded at low aspect ratios of 3 to 4. It is worth noting, however, that some regions ensure that the bridge column design must have an aspect ratio greater than or equal to an aspect ratio of 4. Although the data suggests that a satisfactory design at column aspect ratios greater than 4 is being achieved, these records do not take into account recent earthquakes such as the 2011 Great East Japan Earthquake (Tohoku), which had large ground accelerations and an associated high intensity. Furthermore, upon closer inspection of the data set, it can be concluded that a bridge column designed with the exact same level of reinforcement and natural period could experience a demand greater than the capacity as indicated by the higher levels of inelastic deformation occurring with the 2.0 sec period systems. This is more prevalent in the curvature ductility demand data set depicted in Figure 6-9 for the Northridge event.

This data, when combined with the comparison of reinforcement equations, suggests that a constant level of ductility may not be appropriate for all design cases. In this study, it was observed that the displacement ductility demand exceeded capacity for the low aspect ratios; thus, it may be more appropriate to account for the expected demand to be seen within the sytem. Although the demand level is hard to specify, additional analyses could provide a reasonable approach that takes into account the column aspect ratio as well as the magnitude and intensity of the design level event.

6.5 Conclusions

A brief summary on the work performed by the research team at Iowa State University into the design of transverse confinement reinforcement was provided within this paper. This summary consisted of a brief discussion on the current approaches available to design engineers for the establishment of transverse confinement as well as their impacts on the seismic design of reinforced concrete bridge columns. Based on this information, the following conclusions were drawn:

1. Existing methodologies require different amounts of confinement reinforcement in the critical plastic hinge regions. The transverse confinement reinforcement amount required by current methods can vary by a factor as high as 2 to 3 times the smallest value.

2. The equation as established by ATC-32 (1996) for Caltrans and presented in Priestley et al. (1996) along with the requirements of AASHTO (2012) fall in the upper range of the confinement reinforcement requirements provided by the different approaches. To provide a better design equation, the establishment of a target curvature demand as a function of column geometry, axial load ratio, longitudinal reinforcement, and column aspect ratio is suggested to formulate a more dependable ρ_s requirement.

3. To further examine the impact of the confinement equations, a ρ_s value was established using the Priestley et al. (1996) approach which takes into account material properties and some initial section designs. Using this approach, a series of additional conclusions were drawn and are as follows:

    a. Current confinement equations provide sufficient amounts of reinforcement to meet the intended design procedure of SDC (2010) and AASHTO (2010) for a

minimum displacement ductility of 3 and the preferred displacement ductility level of 4 or greater. However, the demand on the analyzed system exceeds column capacity based on a pushover analysis at column aspect ratios between 3 and 4.

b. Aspect ratios greater than 4 for the specific column analyzed may experience a lateral earthquake demand greater than the column capacity under a larger magnitude or more intense earthquake event. This possibility along with the dependency of curvature and displacement ductility demands on aspect ratio indicates the need to consider a demand level displacement or curvature ductility level in the design of transverse confinement reinforcement.

c. Based on the dynamic analyses, it was found that a constant value of displacement ductility may not be appropriate for all column designs and should take into account the events being considered in the design process. This was indicated in the data based on the decreasing curvilinear trend that developed in the displacement ductility (Figure 6-8) as a function of earthquake demand, column aspect ratio and natural period of the structure being analyzed.

6.6 Acknowledgements

6.7 References

American Association of State Highway and Transportation Officials (AASHTO), 2010. *Guide Specifications for LRFD Seismic Bridge Design 1st Edition with 2010 Interim Revisions*, Washington D.C.

AASHTO, 2012. *LRFD Bridge Design Specifications, customary U.S. units 6th Edition*, Washington D.C.

Applied Technology Council (ATC), 1996. *Improved Seismic Design Criteria for California Bridges: Provisional Recommendations*, Applied Technology Council, Redwood City, CA

Caltrans, 2010. *Seismic Design Criteria Version 1.6*. Sacramento, CA

Chopra, A. K., 2007. *Dynamics of Structures 3rd Edition.* Upper Saddle River, NJ: Pearson, Prentice Hall.

Kawashima, K., Kosa, K., Takahashi, Y., Akiyama, M., Nishioka, T., Watanabe, G. Koga, H. and Matsuzaki, H., 2011. "Damage of Bridges during 2011 Great East Japan Earthquake." *Proceeding of 43rd Joint Meeting, US-Japan Panel on Wind and Seismic Effects*, UJNR, Tsukuba, Japan

Open System for Earthquake Engineering Simulation (OpenSEES), 2012. *OpenSees Version 2.3.2*. http://opensees.berkeley.edu/

Park, R., 1996. "The Revised New Zealand Concrete Design Standard". *Proceedings of the Eleventh World Conference on Earthquake Engineering – Acapulco*, Elsevier Science Ltd., Mexico

Priestley, M. J. N., Seible, F. & Calvi, G. M., 1996. *Seismic Design and Retrofit of Bridges*, John Wiley & Sons, Inc., New York

Priestley, M. J. N., 2000. "Performance-Based Seismic Design". *Proceedings of the 12th World Conference on Earthquake Engineering*, Auckland, New Zealand

Priestley, M. J. N. and Grant, D. N., 2004. "Viscous Damping in Seismic Design and Analysis", *Journal of Earthquake Enginering*

Shelman, A. and Sritharan, S., 2013 (In Progress). *A critical review of column confinement reinforcement used in current seismic bridge design practice*, Final report prepared for Caltrans

Standards New Zealand, 1995. *The Design of Concrete Structures (NZS 3101:1995)*, Standards New Zealand, Wellington, New Zealand

Standards New Zealand, 2008. *Concrete Structures Standard: Part 1 – The Design of Concrete Structures (NZS 3101: 2008)*, Standards New Zealand, Wellington, New Zealand

Figure 6-1: Nakasone Viaduct after the 2011 Great East Japan Earthquake (Kawashima et al. 2011)
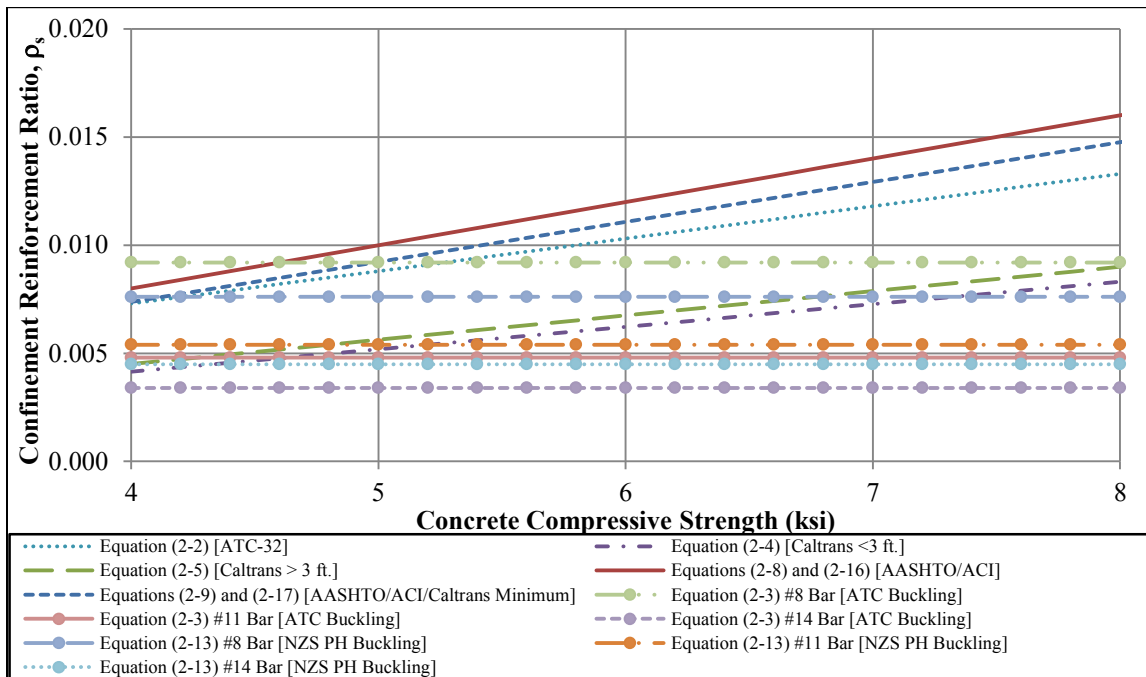
(a) Concrete Compressive Strength
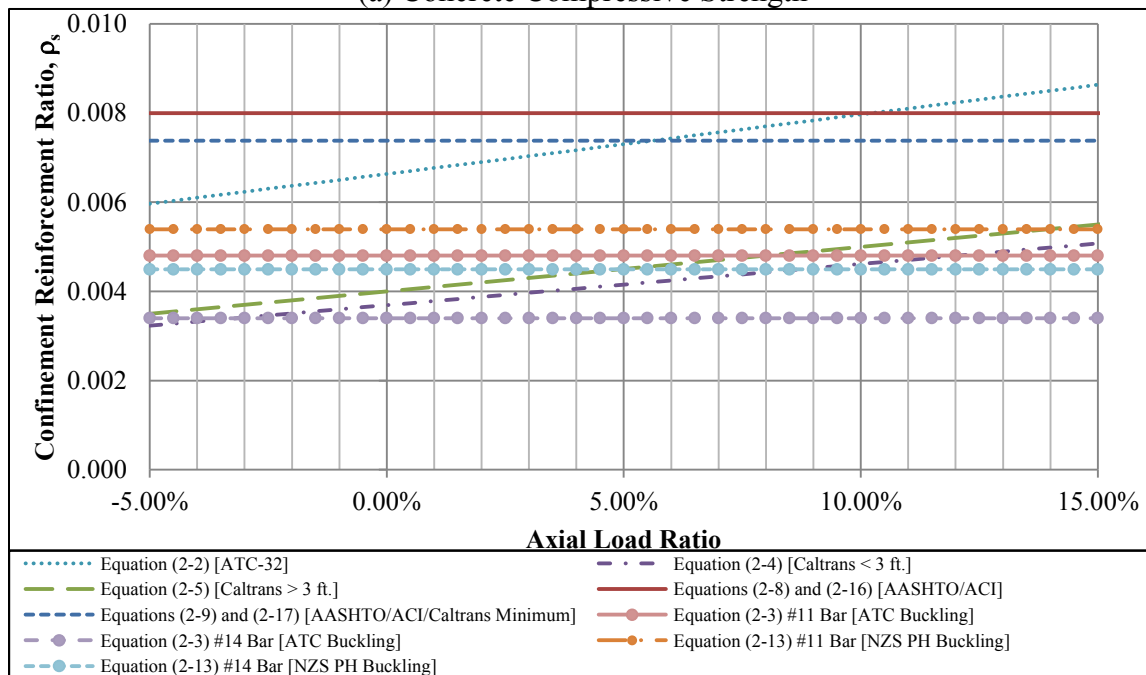
(b) Axial Load Ratio

Figure 6-2: Example comparison of transverse confinement reinforcement requirements for the concrete compressive strength and axial load ratio [after Shelman and Sritharan 2013]
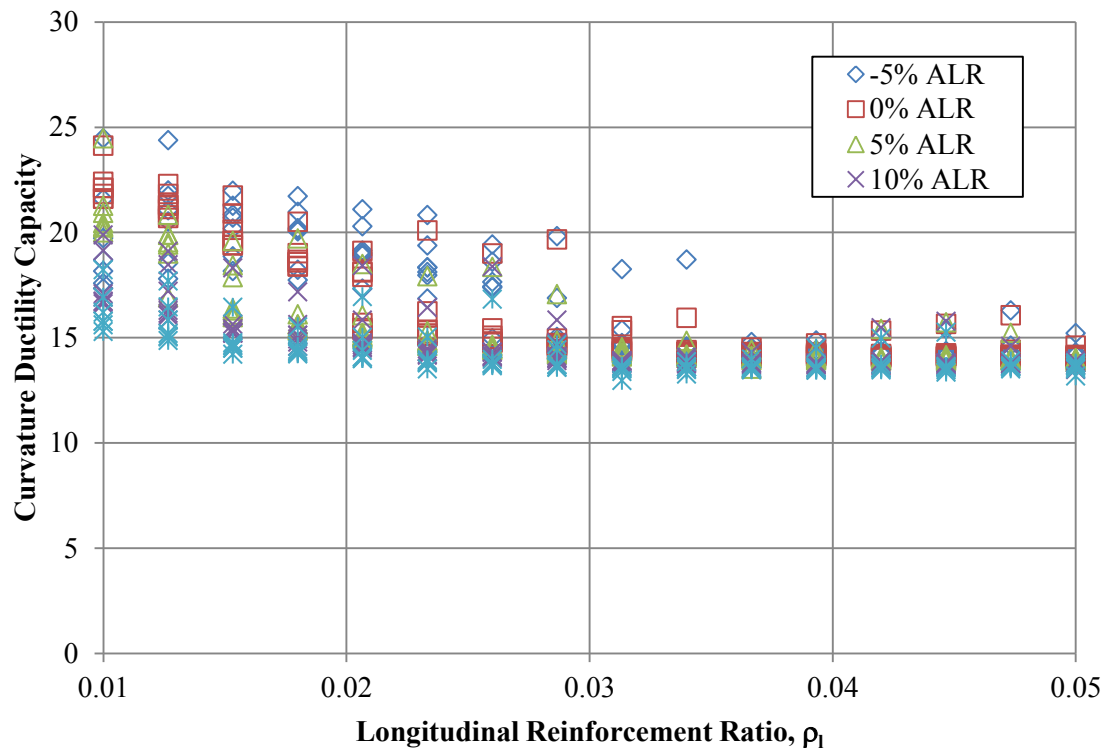
Figure 6-3: Curvature ductility capacity of bridge columns using Eq. (6-3)
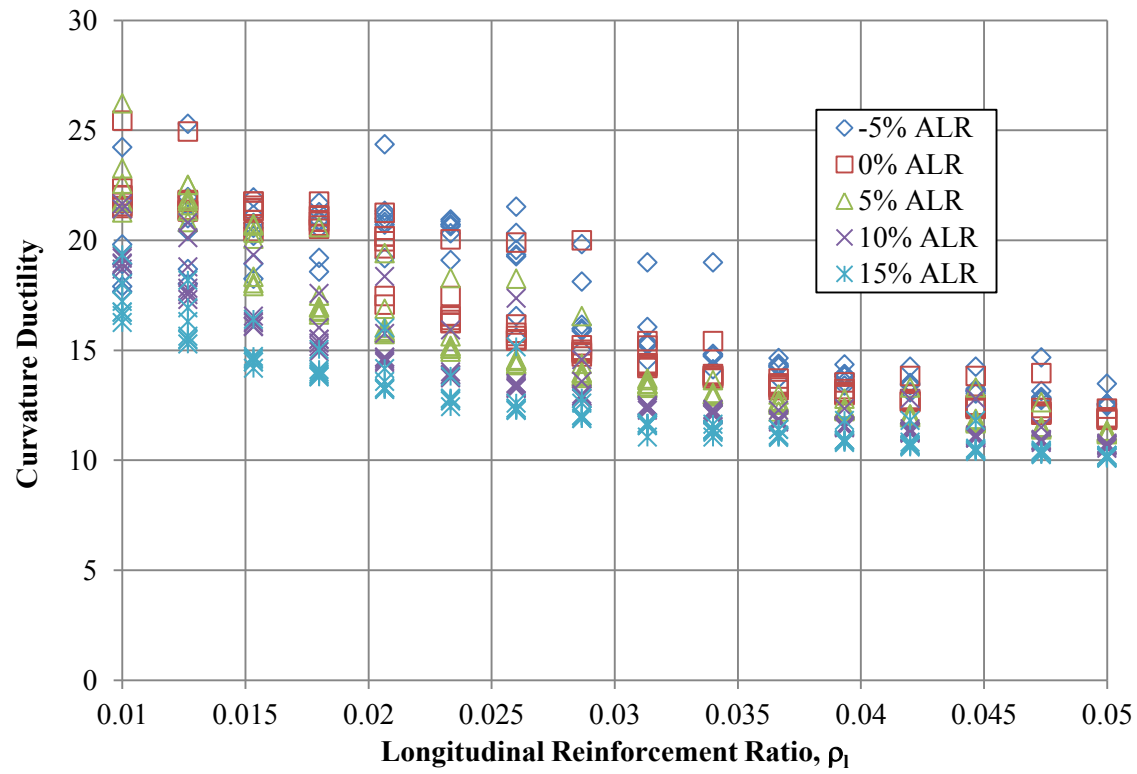
Figure 6-4: Curvature ductility capacity of bridge columns using Eq. (6-2)
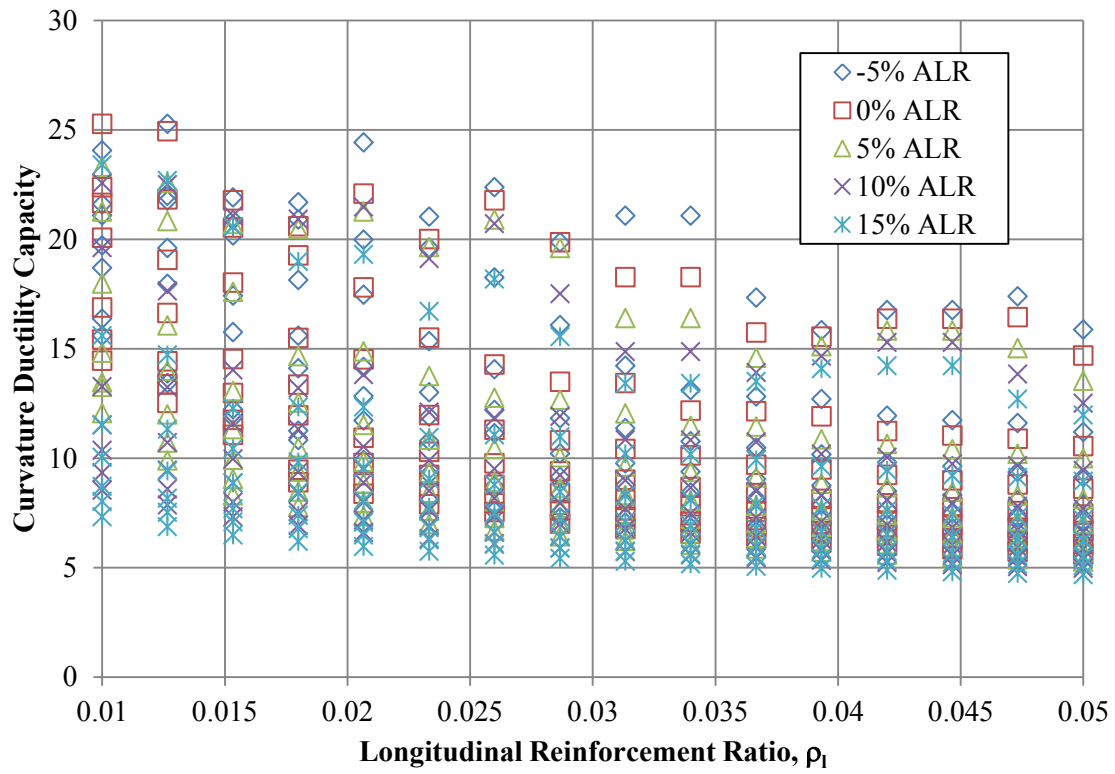
Figure 6-5: Curvature ductility capacity of bridge columns using Eq. (6-1)
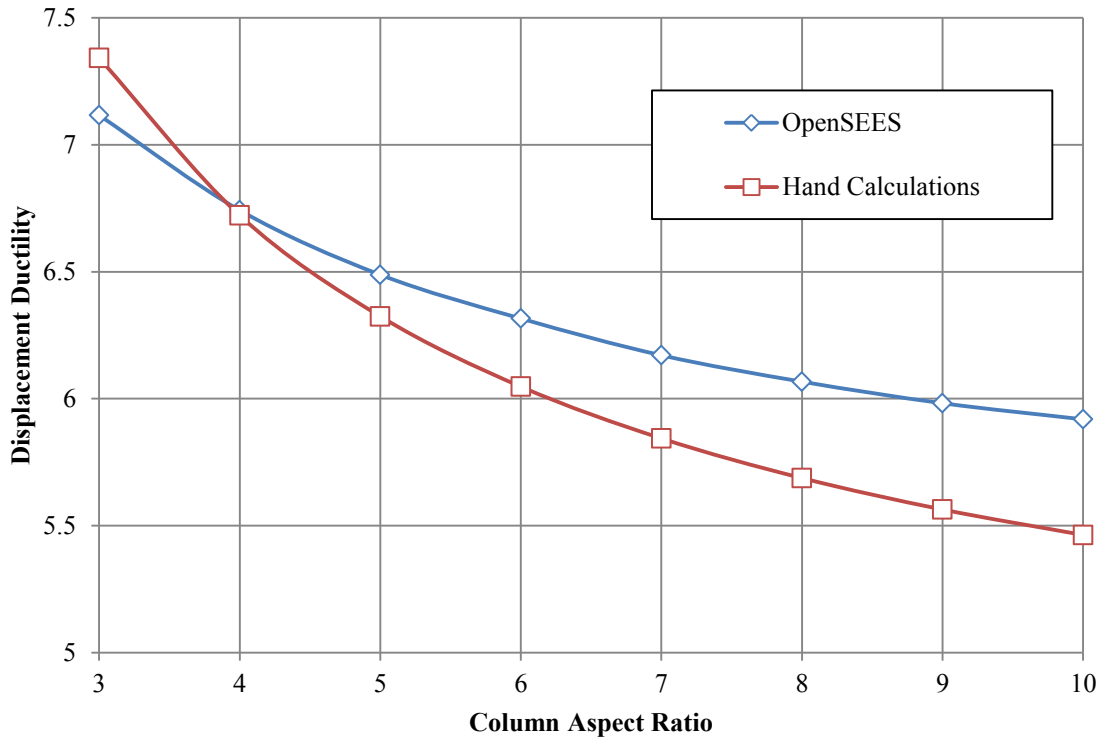
Figure 6-6: Displacement ductility capacity of bridge columns using Eq. (6-3)
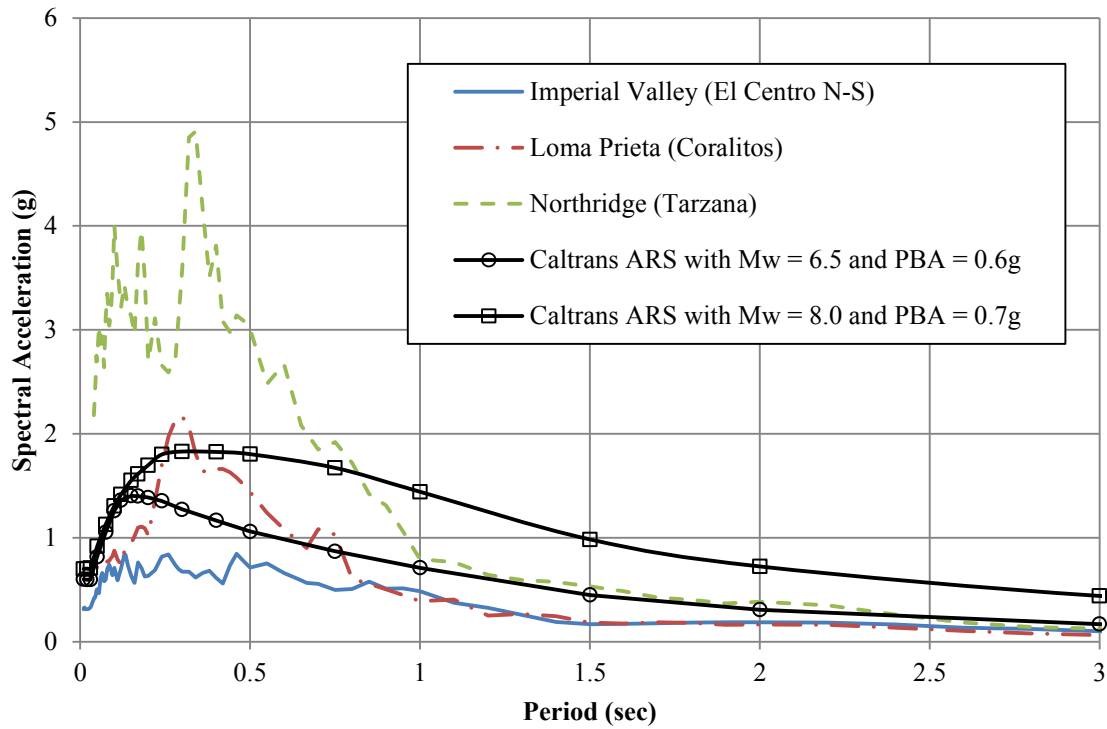
Figure 6-7: 5% damped spectral acceleration curves for selected earthquake records with

two design curves
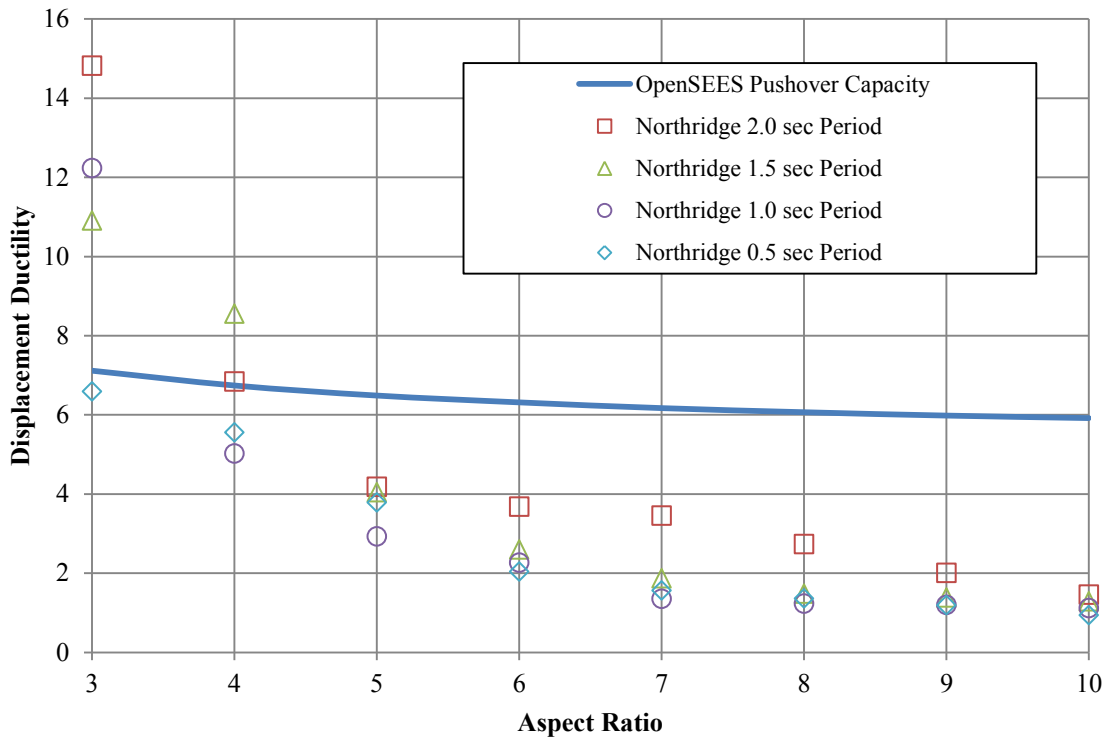
Figure 6-8: Comparison of the displacement ductility capacity and demand obtained from dynamic analyses of bridge columns subjected to the Northridge Earthquake record
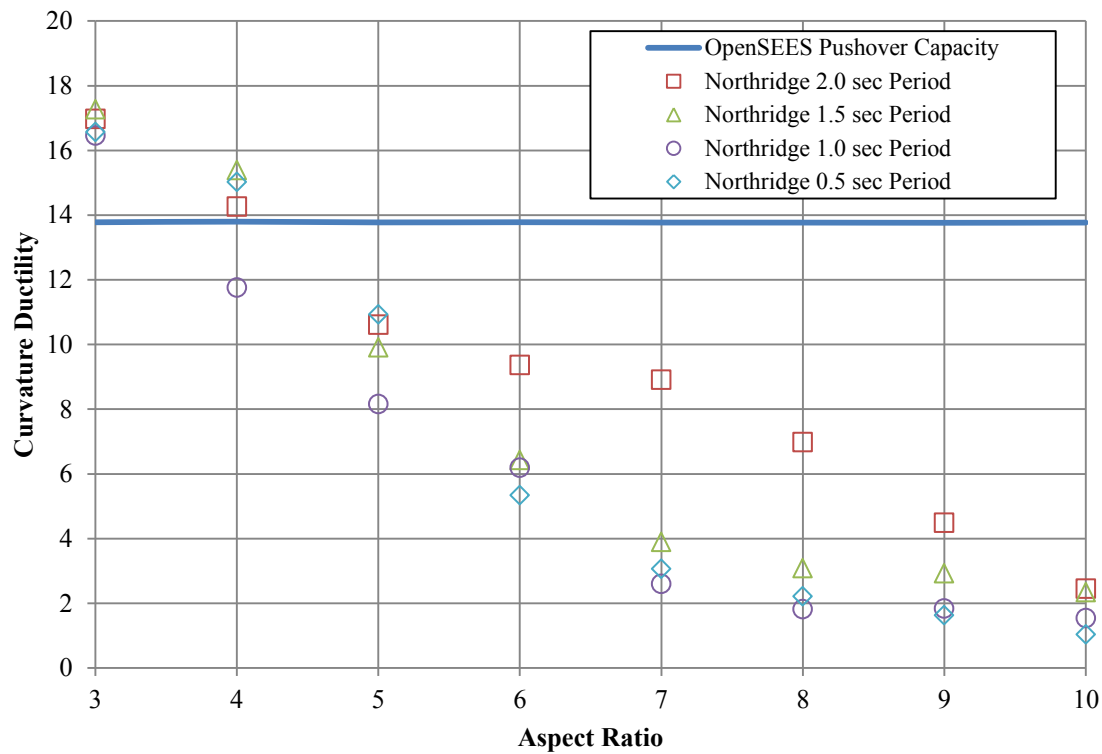
Figure 6-9: Comparison of the curvature ductility capacity and demand obtained from dynamic analyses of bridge columns subjected to the Northridge Earthquake record

CHAPTER 7: SUMMARY, CONCLUSIONS AND RECOMMENDATIONS

7.1 Introduction

Research presented herein on the seismic design of reinforced concrete bridge columns was motivated by the desire to take a proactive approach at advancing current design procedures. The objectives of this research were to: (1) construct a simplified model that is consistent with a previously developed model by the Iowa State University research team for the design of columns continuously supported on drilled shaft foundation; (2) improve the understanding of material behavior of soil and concrete for areas that may experience seasonal freezing; and (3) examine the impacts of current design methodologies for the establishment of transverse confinement reinforcement. The sections presented below provide a summary of the completed work, conclusions drawn from the multiple projects and recommendations developed throughout the process.

7.2 Summary

The research presented within this series of investigations started with a general introduction on the recent history of major seismic events throughout the world and their impact on current infrastructure. This transitioned towards the history of seismic design within the United States and its evolution over the decades. Based on the idea of using a proactive approach, areas for improvement within the current state of practice were discussed including the impact of transverse confinement reinforcement, soil-foundation-structure-interaction and seasonal temperature effects. The scope of research for this document was discussed with respect to the multiple experimental and analytical investigations to be undertaken and presented as a series of journal and conference papers.

An extensive literature review was completed with the goal of providing additional information on advancing the seismic design of reinforced concrete bridge columns that could not be provided in the selected form for this document. The first portion examined was the variation within design equations and methodologies for the establishment of transverse confinement reinforcement. This was followed by a discussion on the influence of SFSI on the seismic design of bridge columns with the impacts of seasonal freezing on its overall response. This process included an examination on the broad impacts of temperature variation on the infrastructure within the United States and Japan. Due to the drastic changes in behavior associated with seasonal freezing, a study on the current knowledge base associated with material behavior of soil and concrete at freezing temperatures was conducted to highlight possible areas of improvement and further demonstrate the need for inclusion of temperature effects in routine design.

A simplified model for determining the lateral response of drilled shafts in non-cohesive soils was developed to create a consistent approach with the one discussed in Appendix A. The proposed methodology consisted of a cantilever supported on a flexible base such that the effective height was from the column tip to the point of maximum moment. Properties of the system and the three springs were established using a series of simple equations. These equations allow for the establishment of a bilinear force-displacement curve representing the lateral load response of the system with limit states defined at the first occurrence of yielding in the longitudinal steel reinforcement and the ultimate flexural failure of the cross-section.

The accuracy of the method was verified against experimental data from Chai and Hutchinson (2002) and detailed analyses performed in LPILE.

The next topic tackled was the material behavior of soil at freezing temperatures. This was performed using an experimental investigation on five soil types expected to be encountered near bridge locations throughout the United States. Testing was performed at three different temperatures in an unconsolidated and undrained manner using a specially designed triaxial testing apparatus in New York City. Preliminary recommendations for adjusting material properties and their impacts on the seismic design of bridge columns continuously supported on drilled shaft foundations were included.

Improvement of the overall design process was then extended to the behavior of confined concrete at subzero temperatures. This was performed using an experimental investigation on multiple confined concrete specimens using three mix designs, five levels of reinforcement and four different levels of subzero temperatures. Preliminary trends were presented for the impacts of temperature on the mechanical properties of confined and unconfined concrete that could be used in the design of reinforced concrete in high seismic regions. Additional information was provided to indicate the need to improve theoretical design models used for defining the confined concrete behavior; thus improving the understanding of curvature and displacement ductility for seismic design of reinforced concrete bridge columns.

Assuming the temperature effects could be adequately addressed, it was important to ensure that enough transverse confinement reinforcement was being provided to attain the

desired ductile response. The requirements associated with different standards and recommendations for the establishment of transverse confinement reinforcement in the critical plastic hinge region were investigated. After highlighting the large variation in the requirements, a brief discussion on the impacts of the highest levels of provided reinforcement were investigated using pushover and dynamic analyses.

7.3 Conclusions

Based on the information attained from the multiple studies within this document, the following conclusions were drawn:

- Recent earthquakes have indicated that there is still room for improvement within the current seismic design of reinforced concrete bridges. SFSI and seasonal freezing were found to highly influence the overall lateral load response as indicated by researchers such as Chai (2002), Sritharan et al. (2007) and Wotherspoon et al. (2010).

- A new simplified method was developed for the establishment of the lateral load response of bridge columns continuously supported on drilled shaft foundations using a series of equations. The method was constructed to be consistent with the approach described in Appendix A and adequately verified against the work of Chai and Hutchinson (2002).

- Within the experimental investigation into the behavior of soil subjected to frozen temperatures a number of conclusions were produced. Those conclusions are presented below:

o The unconfined compressive strength of soil significantly increases with colder temperatures. The multiple soil types tested (Type I through V, excluding II) typically had the strength ratio increase by a factor of 10 at -1°C (30.2°F) and 100 at -20°C (-4°F).

o The strain at the unconfined compressive strength decreased by 0.05 ε between the upper and lower limit testing temperatures for all soils. This corresponds to a drop in strain of 1.25E-3 ε/°C (6.5E-4 ε/°F) as a function of temperature for all the soil types tested.

o The stiffness ratio increased in an exponential manner to an average factor of 300 at -20°C (-4°F) for Type I through Type V soils, excluding Type II soils.

o Increasing the moist unit weight of the soil specimens caused an increase in the unconfined compressive strength at -20°C (-4°F). Additionally, the increased moisture content caused a higher amount of ice in the void spaces, which led to an increased unconfined compressive strength at -20°C (-4°F).

o The Type II soils tested in this program did not follow the same magnitudes of increase for the UCS and soil modulus of elasticity. In this instance, the UCS ratio increased by 140 and 740 at -1°C (30.2°F) and -20°C (-4°F), respectively. The stiffness ratio increased by a factor of 1000 to 1800 at -20°C (-4°F).

o Additional testing of Type I soils was performed to examine the influence of moist unit weight, moisture content and strain rate. The increasing trends for

the moist unit weight and moisture content tests were as expected based on the current understanding of warm weather behavior. Variation in the rate of monotonic loading of the Type I soils between 0.1% and 10% strain per minute resulted in an increase of the unconfined compressive strength and strain at the associated level. However, the modulus of elasticity was unaffected by strain rate over the testing range.

- o Cyclic loading of the warm and frozen soil specimens produced data trends similar to that of the monotonic testing for the strength ratio, stiffness ratio and strain at the unconfined compressive strength. The residual deformation of the soil type tested was 93% of the peak strain value at -1°C (30.2°F) and 80% of the peak strain at -20°C (-4°F). Additionally, strain rate effects were the same as the monotonic specimens at -20°C (-4°F).

- o The influence of frozen soil on the lateral load response of a column continuously supported on a CIDH was found to be significant. The column and foundation shear demands increased by 19% to 128%, depending on the depth of frozen soil and temperature being examined. Additionally, the critical design location shifted towards the ground surface by over a meter at the extreme testing temperature of -20°C (-4°F), emphasizing the importance of accounting for seasonal temperature variation.

- Within the experimental investigation into the behavior of confined concrete

  subjected to seasonal freezing a number of conclusions were produced. Those

  conclusions are presented below:

  - The unconfined concrete compressive strength of concrete increased an

    average of 28% when temperature decreased from 20 °C (68 °F) to -40 °C (-40

    °F).

  - The concrete strain at the peak of the unconfined concrete curve (ε_{co}) was

    found to be approximately 0.002 at 20 °C (68 °F). This value will decrease in

    a linear manner by approximately 23% as the temperature decreases to -40 °C

    (-40 °F).

  - The modulus of elasticity for unconfined concrete (E_c) was found to increase

    by 13%, based on a square root relationship to compressive strength, as

    temperature decreased to -40°C (-40°F) from 20°C (68°F). Furthermore, the

    confined concrete modulus of elasticity was the same as the unconfined

    concrete modulus of elasticity.

  - Similar to the unconfined compressive stress, the confined concrete

    compressive stress (f'_{cc}) was found to increase as temperature decreased from

    20°C (68°F) to -40°C (-40°F). Additionally, the rate of increase in f'_{cc} was

    determined to be affected by the increase in Poisson's ratio of the concrete

    specimen as temperature decreases. The changing Poisson's ratio decreased

    the effectiveness of the confinement thus reducing the overall strength gain

possible. However, additional steel added to the specimen will increase the ductility of the confined region as it does during a warm weather condition.

- o In contrast to the unconfined concrete, the strain at the peak confined compressive strength increased between 0% and 40%, depending on the amount of horizontal reinforcement present in the specimen, as temperature went from 20°C (68°F) to -40°C (-40°F).

- o The modification of material properties alone in Mander's model (1988) will not adequately capture the behavior of confined concrete subjected to seasonal freezing as shown in Figure 5-8. The confined concrete curve must therefore be established through modification of the key parameters using its own relationships.

- o The ultimate confined compressive strain was found to not be affected by decreasing temperature and recommended that the cold temperature value be the same as the warm temperature value.

- Within the analytical study on the requirements of transverse confinement reinforcement and its impacts on the seismic design of reinforced concrete bridge columns resulted in a number of conclusions. A large variation was noted in the different requirements and the final conclusions are provided below:

- o The equation as established by ATC-32 (1996) for Caltrans and presented in Priestley et al. (1996) along with the requirements of AASHTO (2012) fall in the upper range of the confinement reinforcement requirements provided by

the different approaches. To provide a better design equation, the establishment of a target curvature demand as a function of column geometry, axial load ratio, longitudinal reinforcement, and column aspect ratio is suggested to formulate a more dependable ρ_s requirement.

o   To further examine the impact of the confinement equations, a ρ_s value was established using the Priestley et al. (1996) approach which takes into account material properties and some initial section designs. Using this approach, a series of additional conclusions were drawn and are as follows:

   ▪   Current confinement equations provide sufficient amounts of reinforcement to meet the intended design procedure of SDC (2010) and AASHTO (2010) for a minimum displacement ductility of 3 and the preferred displacement ductility level of 5. However, the demand on the analyzed system exceeds column capacity based on a pushover analysis at column aspect ratios between 3 and 4.

   ▪   Aspect ratios greater than 4 for the specific column analyzed may experience a demand greater than the column capacity under a larger magnitude or more intense earthquake event. This possibility indicates the need to consider a demand level displacement or curvature ductility level in the design of transverse confinement reinforcement.

   ▪   Based on the dynamic analyses, it was found that a constant value of displacement ductility may not be appropriate for all column designs

and should take into account the events being considered in the design process. This was indicated in the data based on the decreasing curvilinear trend that developed in the displacement ductility (Figure 6-8) as a function of earthquake demand, column aspect ratio and natural period of the structure being analyzed.

7.4 Recommendations

A number of recommendations towards the seismic design of reinforced concrete bridge columns were presented within this series of papers and are as follows:

- The influence of frozen temperatures on the behavior of soil can be addressed using the equations presented within Chapter 4. When using these equations, it is assumed that the design engineer has established an appropriate starting strength by taking into account the influence of freezing and thawing, in-situ strength, possible degradation from cyclic loading, etc.

- The influence of frozen temperatures on the behavior of confined and unconfined concrete can be addressed using the equations presented within Chapter 5. When using these equations, it is assumed that the design engineer has established an appropriate starting strength by taking into account the influence of freezing and thawing, possible degradation from chemicals, etc.

- Simplified models were developed that can be applied to the design of columns continuously supported on drilled shaft foundations in cohesive and non-cohesive

soils. The proposed models are recommended to improve current practice as they provide both the lateral displacement and force response with a single model.

7.5 Future Research

Throughout the studies within this project a number of different topics were addressed including: (1) the development of a new simplified method for the lateral load response of columns continuously supported on drilled shafts in non-cohesive soils; (2) the influence of seasonal freezing on the behavior of confined and unconfined concrete; (3) the impacts of seasonal freezing on the behavior of five soil types expected to be encountered near bridge sites throughout the United States; and (4) the variation and impacts of current design methodologies for transverse confinement reinforcement to the seismic design of reinforced concrete bridge columns. During this process, a number areas were identified for future areas of research and further refinement of the studies presented within this series of papers. The recommendations are as follows:

- The use of a tri-linear curve in determining the lateral response could be investigated to more accurately capture the shear demands experienced by a column supported continuously supported on a drilled shaft foundation.

- Alternative materials, such as steel and ultra-high performance concrete, should be investigated to expand on the capabilities of the improved model in capturing the lateral loading response.

- Additional testing on the behavior of soil at frozen temperatures for use in the seismic design of bridge columns could be completed. This should include triaxial testing to

identify variations in the friction angle of sand soils as well as additional tests to produce a larger data set using multiple soils and temperatures.

- Additional testing on the behavior of confined concrete at frozen temperatures could be completed to populate a larger data set and construct a theoretical model for use in frozen conditions. This data set should take into account potential size effect concerns as well as the presence of longitudinal reinforcement in the cross-section.

- A new equation for the establishment of transverse reinforcement could be developed that takes into account the expected demand from an earthquake event as well as axial load ratio, the amount of longitudinal reinforcement, material properties and the ratio of the gross to core concrete cross-sectional area. This would help to improve the efficiency of the design process.

- The impacts of a dynamic versus a pushover analysis should be further investigated to ensure that all effects are sufficiently captured during the design process.

7.6 References

American Association of State Highway and Transportation Officials (AASHTO), 2010. *Guide Specifications for LRFD Seismic Bridge Design 1st Edition with 2010 Interim Revisions*, Washington D.C.

AASHTO, 2012. *LRFD Bridge Design Specifications, customary U.S. units 6th Edition*, Washington D.C.

Applied Technology Council (ATC), 1996. *Improved Seismic Design Criteria for California Bridges: Provisional Recommendations*, Applied Technology Council, Redwood City, CA

Caltrans, 2010. *Seismic Design Criteria Version 1.6*. Sacramento, CA

Chai, Y. H. (2002). "Flexural strength and ductility of extended pile-shafts. I: analytical model." *Journal of Structural Engineering* 128(5), 586-594.

Chai, Y. H. & Hutchinson, T. C. (2002). "Flexural strength and ductility of extended pile-shafts. II: experimental study." *Journal of Structural Engineering* 128(5), 595-602.

Mander, J. B., Priestley, M. J. N. and Park, R. (1988a). "Theoretical stress-strain model for confined concrete." *Journal of structural engineering* 114(8): 1804-1826.

Mander, J. B., Priestley, M. J. N. and Park, R. (1988b). "Observed stress-strain behavior of confined concrete." *Journal of structural engineering* 114(8): 1827-1849.

Priestley, M. J. N., Seible, F. & Calvi, G. M., 1996. *Seismic Design and Retrofit of Bridges*, John Wiley & Sons, Inc., New York

Sritharan, S., Suleiman, M. T. and White, D. J. (2007). "Effects of seasonal freezing on bridge column-foundation-soil interaction and their implications." *Earthquake spectra* 23(1): 199-222.

Wotherspoon, L. M., Sritharan, S., Pender, M. J. and Carr, A. J. (2010). "Investigation on the impact of seasonally frozen soil on seismic response of bridge columns." *Journal of bridge engineering* 15(5): 473-481.

APPENDIX A: A RATIONAL MODEL FOR CHARACTERIZING THE MONOTONIC LATERAL RESPONSE OF DRILLED SHAFTS IN COHESIVE SOILS

A paper to be submitted to the American Society of Civil Engineers (ASCE) Journal of Structural Engineering

Aaron Shelman[11] and Sri Sritharan[12]

A.1: Abstract

The influence of soil on a foundation subjected to lateral loading impacts the behavior of both the foundation and the column to which it is typically connected. This paper examines the current state of practice for accounting for characterizing the column-shaft-soil system using simplified means and proposes a new rational model with improved capabilities. The proposed model is aimed to establish a bilinear response for the overall behavior of the system using a set of three springs to create a flexible base for the column at the maximum moment location. Spring properties and overall length of the new system are based on a series of simple equations that allow the response to be computed quickly by hand. Additional features of the model include: (1) the ability to estimate ultimate shear demand and its associated location, and; (2) the ability to account for the effects of seasonal temperature variations. Verification, both analytical

---

[11] Primary Author and Researcher; Research Assistant, Department of Civil, Construction and Environmental Engineering, Iowa State University, Ames, IA 50011

[12] Wilson Engineering Professor, Department of Civil, Construction and Environmental Engineering, Iowa State University, Ames, IA 50011

and experimental, of the model is provided, demonstrating adequacy of the model in representing the columns supported on drilled shaft foundations in cohesive soils.

CE Database Keywords: Foundations; Seismic design; Soil-Structure Interaction; Models; Concrete; Cold Temperature; Cohesive Soil

A.2: Introduction

Lateral loading on structures (e.g., wind and seismicity) requires the design of their foundations to resist overturning and prevent collapse. In regions of high seismicity, a common bridge design practice is the use of columns continued directly into the ground as drilled shaft foundations due to reduction of construction costs. The effects of soil-foundation-structure-interaction (SFSI), however, increase the difficulty of characterizing the monotonic lateral response of column-shaft systems as equilibrium must be maintained between soil and foundation at all points while taking into account the nonlinear behavior of soil and reinforced concrete. Establishing the monotonic behavior is further complicated by the effects of seasonally frozen temperatures where critical locations shift upwards, drastically increasing force demands [Suleiman et al. 2006; Sritharan et al. 2007; Wotherspoon et al. 2009 and 2010]. Detailed approaches to solving this interaction commonly use computationally heavy techniques such as finite element programs or Winkler soil springs to model every aspect of the system. Simplified models are constructed to reduce the computation time while minimizing the necessary amount of input information to ensure that the displacements at the column top are in agreement with the SFSI system built in the field. This paper describes a rational model for characterizing the monotonic lateral response of drilled shafts through the use of a flexible foundation.

A.3: Current Design Models

Current practices for the lateral design of drilled shafts employ pushover analyses to ensure that capacity exceeds demand for a design-level event. Pushover analyses are commonly employed using the Winkler spring approach to get the typical behavior depicted in Figure A-1. Programs such as LPILE (Reese et al. 2004) are used in current practice to produce such results; however, they are used to solely perform the lateral design of a pile foundation or drilled shaft. This approach or even more refined finite element methods may produce inaccurate results due to not accurately modeling both nonlinear soil behavior and moment-curvature response of the foundation shaft, especially in the critical region. Another drawback to this approach for accounting for SFSI is that the results are not easily integrated into a global analysis of the full structural system to capture the realistic response. Incorporation of the effects of SFSI into such global analyses commonly employ simplified methodologies that define an equivalent fixed based cantilever system for a column supported by a drilled shaft [e.g., Priestley et al. (1996, 2007); Chai (2002)]. Such a fixed based cantilever requires two separate models to realistically capture both the force and displacement resistance associated with the inclusion of SFSI.

A.3.1: Guide Specifications for LRFD Seismic Bridge Design (AASHTO 2010)

Multiple methods are presented in the guidelines and commentary for determining the lateral response of deep foundations based on site location, bridge design and importance. The simple method discussed in the main portion of the specification models the bridge column by extending the above ground column into the ground to an equivalent point of fixity within the soil using empirical means and eliminating the presence of soil. The goal of this approach is to match the stiffness of the cantilever such that the displacement at the top of the column corresponds to the

displacement with the presence of soil. This method relies on a ratio of the pile's flexural

rigidity and the soil's modulus of elasticity and applies only when the system behaves in a linear

elastic manner. The commentary of AASHTO (2010) suggests additional simple approaches,

Chai (2002) and Priestley et al. (2007), in lieu of the point of fixity method if the systems are

believed to not behave in a linear elastic manner, which is the case in most seismic design

situations.

A.3.2: Chai (2002)

Chai's model relies on the use of two points, the point of fixity and the maximum moment, to

adequately define the flexural strength and ductility of the system with the assumption that the

stiffness of the second slope is zero for the force-displacement response. The fixity and

maximum moment location were developed by relating soil models such as Poulos and Davis

(1980) and Broms (1964) to an equivalent cantilever system. These locations define the flexural

strength and ductility of the system based on an idealized elasto-plastic moment-curvature

response of the cross section, thus ignoring the strain hardening associated with steel and

concrete. The plastic rotation of the system was assumed to be concentrated at the maximum

moment location with an analytical plastic hinge length determined based off of four full-scale

columns supported on drilled shafts tested in a uniform cohesionless soil (Chai and Hutchinson

2002).

A.3.3: Priestley et al. (2007)

For a bridge column supported by a drilled shaft, a method for determining the design

displacement of the system based off of the work of Suarez and Kowalsky (2007) is provided.

The method determines the design displacement using a series of nomographs or equations to

locate the in-ground plastic hinge location and a coefficient that accounts for the boundary conditions at the column tip and the type of soil surrounding the foundation shaft. Plastic action within the in-ground plastic hinge is accounted for based on the recommendations of Chai (2002). Lateral shear demand is found by approximating the viscous damping of the system due to the elastic and hysteretic damping and then relating to a predetermined spectral displacement and acceleration curve to find a stiffness of the system. The application of this method is restricted to drilled shafts in soils for undrained shear strengths, c_u, between 20 kPa (420 psf) and 40 kPa (840 psf).

A.4: Challenges

Although some models are in existence, challenges associated with their use in the lateral design of a drilled shaft subjected to a design-level or greater earthquake exist. Advancements in the simplified models can be made to better define the behavior of a continuous column/shaft system over the entire loading range on both a global and local level. A recent study (Shelman et al. 2010) found the following shortcomings with the existing SFSI design models:

1) The maximum moment location must be adequately identified to ensure an adequate ductile design for all conditions. Elastic approaches tend to define the maximum moment to occur at the point of fixity used for the individual model although the maximum moment is typically above this location as shown in Figure A-1.

2) Both the elastic and inelastic response of materials must be adequately captured as drilled shafts may experience plastic deformation due to a design-level or greater event. The inelastic range must consider the nonlinearity of soil, concrete and steel as these parameters largely influence the overall lateral load behavior of the SFSI system.

3) An analytical plastic hinge length established based off of experimental or analytical techniques in cohesive soils should be used instead of methods established in non-cohesive soils. Drilled shafts in cohesive soils typically experience a longer plastic hinge length since cohesionless soils are generally stiffer, limiting the inelasticity over a smaller shaft length.

4) A large range in soil parameters should be accommodated as cohesive soil varies from soft to stiff with the upper range of c_u being closer to 400 kPa (8350 psf) – a tenfold increase beyond that used for developing some existing models.

5) Use of one model to capture strength and another to obtain displacement should be avoided as this approach will not allow the simplified method to be incorporated into finite element models used for bridge analysis.

6) Given the significant impacts of seasonally cold temperatures on SFSI, inclusion of the standard variations in design temperature range that the structure and soil experience over the specified lifetime would be desirable in the development of suitable SFSI models.

A.5: Proposed Rational Method

Upon assessment of the needed advancements, a new equation based method was constructed to define the local and global lateral load response of a column supported on a drilled shaft using an equivalent cantilever system by addressing all of the aforementioned concerns. The rational method established uniquely captures the realistic response through the development of an equivalent cantilever with a flexible foundation that identifies the critical design locations as well as capturing the ground movement associated with the shaft deformation. A set of three springs are used to define the effects of soil on the foundation shaft. Two of the springs, one rotational

and one translational, are located at the point of maximum moment to capture the rotation and translation of the overall system (see Figure A-1), which corresponds to the critical location for damage and plastic deformation. The rotational spring (i.e., 3 in Figure A-2) accounts for the elastic shaft rotation below the maximum moment location as well as the plastic action in the shaft above and below the maximum moment location. The translational spring at the flexible base (i.e., 2 in Figure A-2) models the translational movement of the shaft from below the maximum moment location. The second translational spring (i.e., 1 in Figure A-2) represents the resistance of the soil between the ground surface and the maximum moment location. Although springs are used in the model, simple equations relying on the compatibility of the structure at certain limit states (i.e., first yield and ultimate) can be used to define a global force-displacement response over the elastic and inelastic loading range. The springs improve the method's versatility through the use of a structural analysis program capable of handling nonlinear spring behavior.

A.6: Formulation of Model

Based on the model provided in Figure A-2, a number of key parameters for a base model were established using the following variables: (1) a uniform layer of cohesive soil; (2) undrained shear strength, c_u, between 48.3 kPa (7 psi) and 380 kPa (55 psi); (3) axial load ratio of five percent; (4) circular column and shaft diameter of 0.6 m (2 ft); (5) longitudinal reinforcement ratio of two percent; (6) transverse spiral reinforcement specified to ensure flexural failure of the shaft; (7) column above the ground between 0D and 10D, where D is the diameter of the shaft; and, (8) foundation shaft long enough to ensure complete fixity and beam behavior. Using a series of analytical models constructed in LPILE Plus v 5.0 (Reese et al.

2004) with accurate representation of material nonlinearity and identifying trends within the resulting data sets appropriate equations for the parameters of the proposed method were established. A more detailed description of the establishment of equations can be found in the work of Shelman et al. (2010).

A.6.1: Maximum Moment Location

The maximum moment location, the most critical region where plastic strains are expected to develop in the shaft, defines the effective height of the cantilever model supported on a flexible base and locates the rotational and translational spring. Based on the results of the pushover analyses, provided in Figure 3, the non-dimensional maximum moment location (L_{ma}/D) varied in a quadratic manner as a function of the above ground column aspect ratio. Normalization of the data with respect to the column diameter was performed to expand the methods range of applicability. Furthermore, the data indicated that the coefficients of the quadratic trends would be a function of c_u as noted by the stacking of the lines where a softer soil is expected to have a larger depth to the point of maximum moment. The maximum moment location can be found using Eq. (A-1), where α_{ma}, β_{ma} and χ_{ma} are coefficients calculated based off of the soils undrained shear strength with a comparison between the equation and analytical data set provided in Figure 3.

$$L_{ma}=D\left[\alpha_{ma}\left(\tfrac{L_{col}}{D}\right)^2+\beta_{ma}\left(\tfrac{L_{col}}{D}\right)+\chi_{ma}\right]$$ Eq. (A- 1)

where, $\alpha_{ma}=-0.000005*a*c_u^2+0.0003*b*c_u+0.028$

$$\beta_{ma} = 0.0038 * b * c_u + 0.3247$$

$\chi_{ma}=-1.28*\ln[c_u(psi)]+7.1307=-1.28*\ln[c_u(kPa)]+9.6021$

$a = 1.0$ for psi and 0.021 for kPa

$b = 1.0$ for psi and 0.145 for kPa

A.6.2: Zero Moment Location

The next point determined in the model identifies the point on the expected moment profile where zero moment first occurs below the maximum moment location and the lateral displacement in the foundation shaft at this point has nearly been dissipated. This point defines the translation, elastic rotation and plastic rotation occurring at the maximum moment location due to movement below this point. The pushover data in Figure A-3 led to the non-dimensional zero moment location (L_{m0}/D) being a power series relation based on the undrained shear strength of the soil and the above ground column aspect ratio. The zero moment location can be found using Eq. (A-2), where α_{m0} and β_{m0} are coefficients based on the above ground height of the column with a comparison between the equation and analytical data provided in Figure A-3.

$$L_{m0} = D\zeta\alpha_{m0}[c_u(\text{psi})]^{\beta_{m0}} \text{ or } L_{m0} = D\zeta\alpha_{m0}[0.145*c_u(\text{kPa})]^{\beta_{m0}} \qquad \text{Eq. (A- 2)}$$

where, $\alpha_{m0} = 0.11\left(\frac{L_{col}}{D}\right) + 22.3$

$\beta_{m0} = 0.021\left(\frac{L_{col}}{D}\right) - 0.33$

A.6.3: Translational Spring at Maximum Moment Location

At the maximum moment location, the drilled shaft experiences lateral deformation, as depicted in Figure 1, due to development of shear and moment below the maximum moment location. Due to the presence of a flexible base in the equivalent cantilever model, the properties of a bilinear spring in the lateral translational direction (i.e., 2 in Figure A-2) can be constructed

to account for this movement. From the pushover analyses, it was found that a linear relationship between the non-dimensional translation (Δ_t/D) and the non-dimensional distance between the maximum moment and zero moment location (L_{mb}/D) would be sufficient. The translation at the ultimate condition can be found using Eq. (A-3) while the translation at the first yielding of the steel is found using Eq. (A-4), where ψ is a correction factor used only if c_u is less than ~70 kPa (10 psi); otherwise the value is input as 1. Spring forces are computed using equilibrium of a free-body diagram associated with the proposed cantilever system at the ultimate and first yield limit states.

$$\Delta_{tu} = D\left[0.0255\psi\left(\frac{L_{mb}}{D}\right) - 0.0652\right]$$
<div align="right">Eq. (A- 3)</div>

$$\text{where, } \psi = 0.0157\left(\frac{L_{col}}{D}\right) + 0.9342$$

$$\Delta_{ty} = \frac{\Delta_{tu}}{4.37}$$
<div align="right">Eq. (A- 4)</div>

A.6.4: Rotational Spring at Maximum Moment Location

The amount of elastic rotation within the bilinear spring at the ultimate and first yield limit states were found to be linearly related to L_{mb}/D. To account for the plastic action within the system, an analytical plastic hinge length, L_p, relating the section curvature to the total plastic rotation, θ_p, was established as a function of L_{mb}/D. Eqs. (A-5) to (A-8) establish the rotational aspects of the bilinear spring at the ultimate limit state based on flexural failure of the cross-section. At the first yield limit state, the elastic rotation component is defined using Eq. (A-9). The moment value for each of the limit states is taken as the ultimate and first yield moments of the foundation shaft within the expected plastic region produced from a moment-curvature

analysis that adequately addresses material behavior through all seasons (e.g., see Shelman et al. 2010 and Levings and Sritharan 2012).

$$\theta_{ebu}=0.0031 \left(\tfrac{L_{mb}}{D}\right)+0.0006 \qquad\qquad \text{Eq. (A- 5)}$$

$$L_p=2(0.16L_{mb}) \qquad\qquad \text{Eq. (A- 6)}$$

$$\theta_p=\phi_p L_p=\left(\phi_u-\phi_e\right)L_p \qquad\qquad \text{Eq. (A- 7)}$$

$$\theta_u=\theta_{ebu}+\theta_p \qquad\qquad \text{Eq. (A- 8)}$$

$$\theta_y=\theta_{eby}=0.002 \left(\tfrac{L_{mb}}{D}\right)+0.00001 \qquad\qquad \text{Eq. (A- 9)}$$

A.6.5: Translational Spring representing Soil

This translational spring specified as a single spring halfway between the maximum moment location and the ground surface can be modeled as multiple springs to produce a more accurate soil model. The soil spring improves the rational methods ability to handle P-Δ effects that arise from large deformations as well as the impacts associated with seasonal freezing. The p-y curve for the soil spring is found using the procedures suggested by Reese et al. (1975) with adjustments for the soil material behavior as discussed in Shelman et al. (2010).

When a hand calculation is desired for establishing the tip lateral load and displacement, the ultimate soil pressure, p_u, is computed and then multiplied by the effective height of the spring, h ($h = L_{ma} - L_{col}$ for a single spring), to determine the resistance of the soil at the ultimate limit state, V_{su}. A similar process is needed at the first yield limit state, but calibration of the pushover data sets found that a coefficient η, Eq. (A-10), could adjust the ultimate limit state to the first yield limit state as a function of the undrained shear strength of the soil (Shelman et al. 2010) by multiplying the soil resistance at the ultimate limit state by the coefficient η.

$$\eta=-0.03*\ln[c_u(\text{psi})]+0.7536 \text{ or } \eta=-0.03*\ln[c_u(\text{kPa})]+0.8115 \qquad \text{Eq. (A- 10)}$$

A.6.6: Force-Displacement Response at Tip

The global force-displacement bilinear response envelope can be found by summing the following individual components: (1) the total elastic displacement of the sytem, Δ_e; the total plastic displacement, Δ_p; and (3) the initial translation at the maximum moment location, Δ_t. The total elastic displacement accounts for the elastic rotation below the maximum moment location, Δ_{eb}, and the elastic displacement above the maximum moment location, Δ_{ea}, due to the cantilever action produced from loading applied at the column tip. The initial translation at the maximum moment location is found using Eq. (A-3) or (A-4) depending on the limit state that is being analyzed. The plastic displacement is due to the plastic rotation, θ_p, concentrated at the maximum moment location. The final equation, Eq. (A-11), requires iteration on the tip elastic displacement, Δ_{ea}, to account for the P-Δ effects present in the overall system. The force at the column top, V_{top}, is found at each limit state using a summation of moments about the flexible base accounting for the P-Δ effects.

$$\Delta_{final}=(\Delta_{eb}+\Delta_{et})+\Delta_p+\Delta_t \qquad \text{Eq. (A- 11)}$$

where, $\Delta_{eb}=\theta_{eb}L_{ma}$

$$\Delta_{et}=\frac{V_{top}L_{ma}{}^3}{3EI_e}$$

$$\Delta_p=\theta_pL_{ma}$$

$$\Delta_t=\Delta_{tu} \text{ or } \Delta_{ty}$$

A.7: Maximum Shear Calculations

Although the maximum moment location and top lateral force has been effectively established, the maximum shear does not typically occur within this region but rather deeper into the soil. Two methods were established as part of the rational model to adequately define the maximum shear and its location. Both methods establish the point of maximum shear, Eq. (A-12), by relating to the maximum moment and a ratio of the column clear height and diameter that is greater than 2. If it is less than 2, the maximum shear typically occurs at the column tip.

$$L_{vu} = L_{ma}\left[-0.035\left(\frac{L_{col}}{D}\right) + 1.75\right]$$

Eq. (A- 12)

The first method computes the maximum shear based on the soil causing a distributed loading on the foundation shaft between the maximum moment and maximum shear locations as shown in Figure A-4. The loading is approximately parabolic in shape with a zero slope at the point of maximum moment and an ordinate value of the ultimate soil pressure. In this method, the shear at the maximum moment location is taken to be a value of zero - as expected from general beam theory - and the maximum shear is then calculated as $\alpha(p_u)(L_{vu}-L_{ma})$, where α defined in Eq. (A-13) is a coefficient that better defines the shape of the distributed load based on the strength of the soil. The α value computed by Eq. (A-13) approximately varies between 0.5 and 0.9, corresponding to a shape somewhere between a linear relationship and a cubic relationship. Alternatively, Eq. (A-14) may be used to conservatively compute the maximum shear associated with the distributed loading of soil along the foundation shaft.

$$\alpha = 1.6[c_u(psi)]^{-0.28} \text{ or } \alpha = 1.6[0.145c_u(kPa)]^{-0.28} \qquad \text{Eq. (A-13)}$$

$$V_u = V_{top}\left[0.75e^{0.26\left(\frac{L_{col}}{D}\right)}\right] \qquad \text{Eq. (A-14)}$$

A.8: Influence of Additional Parameters

In addition to the parameters used to establish the base model, a number of other properties influence the lateral load response in a pushover style analysis. Extension of the model to account for some of these parameters included an examination of the axial load ratio and the amount of longitudinal reinforcement within the shaft cross-section.

A.8.1: Axial Load Ratio (ALR)

Although not expected to highly impact the results of the model, the impact of axial load ratio was investigated by varying the ALR between 0% and 10%. The results of the comparison are provided in Figure A-5 where the influence of ALR was compared with the main parameters of L_{ma} and L_{m0} that are used to construct the majority of the final model. Data indicated that the variation in ALR would alter these two parameters between 0.2% and 2.5% depending on the aboveground column height and applied axial load. Based on the results of this comparison it was concluded that the model does not need to be adjusted for the axial load ratio, thus expanding the applicability of the model to a column and shaft system with an ALR between 0% and 10%.

A.8.2: Longitudinal Reinforcement Ratio

The impact of the amount of longitudinal reinforcement within a column and shaft cross-section was examined by varying the volumetric ratio of steel to concrete between 1% and 4%. Figure A-6 indicates that both the normalized maximum moment and zero moment locations are

influenced by the amount of longitudinal reinforcement in the system with the maximum

moment location experiencing a larger variation in the data. Within the model, the normalized

locations can be corrected for the presence of different amounts of longitudinal reinforcement by

taking the original equations and multiplying them by a factor determined from the information

provided in Figure A-6. The factor applied to the maximum moment location shall be a factor of

the aboveground column height to ensure that the length of soil influence does not overtake the

P-Δ effects within the free-body diagram of the system at the first yield and ultimate limit states.

The variation within the normalized zero moment location was such that a constant based on the

amount of longitudinal reinforcement alone could be applied to Eq. (A-2). This constant, using

Eq. (A-15), ranges from 0.9 at 1% longitudinal reinforcement to 1.15 at 4% longitudinal

reinforcement. Furthermore, the ultimate shear estimation should be modified with Eq. (A-15)

and the same approach technique stated for the adjustment of the normalized zero moment

location.

$$\zeta_{m0} = 0.08[\rho_l(in\ \%)] + 0.83 \qquad\qquad \text{Eq. (A- 15)}$$

where, ρ_l = volumetric ratio of longitudinal reinforcing steel to gross-concrete

A.9: Verification of Proposed Method

Model verification was performed using data from full-scale testing of CIDH shafts in

cohesive style soils [Suleiman et al. (2006) and Stewart et al. (2007)] and multiple nonlinear

analyses of column-foundation systems using LPILE Plus v 5.0 (Reese et al. 2004). This

included an examination of the global force-displacement response, the maximum moment

location, the elastic and plastic rotations, the displacement at the maximum moment location, and

the location of the zero moment. The proposed rational model adequately captures the lateral response for a wide range of soil undrained shear strengths, column loadings, column/shaft diameters and longitudinal reinforcement ratio.

A.9.1: Experimental Verification – Iowa State University field testing

At Iowa State University (ISU) a series of full-scale field tests on two identical continuous column/foundation systems that closely resembled the base model developed in the paper were tested in summer and winter to examine the impacts of seasonal freezing on the lateral load response (Suleiman et al. 2006). Using the structural and geotechnical parameters provided by the researchers, the experimental tests and the proposed rational method were compared graphically for the column top force-displacement response in Figure A-7 and found to adequately capture the overall behavior. A numerical comparison was conducted with analytical models in LPILE (Reese et al. 2004) and the maximum moment location was determined within 7%, the top lateral force within 5% at the ultimate condition and the ultimate displacement within approximately 20%. Variation in the ultimate displacement generally arose from the conservatism within the model used for the determination of the plastic displacement of the overall system. Comparing the warm weather model directly to the experimental data of Suleiman et al. (2006), the maximum moment location was located within 10% of the full-scale test results. Furthermore, the yield lateral force was found within 5% and the column tip displacement at yield was within 17%, an adequate approximation due to variation in material properties and identification of correct displacement from available strain data.

A.9.2: Experimental Verification – University of California, Los Angeles (UCLA)

As part of a project for the California Department of Transportation (Caltrans) researchers at the University of California, Los Angeles (UCLA) performed field testing on a 1/3 geometrically scaled model of a typical 1.83 m (6 ft) diameter bridge column that continued into the ground as a drilled shaft foundation. The site consisted of a silty clay material with a plasticity index between 12 and 15 with 30% - 60% fines, and included a definitive layer of silty sand. Using the information provided by the researchers, the proposed rational method was performed and Figure A-8 presents a graphical comparison of the force-displacement response at the column tip. The initial stiffness was in reasonable agreement with the data producing a value of 4.1 kip/in in the rational method compared to 5.1 kip/in for the experimental data. The global comparison of Figure A-8 indicates that the yield force and displacement are reasonably captured as noted by the consistent appearance of inelastic behavior. The comparison, albeit reasonable, has noted differences that are mostly due to the large presence of sand and silt at the testing site that causes a purely cohesive environment to not exist at all times as specified in the model development. The results, however, demonstrate the ability of the model for different types of cohesive soils that may be encountered near a bridge site.

A.9.3: Analytical Comparison – LPILE Results

Additional analytical comparisons using LPILE (Reese et al. 2004) were conducted as part of a sensitivity study to better determine the range of applicability of the proposed new model. This study included the examination of 0.61 m (2 ft), 1.22 m (4 ft) and 1.83m (6 ft) diameter columns with varying soil strengths, shaft longitudinal reinforcement ratios, and column heights above ground. Graphical results of a few of the global force-displacement responses are provided in

Figure A-9. The results of the multiple analyses indicated that the base model and its extensions would sufficiently capture the critical locations, differences less than 5%, and the local and global response, differences less than 15%.

A.10: Conclusions

A rational method accounting for the effects of SFSI was presented within this paper that improves upon the traditional approaches used for simplifying detailed finite element approaches. The typical approach relies on the use of an equivalent cantilever that matches displacement at the tip of the column shaft, but the rational method was developed to capture both the force and displacement response. This was accomplished by constructing an equivalent cantilever supported by a flexible foundation at the critical design location for maximum moment using an equation based approach. Verification of the proposed rational method was performed against experimental test specimens in a wide range of soils and analytical models using varying soil and structural parameters. Results indicated that critical design locations could be captured within 10% while displacements at the first yield and ultimate limit states were within 20%. These verifications ensure the applicability of the model within the following parameters: (1) axial load ratio between zero and ten percent; (2) longitudinal reinforcement ratio between one percent and four percent with the horizontal reinforcement ratio designed to meet the requirements of the governing standards and experience a flexural failure; (3) the column and shaft diameter are between 0.6 m (2 ft) and 1.83 m (6 ft); (4) the column above the ground surface can range in length from 0D to 10D, where D is the cross-sectional diameter of the pile shaft; and, (5) the undrained shear strength of the soil lies between 48.3 kPa (7 psi) and 380 kPa (55 psi).

A.11: Acknowledgements

A.12: References

American Association of State Highway and Transportation Officials (AASHTO). (2009). *Guide Specifications for LRFD Seismic Bridge Design,* Washington D.C.

Chai, Y. H. (2002). "Flexural strength and ductility of extended pile-shafts. I: analytical model." *Journal of Structural Engineering* 128(5), 586-594.

Chai, Y. H. & Hutchinson, T. C. (2002). "Flexural strength and ductility of extended pile-shafts. II: experimental study." *Journal of Structural Engineering* 128(5), 595-602.

Crowther, G. S. (1990). "Analysis of laterally loaded piles embedded in layered frozen soil." *Journal of geotechnical engineering* 116(7): 1137-1152.

Levings, J. and Sritharan, S. (2012). "Effects of cold temperature and strain rate on the stress-strain behavior of ASTM A706 Grade 420 (60) steel reinforcement." *Journal of Materials in Civil Engineering* 24(12): 1441-1449.

Priestley, M. J. N., Seible, F. & Calvi, G. M. (1996). *Seismic Design and Retrofit of Bridges,* John Wiley & Sons, Inc., New York

Priestley, M. J. N., Calvi, G. M. & Kowalsky, M. J. (2007). *Displacement-Based Seismic Design of Structures*, IUSS Press, Pavia, Italy.

Reese, L. C., Wang, S. T., Isenhower, W. M., Arrellaga, J. A. and Hendrix, J. (2004). *LPILE plus 5.0, user's manual.* Austin: Ensoft, Inc.

Reese, L. C., Wang, S. T.. Isenhower, W. M. and Arrellaga, J. A. (2004). *LPILE plus 5.0, technical manual.* Austin: Ensoft, Inc.

Reese, L. C. and Welch, R. C. (1975). "Lateral loading of deep foundations in stiff clay." *Journal of geotechnical engineering division* 101(GT7): 633-649.

Shelman, A., Levings, J. and Sritharan, S. (2010) "Seismic design of deep bridge pier foundations in seasonally frozen ground." *Final Report submitted to AUTC and ADOT&PF.*

Sritharan, S., Suleiman, M. T. and White, D. J. (2007). "Effects of seasonal freezing on bridge column-foundation-soil interaction and their implications." *Earthquake spectra* 23(1): 199-222.

Sritharan, S. and Shelman, A. (2008). "An assessment of broad impact of seasonally frozen soil on seismic response of bridges in the U.S. and Japan." *Proceedings of the 24th US-Japan bridge engineering workshop, Minneapolis.* FHWA: 429-440.

Stewart, J. P., Taciroglu, E., Wallace, J. W., Ahlberg, E. R., Lemnitzer, A., Rha, C., Khalili-Tehrani, P., Keowen, S., Nigbor, R. L. and Salamance, A. (2007). "Full scale cyclic large deflection testing of foundation support systems for highway bridges. Part I: Drilled shaft foundations." *Research report for Grant No. 59A0247 for the California Department of Transportation.* University of California, Los Angeles.

Suarez, V. & Kowalsky, M. J. (2007). "Displacement-based seismic design of drilled shaft bents with soil-structure interaction." *Journal of Earthquake Engineering* 11, 1010-1030.

Suleiman, M. T., Sritharan, S. and White, D. J. (2006). "Cyclic lateral load response of bridge column-foundation-soil systems in freezing conditions." *Journal of structural engineering* 132(11): 1745-1754

Wotherspoon, L. M., Sritharan, S., Pender, M. J. (2009). "Modelling the response of cyclically loaded bridge columns embedded in warm and seasonally frozen soils." *Engineering structures* 32(2010): 933-943.

Wotherspoon, L. M., Sritharan, S., Pender, M. J. and Carr, A. J. (2010). "Investigation on the impact of seasonally frozen soil on seismic response of bridge columns." *Journal of bridge engineering* 15(5): 473-481.

Ground Surface

Maximum Moment
Location

Typical Fixity
Location for
Displacement
Equivalency

Equivalent System

Typical System   Expected Displacement   Expected Moment Profile

Figure A-1: Typical response of a drilled shaft subjected to a lateral force
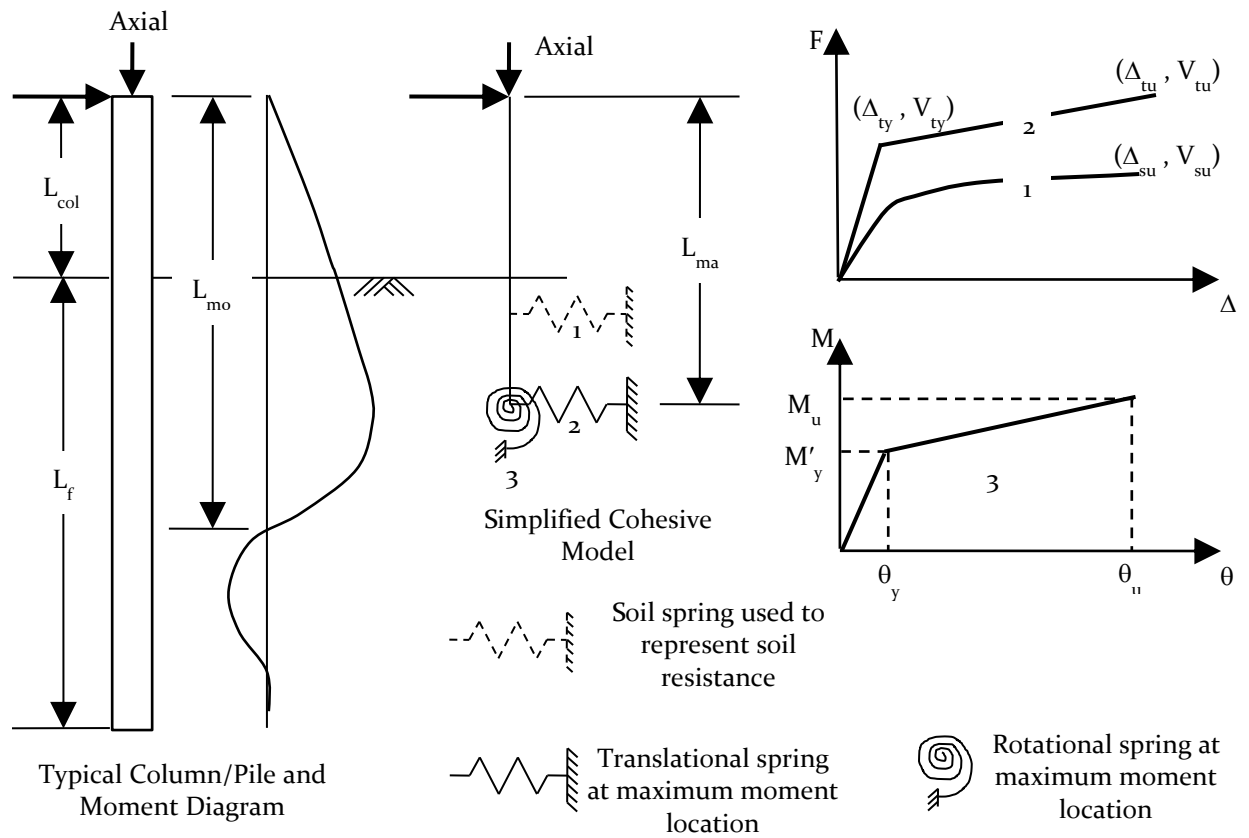
Figure A-2: Proposed new method
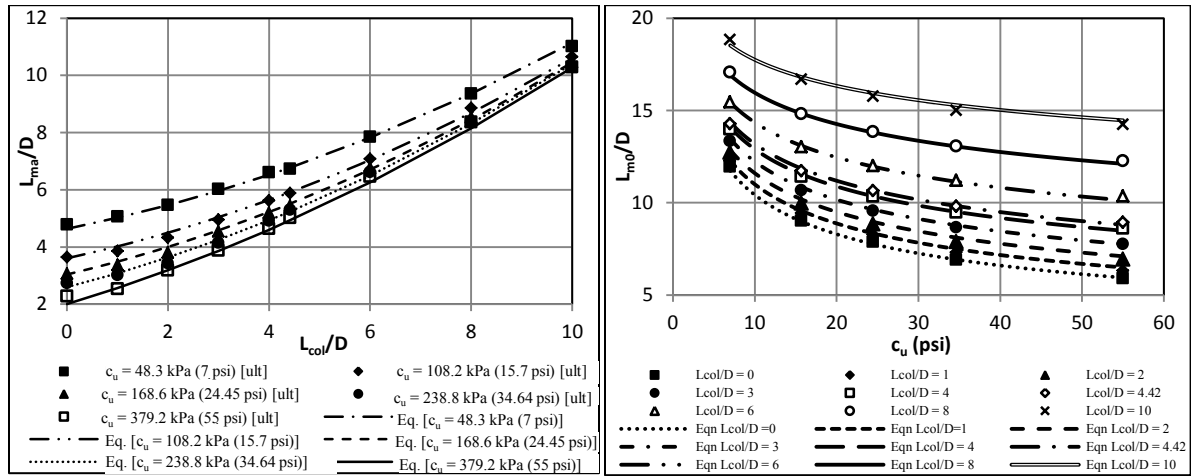
Figure A-3: Comparison of Equation based methods to analytical LPILE (Reese et al. 2004) models (left) maximum moment location; (right) zero moment location [Note: 1 psi = 6.895 kPa]
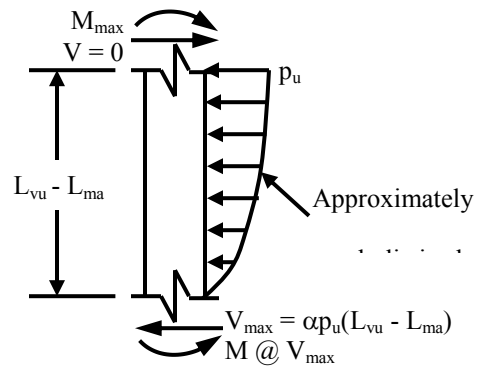
Figure A-4: Free body diagram for determining the ultimate shear in the foundation shaft

Figure A-5: Influence of axial load ratio on the model developed assuming a 5% axial load ratio (left) maximum moment location; (right) zero moment location [Note: 1 psi = 6.895 kPa]
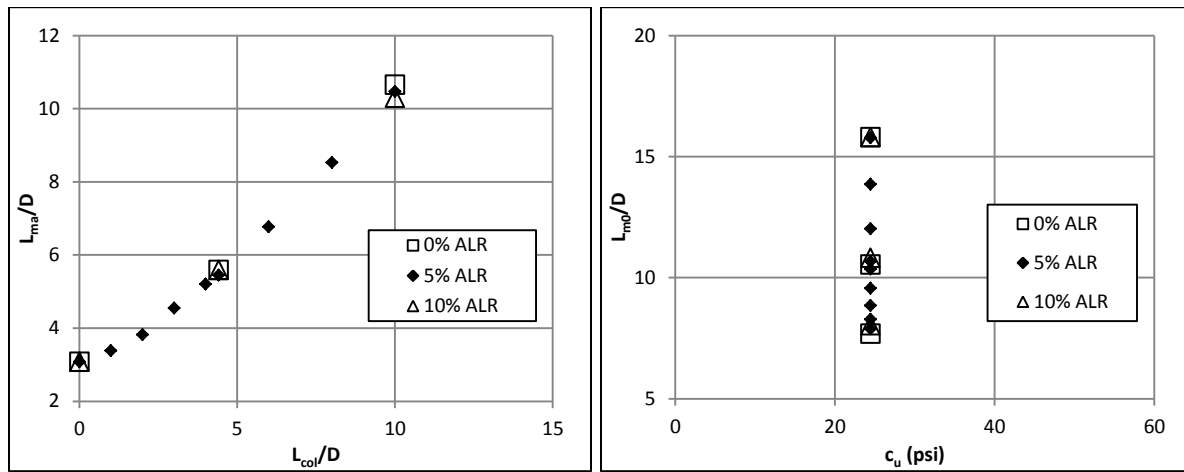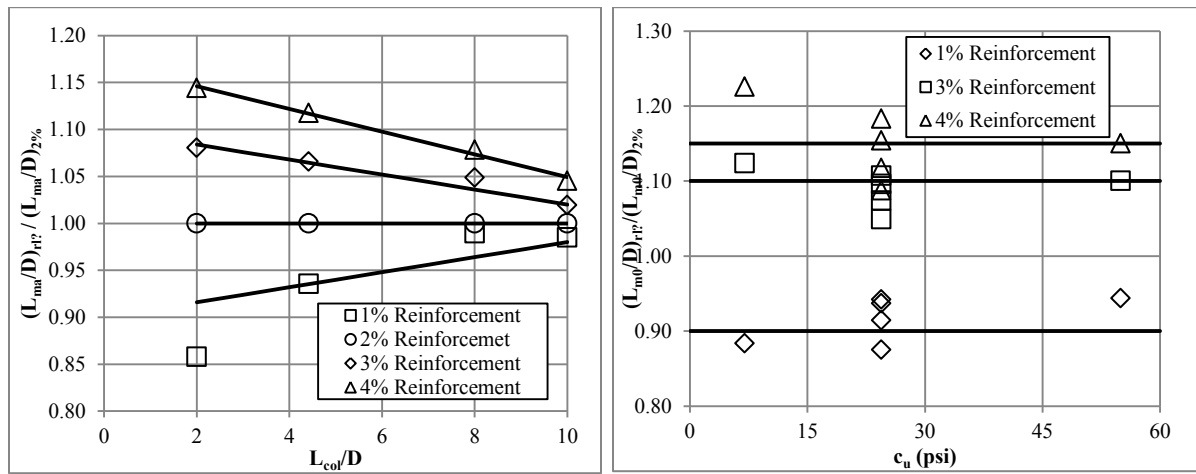
Figure A-6: Effects of longitudinal reinforcement on the model (left) maximum moment location; (right) zero moment location [Note: 1 psi = 6.895 kPa]
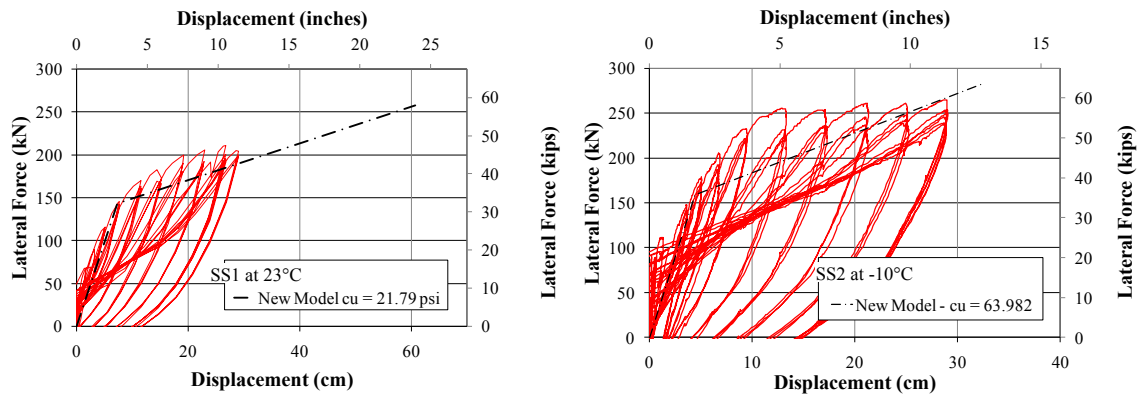
Figure A- 7: Graphical comparison of proposed simplified model with experimental testing of Suleiman et al. (2006)
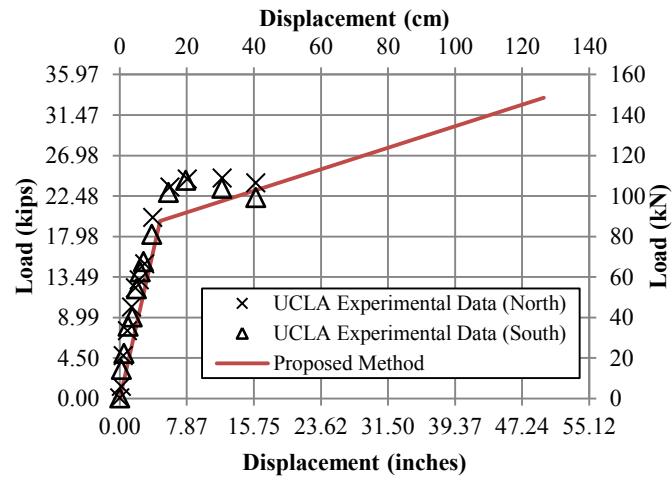
Figure A-8: Graphical comparison of Stewart et al. (2007) experimental testing with the proposed simplified model
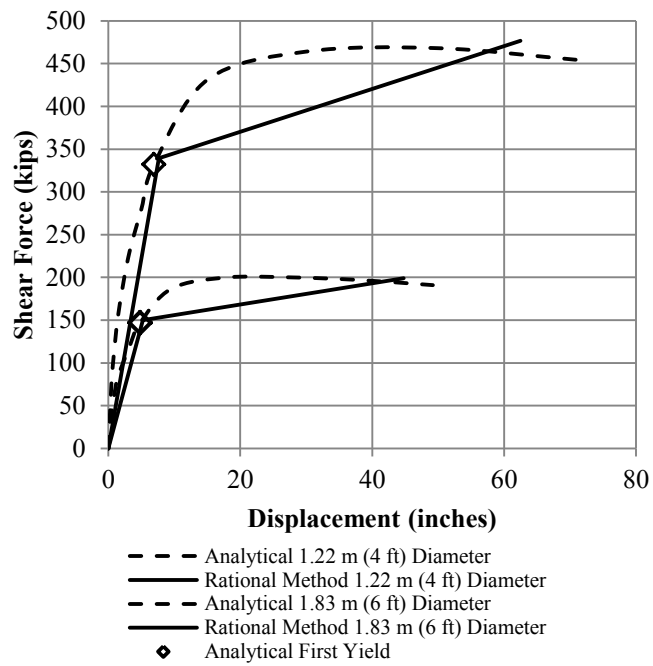
Figure A-9: Graphical comparison of analytical approaches with the rational method for 4 ft and 6 ft diameter columns and drilled shafts [Note: 1 inch = 2.54 cm and 1 kip = 4.448 kN]

APPENDIX B: MATLAB AND OPENSEES CODE

B.1: Establishment of Input Files for OpenSEES using Matlab

This portion of Appendix B contains the coding files used in Matlab for establishing the input behavior for the moment-curvature, pushover and dynamic analyses conducted using OpenSEES.

B.1.1: Material Section Behavior using Priestley et al. (1996)

```
function Priestley(index,colD,cover,rhol,ALR,BarNumLong,fc,fy,Es,Esh,esu,maxK,numIncr,AspectRatio)


% Define areas and cross-sectional dimensions of steel reinforcement based on bar number
Bar=[3,0.375,0.11;4,0.5,0.2;5,0.625,0.31;6,0.75,0.44;7,0.875,0.60;8,1,0.79;
    9,1.128,1.00;10,1.270,1.27;11,1.410,1.56;14,1.693,2.25;18,2.257,4];


% establishing the properties of the longitudinal reinforcing bar
barindex=find(Bar(1:end)==BarNumLong,1,'first');
Abl=Bar(barindex,3);
dbl=Bar(barindex,2);


%establishing the properties of the horizontal reinforcing bar
if BarNumLong <= 9
   BarNumHor=4;
else
   BarNumHor=5;
end


barindexh=find(Bar(1:end)==BarNumHor,1,'first');
```

```
Abh=Bar(barindexh,3);

dbh=Bar(barindexh,2);


% Establish the cross-section dimensions and longitudinal r/f details based on the starting assumption of a #11 bar or

% smaller longitudinally

Dc=colD-2*cover+dbh;

Ag=pi*(colD^2)/4;

Ac=pi*(Dc^2)/4;

Asl=rhol*Ag;

ns1=round(ceil(Asl/Abl));

if ns1 >= 8

    ns=ns1;

else

    while ns1 < 8

        barindex=find(Bar(1:end)==BarNumLong);

        Abl=Bar(barindex,3);

        dbl=Bar(barindex,2);

        ns1=round(ceil(Asl/Abl));

        BarNumLong=BarNumLong-1;

    end

    ns=ns1;

    BarNumLong=BarNumLong+1

    Abl

    dbl

    ns

end
```

%establishing the properties of the horizontal reinforcing bar after adjusting the longitudinal bar if needed

if BarNumLong <= 9

   BarNumHor=4

else

   BarNumHor=5

end

barindexh=find(Bar(1:end)==BarNumHor,1,'first');

Abh=Bar(barindexh,3)

dbh=Bar(barindexh,2)

% Redefine the column sections based on the adjusted longitudinal bar

Dc=colD-2*cover+dbh;

Ag=pi*(colD^2)/4;

Ac=pi*(Dc^2)/4;

% Going to determine the unconfined concrete properties

Ec=185000*((fc*1000)^0.375)/1000;

ec1=((fc*1000)^0.25)/4000;

ft1=7.5/1000; % Could also look at 7.5*sqrt(fc)

et1=2*ft1/Ec;

r1=(fc*1000/750)-1.9;

xp1=1.23;

xn1=2.3;

% Specify the steel properties of the system

```
fye=1.1*fy;

fsu=1.5*fye;

esh=3.24*(fye/Es);

Eratio=0.02;  % ratio between the plastic and elastic moduli in model


% Determine the horizontal reinforcement properties of the system

rhola=ns*Abl/Ag

rhos=0.16*(fc/fy)*(0.5+1.25*ALR)+0.13*(rhola-0.01);


s=4*Abh/(Dc*rhos);


% Establish the confined concrete properties

sclear=s-dbh;

rhocc=ns*Abl/Ac;

Ke=min(1,(1-0.5*sclear/Dc)/(1-rhocc));

flp=Ke*fy*rhos/2;

fcc=fc*(2.254*sqrt(1+7.94*flp/fc)-2*flp/fc-1.254);

ecc=0.002*(1+5*(fcc/fc-1));

Ecc=185000*((fcc*1000)^0.375)/1000;

ft2=7.5/1000; % Could also look at 7.5*sqrt(fc)

et2=2*ft2/Ecc;

xp2=1.23;

xn2=20; % This is supposed to be between 20-30

n2=Ecc*ecc/fcc;

r2=n2/(n2-1);

ecu=-1*(0.004+1.4*rhos*fy*esu/fcc);
```

% Want to establish the necessary information for loading and material property definition with the sign convention

% being (-) for compression and (+) for tension

P=1*ALR*fc*Ag;

fccmat=-1*fcc;

eccmat=-1*ecc;

fcmat=-1*fc;

ecmat=-1*ec1;

Esh=Esh;

% Set a few parameters for the building of the circular fiber sections

rcon=Dc/2;

rcov=colD/2;

rsteel=Dc/2-dbh/2-dbl/2;

theta=360/ns;

% Establish the number of fibers in the section based on the fiber edge size wanted in the model

length=1.0;

lcover=1.0;

nfcradial=round(ceil(0.5*Dc/length));

nfccirc=round(ceil(pi*Dc/length));

nfuradial=round(ceil(cover/lcover));

nfucirc=round(ceil(pi*colD/lcover));

% Writing the .tcl input file to go into OpenSees for analysis

fid=fopen('input.tcl','w');

fprintf(fid,'set id %d\n',index);

fprintf(fid,'set smodel Steel02\n');

```
fprintf(fid,'set cmodel Concrete03\n');

fprintf(fid,'set P %f\n',P); %Defining the Axial Load

fprintf(fid,'set colD %f\n',colD); %Defining the cross-section props.

fprintf(fid,'set D %d\n',colD); %Need a second term for File ID

fprintf(fid,'set Dc %f\n',Dc);

fprintf(fid,'set cover %f\n',cover)

fprintf(fid,'set Ag %f\n',Ag);

fprintf(fid,'set rcon %f\n',rcon);

fprintf(fid,'set rcov %f\n',rcov);

fprintf(fid,'set rsteel %f\n',rsteel);

fprintf(fid,'set theta %f\n',theta);

fprintf(fid,'set ns %d\n',ns);

fprintf(fid,'set Abar %f\n',Abl);

fprintf(fid,'set dbl %f\n',dbl);

fprintf(fid,'set Abh %f\n',Abh);

fprintf(fid,'set dbh %f\n',dbh);

fprintf(fid,'set rhos %f\n',rhos);

fprintf(fid,'set s %f\n',s)

fprintf(fid,'set Ke %f\n',Ke)

fprintf(fid,'set fccmat %f\n',fccmat); %Start of Confined Concrete Props.

fprintf(fid,'set eccmat %f\n',eccmat);

fprintf(fid,'set Ecc %f\n',Ecc);

fprintf(fid,'set ft2 %f\n',ft2);

fprintf(fid,'set et2 %f\n',et2);

fprintf(fid,'set xp2 %f\n',xp2);

fprintf(fid,'set xn2 %f\n',xn2);

fprintf(fid,'set r2 %f\n',r2);
```

```
fprintf(fid,'set ecu %f\n',ecu);

fprintf(fid,'set fcmat %f\n',fcmat); %Start of Unconfined Concrete Props.

fprintf(fid,'set ecmat %f\n',ecmat);

fprintf(fid,'set Ec %f\n',Ec);

fprintf(fid,'set ft1 %f\n',ft1);

fprintf(fid,'set et1 %f\n',et1);

fprintf(fid,'set xp1 %f\n',xp1);

fprintf(fid,'set xn1 %f\n',xn1);

fprintf(fid,'set r1 %f\n',r1);

fprintf(fid,'set fye %f\n',fye); %Start of Steel R/F Material Props.

fprintf(fid,'set fy %f\n',fy);

fprintf(fid,'set fsu %f\n',fsu);

fprintf(fid,'set Es %f\n',Es);

fprintf(fid,'set Eratio %f\n',Eratio);

fprintf(fid,'set Esh %f\n',Esh);

fprintf(fid,'set esh %f\n',esh);

fprintf(fid,'set esu %f\n',esu);

fprintf(fid,'set nfcradial %d\n',nfcradial);

fprintf(fid,'set nfccirc %d\n',nfccirc);

fprintf(fid,'set nfuradial %d\n',nfuradial);

fprintf(fid,'set nfucirc %d\n',nfucirc);

fprintf(fid,'set maxK %f\n',maxK); %Establish the Analysis Parameters

fprintf(fid,'set numIncr %f\n',numIncr);

fclose(fid);


%Need an input file for reading into the

colH=colD/AspectRatio;
```

```
Parameters=[Abl;rhol;ns;Abh;rhos;s;Ke;fccmat;eccmat;fcmat;ecmat;ecu;colH];

[r,c]=size(Parameters);

fid2=fopen(['param_',num2str(colD),'_',num2str(rhol),'_',num2str(ALR),'_',num2str(index),'.txt'],'w');

for x = 1:r

    fprintf(fid2,'%e\t',Parameters(x,:));

    fprintf(fid2,'\r\n');

end

fclose(fid2);
```

B.1.2:Material Section Behavior using the AASHTO (2012) approach for minimum flexural curvature capacity

```
function ACI1(index,colD,cover,rhol,ALR,BarNumLong,fc,fy,Es,Esh,esu,maxK,numIncr,AspectRatio)


% Define areas and cross-sectional dimensions of steel reinforcement based on bar number

Bar=[3,0.375,0.11;4,0.5,0.2;5,0.625,0.31;6,0.75,0.44;7,0.875,0.60;8,1,0.79;

    9,1.128,1.00;10,1.270,1.27;11,1.410,1.56;14,1.693,2.25;18,2.257,4];


% establishing the properties of the longitudinal reinforcing bar

barindex=find(Bar(1:end)==BarNumLong,1,'first');

Abl=Bar(barindex,3);

dbl=Bar(barindex,2);


%establishing the properties of the horizontal reinforcing bar

if BarNumLong <= 9

    BarNumHor=4;

else

    BarNumHor=5;
```

```
end

barindexh=find(Bar(1:end)==BarNumHor,1,'first');

Abh=Bar(barindexh,3);

dbh=Bar(barindexh,2);


% Establish the cross-section dimensions and longitudinal r/f details based on the starting assumption of a #11 bar or

% smaller longitudinally

Dc=colD-2*cover+dbh;

Ag=pi*(colD^2)/4;

Ac=pi*(Dc^2)/4;

Asl=rhol*Ag;

ns1=round(ceil(Asl/Abl));

if ns1 >= 8

   ns=ns1;

else

   while ns1 < 8

      barindex=find(Bar(1:end)==BarNumLong);

      Abl=Bar(barindex,3);

      dbl=Bar(barindex,2);

      ns1=round(ceil(Asl/Abl));

      BarNumLong=BarNumLong-1;

   end

   ns=ns1;

   BarNumLong=BarNumLong+1

   Abl

   dbl
```

```
    ns

end


%establishing the properties of the horizontal reinforcing bar after adjusting the longitudinal bar if needed


if BarNumLong <= 9

    BarNumHor=4

else

    BarNumHor=5

end


barindexh=find(Bar(1:end)==BarNumHor,1,'first');

Abh=Bar(barindexh,3)

dbh=Bar(barindexh,2)


% Redefine the column sections based on the adjusted longitudinal bar

Dc=colD-2*cover+dbh;

Ag=pi*(colD^2)/4;

Ac=pi*(Dc^2)/4;


% Going to determine the unconfined concrete properties

Ec=185000*(fc^0.375);

ec1=(fc^0.25)/4000;

ft1=7.5; % Could also look at 7.5*sqrt(fc)

et1=2*ft1/Ec;

r1=(fc/750)-1.9;

xp1=1.23;
```

```
xn1=2.3;


% Specify the steel properties of the system

fye=1.1*fy;

fsu=1.5*fye;

esh=3.24*(fye/Es);

Eratio=0.02; % ratio between the plastic and elastic moduli in model


% Determine the horizontal reinforcement properties of the system

rhos=0.12*(fc/fy);


s=4*Abh/(Dc*rhos);


% Establish the confined concrete properties

sclear=s-dbh;

rhocc=ns*Abl/Ac;

Ke=min(1,(1-0.5*sclear/Dc)/(1-rhocc));

flp=Ke*fy*rhos/2;

fcc=fc*(2.254*sqrt(1+7.94*flp/fc)-2*flp/fc-1.254);

ecc=0.002*(1+5*(fcc/fc-1));

Ecc=185000*(fcc^0.375);

ft2=7.5; % Could also look at 7.5*sqrt(fc)

et2=2*ft2/Ecc;

xp2=1.23;

xn2=20; % This is supposed to be between 20-30

n2=Ecc*ecc/fcc;

r2=n2/(n2-1);
```

```
ecu=-1*(0.004+1.4*rhos*fy*esu/fcc);


% Want to establish the necessary information for loading and material property definition with the sign convention

% being (-) for compression and (+) for tension

P=1*ALR*fc*Ag;

fccmat=-1*fcc;

eccmat=-1*ecc;

fcmat=-1*fc;

ecmat=-1*ec1;

Esh=Esh;


% Set a few parameters for the building of the circular fiber sections

rcon=Dc/2;

rcov=colD/2;

rsteel=Dc/2-dbh/2-dbl/2;

theta=360/ns;


% Establish the number of fibers in the section based on the fiber edge size wanted in the model.

length=1.0;

nfcradial=round(ceil(0.5*Dc/length));

nfccirc=round(ceil(pi*Dc/length));

nfuradial=round(ceil(cover/length));

nfucirc=round(ceil(pi*colD/length));


% Writing the .tcl input file to go into OpenSees for analysis

fid=fopen('input.tcl','w');

fprintf(fid,'set id %d\n',index);
```

```
fprintf(fid,'set smodel Steel02\n');

fprintf(fid,'set cmodel Concrete07\n');

fprintf(fid,'set P %f\n',P); %Defining the Axial Load

fprintf(fid,'set colD %f\n',colD); %Defining the cross-section props.

fprintf(fid,'set D %d\n',colD); %Need a second term for File ID

fprintf(fid,'set Dc %f\n',Dc);

fprintf(fid,'set rcon %f\n',rcon);

fprintf(fid,'set rcov %f\n',rcov);

fprintf(fid,'set rsteel %f\n',rsteel);

fprintf(fid,'set theta %f\n',theta);

fprintf(fid,'set ns %d\n',ns);

fprintf(fid,'set Abar %f\n',Abl);

fprintf(fid,'set fccmat %f\n',fccmat); %Start of Confined Concrete Props.

fprintf(fid,'set eccmat %f\n',eccmat);

fprintf(fid,'set Ecc %f\n',Ecc);

fprintf(fid,'set ft2 %f\n',ft2);

fprintf(fid,'set et2 %f\n',et2);

fprintf(fid,'set xp2 %f\n',xp2);

fprintf(fid,'set xn2 %f\n',xn2);

fprintf(fid,'set r2 %f\n',r2);

fprintf(fid,'set ecu %f\n',ecu);

fprintf(fid,'set fcmat %f\n',fcmat); %Start of Unconfined Concrete Props.

fprintf(fid,'set ecmat %f\n',ecmat);

fprintf(fid,'set Ec %f\n',Ec);

fprintf(fid,'set ft1 %f\n',ft1);

fprintf(fid,'set et1 %f\n',et1);

fprintf(fid,'set xp1 %f\n',xp1);
```

```
fprintf(fid,'set xn1 %f\n',xn1);

fprintf(fid,'set r1 %f\n',r1);

fprintf(fid,'set fye %f\n',fye); %Start of Steel R/F Material Props.

fprintf(fid,'set fsu %f\n',fsu);

fprintf(fid,'set Es %f\n',Es);

fprintf(fid,'set Eratio %f\n',Eratio);

fprintf(fid,'set Esh %f\n',Esh);

fprintf(fid,'set esh %f\n',esh);

fprintf(fid,'set esu %f\n',esu);

fprintf(fid,'set nfcradial %d\n',nfcradial);

fprintf(fid,'set nfccirc %d\n',nfccirc);

fprintf(fid,'set nfuradial %d\n',nfuradial);

fprintf(fid,'set nfucirc %d\n',nfucirc);

fprintf(fid,'set maxK %f\n',maxK); %Establish the Analysis Parameters

fprintf(fid,'set numIncr %f\n',numIncr);

fclose(fid);


%Need an input file for reading into the

colH=colD/AspectRatio;

Parameters=[Abl;rhol;ns;Abh;rhos;s;Ke;fccmat;eccmat;fcmat;ecmat;ecu;colH];

[r,c]=size(Parameters);

fid2=fopen(['param_',num2str(colD),'_',num2str(rhol),'_',num2str(ALR),'_',num2str(index),'.txt'],'w');

for x = 1:r

    fprintf(fid2,'%e\t',Parameters(x,:));

    fprintf(fid2,'\r\n');

end

fclose(fid2);
```

B.1.3: Material Section Behavior using the AASHTO (2012) approach for maintaining the axial load capacity

```
function CalTransMin(index,colD,cover,rhol,ALR,BarNumLong,fc,fy,Es,Esh,esu,maxK,numIncr,AspectRatio)


% Define areas and cross-sectional dimensions of steel reinforcement based on bar number

Bar=[3,0.375,0.11;4,0.5,0.2;5,0.625,0.31;6,0.75,0.44;7,0.875,0.60;8,1,0.79;

    9,1.128,1.00;10,1.270,1.27;11,1.410,1.56;14,1.693,2.25;18,2.257,4];


% establishing the properties of the longitudinal reinforcing bar

barindex=find(Bar(1:end)==BarNumLong,1,'first');

Abl=Bar(barindex,3);

dbl=Bar(barindex,2);


%establishing the properties of the horizontal reinforcing bar

if BarNumLong <= 9

    BarNumHor=4;

else

    BarNumHor=5;

end


barindexh=find(Bar(1:end)==BarNumHor,1,'first');

Abh=Bar(barindexh,3);

dbh=Bar(barindexh,2);


% Establish the cross-section dimensions and longitudinal r/f details based on the starting assumption of a #11 bar or

% smaller longitudinally

Dc=colD-2*cover+dbh;
```

```
Ag=pi*(colD^2)/4;

Ac=pi*(Dc^2)/4;

Asl=rhol*Ag;

ns1=round(ceil(Asl/Abl));

if ns1 >= 8

    ns=ns1;

else

    while ns1 < 8

        barindex=find(Bar(1:end)==BarNumLong);

        Abl=Bar(barindex,3);

        dbl=Bar(barindex,2);

        ns1=round(ceil(Asl/Abl));

        BarNumLong=BarNumLong-1;

    end

    ns=ns1;

    BarNumLong=BarNumLong+1

    Abl

    dbl

    ns

end


%establishing the properties of the horizontal reinforcing bar after adjusting the longitudinal bar if needed


if BarNumLong <= 9

    BarNumHor=4

else

    BarNumHor=5
```

```
end


barindexh=find(Bar(1:end)==BarNumHor,1,'first');

Abh=Bar(barindexh,3)

dbh=Bar(barindexh,2)


% Redefine the column sections based on the adjusted longitudinal bar

Dc=colD-2*cover+dbh;

Ag=pi*(colD^2)/4;

Ac=pi*(Dc^2)/4;


% Going to determine the unconfined concrete properties

Ec=185000*(fc^0.375);

ec1=(fc^0.25)/4000;

ft1=7.5; % Could also look at 7.5*sqrt(fc)

et1=2*ft1/Ec;

r1=(fc/750)-1.9;

xp1=1.23;

xn1=2.3;


% Specify the steel properties of the system

fye=1.1*fy;

fsu=1.5*fye;

esh=3.24*(fye/Es);

Eratio=0.02; % ratio between the plastic and elastic moduli in model


% Determine the horizontal reinforcement properties of the system
```

```
rhos=0.45*((Ag/Ac)-1)*(fc/fy);


s=4*Abh/(Dc*rhos);


% Establish the confined concrete properties

sclear=s-dbh;

rhocc=ns*Abl/Ac;

Ke=min(1,(1-0.5*sclear/Dc)/(1-rhocc));

flp=Ke*fy*rhos/2;

fcc=fc*(2.254*sqrt(1+7.94*flp/fc)-2*flp/fc-1.254);

ecc=0.002*(1+5*(fcc/fc-1));

Ecc=185000*(fcc^0.375);

ft2=7.5; % Could also look at 7.5*sqrt(fc)

et2=2*ft2/Ecc;

xp2=1.23;

xn2=20; % This is supposed to be between 20-30

n2=Ecc*ecc/fcc;

r2=n2/(n2-1);

ecu=-1*(0.004+1.4*rhos*fy*esu/fcc);


% Want to establish the necessary information for loading and material  property definition with the sign convention

% being (-) for compression and (+) for tension

P=1*ALR*fc*Ag;

fccmat=-1*fcc;

eccmat=-1*ecc;

fcmat=-1*fc;

ecmat=-1*ec1;
```

Esh=Esh;

% Set a few parameters for the building of the circular fiber sections

rcon=Dc/2;

rcov=colD/2;

rsteel=Dc/2-dbh/2-dbl/2;

theta=360/ns;

% Establish the number of fibers in the section based on the fiber edge size wanted in the model.

length=1.0;

nfcradial=round(ceil(0.5*Dc/length));

nfccirc=round(ceil(pi*Dc/length));

nfuradial=round(ceil(cover/length));

nfucirc=round(ceil(pi*colD/length));

% Writing the .tcl input file to go into OpenSees for analysis

fid=fopen('input.tcl','w');

fprintf(fid,'set id %d\n',index);

fprintf(fid,'set smodel Steel02\n');

fprintf(fid,'set cmodel Concrete07\n');

fprintf(fid,'set P %f\n',P); %Defining the Axial Load

fprintf(fid,'set colD %f\n',colD); %Defining the cross-section props.

fprintf(fid,'set D %d\n',colD); %Need a second term for File ID

fprintf(fid,'set Dc %f\n',Dc);

fprintf(fid,'set rcon %f\n',rcon);

fprintf(fid,'set rcov %f\n',rcov);

fprintf(fid,'set rsteel %f\n',rsteel);

```
fprintf(fid,'set theta %f\n',theta);

fprintf(fid,'set ns %d\n',ns);

fprintf(fid,'set Abar %f\n',Abl);

fprintf(fid,'set fccmat %f\n',fccmat); %Start of Confined Concrete Props.

fprintf(fid,'set eccmat %f\n',eccmat);

fprintf(fid,'set Ecc %f\n',Ecc);

fprintf(fid,'set ft2 %f\n',ft2);

fprintf(fid,'set et2 %f\n',et2);

fprintf(fid,'set xp2 %f\n',xp2);

fprintf(fid,'set xn2 %f\n',xn2);

fprintf(fid,'set r2 %f\n',r2);

fprintf(fid,'set ecu %f\n',ecu);

fprintf(fid,'set fcmat %f\n',fcmat); %Start of Unconfined Concrete Props.

fprintf(fid,'set ecmat %f\n',ecmat);

fprintf(fid,'set Ec %f\n',Ec);

fprintf(fid,'set ft1 %f\n',ft1);

fprintf(fid,'set et1 %f\n',et1);

fprintf(fid,'set xp1 %f\n',xp1);

fprintf(fid,'set xn1 %f\n',xn1);

fprintf(fid,'set r1 %f\n',r1);

fprintf(fid,'set fye %f\n',fye); %Start of Steel R/F Material Props.

fprintf(fid,'set fsu %f\n',fsu);

fprintf(fid,'set Es %f\n',Es);

fprintf(fid,'set Eratio %f\n',Eratio);

fprintf(fid,'set Esh %f\n',Esh);

fprintf(fid,'set esh %f\n',esh);

fprintf(fid,'set esu %f\n',esu);
```

```matlab
fprintf(fid,'set nfcradial %d\n',nfcradial);

fprintf(fid,'set nfccirc %d\n',nfccirc);

fprintf(fid,'set nfuradial %d\n',nfuradial);

fprintf(fid,'set nfucirc %d\n',nfucirc);

fprintf(fid,'set maxK %f\n',maxK); %Establish the Analysis Parameters

fprintf(fid,'set numIncr %f\n',numIncr);

fclose(fid);


%Need an input file for reading into the

colH=colD/AspectRatio;

Parameters=[Abl;rhol;ns;Abh;rhos;s;Ke;fccmat;eccmat;fcmat;ecmat;ecu;colH];

[r,c]=size(Parameters);

fid2=fopen(['param_',num2str(colD),'_',num2str(rhol),'_',num2str(ALR),'_',num2str(index),'.txt'],'w');

for x = 1:r

   fprintf(fid2,'%e\t',Parameters(x,:));

   fprintf(fid2,'\r\n');

end

fclose(fid2);
```

B.2: Batching Processes using Matlab

This portion of Appendix B contains the coding files used in Matlab for conducting the

batching process for moment-curvature, pushover and dynamic analyses conducted using

OpenSEES.

B.2.1: Moment-Curvature Analyses

```matlab
id=1

a=0.01;
```

```
b=0.05;

Es=29000000;

fy=60000;

fc=4000;

N=15;

AspectRatio=1/4;

cvr=2.0;

esu=0.12;

maxCurv=0.005;

Incr=300;

for colD = 24:12:96

   for ALR = [-0.05, 0.001, 0.05, 0.1, 0.15]

     for rl = a:(b-a)/N:b

     BarNumLong=11;

     ACI1(id,colD,cvr,rl,ALR,BarNumLong,fc,fy,Es,85e04,esu,maxCurv,Incr,AspectRatio)

     !OpenSees.exe "CircMPhiSteel.tcl"

     % Post Processing of the Data

     a1=load(['MCNode_',num2str(colD),'_',num2str(id),'.out']);

     b1=load(['ConcStrainUnConf_',num2str(colD),'_',num2str(id),'.out']);

     c1=load(['ConcStrainConf_',num2str(colD),'_',num2str(id),'.out']);

     d1=load(['BarStrain_',num2str(colD),'_',num2str(id),'.out']);

     MPhi=horzcat(a1,[b1(:,3)],[c1(:,3)],[d1(:,3)]);

     fid2=fopen(['MPhi_',num2str(colD),'_',num2str(rl),'_',num2str(ALR),'_',num2str(id),'.txt'],'w');

     [row,col]=size(MPhi);

     for x = 1:row

        fprintf(fid2,'%e\t',MPhi(x,:));

        fprintf(fid2,'\r\n');
```

```
        end

        fclose(fid2);

        id=id+1

        end

    end

end


a = 0.01;

b = 0.05;

K = 1;

count = 1;

J = 1;

Es=29000000;

fy=60000;

N=15;


% Loading of the full matrices for establishing the M-Phi response

for colD =

[24,24,24,24,24,36,36,36,36,36,48,48,48,48,48,60,60,60,60,60,72,72,72,72,72,84,84,84,84,84,96,96,96,96,96]

    for n = 1+16*(K-1):(N+1)+16*(K-1)

    rl2=a+(n-1-16*(K-1))*(b-a)/N

    if count <= 80

        ALR1 = -0.05*J+0.05*(K-1)

        if ALR1 == 0

            ALR = 0.001

        else

            ALR =  -0.05*J+0.05*(K-1)
```

```
        end

        count = count + 1

    else

        J = J + 5

        ALR = -0.05*J + 0.05*(K-1)

        count = 2

    end

    A{n}=load(['MPhi_',num2str(colD),'_',num2str(rl2),'_',num2str(ALR),'_',num2str(n),'.txt']);

    B{n}=load(['param_',num2str(colD),'_',num2str(rl2),'_',num2str(ALR),'_',num2str(n),'.txt']);

    end

K = K + 1

end


% Plotting the matrices constructed for M-Phi; M-ec,cover; M-ec,conf; M-es
figure;
for x = 1:(K-1)*(N+1)

    subplot(2,2,1)

    plot(A{x}(:,2),A{x}(:,1));

    hold all

    grid

    xlabel('Curvature (1/in)')

    ylabel('Moment (lb-in)')

    title('M-Phi')

    subplot(2,2,2)

    plot(A{x}(:,3),A{x}(:,1))

    hold all

    grid
```

```
    xlabel('Axial Strain')

    ylabel('Moment (lb-in)')

    title('M - ec,cover')

    subplot(2,2,3)

    plot(A{x}(:,4),A{x}(:,1))

    hold all

    grid

    xlabel('Axial Strain')

    ylabel('Moment (lb-in)')

    title('M - ec,conf')

    subplot(2,2,4)

    plot(A{x}(:,5),A{x}(:,1))

    hold all

    grid

    xlabel('Axial Strain')

    ylabel('Moment (lb-in)')

    title('M - es')

end

% Putting a grid to the plots created above

subplot(2,2,1)

grid

subplot(2,2,2)

grid

subplot(2,2,3)

grid

subplot(2,2,4)

grid
```

```
% Want to determine the first yield curvature of the section

phi1all=[];

myprall=[];

for n = 1:(K-1)*(N+1)

    for y=1:length(A{n})

        if (A{n}(y,5) >= fy/Es) && (A{n}([y-1],5) <= fy/Es)

            m=((A{n}(y-1,2))-(A{n}(y-2,2)))/((A{n}(y-1,5))-(A{n}(y-2,5)));

            b2=(A{n}(y-1,2))-m*(A{n}(y-1,5));

            phi1 = m*(fy/Es)+b2;

            m3=((A{n}(y-1,1))-(A{n}(y-2,1)))/((A{n}(y-1,5))-(A{n}(y-2,5)));

            b3=(A{n}(y-1,1))-m3*(A{n}(y-1,5));

            mypr1=m3*(fy/Es)+b3;

        else

            'NA';

        end

    end

    phi1all = [phi1all;phi1];

    myprall = [myprall;mypr1];

end


% Want to establish the yield curvature of the section

phi2all=[];

mnall=[];

for n = 1:(K-1)*(N+1)

    for y=1:length(A{n})

        if (A{n}(y,4) >= -0.004) && (A{n}([y+1],4) <= -0.004) && (A{n}(y,5) <= 0.015)
```

```
      m1=A{n}(y,1);

      m2=A{n}(y+1,1);

      e1=A{n}(y,4);

      e2=A{n}(y+1,4);

      mn=m1+(-0.004-e1)*(m2-m1)/(e2-e1);

      phi2 = phi1all(n,1)*(mn/myprall(n,1));

    elseif (A{n}(y,5) >= 0.015) && (A{n}(y-1,5) <= 0.015) && (A{n}(y,4) >= -0.004)

      m1=A{n}(y,1);

      m2=A{n}(y-1,1);

      e1=A{n}(y,5);

      e2=A{n}(y-1,5);

      mn=m1+(-0.004-e1)*(m2-m1)/(e2-e1);

      phi2 = phi1all(n,1)*(mn/myprall(n,1));

    else

      'NA';

    end

  end

  phi2all = [phi2all;phi2];

  mnall=[mnall;mn];

end


% Want to establish the ultimate curvature of the section

phi3all=[];

muall=[];

for n = 1:(K-1)*(N+1)

  for y=1:length(A{n})

    if (abs(A{n}(y,4)) >= abs(B{n}(12,1))) && (abs(A{n}([y-1],4)) <= abs(B{n}(12,1))) && (A{n}(y,5) <= 0.07)
```

```
        m1=A{n}(y,1);

        m2=A{n}(y-1,1);

        e1=A{n}(y,4);

        e2=A{n}(y-1,4);

        f1=A{n}(y,2);

        f2=A{n}(y-1,2);

        mu=m1+(B{n}(12,1)-e1)*(m2-m1)/(e2-e1);

        phi3=f1+(B{n}(12,1)-e1)*(f2-f1)/(e2-e1);

    elseif (A{n}(y,5) >= 0.07) && (A{n}(y-1,5) <= 0.07) && (abs(A{n}(y,4)) <= abs(B{n}(12,1)))

        m1=A{n}(y,1);

        m2=A{n}(y-1,1);

        e1=A{n}(y,5);

        e2=A{n}(y-1,5);

        f1=A{n}(y,2);

        f2=A{n}(y-1,2);

        mu=m1+(0.07-e1)*(m2-m1)/(e2-e1);

        phi3=f1+(0.07-e1)*(f2-f1)/(e2-e1);

    else

        'NA';

    end

    end

  phi3all = [phi3all;phi3];

  muall=[muall;mu];

end


Mideal=[myprall phi1all mnall phi2all muall phi3all];
```

```
fid3=fopen(['Mideal.txt'],'w');

[rows,col]=size(Mideal);

for x = 1:rows

    fprintf(fid3,'%e\t',Mideal(x,:));

    fprintf(fid3,'\r\n');

end

fclose(fid3);
```

B.2.2: Pushover Analyses

% Going to run a series of pushover analyses based on same cross-section modifying the aspect ratio of this system.

% This is for a circular column using the rhos as specified in the program (currently set at Priestley)

%Trial Number

id=1

%Ultimate Curvature of the section based on M-phi analysis

phiu=0.002

%Axial Load Ratio

ALR=0.05

%Column Diameter

colD=48

%cover to main longitudinal bar

cover=2

% diameter and area of main longitudinal r/f based on the BarNumber in thecross-section. Establish the horizontal

% bar area based on the longitudinal bar being used in the cross-section

BarNumLong=11

%desired amount of longitudinal r/f

rhold=0.02

%material properties for concrete and steel

fc=4;

fy=60;

Es=29000

% Need to establish some additional parameters for use in the Priestley function which writes the material properties

% input file

maxK=0.005

Incr=300

%setting up the actual batching process and writing the appropriate input file for the analysis

for ARatio = [0.1,1/9,1/8,1/7,1/6,1/5,1/4,1/3]

  %Establishing the length of the element to be used in the analysis

  Lele=(1.2973*(ARatio^-1))

  %Going to establish the material values and section properties using matlab

  %instead of OpenSees in the *.tcl file

  Priestley(id,colD,cover,rhold,ALR,BarNumLong,fc,fy,Es,850,0.12,maxK,Incr,ARatio)

  fid=fopen('input2.tcl','w');

  fprintf(fid,'set Trial %d\n',id);

  fprintf(fid,'set Analoption Pushover\n');

```
    fprintf(fid,'set concMat c03\n');

    fprintf(fid,'set steelMat s02\n');

    fprintf(fid,'set rhold %f\n',rhold);

    fprintf(fid,'set Lele %f\n',Lele);

    fprintf(fid,'set phiu %f\n',phiu);

    fprintf(fid,'set ALR %f\n',ALR);

    fprintf(fid,'set ARatio %f\n',ARatio);

    fclose(fid);

    !OpenSees.exe "CalTransPushCyclicSP.tcl"

    id=id+1

end


%Writing a code to post process the output files created by OpenSEES. The goal is to get a final text document that

% has the force, displacement,unconfined concrete strain, confined concrete strain, reinforcement strain at the

% extreme layer


% Start the process by loading the necessary files into matlab


Disp=load('Dtop.out');

Force=load('FColTop.out');

BotUnSe=load('BotUCse2.out');

BotCCSe=load('BotCCse2.out');

BotRFse=load('BotRFse2.out');


% Combine the appropriate columns from each file into a single matrix


Results=[Disp(:,2) Force(:,5) BotUnSe(:,3) BotCCSe(:,3) BotRFse(:,3)];
```

% Want to establish the ultimate force and displacement of the analysis to write it into the final file. This is going to

% be based on the ultimate curvature as established in a moment-curvature analysis. Using a 48 inch column with 2

% inch cover and #11 bar longitudinally and #5 bar horizontally.


```
phiu=0.001662917;

cover = 2;

D = 48;

dbl = 1.410;

dbh = 0.625;

Dpr = D-2*cover+dbh;

Dbar = D-2*cover-dbl;

Aspect=3;

nele=37;


NADepth = [];

phi = [];

for y=1:length(Results)

   ccon=(Results(y,4)*(Dpr/2+Dbar/2)/(Results(y,4)-Results(y,5)));

   phi1=abs(Results(y,4))/ccon;

  if (phi <= phiu);

     DispU = Results(y,1);

     ForceU = Results(y,2);

   else

      'NA';

   end

   NADepth = [NADepth;ccon];
```

```
    phi = [phi;phi1];

end


MFinal=[Results NADepth phi];


for y=1:length(MFinal);

  if (MFinal(y,2) == ForceU);

    phiu=MFinal(y,7);

  end

end


% Need to establish the first yield displacement and force of the column system

for y=1:length(Results);

  if(Results(y,5) >= 66/29000) && (Results(y-1,5) <= 66/29000);

    m=((Results(y-1,2))-(Results(y-2,2)))/((Results(y-1,5))-(Results(y-2,5)));

    b2=(Results(y-1,2))-m*(Results(y-1,5));

    Fypr = m*(66/29000)+b2;

    m3=((Results(y-1,1))-(Results(y-2,1)))/((Results(y-1,5))-(Results(y-2,5)));

    b3=(Results(y-1,1))-m3*(Results(y-1,5));

    Dpry=m3*(66/29000)+b3;

    m4=((MFinal(y-1,7))-(MFinal(y-2,7)))/((MFinal(y-1,5))-(MFinal(y-2,5)));

    b4=(MFinal(y-1,7))-m4*(MFinal(y-1,5));

    phipry=m4*(66/29000)+b4;

  end

end


%Need to establish the idealized yield displacement and force of the column based on the confined concrete strain
```

% and steel strain in the system

```
for y=1:length(Results)

    if (Results(y,4) >= -0.004) && (Results([y+1],4) <= -0.004) && (Results(y,5) <= 0.015)

        m1=Results(y,2);

        m2=Results(y+1,2);

        e1=Results(y,4);

        e2=Results(y+1,4);

        Fy=m1+(-0.004-e1)*(m2-m1)/(e2-e1);

        Dy = Dpry*(Fy/Fypr);

        phiy = phipry*(Fy/Fypr);

    elseif (Results(y,5) >= 0.015) && (Results(y-1,5) <= 0.015) && (Results(y,4) >= -0.004)

        m1=Results(y,2);

        m2=Results(y-1,2);

        e1=Results(y,5);

        e2=Results(y-1,5);

        Fy=m1+(-0.004-e1)*(m2-m1)/(e2-e1);

        Dy = Dpry*(Fy/Fypr);

        phiy = phipry*(Fy/Fypr);

    end

end


% Want to establish the moment and curvature along the length of the column at the ultimate condition

FLength=load('FLength.out');

RFLength=load('RFseLength.out');

UCLength=load('UCseLength.out');

CCLength=load('CCseLength.out');

MLength=[];
```

```
for y=1:length(FLength);

    if (FLength(y,1) == ForceU);

        for i=1:1:37;

            ML1=FLength(y,4+6*(i-1));

            UC1=UCLength(y,3+10*(i-1));

            CC1=CCLength(y,3+10*(i-1));

            RF1=RFLength(y,3+10*(i-1));

            NAD=(CC1*(Dpr/2+Dbar/2)/(CC1-RF1));

            curv=abs(CC1)/NAD;

            MLength = [MLength;ML1 UC1 CC1 RF1 NAD curv];

        end

    end

end


fid2=fopen('MomentLength.txt','w');

[rows,col]=size(MLength);

for x=1:rows;

    fprintf(fid2,'%e\t',MLength(x,:));

    fprintf(fid2,'\r\n');

end

fclose(fid2);


% Next up want to also establish an additional file that has curvature along the length at additional point from the

% Gauss-Lobatto Integration technique

curvature=[];

for y=1:length(FLength)

    Lele=Aspect*D/nele;
```

```
Loc1=0;

Loc2=(Lele/2)*(1-0.65465367);

Loc3=Lele/2;

Loc4=Lele/2+(Lele/2)*0.65465367;

Loc5=Lele;

if (FLength(y,1)==ForceU);

    for i=1:1:37

        Loca=(i-1)*Lele+Loc1;

        UC1a=UCLength(y,3+10*(i-1));

        CC1a=CCLength(y,3+10*(i-1));

        RF1a=RFLength(y,3+10*(i-1));

        NADa=(CC1a*(Dpr/2+Dbar/2)/(CC1a-RF1a));

        curva=abs(CC1a)/NADa;

        Locb=(i-1)*Lele+Loc2;

        UC1b=UCLength(y,5+10*(i-1));

        CC1b=CCLength(y,5+10*(i-1));

        RF1b=RFLength(y,5+10*(i-1));

        NADb=(CC1b*(Dpr/2+Dbar/2)/(CC1b-RF1b));

        curvb=abs(CC1b)/NADb;

        Locc=(i-1)*Lele+Loc3;

        UC1c=UCLength(y,7+10*(i-1));

        CC1c=CCLength(y,7+10*(i-1));

        RF1c=RFLength(y,7+10*(i-1));

        NADc=(CC1c*(Dpr/2+Dbar/2)/(CC1c-RF1c));

        curvc=abs(CC1c)/NADc;

        Locd=(i-1)*Lele+Loc4;

        UC1d=UCLength(y,9+10*(i-1));
```

```
        CC1d=CCLength(y,9+10*(i-1));

        RF1d=RFLength(y,9+10*(i-1));

        NADd=(CC1d*(Dpr/2+Dbar/2)/(CC1d-RF1d));

        curvd=abs(CC1d)/NADd;

        Loce=(i-1)*Lele+Loc5;

        UC1e=UCLength(y,11+10*(i-1));

        CC1e=CCLength(y,11+10*(i-1));

        RF1e=RFLength(y,11+10*(i-1));

        NADe=(CC1e*(Dpr/2+Dbar/2)/(CC1e-RF1e));

        curve=abs(CC1e)/NADe;

        curvature=[curvature;Loca UC1a CC1a RF1a NADa curva;Locb UC1b CC1b RF1b NADb curvb;Locc

UC1c CC1c RF1c NADc curvc;Locd UC1d CC1d RF1d NADd curvd;Loce UC1e CC1e RF1e NADe curve];

     end

   end

end


% Write the curvature against length file

fid3=fopen('CurvatureLength.txt','w');

[rows,col]=size(curvature);

for x=1:rows;

   fprintf(fid3,'%e\t',curvature(x,:));

   fprintf(fid3,'\r\n');

end

fclose(fid3);


Rotation=load('DBase2.out');

for y=1:length(Rotation);
```

```
    if (Rotation(y,1)==ForceU);

        Qsp = Rotation(y,4);

    end

end


% Write the final matrix to file


fid=fopen('ForceDisp.txt','w');

fprintf(fid,'This is a file that contains the force and displacement results of an OpenSees Pushover Analysis.\n');

fprintf(fid,'\n');

fprintf(fid,'The analysis was taken to the ultimate curvature of the section based on an M-Phi Analysis\n');

fprintf(fid,'and the input file must be checked to determine the ultimate concrete strain to determine failure location

of the column.\n');

fprintf(fid,'\n');

fprintf(fid,'The data is presented in the following form:\n');

fprintf(fid,'\n');

fprintf(fid,'Displacement (inches)  Force (kips)    Unconfined Concrete Strain (in/in)  Confined Concrete Strain

(in/in)    Steel Strain (in/in)\n    NADepth (in)    Curvature(1/in)');

fprintf(fid,'\n');

[rows,col]=size(MFinal);

for x = 1:rows

    fprintf(fid,'%e\t',MFinal(x,:));

    fprintf(fid,'\r\n');

end

fprintf(fid,'\n');

fprintf(fid,'First Yield Displacement = %e\n',Dpry);

fprintf(fid,'First Yield Force = %e\n',Fypr);
```

```
fprintf(fid,'First Yield Curvature = %e\n',phipry);

fprintf(fid,'Yield Displacement = %e\n',Dy);

fprintf(fid,'Yield Force = %e\n',Fy);

fprintf(fid,'Yield Curvature = %e\n',phiy);

fprintf(fid,'Ultimate Displacment = %e\n',DispU);

fprintf(fid,'Ultimate Force = %e\n',ForceU);

fprintf(fid,'Ultimate Curvature = %e\n',phiu);

fprintf(fid,'\n');

fprintf(fid,'Rotation due to Strain Penetration = %e\n',Qsp);

fclose(fid);


figure;

plot(Results(:,1),Results(:,2))

grid

xlabel('Displacement (in)')

ylabel('Force (kip)')

title('Force - Displacment')

axis([0 Inf 0 Inf])

saveas(gcf,'Force_Disp.fig')


figure;

plot(curvature(:,6),curvature(:,1))

grid

xlabel('Curvature (1/in)')

ylabel('Length Along Column (in)')

title('Curvature along Length')

axis([0 Inf 0 Inf])
```

saveas(gcf,'Curv_Length.fig')

B.2.3: Dynamic Analyses

%Earthquake Batch based on the stiffnesses that are selected based on the data from the Pushover analyses

%Axial Load Ratio

ALR=0.05

%Column Diameter

colD=48

%cover to main longitudinal bar

cover=2

%diameter and area of main longitudinal r/f

dbl=1.410;

Abl=1.56;

BarNumLong=11

%diameter and area of hoop r/f

dbh=0.625;

Abh=0.31;

%desired amount of longitudinal r/f

rhold=0.02;

%material properties for concrete and steel

fc=4;

fy=60;

Es=29000;

%Some additional Parameters are needed for the analysis

maxK=0.005;

Incr=300;

% Time Stepping Information

```
DtAnalysis=0.005;

TmaxAnalysis=39.945;

% The actual time step size of the ground motion file

dt=0.005;

%setting up the actual batching process and writing the appropriate input file for the analysis

id=1;

for ARatio = [1/10,1/9,1/8,1/7,1/6,1/5,1/4,1/3]

    %Establishing the length of the element to be used in the analysis

    Lele=1.2973*(ARatio^-1);

    Priestley(id,colD,cover,rhold,ALR,BarNumLong,fc,fy,Es,850,0.12,maxK,Incr,ARatio);

    Stiffness=8348.9*((1/ARatio)^-2.858)

    fid=fopen('inputeq.tcl','w');

    fprintf(fid,'set Analoption Earthquake\n');

    fprintf(fid,'set concMat c03\n');

    fprintf(fid,'set steelMat s02\n');

    fprintf(fid,'set rhold %f\n',rhold);

    fprintf(fid,'set ALR %f\n',ALR);

    fprintf(fid,'set ARatio %f\n',ARatio);

    fprintf(fid,'set Lele %f\n',Lele);

    fprintf(fid,'set Stiffness %f\n',Stiffness);

    fprintf(fid,'set GMfile "LPRIETA.acc"\n');

    fprintf(fid,'set DtAnalysis %f\n',DtAnalysis);

    fprintf(fid,'set TmaxAnalysis %f\n',TmaxAnalysis);

    fprintf(fid,'set dt %f\n',dt)

    fclose(fid);

    !OpenSees.exe "CalTransEQSP2.tcl"

    id=id+1
```

end

% Writing a code to process the output files produced from the multiple earthquake runs. Creating a final text
% document and figures of the data to help understand what is going on.

```
colD=input('What is the column diameter?');

cover=input('What is the cover to longitudinal reinforcement?');

dbh=input('What is the diameter of the horizontal reinforcing bar?');

dbl=input('What is the diameter of the longituidnal reinforcing bar?');

Period=input('What is the period of the structure being analyzed?');

ARatio=input('What is the aspect ratio of the column?');

EQ=input('What was the Earthquake Record used in the Analysis?','s');
```

% Loading the Files that are needed to produce the final files

```
Disp=load('Dtop.out');

Force=load('FcolTop.out');

BotUCse=load('BotUCse2.out');

BotCCse=load('BotCCse2.out');

BotRFse=load('BotRFse2.out');
```

% Need to combine the appropriate columns into a matrix that is easier to work with.

```
FDResults=[Disp,Force(:,2),Force(:,3),Force(:,4),Force(:,5),Force(:,6),Force(:,7)];
```

```
SEResults=[BotUCse(:,2),BotUCse(:,3),BotCCse(:,2),BotCCse(:,3),BotRFse(:,2),BotRFse(:,3)];
```

% Create the Final Matrix that is fully combined with Force-Disp and Stress-Strain Information

Final=[FDResults SEResults];

% Want to perform a couple of calculations to produce the Neutral Axis, Depth and the Curvature of the local

% section at any given time

% Define the depth of steel from the edge of the cover concrete section

dsteel=colD-cover-dbl/2;

NADepth=[];

curvature=[];

for y=1:length(Final);

   ccov=Final(y,12)*dsteel/(Final(y,12)-Final(y,16));

   phi1=abs(Final(y,12))/ccov;

   NADepth=[NADepth;ccov];

   curvature=[curvature;phi1];

end

% Define the final matrix that now takes into account the neutral axis depth and curvature of the section

Final2=[Final NADepth curvature];

% Going to write the fianl data set to a file called EQCompiledData.txt

fid=fopen('EQCompiledData.txt','w');

fprintf(fid,'This is a file that contains the force, displacement, stress, strain and curvature results of an OpenSees

Earthquake Analysis.\n');

fprintf(fid,'\n');

fprintf(fid,'Some of the important input information parameters are as follows:\n');

```
fprintf(fid,'Column Diameter = %e\n',colD);

fprintf(fid,'Aspect Ratio = %e\n',ARatio);

fprintf(fid,'Period of the Structure = %e\n',Period);

fprintf(fid,'Earthquake Ground Motion Record = %s\n',EQ);

fprintf(fid,'\n');

fprintf(fid,'The data is presented in the following form:\n');

fprintf(fid,'\n');

fprintf(fid,'Time(sec) Dx(inches) Dy(inches) ThetaZ(rad) FxLow(kips) FyLow(kip) MzLow(kip-in) FxHigh(kips)

FyHigh(kip) MzHigh(kip-in)\n');

fprintf(fid,'UCStress(ksi) UCStrain(in/in) CCStress(ksi) CCStrain(in/in) RFStress(ksi) RFStrain(in/in) NADepth(in)

Curvature(1/in)\n');

fprintf(fid,'\n');

[rows,col]=size(Final2);

for x = 1:rows

    fprintf(fid,'%e\t',Final2(x,:));

    fprintf(fid,'\r\n');

end

fclose(fid);


figure;

plot(Final2(:,2),Final2(:,8))

grid

xlabel('Displacement (in)')

ylabel('Force (kips)')

title('EQ Force-Displacement')

saveas(gcf,'EQForceDisp.emf')
```

figure;

plot(Disp(:,1),Disp(:,2))

grid

xlabel('Time (sec)')

ylabel('Displacement (inches)')

title('Displacement with Time')

saveas(gcf,'DispTimeHistory.emf')

B.3: OpenSEES Codes

This portion of Appendix B contains the coding files used in OpenSEES that were accessed during the batching process within Matlab.

B.3.1: Moment-Curvature Analysis

```
#units of lbs and in


#Clear the system of any previous operations
wipe


# Bring in the important design information from the Matlab coded input file
source "input.tcl"


# Establish information for the writing of the file name during recording of data
set Specimen1 $D
set Specimen2 _$id


# The term below defines the edge of the confined concrete region
set rrec [expr $rcov-2.0]
```

```
# Define the model (Two Dimensions and 3 DOF/node)

model BasicBuilder -ndm 2 -ndf 3


# Define the concrete material behavior using Concrete07 (tag, fc, ec, Ec, ft, et, xp, xn, r)

# ----------------------------------------------------------------------------------------

# For the Confined Concrete Model Going to Need


if {$cmodel == "Concrete02"} {

    uniaxialMaterial Concrete02 1 $fccmat $eccmat [expr 0.1*$fccmat] $ecu .1 $ft2 [expr $Ec/10]

    } else {

    uniaxialMaterial Concrete07 1 $fccmat $eccmat $Ecc $ft2 $et2 $xp2 $xn2 $r2

}


# Cover Concrete


if {$cmodel == "Concrete02"} {

    uniaxialMaterial Concrete02 2 $fcmat $ecmat [expr 0.1*$fcmat] -0.008 .1 $ft1 [expr $Ec/10]

    } else {

    uniaxialMaterial Concrete07 2 $fcmat $ecmat $Ec $ft1 $et1 $xp1 $xn1 $r1

}


# Define the steel material behavior using ReinforcingSteel (tag fy fu Es esh eu)

# Also going to define a second steel model in case it is needed use Steel02 (tag fy E b R0 cR1 cR2)


if {$smodel == "ReinforcingSteel"} {

    uniaxialMaterial ReinforcingSteel 3 $fye $fsu $Es $Esh $esh $esu

    } else {
```

```
        uniaxialMaterial Steel02 3 $fye $Es $Eratio 18 0.925 0.15 0 5 0 5

}


# Create the section itself using fibers

section Fiber 1 {

        # Confined Concrete Fibers

        patch circ 1 $nfccirc $nfcradial 0 0 0 $rcon 0 360

        # Unconfined Concrete Fibers

        patch circ 2 $nfucirc $nfuradial 0 0 $rcon $rcov 0 360

        # Reinforcing Steel Fibers (Tag nFiber AFiber yCenter zCenter radius <startAng endAng>

        layer circ 3 $ns $Abar 0.00 0.00 $rsteel 0 360

}




#Need to create the Nodes for the System itself

node 1 0.0 0.0

node 2 0.0 0.0


# Apply Boundary Conditions (for this problem x, y, rotation)

# The y direction is fixed at Node 2 as the axial load is in the local x-direction of the zerolength element

fix 1 1 1 1

fix 2 0    1 0


# Define the element so that the moment curvature procedure can be run

element zeroLengthSection 1 1 2 1


#Create a series of recorders for monitoring the overall system response
```

Record the Moment-Curvature behavior based on the 2nd node of the system

--

recorder Node -file MCNode_$Specimen1$Specimen2.out -time -node 2 -dof 3 disp

Record the material behaviors of the system within the cross-section

--

recorder Element -file BarStrain_$Specimen1$Specimen2.out -time -ele 1 section fiber -$rrec 0 3 stressStrain

recorder Element -file ConcStrainT_$Specimen1$Specimen2.out -time -ele 1 section fiber -$rcov 0 2 stressStrain

recorder Element -file ConcStrainConf_$Specimen1$Specimen2.out -time -ele 1 section fiber $rrec 0 1 stressStrain

recorder Element -file ConcStrainUnConf_$Specimen1$Specimen2.out -time -ele 1 section fiber $rcov 0 2

stressStrain

Record the Forces of the element at the top and bottom nodes to verify the Moment Behavior

--

recorder Element -file Forces_$Specimen1$Specimen2.out -time -ele 1 section force

puts "recorder ok"

Define constant axial load using pattern (type tag tsTag {

using a nodal load with load (node $ndfLoadValues)

pattern Plain 1 "Constant" {

    load 2 [expr -1*$P] 0.0 0.0

}

```
puts "loading ok"

puts "Ultimate Strain"

puts $ecu


# Define the analysis parameters

integrator LoadControl 0.0

system SparseGeneral -piv

#test NormDispIncr 1.0e-8 100 0

test NormUnbalance 1.0e-04 600 0

numberer Plain

constraints Plain

algorithm KrylovNewton

analysis Static


# Do a single analysis for constant axial load

analyze 1


# Define a reference moment

pattern Plain 2 "Linear" {

    load 2 0.0 0.0 1.0

}


# Compute curvature and increments

set dK [expr $maxK/$numIncr]


# Use displacement control at node 2 for section analysis

integrator DisplacementControl 2 3 $dK
```

set a [eleResponse 1 section fiber -$rrec 0.0 3 strain]

#Perform the section analysis

while {$a <= 0.07} {

    analyze 1

    set a [eleResponse 1 section fiber -$rrec 0.0 3 strain]

    }

exit

B.3.2: Pushover Analysis

Start the development of the model

units: kip, inch, sec

#

clear any data from any previous analyses

wipe;

Establish the type of analysis to be used for this column section and some basic information about the materials

#set Analoption Pushover;   # want this to be "Cyclic" for a cyclic analysis otherwise something else to run

pushover analysis

#set Trial 1

#set concMat c03;   # Options are c07, c02, c03

#set steelMat s02;   # Options are rs, s02

#set phiu 0.00144995;   # Ultimate curvature of the concrete section (from moment-curvature analysis)

#set ARatio 0.25; # Column Aspect Ratio

```
#set ALR 0.05;    # Column Axial Load Ratio

#set colD 48;    # Column Diameter


#Going to call up the above information using Matlab to do the batching process

source input.tcl

source input2.tcl


# Create a file folder location for all of the data in the OpenSees folder

set File

Data_multDispEle_ATC_D{$colD}_ConcMat{$concMat}_SteelMat{$steelMat}_ALR{$ALR}_Aspect{$ARatio}

_{$Analoption}_Trial{$Trial}_SP;

file mkdir $File;


# define the model builder and how many dimensions and degrees of freedom

model BasicBuilder -ndm 2 -ndf 3


# define some important constants for calculations

#set pi [expr 4*atan(1)];

#set g 386.4;    # establshing the gravity constant in in/sec^2


# Define some geometry of the section

#set colD 48;

#set Ag [expr $pi*pow($colD,2)/4];

#set cover 2.;    # Cover to Longitudinal Bar

#set dbl 1.410;    # Longitudinal Bar Diameter

#set Abl 1.56;    # Longitudinal Bar Area

#set dbh 0.625;    # Hoop Bar Diameter
```

```
#set Abh 0.31;    # Hoop Bar Area

#set Dpr [expr $colD-2*$cover+$dbh];

#set Ac [expr $pi*pow($Dpr,2)/4];

#set Dbar [expr $colD-2*$cover-$dbl];


# Establish the important radii for the section definition

#set rout [expr $colD/2];

#set rpr [expr $Dpr/2];

#set rbar [expr $Dbar/2];

set dconf [expr $rcon+$rsteel];    # depth of steel bar from the confined concrete region definition


# Define the geometry of the column above the foundation

set Lcol [expr $colD/$ARatio];

#set Lele [expr 1.2973*pow($ARatio,-1)];

set colNumIncr [expr int(ceil($Lcol/$Lele))];

puts "colNumIncr = $colNumIncr"

set colIncr [expr $Lcol/$colNumIncr];


# Define the number of longitudinal bars to be used in the section model

#set rhold 0.02;

#set Asd [expr $rhold*$Ag];

#set ns [expr int(ceil($Asd/$Abl))];

set rhola [expr $ns*$Abar/$Ag];


# nodal coordinates for the model - node(node#, X, Y)


node 1 0.0 0.0
```

```
node 2 0.0 0.0

for {set i 1} {$i <= $colNumIncr} {incr i 1} {

    node [expr $i+2] 0 [expr $i*$colIncr]

    puts "node [expr $i+2] = [expr $i*$colIncr]"

}
puts "nodes established"


# Single point constraints -- Boundary Conditions fix(node #, DX, DY, RZ)

fix 1 1 1 1


# Going to establish the nodal conditions at the top of the strain penetration element

# Creating an equal dof such that the element can slip along the length of the element in

# local coordinate system.  Thus only constrain the dof 2 using:

# equalDOF (Master Node, Slave Node, DOF to match)

equalDOF 1 2 1


# Define the material properties that are going to be used in the fiber section

#

# Unconfined Concrete Properties First

#set fc 4;

#set Ec [expr 57*pow($fc*1000,0.5)];

#set ec [expr pow($fc*1000,0.25)/4000];

#set ft1 0.0005;

#set et1 [expr 2*$ft1/$Ec];

#set xp1 1.23;

#set xn1 2.3;
```

```
#set r1 [expr ($fc*1000/750)-1.9];

#set fc1 [expr -1*$fc];

#set ec1 [expr -1*$ec];


# Reinforcing Steel Properties

#set fy 60.;

#set fye [expr 1.1*$fy];

#set fsu [expr 1.5*$fye];

#set Es 29000.;

#set Esh 850.;

#set esh [expr 3.24*$fye/$Es];

#set esu 0.12;

#set Eratio 0.02;


# Define the column axial load

#set PCol [expr $ALR*$fc1*$Ag];


# Confined Concrete Properties

#set rhos [expr 0.16*($fc/$fy)*(0.5+1.25*$ALR)+0.13*($rhola-0.01)];    # ATC-32 Reccommendation and values
in Priestley (1996)

#set rhos [expr 0.45*($fc/$fy)*(($Ag/$Ac)-1)];    #This is the Caltrans Minimum Equation

#set s [expr 4*$Abh/($Dpr*$rhos)];

#set sclear [expr $s-$dbh];

#set rhocc [expr $ns*$Abl/$Ac];

#set Ke [expr (1-0.5*$sclear/$Dpr)/(1-$rhocc)];

#puts "Ke = $Ke"

#set flp [expr $Ke*$fy*$rhos/2];
```

```
#set fcc [expr $fc*(2.254*pow((1+7.94*$flp/$fc),0.5)-2*$flp/$fc-1.254)];

#set ecc [expr 0.002*(1+5*($fcc/$fc-1))];

#set Ecc [expr 57*pow($fc*1000,0.5)];

#set ft2 0.0005;

#set et2 [expr 2*$ft2/$Ecc];

#set xp2 1.23;

#set xn2 20;     # this is supposed to be between 20-30 based on information provided by others using Concrete07

#set n2 [expr $Ecc*$ecc/$fcc];

#set r2 [expr $n2/($n2-1)];

#set ecu [expr -1*(0.004+1.4*$rhos*$fy*$esu/$fcc)];

set rmander [expr $Ecc/($Ecc-($fccmat/$eccmat))];

set xult [expr $ecu/$eccmat];

puts "xult = $xult"

set fccu [expr ($fccmat*$xult*$rmander)/($rmander-1+pow($xult,$rmander))];

#set fc2 [expr -1*$fcc];

#set ec2 [expr -1*$ecc];

set fcu2 [expr $fccu];

#set fcu2 -4.;

puts "ultimate compressive strength = $fcu2"

puts "confined concrete properties ok"


# Writing a text file of the information used for the analysis

set out [open "$File/Input.txt" w]

puts $out "Units in the Program"

puts $out "Forces are in kips"

puts $out "Displacements and Dimensions are in inches"

puts $out "Time is in Seconds"
```

```
puts $out ""

puts $out ""

puts $out "Analysis Type = $Analoption"

puts $out ""

puts $out ""

puts $out "Section Geometry"

puts $out ""

puts $out "Column Diameter = $colD"

puts $out "Cover to Main Bar = $cover"

puts $out "Longitudinal Bar Diameter = $dbl"

puts $out "Longitudianl Bar Area = $Abar"

puts $out "Number Longitudinal Bars = $ns"

puts $out "Longitudinal Reinforcement Ratio = $rhola"

puts $out "Hoop Bar Diameter = $dbh"

puts $out "Hoop Bar Area = $Abh"

puts $out "Hoop Spacing = $s"

puts $out "Horizontal Reinforcement Ratio = $rhos"

puts $out ""

puts $out ""

puts $out "Column Geometry above the Spread Footing"

puts $out ""

puts $out "Column Height = $Lcol"

puts $out "Aspect Ratio = $ARatio"

puts $out "Element Length = $colIncr"

puts $out "Number of Elements = $colNumIncr"

puts $out ""

puts $out ""
```

```
puts $out "Applied Loads"

puts $out ""

puts $out "Column Axial Load At Top = $P"

puts $out ""

puts $out ""

puts $out "Unconfined Concrete Material Properties"

puts $out ""

puts $out "Compressive Strength = $fcmat"

puts $out "Strain at Compressive Strength = $ecmat"

puts $out "Modulus of Elasticity = $Ec"

puts $out "Tensile Strength = $ft1"

puts $out "Tensile Strain = $et1"

puts $out "Concrete Model is $concMat"

puts $out ""

puts $out ""

puts $out "Confined Concrete Material Properties"

puts $out ""

puts $out "Confinement Effectiveness, Ke = $Ke"

puts $out "Compressive Strength = $fccmat"

puts $out "Strain at Compressive Strength = $eccmat"

puts $out "Modulus of Elasticity = $Ecc"

puts $out "Ultimate Compressive Strain = $ecu"

puts $out "Ultimate Compressive Stress = $fcu2"

puts $out "Tensile Strength = $ft2"

puts $out "Tensile Strain = $et2"

puts $out "Concrete Model is $concMat"

puts $out ""
```

```
puts $out ""

puts $out "Reinforcing Steel Material Properties"

puts $out ""

puts $out "Hoop Yield Stress = $fy"

puts $out "Longitudinal Yield Stress = $fye"

puts $out "Ultimate Stress = $fsu"

puts $out "Modulus of Elasticity = $Es"

puts $out "Hardening Steel Strain = $esh"

puts $out "Hardening Modulus of Elasticity = $Esh"

puts $out "Ultimate Steel Strain = $esu"

puts $out "Steel Model is $steelMat"

close $out




# Write the actual material property definitions in OpenSees

# Concrete Properties using Concrete07(tag, fc, ec, Ec, ft, et, xp, xn, r)

# Concrete Properties using Concrete02(tag,fc, ec, fc(crushing), ec(crushing), lambda, ft, Ets)

# Concrete Properties using Concrete03(tag, fc, ec, fc (crushing), ec (crushing), lambda (0.1), ft, ets0 (tension

transition to strain softening), ft0 (tesnsion stress at softening transition), beta (exponent tension soft), etu (ultimate

tensile strain))

# Steel Properties using ReinforcingSteel(tag, fy, fu, Es, Esh, esh, esu)

# Steel Properties using Steel02(tag, fy, Es, b(0.015), R0 (between 10 and 20), CR1 (0.925), CR2(0.15), a1(0),

a2(5), a3(0), a4(5)

# ----------------------------------------------------------------------------------------------

# Unconfined Concrete Models

if {$concMat == "c07"}  {
```

```
    uniaxialMaterial Concrete07 2 $fcmat $ecmat $Ec $ft1 $et1 $xp1 $xn1 $r1

} elseif {$concMat == "c02"} {

    uniaxialMaterial Concrete02 2 $fcmat $ecmat [expr 0.1*$fcmat] -0.008 0.1 $ft1 [expr $Ec/10]

} else {

    uniaxialMaterial Concrete03 2 $fcmat $ecmat -0.01 -0.0091 0.1 $ft1 0.003 0.0004 2.5 0.004

}


# Confined Concrete Models

if {$concMat == "c07"} {

    uniaxialMaterial Concrete07 1 $fccmat $eccmat $Ecc $ft2 $et2 $xp2 $xn2 $r2

} elseif {$concMat == "c02"} {

    uniaxialMaterial Concrete02 1 $fccmat $eccmat [expr 0.1*$fccmat] $ecu 0.1 $ft2 [expr $Ec/10]

} else {

    uniaxialMaterial Concrete03 1 $fccmat $eccmat $fcu2 $ecu 0.1 $ft2 0.003 0.0004 2.5 0.004

}


# Reinforcing Steel Models

if {$steelMat == "rs"} {

    uniaxialMaterial ReinforcingSteel 3 $fye $fsu $Es $Esh $esh $esu

} else {

    uniaxialMaterial Steel02 3 $fye $Es $Eratio 18 0.925 0.15 0 5 0 5

}


# Strain Penetration Model Needs to be Defined

# Defining the Slip Curve using Bond_SP01 $matTag $Fy $Sy $Fu $Su $b $R

# Fy = yield stress of r/f steel

# Sy = rebar slip at member interface under yield stress
```

```
# Fu = ultimate strength of reinforcing steel

# Su = rebar slip at the loaded end at the bar fracture strength

# b = initial hardening ratio in the monotonic slip vs. bar stress response (0.3 ~ 0.5) (Paper says 0.5 in columns)

# R = Pinching factor for the cyclic slip vs. bar response (0.5 ~ 1.0) (Paper says 1.0 columns and 0.7 tee-joint)


set alpha 0.4;

set alphain [expr 1/$alpha];

set Fy [expr $fye*1000];

set bracket [expr ($dbl/4000)*($Fy/pow(-1*$fccmat*1000,0.5))*(2*$alpha+1)];

set Sy [expr 0.1*pow($bracket,$alphain)+0.013]

set Su [expr 40*$Sy]

set b 0.5;

set R 1.0;

puts "Yield Slip = $Sy"

puts "Ultimate Slip = $Su"


uniaxialMaterial Bond_SP01 4 $fye $Sy $fsu $Su $b $R


puts "Materials Defined"


# Create the fiber section to be used in the analysis for this model of a circular column

# --------------------------------------------------

# Define the number of fibers to be used in the cross-section

#set length 0.5

#set nfcradial [expr int(ceil(0.5*$Dpr/$length))]

#set nfccirc [expr int(ceil($pi*$Dpr/$length))]

#set nfuradial [expr int(ceil($cover/$length))]
```

```
#set nfucirc [expr int(ceil($pi*$colD/$length))]


# Define the cross-section using fibers


section Fiber 1 {

    patch circ 1 $nfccirc $nfcradial 0 0 0 $rcon 0 360

    patch circ 2 $nfucirc $nfuradial 0 0 $rcon $rcov 0 360

    layer circ 3 $ns $Abar 0 0 $rsteel 0 360

    }


section Fiber 2 {

    patch circ 1 $nfccirc $nfcradial 0 0 0 $rcon 0 360

    patch circ 2 $nfucirc $nfuradial 0 0 $rcon $rcov 0 360

    layer circ 4 $ns $Abar 0 0 $rsteel 0 360

    }


# define geometric transformation to transform basic system to global system

geomTransf Linear 101

#geomTransf PDelta 101


# establish the element(s) for use in the model

set numIntgrPts 5;


element zeroLengthSection 1 1 2 2 -orient 0 1 0 1 0 0

# in the orientation term $x1 $x2 $x3 define the local x-axis in global coordinates

# the yp terms can be found as the x vector crossed with yp equals your z-vector direction
```

```
for {set i 1} {$i <= $colNumIncr} {incr i 1} {

    element dispBeamColumn [expr $i+1] [expr $i+1] [expr $i+2] $numIntgrPts 1 101

    puts "element = [expr $i+1] for node [expr $i+1] and [expr $i+2]"

}


puts "elements defined"


# Define RECORDERS -------------------------------------------------------------

recorder Node -file $File/DFree1.out -time -node 2 -dof 1 2 3 disp;

recorder Node -file $File/Dtop.out -time -node [expr $colNumIncr+2] -dof 1 2 3 disp;

recorder Node -file $File/DBase1.out -time -node 1 -dof 1 2 3 disp;

recorder Node -file $File/RBase1.out -time -node 1 -dof 1 2 3 reaction;

recorder Node -file $File/DBase2.out -time -node 2 -dof 1 2 3 disp;

recorder Node -file $File/Rbase2.out -time -node 2 -dof 1 2 3 reaction;

#recorder Drift -file $File/Drift1.out -time -iNode 1 -jNode 2 -dof 1 -perpDirn 2;

#recorder Drift -file $File/Drift2.out -time -iNode 2 -jNode 3 -dof 1 -perpDirn 2;

#recorder Drift -file $File/DriftTot.out -time -iNode 1 -jNode [expr $colNumIncr+1] -dof 1 -perpDirn 2;

recorder Element -file $File/FCol1.out -time -ele 1 globalForce;

recorder Element -file $File/Fcol2.out -time -ele 2 globalForce

recorder Element -file $File/FColTop.out -time -ele [expr $colNumIncr+1] globalForce;

recorder Element -file $File/TopUCse.out -time -ele [expr $colNumIncr+1] section fiber -$rcov 0.0 2 stressStrain

recorder Element -file $File/BotUCse1.out -time -ele 1 section fiber -$rcov 0.0 2 stressStrain

recorder Element -file $File/BotUCse2.out -time -ele 2 section fiber -$rcov 0.0 2 stressStrain

recorder Element -file $File/TopCCse.out -time -ele [expr $colNumIncr+1] section fiber -$rcon 0.0 1 stressStrain

recorder Element -file $File/BotCCse1.out -time -ele 1 section fiber -$rcon 0.0 1 stressStrain

recorder Element -file $File/BotCCse2.out -time -ele 2 section fiber -$rcon 0.0 1 stressStrain

recorder Element -file $File/TopRFse.out -time -ele [expr $colNumIncr+1] section fiber $rsteel 0.0 3 stressStrain
```

recorder Element -file $File/BotRFse1.out -time -ele 1 section fiber $rsteel 0.0 4 stressStrain

recorder Element -file $File/BotRFse2.out -time -ele 2 section fiber $rsteel 0.0 3 stressStrain

#recorder Element -file $File/DefoCol1.out -time -ele 1 basicDeformation;

#recorder Element -file $File/DefoCol2.out -time -ele 2 basicDeformation;

#recorder Element -file $File/FColSec1_1.out -time -ele 1 section 1 force;

#recorder Element -file $File/FColSec1_2.out -time -ele 2 section 1 force;

#recorder Element -file $File/DefoColSec1_1.out -time -ele 1 section 1 deformation;

#recorder Element -file $File/DefoColSec1_2.out -time -ele 2 section 1 deformation;

#recorder Element -file $File/FColSec{$numIntgrPts}_1.out -time -ele 1 section $numIntgrPts force;

#recorder Element -file $File/FColSec{$numIntgrPts}_2.out -time -ele 2 section $numIntgrPts force;

#recorder Element -file $File/DefoColSec{$numIntgrPts}_1.out -time -ele 1 section $numIntgrPts deformation;

#recorder Element -file $File/DefoColSec{$numIntgrPts}_2.out -time -ele 1 section $numIntgrPts deformation;

recorder Element -file $File/FLength.out -time -eleRange 2 [expr $colNumIncr+1] globalForce

recorder Element -file $File/RFseLength.out -time -eleRange 2 [expr $colNumIncr+1] section fiber $rsteel 0 3 stressStrain

recorder Element -file $File/CCseLength.out -time -eleRange 2 [expr $colNumIncr+1] section fiber -$rcon 0 1 stressStrain

recorder Element -file $File/UCseLength.out -time -eleRange 2 [expr $colNumIncr+1] section fiber -$rcov 0 2 stressStrain

puts "recorders started"

define the Gravity Load on the column ---

pattern Plain 1 Linear {

    load [expr $colNumIncr+2] 0 [expr -1*$P] 0

}

```
set Tol 1.0e-8;

constraints Plain;

numberer Plain;

system BandGeneral;

test NormDispIncr $Tol 10;

algorithm Newton;

set NstepGravity 10;

set DGravity [expr 1./$NstepGravity];

integrator LoadControl $DGravity;

analysis Static

analyze $NstepGravity


# Maintain the applied gravity load and reset the time of the program to 0

loadConst -time 0.0

puts "Gravity load applied, moving to cyclic analysis"


# define the cyclic lateral load analysis ----------------------------------------------------

#

# Establish the model parameters specific to this analysis

set IDctrlNode [expr $colNumIncr+2];

puts "IDctrlNode = $IDctrlNode"

set IDctrlDOF 1;     # This is for the Global X-Direction, 2 is the Global Y-Direction, 3 is the Global Rotation about
z

set du [expr -25.55*$ARatio+32.55];

set nsteps 600;

set Dincr [expr $du/$nsteps];
```

```
# Define the static analysis parameters for this process

set tolerance 1.0e-5

set nItr 100

set maxNumItrStatic 5000

#constraints Plain;

#numberer Plain;

#system SparseGeneral -piv

#test EnergyIncr $tolerance $nItr 1

#test NormUnbalance $tolerance $nItr 1

#algorithm KrylovNewton

#analysis Static


pattern Plain 200 Linear {

    load $IDctrlNode 1.0 0.0 0.0

}


if {$Analoption != "Cyclic"} {

    puts "running the pushover analysis"

    set a [eleResponse 2 section 1 fiber -$rcon 0.0 1 strain]

    set b [eleResponse 2 section 1 fiber $rcov 0.0 3 strain]

    set cconf [expr $a*$dconf/($a-$b)];    # This is the neutral axis depth of concrete from the confined region

    set curv [expr abs($a)/$cconf];    # This is the curvature of the concrete section at the bottom node

    while {$curv <= $phiu} {

        set ok 0

        constraints Plain

        numberer Plain

        system SparseGeneral -piv
```

```
test EnergyIncr $tolerance $nItr 1

algorithm KrylovNewton

integrator DisplacementControl $IDctrlNode $IDctrlDOF $Dincr

analysis Static

set ok [analyze 1]

if {$ok != 0} {

        puts "Trying Krylov Newton with Different Tolerance and # of Iterations and NormDispIncr test"

        set tolerance 1.0e-4

        set nItr $maxNumItrStatic

        constraints Plain

        numberer Plain

        system SparseGeneral -piv

        test normDispIncr $tolerance $nItr 1

        algorithm KrylovNewton

        analysis Static

        set ok [analyze 1]

}

if {$ok != 0} {

        puts "Trying KylovNewton with NormUnbalance Test"

        set tolerance 1.0e-4

        set nItr $maxNumItrStatic

        constraints Plain

        numberer Plain

        system SparseGeneral -piv

        test NormUnbalance $tolerance $nItr 1

        algorithm KrylovNewton

        analysis Static
```

```
        set ok [analyze 1]

}

if {$ok != 0} {

        puts "Trying Newton algorithm with NormDispIncr test"

        set tolerance 1.0e-4

        set nItr $maxNumItrStatic

        test NormDispIncr $tolerance $nItr 1

        algorithm Newton

        set ok [analyze 1]

}

if {$ok != 0} {

        puts "Trying Newton algorithm with NormUnbalance Test"

        set tolerance 1.0e-4

        set nItr $maxNumItrStatic

        test NormUnbalance $tolerance $nItr 1

        algorithm Newton

        set ok [analyze 1]

}

if {$ok == 0} {

        puts "Convergence Met"

        set tolerance 1.0e-4

        set nItr $maxNumItrStatic

        #test NormUnbalance $tolerance $nItr 1

        test EnergyIncr $tolerance $nItr 1

        algorithm KrylovNewton

        set currentdisp [nodeDisp $IDctrlNode $IDctrlDOF]

        puts "displacement of column is $currentdisp"
```

```
        }

        set a [eleResponse 2 section 1 fiber -$rcon 0.0 1 strain]

        set b [eleResponse 2 section 1 fiber $rsteel 0.0 3 strain]

        set cconf [expr $a*$dconf/($a-$b)];    # This is the neutral axis depth of concrete from the confined region

        set curv [expr abs($a)/$cconf];    # Curvature of the concrete section at the bottom node

        puts "curvature of section is $curv"

    }

} else {

# ----------------------------------------------------------------

# -------------------------Cyclic Analysis-----------------------

# ----------------------------------------------------------------

puts "running the cyclic analysis"

set Dmax1 0.0

set Dmaxa 0.0

    foreach {Dmax} {0.01 -0.01 0.1 -0.1 0.2 -0.2 0.4 -0.4 0.8 -0.8 1.0 -1.0 1.4 -1.4 1.8 -1.8 2.0 -2.0 2.5 -2.5 3.0 -3.0

4.0 -4.0 5.0 -5.0 6.0 -6.0 7.0 -7.0 0.1} {

        if {[expr abs($Dmax)] < 0.2 && [expr abs($Dmaxa)] < 0.2} {

                set stepSize 0.01

        } elseif {[expr abs($Dmax)] >= 0.2 && [expr abs($Dmax)] <=1.0 && [expr abs($Dmaxa)] <=1.0} {

                set stepSize 0.02

        } else {

                set stepSize 0.05

        }

        set numSteps [expr int(abs($Dmax-$Dmax1)/$stepSize)]

        for {set i 1} {$i <= $numSteps} {incr i 1} {

                set ok 0

                if {$Dmax < 0} {
```

```
                set stepSize1 [expr -1.*$stepSize]

        } else {

                set stepSize1 $stepSize

}

integrator DisplacementControl $IDctrlNode $IDctrlDOF $stepSize1

analysis Static

# --------------------first analyze procedure--------------------------

set ok [analyze 1]

# --------------------if convergence failure--------------------------

# if the analysis failed, trying some other stuff to find convergence

if {$ok != 0} {

                puts "Increasing the number of iterations and changing tolerance"

                set tolerance 1.0e-4

                set nItr $maxNumItrStatic

                test EnergyIncr $tolerance $nItr 1

                algorithm KrylovNewton

                set ok [analyze 1]

}

if {$ok != 0} {

                puts "Trying Krylov Newton with Different Tolerance and # of Iterations and

NormDispIncr test"

                set tolerance 1.0e-4

                set nItr $maxNumItrStatic

                test normDispIncr $tolerance $nItr 1

                algorithm KrylovNewton

                set ok [analyze 1]

}
```

```
if {$ok != 0} {

        puts "Trying KylovNewton with NormUnbalance Test"

        set tolerance 1.0e-4

        set nItr $maxNumItrStatic

        test NormUnbalance $tolerance $nItr 1

        algorithm KrylovNewton

        set ok [analyze 1]

}

if {$ok != 0} {

        puts "Trying Newton algorithm with NormDispIncr test"

        set tolerance 1.0e-4

        set nItr $maxNumItrStatic

        test NormDispIncr $tolerance $nItr 1

        algorithm Newton

        set ok [analyze 1]

}

if {$ok != 0} {

        puts "Trying Newton algorithm with NormUnbalance Test"

        set tolerance 1.0e-4

        set nItr $maxNumItrStatic

        test NormUnbalance $tolerance $nItr 1

        algorithm Newton

        set ok [analyze 1]

}

if {$ok == 0} {

        puts "Convergence met"

        set tolerance 1.0e-5
```

```
                    set nItr $maxNumItrStatic

                    #test NormUnbalance $tolerance $nItr 1

                    test NormDispIncr $tolerance $nItr 1

                    #test EnergyIncr $tolerance $nItr 1

                    algorithm KrylovNewton

                    set currentdisp [nodeDisp $IDctrlNode $IDctrlDOF]

                    puts "displacement of column is $currentdisp, displacement cycle of $Dmax"

            }; # end if

        }; # end i procedure

        set Dmaxa $Dmax1

        set Dmax1 $Dmax

    }; # end Dmax cycle

}; # end if statement for analysis type

puts "Analysis is complete"
```

B.3.3: Dynamic Analysis

```
# Start the development of the model

# units: kip, inch, sec

#

# clear any data from any previous analyses

wipe;


# Establish the type of analysis to be used for this column section and some basic information about the materials

#set Analoption Pushover;     # want this to be "Cyclic" for a cyclic analysis otherwise something else to run

pushover analysis

#set Trial 1

#set concMat c03;    # Options are c07, c02, c03
```

```
#set steelMat s02;    # Options are rs, s02

#set phiu 0.00144995;    # Ultimate curvature of the concrete section (from moment-curvature analysis)

#set ARatio 0.25; # Column Aspect Ratio

#set ALR 0.05;    # Column Axial Load Ratio

#set colD 48;    # Column Diameter


#Going to call up the above information using Matlab to do the batching process

source input.tcl

source input2.tcl


# Create a file folder location for all of the data in the OpenSees folder

set File
Data_multDispEle_ATC_D{$colD}_ConcMat{$concMat}_SteelMat{$steelMat}_ALR{$ALR}_Aspect{$ARatio}
_{$Analoption}_Trial{$Trial}_SP;

file mkdir $File;


# define the model builder and how many dimensions and degrees of freedom

model BasicBuilder -ndm 2 -ndf 3


# define some important constants for calculations

#set pi [expr 4*atan(1)];

#set g 386.4;    # establshing the gravity constant in in/sec^2


# Define some geometry of the section

#set colD 48;

#set Ag [expr $pi*pow($colD,2)/4];

#set cover 2.;    # Cover to Longitudinal Bar
```

```
#set dbl 1.410;    # Longitudinal Bar Diameter

#set Abl 1.56;    # Longitudinal Bar Area

#set dbh 0.625;    # Hoop Bar Diameter

#set Abh 0.31;    # Hoop Bar Area

#set Dpr [expr $colD-2*$cover+$dbh];

#set Ac [expr $pi*pow($Dpr,2)/4];

#set Dbar [expr $colD-2*$cover-$dbl];


# Establish the important radii for the section definition

#set rout [expr $colD/2];

#set rpr [expr $Dpr/2];

#set rbar [expr $Dbar/2];

set dconf [expr $rcon+$rsteel];    # depth of steel bar from the confined concrete region definition


# Define the geometry of the column above the foundation

set Lcol [expr $colD/$ARatio];

#set Lele [expr 1.2973*pow($ARatio,-1)];

set colNumIncr [expr int(ceil($Lcol/$Lele))];

puts "colNumIncr = $colNumIncr"

set colIncr [expr $Lcol/$colNumIncr];


# Define the number of longitudinal bars to be used in the section model

#set rhold 0.02;

#set Asd [expr $rhold*$Ag];

#set ns [expr int(ceil($Asd/$Abl))];

set rhola [expr $ns*$Abar/$Ag];
```

```
# nodal coordinates for the model - node(node#, X, Y)


node 1 0.0 0.0

node 2 0.0 0.0


for {set i 1} {$i <= $colNumIncr} {incr i 1} {

    node [expr $i+2] 0 [expr $i*$colIncr]

    puts "node [expr $i+2] = [expr $i*$colIncr]"

}
puts "nodes established"


# Single point constraints -- Boundary Conditions fix(node #, DX, DY, RZ)

fix 1 1 1 1


# Going to establish the nodal conditions at the top of the strain penetration element

# Creating an equal dof such that the element can slip along the length of the element in

# local coordinate system.  Thus only constrain the dof 2 using:

# equalDOF (Master Node, Slave Node, DOF to match)

equalDOF 1 2 1


# Define the material properties that are going to be used in the fiber section

#

# Unconfined Concrete Properties First

#set fc 4;

#set Ec [expr 57*pow($fc*1000,0.5)];

#set ec [expr pow($fc*1000,0.25)/4000];

#set ft1 0.0005;
```

```
#set et1 [expr 2*$ft1/$Ec];

#set xp1 1.23;

#set xn1 2.3;

#set r1 [expr ($fc*1000/750)-1.9];

#set fc1 [expr -1*$fc];

#set ec1 [expr -1*$ec];


# Reinforcing Steel Properties

#set fy 60.;

#set fye [expr 1.1*$fy];

#set fsu [expr 1.5*$fye];

#set Es 29000.;

#set Esh 850.;

#set esh [expr 3.24*$fye/$Es];

#set esu 0.12;

#set Eratio 0.02;


# Define the column axial load

#set PCol [expr $ALR*$fc1*$Ag];


# Confined Concrete Properties

#set rhos [expr 0.16*($fc/$fy)*(0.5+1.25*$ALR)+0.13*($rhola-0.01)];     # ATC-32 Reccommendation and values
in Priestley (1996)

#set rhos [expr 0.45*($fc/$fy)*(($Ag/$Ac)-1)];     #This is the Caltrans Minimum Equation

#set s [expr 4*$Abh/($Dpr*$rhos)];

#set sclear [expr $s-$dbh];

#set rhocc [expr $ns*$Abl/$Ac];
```

```
#set Ke [expr (1-0.5*$sclear/$Dpr)/(1-$rhocc)];

#puts "Ke = $Ke"

#set flp [expr $Ke*$fy*$rhos/2];

#set fcc [expr $fc*(2.254*pow((1+7.94*$flp/$fc),0.5)-2*$flp/$fc-1.254)];

#set ecc [expr 0.002*(1+5*($fcc/$fc-1))];

#set Ecc [expr 57*pow($fc*1000,0.5)];

#set ft2 0.0005;

#set et2 [expr 2*$ft2/$Ecc];

#set xp2 1.23;

#set xn2 20;    # this is supposed to be between 20-30 based on information provided by others using Concrete07

#set n2 [expr $Ecc*$ecc/$fcc];

#set r2 [expr $n2/($n2-1)];

#set ecu [expr -1*(0.004+1.4*$rhos*$fy*$esu/$fcc)];

set rmander [expr $Ecc/($Ecc-($fccmat/$eccmat))];

set xult [expr $ecu/$eccmat];

puts "xult = $xult"

set fccu [expr ($fccmat*$xult*$rmander)/($rmander-1+pow($xult,$rmander))];

#set fc2 [expr -1*$fcc];

#set ec2 [expr -1*$ecc];

set fcu2 [expr $fccu];

#set fcu2 -4.;

puts "ultimate compressive strength = $fcu2"

puts "confined concrete properties ok"


# Writing a text file of the information used for the analysis

set out [open "$File/Input.txt" w]

puts $out "Units in the Program"
```

```
puts $out "Forces are in kips"

puts $out "Displacements and Dimensions are in inches"

puts $out "Time is in Seconds"

puts $out ""

puts $out ""

puts $out "Analysis Type = $Analoption"

puts $out ""

puts $out ""

puts $out "Section Geometry"

puts $out ""

puts $out "Column Diameter = $colD"

puts $out "Cover to Main Bar = $cover"

puts $out "Longitudinal Bar Diameter = $dbl"

puts $out "Longitudianl Bar Area = $Abar"

puts $out "Number Longitudinal Bars = $ns"

puts $out "Longitudinal Reinforcement Ratio = $rhola"

puts $out "Hoop Bar Diameter = $dbh"

puts $out "Hoop Bar Area = $Abh"

puts $out "Hoop Spacing = $s"

puts $out "Horizontal Reinforcement Ratio = $rhos"

puts $out ""

puts $out ""

puts $out "Column Geometry above the Spread Footing"

puts $out ""

puts $out "Column Height = $Lcol"

puts $out "Aspect Ratio = $ARatio"

puts $out "Element Length = $colIncr"
```

```
puts $out "Number of Elements = $colNumIncr"

puts $out ""

puts $out ""

puts $out "Applied Loads"

puts $out ""

puts $out "Column Axial Load At Top = $P"

puts $out ""

puts $out ""

puts $out "Unconfined Concrete Material Properties"

puts $out ""

puts $out "Compressive Strength = $fcmat"

puts $out "Strain at Compressive Strength = $ecmat"

puts $out "Modulus of Elasticity = $Ec"

puts $out "Tensile Strength = $ft1"

puts $out "Tensile Strain = $et1"

puts $out "Concrete Model is $concMat"

puts $out ""

puts $out ""

puts $out "Confined Concrete Material Properties"

puts $out ""

puts $out "Confinement Effectiveness, Ke = $Ke"

puts $out "Compressive Strength = $fccmat"

puts $out "Strain at Compressive Strength = $eccmat"

puts $out "Modulus of Elasticity = $Ecc"

puts $out "Ultimate Compressive Strain = $ecu"

puts $out "Ultimate Compressive Stress = $fcu2"

puts $out "Tensile Strength = $ft2"
```

```
puts $out "Tensile Strain = $et2"

puts $out "Concrete Model is $concMat"

puts $out ""

puts $out ""

puts $out "Reinforcing Steel Material Properties"

puts $out ""

puts $out "Hoop Yield Stress = $fy"

puts $out "Longitudinal Yield Stress = $fye"

puts $out "Ultimate Stress = $fsu"

puts $out "Modulus of Elasticity = $Es"

puts $out "Hardening Steel Strain = $esh"

puts $out "Hardening Modulus of Elasticity = $Esh"

puts $out "Ultimate Steel Strain = $esu"

puts $out "Steel Model is $steelMat"

close $out




# Write the actual material property definitions in OpenSees
# Concrete Properties using Concrete07(tag, fc, ec, Ec, ft, et, xp, xn, r)
# Concrete Properties using Concrete02(tag,fc, ec, fc(crushing), ec(crushing), lambda, ft, Ets)
# Concrete Properties using Concrete03(tag, fc, ec, fc (crushing), ec (crushing), lambda (0.1), ft, ets0 (tension

transition to strain softening), ft0 (tesnsion stress at softening transition), beta (exponent tension soft), etu (ultimate

tensile strain))
# Steel Properties using ReinforcingSteel(tag, fy, fu, Es, Esh, esh, esu)
# Steel Properties using Steel02(tag, fy, Es, b(0.015), R0 (between 10 and 20), CR1 (0.925), CR2(0.15), a1(0),

a2(5), a3(0), a4(5)
```

```
# ---------------------------------------------------------------------------------------

# Unconfined Concrete Models

if {$concMat == "c07"} {

    uniaxialMaterial Concrete07 2 $fcmat $ecmat $Ec $ft1 $et1 $xp1 $xn1 $r1

} elseif {$concMat == "c02"} {

    uniaxialMaterial Concrete02 2 $fcmat $ecmat [expr 0.1*$fcmat] -0.008 0.1 $ft1 [expr $Ec/10]

} else {

    uniaxialMaterial Concrete03 2 $fcmat $ecmat -0.01 -0.0091 0.1 $ft1 0.003 0.0004 2.5 0.004

}


# Confined Concrete Models

if {$concMat == "c07"} {

    uniaxialMaterial Concrete07 1 $fccmat $eccmat $Ecc $ft2 $et2 $xp2 $xn2 $r2

} elseif {$concMat == "c02"} {

    uniaxialMaterial Concrete02 1 $fccmat $eccmat [expr 0.1*$fccmat] $ecu 0.1 $ft2 [expr $Ec/10]

} else {

    uniaxialMaterial Concrete03 1 $fccmat $eccmat $fcu2 $ecu 0.1 $ft2 0.003 0.0004 2.5 0.004

}


# Reinforcing Steel Models

if {$steelMat == "rs"} {

    uniaxialMaterial ReinforcingSteel 3 $fye $fsu $Es $Esh $esh $esu

} else {

    uniaxialMaterial Steel02 3 $fye $Es $Eratio 18 0.925 0.15 0 5 0 5

}


# Strain Penetration Model Needs to be Defined
```

```
# Defining the Slip Curve using Bond_SP01 $matTag $Fy $Sy $Fu $Su $b $R

# Fy = yield stress of r/f steel

# Sy = rebar slip at member interface under yield stress

# Fu = ultimate strength of reinforcing steel

# Su = rebar slip at the loaded end at the bar fracture strength

# b = initial hardening ratio in the monotonic slip vs. bar stress response (0.3 ~ 0.5) (Paper says 0.5 in columns)

# R = Pinching factor for the cyclic slip vs. bar response (0.5 ~ 1.0) (Paper says 1.0 columns and 0.7 tee-joint)


set alpha 0.4;

set alphain [expr 1/$alpha];

set Fy [expr $fye*1000];

set bracket [expr ($dbl/4000)*($Fy/pow(-1*$fccmat*1000,0.5))*(2*$alpha+1)];

set Sy [expr 0.1*pow($bracket,$alphain)+0.013]

set Su [expr 40*$Sy]

set b 0.5;

set R 1.0;

puts "Yield Slip = $Sy"

puts "Ultimate Slip = $Su"


uniaxialMaterial Bond_SP01 4 $fye $Sy $fsu $Su $b $R


puts "Materials Defined"


# Create the fiber section to be used in the analysis for this model of a circular column

# ---------------------------------------------------

# Define the number of fibers to be used in the cross-section

#set length 0.5
```

```
#set nfcradial [expr int(ceil(0.5*$Dpr/$length))]

#set nfccirc [expr int(ceil($pi*$Dpr/$length))]

#set nfuradial [expr int(ceil($cover/$length))]

#set nfucirc [expr int(ceil($pi*$colD/$length))]


# Define the cross-section using fibers


section Fiber 1 {

    patch circ 1 $nfccirc $nfcradial 0 0 0 $rcon 0 360

    patch circ 2 $nfucirc $nfuradial 0 0 $rcon $rcov 0 360

    layer circ 3 $ns $Abar 0 0 $rsteel 0 360

    }


section Fiber 2 {

    patch circ 1 $nfccirc $nfcradial 0 0 0 $rcon 0 360

    patch circ 2 $nfucirc $nfuradial 0 0 $rcon $rcov 0 360

    layer circ 4 $ns $Abar 0 0 $rsteel 0 360

    }


# define geometric transformation to transform basic system to global system

geomTransf Linear 101

#geomTransf PDelta 101


# establish the element(s) for use in the model

set numIntgrPts 5;


element zeroLengthSection 1 1 2 2 -orient 0 1 0 1 0 0
```

```
# in the orientation term $x1 $x2 $x3 define the local x-axis in global coordinates

# the yp terms can be found as the x vector crossed with yp equals your z-vector direction


for {set i 1} {$i <= $colNumIncr} {incr i 1} {

    element dispBeamColumn [expr $i+1] [expr $i+1] [expr $i+2] $numIntgrPts 1 101

    puts "element = [expr $i+1] for node [expr $i+1] and [expr $i+2]"

}


puts "elements defined"


# Define RECORDERS -----------------------------------------------------------------

recorder Node -file $File/DFree1.out -time -node 2 -dof 1 2 3 disp;

recorder Node -file $File/Dtop.out -time -node [expr $colNumIncr+2] -dof 1 2 3 disp;

recorder Node -file $File/DBase1.out -time -node 1 -dof 1 2 3 disp;

recorder Node -file $File/RBase1.out -time -node 1 -dof 1 2 3 reaction;

recorder Node -file $File/DBase2.out -time -node 2 -dof 1 2 3 disp;

recorder Node -file $File/Rbase2.out -time -node 2 -dof 1 2 3 reaction;

#recorder Drift -file $File/Drift1.out -time -iNode 1 -jNode 2 -dof 1 -perpDirn 2;

#recorder Drift -file $File/Drift2.out -time -iNode 2 -jNode 3 -dof 1 -perpDirn 2;

#recorder Drift -file $File/DriftTot.out -time -iNode 1 -jNode [expr $colNumIncr+1] -dof 1 -perpDirn 2;

recorder Element -file $File/FCol1.out -time -ele 1 globalForce;

recorder Element -file $File/Fcol2.out -time -ele 2 globalForce

recorder Element -file $File/FColTop.out -time -ele [expr $colNumIncr+1] globalForce;

recorder Element -file $File/TopUCse.out -time -ele [expr $colNumIncr+1] section fiber -$rcov 0.0 2 stressStrain

recorder Element -file $File/BotUCse1.out -time -ele 1 section fiber -$rcov 0.0 2 stressStrain

recorder Element -file $File/BotUCse2.out -time -ele 2 section fiber -$rcov 0.0 2 stressStrain

recorder Element -file $File/TopCCse.out -time -ele [expr $colNumIncr+1] section fiber -$rcon 0.0 1 stressStrain
```

recorder Element -file $File/BotCCse1.out -time -ele 1 section fiber -$rcon 0.0 1 stressStrain

recorder Element -file $File/BotCCse2.out -time -ele 2 section fiber -$rcon 0.0 1 stressStrain

recorder Element -file $File/TopRFse.out -time -ele [expr $colNumIncr+1] section fiber $rsteel 0.0 3 stressStrain

recorder Element -file $File/BotRFse1.out -time -ele 1 section fiber $rsteel 0.0 4 stressStrain

recorder Element -file $File/BotRFse2.out -time -ele 2 section fiber $rsteel 0.0 3 stressStrain

#recorder Element -file $File/DefoCol1.out -time -ele 1 basicDeformation;

#recorder Element -file $File/DefoCol2.out -time -ele 2 basicDeformation;

#recorder Element -file $File/FColSec1_1.out -time -ele 1 section 1 force;

#recorder Element -file $File/FColSec1_2.out -time -ele 2 section 1 force;

#recorder Element -file $File/DefoColSec1_1.out -time -ele 1 section 1 deformation;

#recorder Element -file $File/DefoColSec1_2.out -time -ele 2 section 1 deformation;

#recorder Element -file $File/FColSec{$numIntgrPts}_1.out -time -ele 1 section $numIntgrPts force;

#recorder Element -file $File/FColSec{$numIntgrPts}_2.out -time -ele 2 section $numIntgrPts force;

#recorder Element -file $File/DefoColSec{$numIntgrPts}_1.out -time -ele 1 section $numIntgrPts deformation;

#recorder Element -file $File/DefoColSec{$numIntgrPts}_2.out -time -ele 1 section $numIntgrPts deformation;

recorder Element -file $File/FLength.out -time -eleRange 2 [expr $colNumIncr+1] globalForce

recorder Element -file $File/RFseLength.out -time -eleRange 2 [expr $colNumIncr+1] section fiber $rsteel 0 3 stressStrain

recorder Element -file $File/CCseLength.out -time -eleRange 2 [expr $colNumIncr+1] section fiber -$rcon 0 1 stressStrain

recorder Element -file $File/UCseLength.out -time -eleRange 2 [expr $colNumIncr+1] section fiber -$rcov 0 2 stressStrain

puts "recorders started"

define the Gravity Load on the column --

pattern Plain 1 Linear {

```
    load [expr $colNumIncr+2] 0 [expr -1*$P] 0

}


set Tol 1.0e-8;

constraints Plain;

numberer Plain;

system BandGeneral;

test NormDispIncr $Tol 10;

algorithm Newton;

set NstepGravity 10;

set DGravity [expr 1./$NstepGravity];

integrator LoadControl $DGravity;

analysis Static

analyze $NstepGravity


# Maintain the applied gravity load and reset the time of the program to 0

loadConst -time 0.0

puts "Gravity load applied, moving to cyclic analysis"


# define the cyclic lateral load analysis ------------------------------------------------------

#

# Establish the model parameters specific to this analysis

set IDctrlNode [expr $colNumIncr+2];

puts "IDctrlNode = $IDctrlNode"

set IDctrlDOF 1;    # This is for the Global X-Direction, 2 is the Global Y-Direction, 3 is the Global Rotation about

z

set du [expr -25.55*$ARatio+32.55];
```

```
set nsteps 600;

set Dincr [expr $du/$nsteps];


# Define the static analysis parameters for this process

set tolerance 1.0e-5

set nItr 100

set maxNumItrStatic 5000

#constraints Plain;

#numberer Plain;

#system SparseGeneral -piv

#test EnergyIncr $tolerance $nItr 1

#test NormUnbalance $tolerance $nItr 1

#algorithm KrylovNewton

#analysis Static


pattern Plain 200 Linear {

    load $IDctrlNode 1.0 0.0 0.0

}


if {$Analoption != "Cyclic"} {

    puts "running the pushover analysis"

    set a [eleResponse 2 section 1 fiber -$rcon 0.0 1 strain]

    set b [eleResponse 2 section 1 fiber $rcov 0.0 3 strain]

    set cconf [expr $a*$dconf/($a-$b)];     # This is the neutral axis depth of concrete from the confined region

    set curv [expr abs($a)/$cconf];     # This is the curvature of the concrete section at the bottom node

    while {$curv <= $phiu} {

        set ok 0
```

```
constraints Plain

numberer Plain

system SparseGeneral -piv

test EnergyIncr $tolerance $nItr 1

algorithm KrylovNewton

integrator DisplacementControl $IDctrlNode $IDctrlDOF $Dincr

analysis Static

set ok [analyze 1]

if {$ok != 0} {

        puts "Trying Krylov Newton with Different Tolerance and # of Iterations and NormDispIncr test"

        set tolerance 1.0e-4

        set nItr $maxNumItrStatic

        constraints Plain

        numberer Plain

        system SparseGeneral -piv

        test normDispIncr $tolerance $nItr 1

        algorithm KrylovNewton

        analysis Static

        set ok [analyze 1]

}

if {$ok != 0} {

        puts "Trying KylovNewton with NormUnbalance Test"

        set tolerance 1.0e-4

        set nItr $maxNumItrStatic

        constraints Plain

        numberer Plain

        system SparseGeneral -piv
```

```
        test NormUnbalance $tolerance $nItr 1

        algorithm KrylovNewton

        analysis Static

        set ok [analyze 1]

}

if {$ok != 0} {

        puts "Trying Newton algorithm with NormDispIncr test"

        set tolerance 1.0e-4

        set nItr $maxNumItrStatic

        test NormDispIncr $tolerance $nItr 1

        algorithm Newton

        set ok [analyze 1]

}

if {$ok != 0} {

        puts "Trying Newton algorithm with NormUnbalance Test"

        set tolerance 1.0e-4

        set nItr $maxNumItrStatic

        test NormUnbalance $tolerance $nItr 1

        algorithm Newton

        set ok [analyze 1]

}

if {$ok == 0} {

        puts "Convergence Met"

        set tolerance 1.0e-4

        set nItr $maxNumItrStatic

        #test NormUnbalance $tolerance $nItr 1

        test EnergyIncr $tolerance $nItr 1
```

```
            algorithm KrylovNewton

            set currentdisp [nodeDisp $IDctrlNode $IDctrlDOF]

            puts "displacement of column is $currentdisp"

        }

        set a [eleResponse 2 section 1 fiber -$rcon 0.0 1 strain]

        set b [eleResponse 2 section 1 fiber $rsteel 0.0 3 strain]

        set cconf [expr $a*$dconf/($a-$b)];    # This is the neutral axis depth of concrete from the confined region

        set curv [expr abs($a)/$cconf];    # Curvature of the concrete section at the bottom node

        puts "curvature of section is $curv"

    }

} else {

# ----------------------------------------------------------------

# -------------------------Cyclic Analysis-----------------------

# ----------------------------------------------------------------

puts "running the cyclic analysis"

set Dmax1 0.0

set Dmaxa 0.0

    foreach {Dmax} {0.01 -0.01 0.1 -0.1 0.2 -0.2 0.4 -0.4 0.8 -0.8 1.0 -1.0 1.4 -1.4 1.8 -1.8 2.0 -2.0 2.5 -2.5 3.0 -3.0

4.0 -4.0 5.0 -5.0 6.0 -6.0 7.0 -7.0 0.1} {

        if {[expr abs($Dmax)] < 0.2 && [expr abs($Dmaxa)] < 0.2} {

            set stepSize 0.01

        } elseif {[expr abs($Dmax)] >= 0.2 && [expr abs($Dmax)] <=1.0 && [expr abs($Dmaxa)] <=1.0} {

            set stepSize 0.02

        } else {

            set stepSize 0.05

        }

        set numSteps [expr int(abs($Dmax-$Dmax1)/$stepSize)]
```

```
for {set i 1} {$i <= $numSteps} {incr i 1} {

        set ok 0

        if {$Dmax < 0} {

                set stepSize1 [expr -1.*$stepSize]

                } else {

                set stepSize1 $stepSize

        }

        integrator DisplacementControl $IDctrlNode $IDctrlDOF $stepSize1

        analysis Static

        # --------------------first analyze procedure-------------------------

        set ok [analyze 1]

        # --------------------if convergence failure-------------------------

        # if the analysis failed, trying some other stuff to find convergence

        if {$ok != 0} {

                puts "Increasing the number of iterations and changing tolerance"

                set tolerance 1.0e-4

                set nItr $maxNumItrStatic

                test EnergyIncr $tolerance $nItr 1

                algorithm KrylovNewton

                set ok [analyze 1]

        }

        if {$ok != 0} {

                puts "Trying Krylov Newton with Different Tolerance and # of Iterations and

NormDispIncr test"

                set tolerance 1.0e-4

                set nItr $maxNumItrStatic

                test normDispIncr $tolerance $nItr 1
```

```
        algorithm KrylovNewton

        set ok [analyze 1]

}

if {$ok != 0} {

        puts "Trying KylovNewton with NormUnbalance Test"

        set tolerance 1.0e-4

        set nItr $maxNumItrStatic

        test NormUnbalance $tolerance $nItr 1

        algorithm KrylovNewton

        set ok [analyze 1]

}

if {$ok != 0} {

        puts "Trying Newton algorithm with NormDispIncr test"

        set tolerance 1.0e-4

        set nItr $maxNumItrStatic

        test NormDispIncr $tolerance $nItr 1

        algorithm Newton

        set ok [analyze 1]

}

if {$ok != 0} {

        puts "Trying Newton algorithm with NormUnbalance Test"

        set tolerance 1.0e-4

        set nItr $maxNumItrStatic

        test NormUnbalance $tolerance $nItr 1

        algorithm Newton

        set ok [analyze 1]

}
```

```
                if {$ok == 0} {

                        puts "Convergence met"

                        set tolerance 1.0e-5

                        set nItr $maxNumItrStatic

                        #test NormUnbalance $tolerance $nItr 1

                        test NormDispIncr $tolerance $nItr 1

                        #test EnergyIncr $tolerance $nItr 1

                        algorithm KrylovNewton

                        set currentdisp [nodeDisp $IDctrlNode $IDctrlDOF]

                        puts "displacement of column is $currentdisp, displacement cycle of $Dmax"

                };  # end if

        };  # end i procedure

        set Dmaxa $Dmax1

        set Dmax1 $Dmax

    };  # end Dmax cycle

};  # end if statement for analysis type

puts "Analysis is complete"
```